ToxStrategies

Innovative solutions
Sound science

November 1, 2022

Supporting Evidence for Petition for Oregon Department of Environmental Quality (ODEQ) Air Toxics Review to Revise the Acute Toxicity Reference Value (TRV) for Acute Manganese Exposure

A petition has been submitted to the Oregon Department of Environmental Quality (ODEQ) to propose an alternative short-term guideline concentration (SGC) and toxicity reference value (TRV) for acute (24-hour) exposure to manganese, as provided in Oregon Administrative Rule (OAR) 340-247-0040(4). This document provides the supporting scientific evidence for a revised SGC and acute TRV **of 5 µg/m^3**. As described below, the evidence supporting an updated SGC and TRV for acute manganese includes the following: authoritative source information; inhalation toxicity reference values established by another state; publicly available and peer-reviewed toxicity testing data; and a peer-reviewed, published physiologically based pharmacokinetic (PBPK) model.

1 The basis for ODEQ's current toxicity reference value (TRV) and short-term guideline concentration (SGC) for acute manganese exposure are not consistent with current authoritative sources, are based on long-term exposure study data, and are not current with the scientific literature.

ODEQ's acute toxicity reference value (TRV) for manganese (0.3 µg/m^3)[1] is applied to exposures up to 24 hours. This TRV was set at the same value as the short-term guideline concentration (SGC) developed by ODEQ and the Oregon Health Authority (OHA).[2] (For simplicity, we will reference only the TRV in our discussion, but the same comments apply to the SGC.) ODEQ's TRV is not set by reference to acute exposure information. Instead, the TRV is based on a long-term exposure guideline (chronic reference exposure level [REL]) published in 2008 by California's Office of Environmental Health Hazard Assessment (OEHHA, 2008b). Although ODEQ air toxics regulations list CalEPA (and thus OEHHA) as an authoritative source from which information can be used to identify TRVs, OEHHA did not set an acute exposure guideline. Moreover, use of a chronic value like the guideline set by OEHHA in 2008 is in direct contrast to the OHA's recommendation that extrapolating from chronic values should be avoided and is to be considered only when the endpoint for the acute exposures is relevant to the chronic effect

[1] Oregon Administrative Rules (OAR 340-247-8010).

[2] Oregon Health Authority. 2019. Short-term guideline concentrations for air toxics. October 29.

(OHA, 2019[2]). As described herein, ODEQ's prior decision to convert OEHHA's chronic REL to an acute value of ODEQ's creation by applying what equates to a chronic-to-acute uncertainty factor is not supported by any authoritative source or published science.

1.1 OEHHA's REL

OEHHA's 2008 REL is based on a study of neurotoxicity in workers exposed for an average of 5.3 years and up to 17 years (Roels et al., 1992). To derive an SGC from OEHHA's chronic REL, ODEQ multiplied the OEHHA REL (0.09 µg/m^3) by an uncertainty factor equal to the square root of 10, to reverse OEHHA's adjustment from subchronic to chronic exposures when setting the REL. OEHHA applied a subchronic adjustment factor to the study results, because, in the underlying study, worker exposures were evaluated for an average exposure of 5.3 years, which is less than the 7 years that OEHHA uses for chronic exposures. Clearly, average exposures of 5.3 years and upper-bound exposures of 17 years in the study are not appropriate evaluation periods for acute 24-hour exposure. In fact, 5.3 years is very close to the chronic exposure timeframe of at least 7 years that would not require adjustment from subchronic to chronic (10% of a lifetime) (OEHHA, 2008a), and data from the Roels et al. (1992) study therefore were appropriate for direct application to evaluate chronic exposures. The same study, however, should not be used to evaluate acute, 24-hour exposures.

While OEHHA has developed acute RELs for some chemicals (to be applied to maximum hourly exposures), OEHHA did not develop an acute REL for manganese, because they did not judge the available data to be appropriate for short-term exposures. In fact, OEHHA specifically concluded that: "No studies of acute manganese inhalation were located that demonstrated a dose-response or evaluated other toxicological endpoints" (OEHHA, 2008b). Therefore, OEHHA did not establish an acute REL.

1.2 ATSDR's Minimal Risk Level

The Agency for Toxic Substance Disease Registry (ATSDR), also listed as an authoritative source in Oregon regulations, developed a chronic inhalation minimum risk level (MRL) for manganese of 0.3 µg/m^3 (ATSDR, 2012). It is important to note that the ATSDR assessment is more current than the OEHHA REL and relies on an enhanced investigation of the same occupational exposure data (Roels et al., 1992). The ATSDR chronic MRL is equal to the ODEQ acute TRV, demonstrating on its face that the acute TRV is unnecessarily conservative.

The ATSDR chronic MRL is based on the neurological endpoint of abnormal hand-eye coordination, as described in Roels et al. (1992). ATSDR calculated a benchmark concentration level for potential adverse effects in 10% of the population ($BMCL_{10}$), as recommended by U.S. EPA (2012), using the individual-level data provided by the authors to calculate the point of departure (POD) of 142 µg/m^3. Following adjustments for worker exposures (5/7 days/week x 8/24 hours per day x 142 ug/m^3 = 34 µg/m^3), ATSDR applied uncertainty factors of 10 for human variability, citing the published PBPK models for demonstrating the lack of effect among neonates and young children, and 10 for

limitations/uncertainties in the database, including that the workers in the Roels et al. (1992) study were exposed to manganese oxide, which is an insoluble form of manganese that is expected to have lower bioavailability than soluble forms. Unlike OEHHA, ATSDR did not include a factor for extrapolating from subchronic to chronic exposure. These uncertainty factors result in the chronic MRL of 0.3 µg/m^3 [34 µg/m^3/(10x10)].

Similar to OEHHA, ATSDR did not develop an acute MRL, or even an intermediate MRL, stating that "The available data on the toxicity of inhaled manganese were considered inadequate for derivation of acute- or intermediate-duration inhalation MRLs" (ATSDR, 2012). In addition, ATSDR highlighted that respiratory effects were relevant to acute exposures. ATSDR summarized, "Several acute- and intermediate-duration studies in animals report various signs of lung inflammation following periods ranging from one day to ten months at manganese concentrations ranging from 0.7 to 69 mg/m^3." No-observed-adverse-effect levels (NOAELs) for respiratory effects from acute exposures reported by ATSDR (2012) range from approximately 2 to 14 mg/m^3. ATSDR concluded that intermediate and acute MRLs based on animal data would be lower[3] than the chronic MRL, which was based on human data, and therefore, these shorter term MRLs were unnecessary.

1.3 Authoritative-Source Information for Chronic Exposure is not Appropriate for Setting an Acute TRV

To summarize, ODEQ set its TRV by relying on OEHHA's chronic values, which were based on a long-term occupational study wherein neurological effects were observed. As noted by ATSDR, although acute health effects on the respiratory system may result from acute inhalation exposure to manganese, neither the OEHHA REL nor the ATSDR MRL were developed from underlying data that represented short-term exposure or effects on the respiratory system. Both agencies, OEHHA and ATSDR, concluded that the data they reviewed were not sufficient to develop an acute exposure value. Given this conclusion from these authoritative sources, it is evident that ODEQ's current TRV is not based on relevant toxicity information from one or more of the authoritative sources listed in OAR 340-247-0030 (i.e., none of the listed authoritative sources have set an acute TRV for manganese) and is inappropriate for continued use. The following section of this document details the evidence that supports revising ODEQ's acute TRV for manganese.

[3] The acute and intermediate MRLs would require additional uncertainty factors because they would be based on animal data, as compared to the chronic MRL based on human data. The ATSDR stated that it believed the chronic value is also adequately protective of acute and intermediate exposures.

2 ODEQ's acute TRV for Mn should be revised to include recent, more applicable regulatory and peer-reviewed, publicly available academic information relevant to acute exposures.

Consistent with OAR 340-247-0040(4), ODEQ should revise its acute TRV for Mn, based on the information used to set acute TRVs for Mn in Texas (Section 2.1) and the most current, peer-reviewed toxicity information that is publicly available (Section 2.2).

2.1 Alternative Regulatory Acute TRVs for Setting an Updated TRV for Mn

The Texas Commission on Environmental Quality (TCEQ) has developed a 24-hour Mn acute toxicity criterion based on short-term toxicity study data (TCEQ, 2017). Specifically, TCEQ[4] developed an air monitoring comparison value (AMCV)[5] for a 24-hour period of 5.0 µg/m^3. "The Texas Commission on Environmental Quality's (TCEQ) Air Monitoring Comparison Values (AMCVs) are used to evaluate the potential for effects to occur as a result of exposure to concentrations of constituents in the air. AMCVs are based on data concerning health effects, odor, and vegetation effects. They are not ambient air standards." TCEQ conducts a thorough literature review to set its criteria.

TCEQ's 24-hour AMCV is based on the non-human primate (NHP) study reporting respiratory effects following exposures to manganese sulfate ($MnSO_4$) by Dorman et al. (2005) (Attachment A).[6] The TCEQ 24-hr AMCV is conservative, because it is based on mild, and transient, respiratory effects observed following exposure to 1,500 µg Mn/m^3 for 6 hours per day, 5 days per week, for 3 weeks, which is 15 exposure days or 90 total hours of exposure (Dorman et al., 2005).[7] TCEQ applied an uncertainty factor of 300, to arrive at the 24-hour AMCV of 5.0 µg/m^3.[8]

---

[4] The Toxicology, Risk Assessment, and Research Division of TCEQ developed the inhalation AMCV. Similar to OEHHA's role in California, this division "helps TCEQ make scientifically sound decisions by applying toxicological principles when evaluating environmental data, issuing authorizations, developing environmental regulations and making policy decisions. TCEQ toxicologists identify chemical hazards, evaluate potential exposures, assess human health risks and communicate risk to the general public and stakeholders." TCEQ Toxicology - Texas Commission on Environmental Quality - www.tceq.texas.gov

[5] Air Monitoring Comparison Values (texas.gov).

[6] Dorman et al. (2005) was reviewed by OEHHA and ATSDR, but was not used to set acute or intermediate MRLs as noted in Footnote 3. OEHHA's acute values are for 1-hr exposures, and the Dorman study was for much longer exposure durations. ATSDR's acute values are for 14 days. ATSDR could have used Dorman et al. (2005), but after adding uncertainty factors appropriate for 14 day exposures (rather than 24-hour exposures), the acute MRL would be lower than the chronic MRL. Using Dorman et al. (2005) for a 24-hour exposure point of departure (POD), as was done by TCEQ, is conservative and appropriate.

[7] Detailed summary of Dorman et al. (2005) is provided herein in Attachment B.

[8] AMCV for Mn $\left(5\frac{\mu g}{m3}\right) = 1.5\frac{mg}{m3} \times 1000\ \frac{\mu g}{mg} \div 300$

The short-term inhalation toxicity guideline concentrations published by ODEQ and TCEQ are compared in Table 1.

Table 1. Acute inhalation guidelines used by ODEQ and TECQ

Agency	Name of Value	Basis	Value ($\mu g/m^3$)	Exposure Term
ODEQ	Cleaner Air Oregon Program Short-Term Guideline Concentration/ Acute Noncancer toxicity reference value (TRV)/ risk-based concentration (RBC)	OEHHA chronic REL Neurological effects observed in workers (Roels et al. 1992); average exposed 5.3 years	0.3	24-hr
TCEQ	Short-term air monitoring comparison value (AMCV)[1]	Mild transient effects in NHPs exposed for 90 hrs over 3 weeks (Dorman et al., 2005)	9.1	1-hr
	24-hour air monitoring comparison value (AMCV)		5.0	24-hr

Abbreviations: $\mu g/m^3$ (microgram per cubic meter); hr (hour)

2.2 Current, Peer-Reviewed Short-Term Toxicity Data for Setting an Updated TRV for Mn

We conducted a current literature and regulatory review to identify the most relevant peer-reviewed toxicology and/or epidemiology data that could be used to set an updated acute TRV for manganese. The review included studies cited in existing regulatory guideline documents developed by TCEQ, ATSDR, and OEHHA to identify points of departure (PODs) (e.g., LOAELs, NOAELs, or benchmark doses [BMD]) for acute exposures. Next, we searched recent publications (since 2005) for relevant inhalation toxicity studies. In April of 2022, we performed a PubMed search for publications from 2005 to 2022 for "manganese inhalation toxicity." The titles and abstracts of the results were mined for newer studies that could help inform a 24-hour inhalation exposure guideline. Of the peer-reviewed articles identified in the initial search, several animal studies were identified as being potentially relevant for developing a short-term inhalation value based on a review of the titles and abstracts. No epidemiology studies were identified. Although the papers were informative, none provide a POD that was lower than that from Dorman et al. (2005). The potentially relevant papers are summarized in Attachment B.

Overall, considering these papers, we concur with the TCEQ's determination that, although exposures were short-term in nature but more than 24 hours, the data set from Dorman et al. (2005) provides the most appropriate POD for an acute TRV. The POD is the LOAEL of 1.5 mg Mn/m^3. As explained in Dorman et al. (2005) (Attachment A), no dosimetric adjustment is required when using these data to assess exposures in humans. Use of the Dorman et al. (2005) LOAEL addresses one of the data gaps identified by ATSDR when it set the chronic MRL in 2012, because exposures in this study were to soluble manganese sulfate ($MnSO_4$), which is bioavailable compared to the form (MnO_2) in Roels et al. (1992) (Chen et al. 2015; Dorman et al. 2005). Further, the reproductive and developmental

toxicity study by McGough and Jardine (2017) addresses the uncertainty associated with selecting the Dorman et al. (2005) POD based on respiratory effects (1.5 mg Mn/m^3), because subchronic exposures in rats at higher levels (up to 8.1 mg/m^3 for up to 714 hours) did not result in reproductive or developmental toxicity.

Although the potential for neurotoxicity from acute exposures seems unlikely, there is uncertainty regarding the potential for neurotoxicity based on the studies reviewed (Attachment B). To address this uncertainty, we cite and apply the currently published PBPK models (Schroeter et al. 2011; Yoon et al. 2019), which consider sensitive human life stages, to assess the potential for neurotoxicity from acute 24-hour exposures at the proposed TRV (5 µg/m^3) (Section 3). It is noteworthy that the data set from the Dorman et al. (2005) study was also used to parametrize the current PBPK models. Finally, Dorman et al. (2006) reported no neurological effects at any dose in the NHPs used in the 2005 study, based on veterinarian observations.

3 The proposed acute TRV/SGC of 5 µg/m^3 is associated with respiratory effects, consistent with the TCEQ AMCV, and would not result in potential neurotoxic effects, based on physiologically based pharmacokinetic (PBPK) modeling of manganese in the target tissue of the brain.

3.1 Proposed Acute TRV Based on Dorman et al. (2005)

It is proposed that ODEQ set an updated acute SGC and TRV for manganese of 5 µg/m^3. This value is consistent with the 24-hour AMCV developed by TCEQ (2017).

The TCEQ Development Support Document (2017) included a detailed literature review when establishing its toxicity criteria. The Dorman et al. (2005) study evaluated several exposure profiles, including exposure of NHPs to 1,500 µg/m^3 (1.5 mg/m^3) for 6 hours per day, 5 days/week, for 3 weeks (15 total exposure events). Dorman et al. (2005) also administered manganese in air for 0.06, 0.3, and 1.5 mg/m^3 for 7 and 13 weeks. Because 1,500 µg/m^3 was the only dose administered at the lowest number of exposures (15 exposure days)—all other dose groups were exposed for more days—1,500 µg/m^3 was selected as a lowest-observed-adverse-effect level (LOAEL). At 1,500 µg/m^3, manganese sulfate was reported to cause inflammatory airway changes (e.g., mild bronchitis, alveolar duct inflammation, see Attachment B). Applying an uncertainty factor of 300 to account for intraindividual variability (10-fold), interspecies variability (10-fold)[9], and an adjustment from mild transient LOAEL to NOAEL (3-fold), results in a proposed TRV of 5 µg/m^3. This TRV is based on NHPs exposed to $MnSO_4$, which is freely soluble and considered the most bioavailable form of manganese. Therefore, in addition to being more

[9] A lower 3-fold interspecies uncertainty factor could also be supported because a dosimetric adjustment between monkeys and humans is not required as discussed in Dorman et al. (2005). Using a 10-fold factor, the proposed TRV is conservative.

appropriate for 24-hour exposures than ODEQ's current TRV, the proposed TRV is more relevant to environmental exposures than the current TRV (which was developed based on workers exposed to less soluble manganese oxide).

3.2 Application of PBPK Model for Manganese to Assess Exposure at the Proposed TRV and SGC

The PBPK model for manganese was developed to satisfy the United States Environmental Protection Agency (EPA) risk assessment requirements under the federal Clean Air Act. The model is able to predict the levels of manganese in the brain from exposure by diet and air for children (birth to 3 years) and youth to adults (3 years to adulthood) (Yoon et al. 2019). The current model code has been reviewed by the EPA's National Center for Environmental Assessment (NCEA).[10] EPA offered recommendations to improve the model, and those recommendations have been incorporated (Campbell et al., 2022; Attachment B). Importantly, the modifications to the model do not affect model predictions of manganese in the brain (Campbell et al., 2022).

Although neurological effects from acute exposures seem improbable, the previously published PBPK model for Mn exposure among infants, toddlers, children, and adults (Schroeter et al., 2011; Yoon et al., 2019) was applied to evaluate the potential for increased manganese concentration in the target tissue of the brain (i.e., globus pallidus) of humans exposed at the proposed TRV and SGC of 5 µg/m^3. Specifically, two scenarios were modeled:

1) 24-hour exposures at the proposed TRV occurring once per month (monthly exposure scenario) throughout life, and
2) A continuous 3-week exposure occurring at the age when the model predicts the highest level of background manganese, which is approximately 3 years old (three week exposure scenario).

Use of the PBPK model reduces uncertainty regarding the potential for neurological effects in humans at the proposed TRV and SGC, which is based on, and specifically protective of, respiratory effects. It also allows for assessment of continuous (24-hour) exposure scenarios and of potentially sensitive exposure during early, sensitive life stages in humans. The PBPK model is based on exposures to $MnSO_4$; therefore, no correction for bioavailability is needed.

The frequency of presumed 24-hour acute exposures is not specified in OAR 340-245-0020 (3). So, for this evaluation, the potential manganese accumulation in the brain from 24-hour exposure at the proposed TRV of 5 µg/m^3 was assumed to occur once per month (monthly exposure scenario) from birth to age 65. This frequency of acute exposures is considered conservative, because the TRV is compared to the highest 24-hour

[10] Personal communication with Paul Schlosser, EPA NCEQ and Deborah Proctor, ToxStrategies.

concentration predicted using an air dispersion model and 5 years of meteorological data. Exposures to background levels of manganese in ambient air (0.015 μg/m^3) (Gentry et al., 2017) were also assumed to occur for the rest of the time period.

The currently available model code, which is in R, does not allow for time-specific exposure periods. Thus, the model was expanded to allow for specifically timed exposures, in this case 24-hour exposures once per month, to predict uptake and distribution in the body. Importantly, this includes accumulation in the target tissue of the brain related to neurotoxic effects from manganese exposure (i.e., globus pallidus). In addition to accounting for age, the model is also specific to sex, so exposure to human females and human males, ages birth to 65 years, were modeled.

3.2.1 PBPK Modeling Methods

The current PBPK human model for Mn were developed from previous models in rats and monkeys (Schroeter et al. 2011; Yoon et al. 2019). These models characterized the toxicokinetics of Mn in the body following exposure by ingestion and inhalation and predict the target tissue concentrations in selected regions of the brain. The models also incorporate direct transport of Mn to the brain via the olfactory nerve (Schroeter et al., 2011). The animal models were extended to humans using tracer studies for verification. The Schroeter et al. (2011) and Yoon et al. (2019) model has simulated the results from ^{54}Mn tracer kinetics from oral and inhalation exposures, and for multiple water-soluble manganese compounds. For inhalation, the model uses the Multiple-Path Particle Dosimetry Mode (MPPD model) to predict particle deposition in species-specific lung regions (Gentry et al., 2017).

We used the "lactation/infant" and the "child/adolescent/adult" model codes, as published most recently in Yoon et al. (2019), to estimate the manganese distribution in different sex and age groups. The full explanation of the human model is available in Schroeter et al. (2011) and Yoon et al. (2019) (Attachment D). The PBPK model accounts for dietary, drinking water, and inhalation exposure. The lactation/infant code simulates manganese kinetics in a lactating mother and a nursing child. It allows the simulation of manganese in a breast-fed and formula-fed infant for the first 6 months of life. Also, the code is applicable to simulate manganese distribution in children for the first three years of life. The child/ adolescent/adult model code is applicable to simulate child, adolescent, and adult human exposure scenarios. The child and adolescent scenarios can simulate an age-dependent increase in tissue volumes, blood flows, and respiratory parameters from age 3 to 18. However, for the adult female and male scenarios simulation (>18 years), the model uses standard parameters for each sex at constant body weight.

3.2.2 Tissue-Based NOAELs in the Brain (Globus Pallidus)

Two studies (Schroeter et al., 2012; Gentry et al., 2017) have evaluated the dose-response for neurological effects associated with Mn exposure using the model-predicted Mn concentrations in the globus pallidus (i.e., target tissue for manganese toxicity in the brain) (Attachment C). In doing so, these authors incorporate the non-linear and dose-dependent kinetics of manganese in humans due to homeostasis. In the first (Schroeter et al., 2012),

the dose response was evaluated in NHPs for time frames of a few months to 2 years, using a categorical regression model (USEPA CatReg) software and severity scores for several neurological observations. For the inhalation studies, the dose was adjusted for particle deposition and solubility (Schroeter et al., 2012), and the Dorman et al. (2006) study, which used the same experimental design as Dorman et al. (2005), required no bioavailability adjustment, because manganese was administered as freely soluble $MnSO_4$.

Schroeter et al. (2012) reported a steep dose-response curve starting at peak manganese concentrations of 7 µg/g globus pallidus for neurological effects. The CatReg-estimated Extra Risk Dose for 10% response (ERD10) for a severity score of 1 was a peak globus pallidus concentration of 0.8 µg/g. For this reason, the ERD10 for a severity score of 1 (0.8 µg/g) is considered the tissue-based NOAEL using NHP data.

Gentry et al. (2017) conducted a similar study using the Schroeter et al. (2011) manganese PBPK model and measures of neurological effects among workers. Gentry et al. (2017) used blood Mn data as a biomarker and predicted the target tissue NOAEL from all available human studies, including Roels et al. (1992). In this study, Gentry et al. (2017) had access to the individual-level data on exposure and outcome from several studies, and blood Mn data from two studies, including Roels et al. (1992). A no-statistical-significance-of-trend (NOSTASOT) test was used with Fisher's exact test to predict target tissue Mn concentrations at the NOAELs for abnormal eye-hand coordination of 0.7 µg/g, and 0.9 µg/g for the endpoint of abnormal hand steadiness.

Schroeter et al. (2012) and Gentry et al. (2017) (Attachment C) provide highly consistent tissue NOAELs or thresholds for adverse effects, ranging from 0.7 to 0.9 µg/g. Both studies also conclude that homeostatic control maintains tissue globus pallidus concentrations below these levels, for chronic inhalation exposures up to 10 $\mu g/m^3$. It is also noteworthy as discussed below, that the tissue-based NOAELs for Mn in the globus pallidus are not substantially different than model predictions for background levels of Mn based on diet and background Mn in ambient air.

3.2.3 Acute Inhalation Exposure Modeling Results

We ran two scenarios using the PBPK model. For the monthly scenario, exposures were assumed to occur at the 5 $\mu g/m^3$ proposed TRV for 24 hours per day, for one day per month. Because the SGC is said to be for exposures of "a few weeks," we also modeled a 3-week scenario, in which exposures occurred at the 5 $\mu g/m^3$ for 24-hours per day, consecutively for three weeks. In both scenarios, all other exposures (oral and inhalation of ambient air) were set to background levels (dietary intake and background ambient air of 0.015 $\mu g/m^3$).

In the monthly scenario, the maximum manganese concentrations in the globus pallidus, whole blood, and liver remain relatively consistent with background levels (Table 2). The results are presented by demographics (age group and sex). The highest concentration in the globus pallidus (0.538 µg/g) of manganese is predicted for male children (3–10 years of age). The second-most susceptible demographic is female children (3 to 10 years of age), with a model-estimated manganese concentration of 0.517 µg/g. These values are predicted

to occur around 3 years of age. The model predictions are only slightly above background and are well below the range of tissue-based NOAELs of 0.7 to 0.9 µg/g based on Schroeter et al. (2012) and Gentry et al. (2017). Thus, exposures to the proposed TRV for 24 hours per day, once per month, would not result in adverse neurotoxic effects.

Table 2. Summary results of the monthly exposure scenario (24-hours per day, once-per-month exposure to 5 µg/m^3)

Age Group	Manganese Concentration (µg/g)			
	Globus Pallidus		Whole Blood	Liver
	Model Predicted	Back-ground	Model Predicted	Model Predicted
0–0.5 years — Male neonate	0.368	0.363	0.024	1.129
0.5–1 years — Male infant	0.327	0.309	0.015	1.145
1–3 years — Male toddler	0.436	0.431	0.018	1.202
3–10 years — Male child	0.538	0.535	0.012	1.197
10–18 years — Male adolescent	0.476	0.466	0.008	1.195
>18 years — Male adult	0.391	0.386	0.005	1.196
0–0.5 years — Female neonate	0.368	0.363	0.024	1.130
0.5–1 years — Female infant	0.327	0.309	0.015	1.145
1–3 years — Female toddler	0.436	0.431	0.018	1.202
3–10 years — Female child	0.517	0.514	0.013	1.199
10–18 years — Female adolescent	0.436	0.429	0.007	1.195
>18 years — Female adult	0.347	0.345	0.005	1.195

Because the TRV is based on the SGC, we also evaluated a 3-week exposure scenario. Because the monthly scenario predicts the highest manganese levels in the globus pallidus at approximately 3 years of age (Table 2), we modeled the 3-week scenario at age three for both females and males. In the 3-week scenario, the maximum globus pallidus concentration was 0.521 µg/g for females and 0.552 µg/g for males, which only slightly exceeds background (Table 3). Whole-blood and total liver concentrations were similar to the monthly scenario. Consistent with the results for the monthly scenario, levels of manganese in the globus pallidus for the 3-week scenario are well below the tissue-based NOAELs (0.7–0.9 µg/g). Thus, the model predicts that exposure for three weeks at the proposed SGC of 5 µg/m^3 would also not result in adverse neurotoxic effects.

These model predictions are consistent with Schroeter et al. (2012) and Gentry et al. (2017) which both predict that homeostasis maintains manganese levels in the target tissue of the brain at airborne exposures less than 10 µg/m^3 for long-term continuous exposures. The

current modeling work is presented in Perry et al. (2022) and in preparation for publication in the peer-reviewed scientific literature.

Table 3. Summary table for the 3-week exposure scenario (daily inhalation exposure at 5 µg/m³ for three weeks)

Age Group	Manganese Concentration (µg/g)			
	Globus Pallidus		Whole-Blood	Liver
	Model Predicted	Background	Model Predicted	Model Predicted
3–10 years — Female child	0.521	0.514	0.012	1.20
3–10 years — Male child	0.552	0.535	0.012	1.20

4 Conclusion

The current TRV (and SGC) for acute manganese should be updated. The current TRV (and SGC) rely on chronic exposure levels provided by OEHHA, with an unsupported correction from chronic to subchronic exposures (reversing the subchronic-to-chronic extrapolation by OEHHA), and no provisions for subchronic to acute exposures. This is not consistent with relying on an "authoritative source." OHA itself explicitly advised against using chronic values for acute exposure TRVs, particularly when (as here) the endpoints are not the same. No authoritative source specified in OAR 340-247-0030 has set TRVs, or their equivalent, for acute manganese exposures. In fact, both ATSDR and OEHHA explicitly declined to because there was insufficient scientific support to do so. Beyond being derived by an unsupported method, ODEQ's current acute TRV for acute manganese exposure is excessively conservative, as evidenced by the fact that it is equal to ATSDR's chronic MRL.

We petition ODEQ to change the acute manganese TRV to 5 µg/m³. The proposed value is consistent with the 24-hour AMCV developed by TCEQ, which was developed after a thorough literature review and addressing public comments. The proposed value is conservative, because it is based on mild, reversible respiratory effects observed after repeated exposures for a total of 60 hours over three weeks to Mn in air at 1,500 µg/m³, as reported by Dorman et al. (2005). To this LOAEL, a 300-fold uncertainty factor is appropriate, resulting in the proposed TRV of 5 µg/m³.

ATSDR (2012) identifies endpoints of potential concern associated with manganese exposure as neurotoxicity, reproductive and developmental toxicity, and respiratory toxicity. The proposed TRV based on Dorman et al. (2005) is protective of respiratory toxicity. Further, the reproductive and developmental toxicity study by McGough and Jardine (2017) involving subchronic exposures in rats at levels much higher than the proposed TRV (up to 8.1 mg/m³ for up to 714 hours) did not result in reproductive or developmental toxicity, which reduces uncertainty associated with potential reproductive

or developmental effects. Additionally, Dorman et al. (2006) reported no observable symptoms of neurotoxicity associated with exposures in the 2005 study.

To further address any uncertainty as to whether neurotoxicity could pose a hazard to humans at the proposed TRV, we used the current human PBPK model to evaluate two exposure scenarios: reoccurring exposures for monthly 24-hour exposures (monthly scenario), and continuous exposure for 3 weeks at the age when manganese levels in brain are predicted to be highest (three week scenario). For both scenarios, the current human PBPK model was used to predict concentrations of manganese in blood, liver, and globus pallidus in males and females. The model predictions indicate that, at all life stages, the levels of manganese in the target tissue of the globus pallidus do not increase significantly over background levels and are lower than tissue NOAELs in the globus pallidus.

The proposed TRV of 5 $\mu g/m^3$ should be adopted by ODEQ, for these primary reasons:

- The current value is not based on authoritative sources.
- The proposed value is based on appropriate, peer-reviewed science that targets a relevant endpoint (respiratory system) for acute exposures.
- Other potential adverse effects related to manganese exposure (neurotoxic and reproductive/developmental) are not observed in peer-reviewed studies of exposures at this level.
- Applying the peer-reviewed PBPK model demonstrates that exposures at the proposed TRV would not result in accumulation in the brain that could result in neurotoxic effects.
- The proposed TRV has been established for 24-hour exposure by another state (Texas).

5. Supporting Information for Proposed Acute TRV for Mn

The following supporting documents are provided as attachments to this petition.

- Attachment A Dorman et al. (2005)
- Attachment B Summary of Relevant Toxicity Studies
- Attachment C Schroeter et al. (2012) and Gentry et al. (2017)
- Attachment D Schroeter et al. (2011), Yoon et al. (2019), Campbell et al. (2022)

6. References

ATSDR (Agency for Toxic Substances Disease Registry). 2012. Toxicological profile for Manganese. September.

Campbell J., Clewell, H, Gentry, R, et al. 2022. Incorporation of rapid association/dissociation processes in tissues into the monkey and human physiologically based pharmacokinetic models for manganese. Society of Toxicology Annual Meeting. San Diego, CA. Abstract 4035. Poster Board P734.

Dorman DC, et al. 2005. Sub-chronic inhalation of high concentrations of manganese sulfate induces lower airway pathology in rhesus monkeys. Respir Res 6:121.

Dorman DC, et al. 2006. Correlation of brain magnetic resonance imaging changes with pallidal manganese concentrations in Rhesus monkeys following subchronic manganese inhalation. Toxicol. Sciences. 92(1) 219-227.

Erikson KM. 2005. Persistent alterations in biomarkers of oxidative stress resulting from combined *in utero* and neonatal manganese inhalation. Biol Trace Element Res 14:151–163.

Gentry PR, et al. 2017. A tissue dose-based comparative exposure assessment of manganese using physiologically based pharmacokinetic modeling — The importance of homeostatic control for an essential metal. Toxicol Appl Pharm 322:27–40.

HaMai D, et al. 2006. Decreased expression of inflammation-related genes following inhalation exposure to manganese. NeuroToxicology 27:395–401.

McGough D, Jardine L. 2017. A two-generation inhalation reproductive toxicity study upon the exposure to manganese chloride. NeuroToxicology 58:194–202.

OEHHA (Office of Environmental Health Hazard Assessment). 2008a. Technical support document for the derivation of noncancer reference exposure levels. June 18.

OEHHA (Office of Environmental Health Hazard Assessment). 2008b. Technical support document for reference exposure levels (RELs). Appendix D. Individual acute, 8-hour, chronic reference exposure levels. Updated July 2014.

Perry, C., Vivanco, S., Antonijevic, T., Verwiel, A., Proctor, D. 2022. Short-Term Environmental Inhalation Toxicity Criteria for Airborne Manganese Protective of Neurological and Respiratory Effects for use in Air Toxics Risk Assessment (Platform Session). Society of Environmental Toxicology and Chemistry North America. 43rd annual meeting. Pittsburgh, PA. November.

Roels HA, et al. 1992. Assessment of the permissible exposure level to manganese in workers exposed to manganese dioxide dust. Brit J Ind Med 49:25–34.

Sapputra D, et al. 2016. Short-term manganese inhalation decreases brain dopamine transporter levels without disrupting motor skills in rats. J Toxicol Sci 41(3):391–402.

Schroeter J, Nong A, Yoon M, et al. 2011. Analysis of manganese tracer kinetics and target tissue dosimetry in monkeys and humans with multi-route physiologically based pharmacokinetic models. Toxicol Sci 120(2):481–498.

Taylor et al., 2006. Effects of inhaled manganese on biomarkers of oxidative stress in the rat brain. Neurotoxicology 27:788–797.

TCEQ (Texas Commission on Environmental Quality). 2015. TCEQ guidelines to develop toxicity factors. Toxicology Division. Revised September 2015.

TCEQ (Texas Commission on Environmental Quality). 2017. Manganese and Inorganic Manganese Compounds, Development Support Document, Final. November 29.

U.S. EPA (U.S. Environmental Protection Agency). 2012. Benchmark dose technical guidance. EPA/100/R-12/001. June.

Yoon, et al. 2019. Assessing children's exposure to manganese in drinking water using a PBPK model. Toxicol Appl Pharm 380:114695.

ATTACHMENT A

Dorman et al. (2005)

Respiratory Research

BioMed Central

Research

Open Access

Sub-chronic inhalation of high concentrations of manganese sulfate induces lower airway pathology in rhesus monkeys

David C Dorman*[1], Melanie F Struve[1], Elizabeth A Gross[1], Brian A Wong[1] and Paul C Howroyd[2]

Address: [1]CIIT Centers for Health Research, 6 Davis Drive, P.O. Box 12137, Research Triangle Park, NC 27709-2137, USA and [2]Experimental Pathology Laboratories, Inc., P.O. Box 12766, Research Triangle Park, NC 27709, USA

Email: David C Dorman* - dorman@ciit.org; Melanie F Struve - struve@ciit.org; Elizabeth A Gross - gross@ciit.org; Brian A Wong - wong@ciit.org; Paul C Howroyd - paul.howroyd@bms.com

* Corresponding author

Published: 21 October 2005

Respiratory Research 2005, **6**:121 doi:10.1186/1465-9921-6-121

Received: 30 March 2005
Accepted: 21 October 2005

This article is available from: http://respiratory-research.com/content/6/1/121

Abstract

Background: Neurotoxicity and pulmonary dysfunction are well-recognized problems associated with prolonged human exposure to high concentrations of airborne manganese. Surprisingly, histological characterization of pulmonary responses induced by manganese remains incomplete. The primary objective of this study was to characterize histologic changes in the monkey respiratory tract following manganese inhalation.

Methods: Subchronic (6 hr/day, 5 days/week) inhalation exposure of young male rhesus monkeys to manganese sulfate was performed. One cohort of monkeys (n = 4–6 animals/exposure concentration) was exposed to air or manganese sulfate at 0.06, 0.3, or 1.5 mg Mn/m^3 for 65 exposure days. Another eight monkeys were exposed to manganese sulfate at 1.5 mg Mn/m^3 for 65 exposure days and held for 45 or 90 days before evaluation. A second cohort (n = 4 monkeys per time point) was exposed to manganese sulfate at 1.5 mg Mn/m^3 and evaluated after 15 or 33 exposure days. Evaluations included measurement of lung manganese concentrations and evaluation of respiratory histologic changes. Tissue manganese concentrations were compared for the exposure and control groups by tests for homogeneity of variance, analysis of variance, followed by Dunnett's multiple comparison. Histopathological findings were evaluated using a Pearson's Chi-Square test.

Results: Animals exposed to manganese sulfate at ≥0.3 mg Mn/m^3 for 65 days had increased lung manganese concentrations. Exposure to manganese sulfate at 1.5 mg Mn/m^3 for ≥15 exposure days resulted in increased lung manganese concentrations, mild subacute bronchiolitis, alveolar duct inflammation, and proliferation of bronchus-associated lymphoid tissue. Bronchiolitis and alveolar duct inflammatory changes were absent 45 days post-exposure, suggesting that these lesions are reversible upon cessation of subchronic high-dose manganese exposure.

Conclusion: High-dose subchronic manganese sulfate inhalation is associated with increased lung manganese concentrations and small airway inflammatory changes in the absence of observable clinical signs. Subchronic exposure to manganese sulfate at exposure concentrations (≤0.3 mg Mn/m^3) similar to the current 8-hr occupational threshold limit value established for inhaled manganese was not associated with pulmonary pathology.

Background

There is growing evidence to suggest that a wide variety of respirable particles can induce lung injury under certain exposure conditions. Clinical recognition of this hazard originally stemmed from occupational studies examining workplace exposure to metals, asbestos, silica, coal, and other biologically active particles [1,2]. However, particulate-induced lung injury is not confined to the workplace. There is strong epidemiologic evidence for significant associations between respiratory morbidity, including exacerbations of asthma and mortality, with exposure to relatively low ambient particulate matter concentrations [3,4]. This association has contributed to the adoption of more stringent ambient air quality standards for respirable particulate matter by the United States Environmental Protection Agency and other health organizations.

Particulate matter is not a single entity but rather a mixture of many subclasses of pollutants including metals, sulfate, acids, ammonium, nitrate, organic compounds, and minerals. Depending on emission source, metals may represent a significant proportion of a particulate matter sample [5]. Soluble metals have been implicated in particulate matter-associated cardiopulmonary disease in healthy and compromised individuals [6-8]. One metal found in ambient air is manganese. Airborne manganese sources include wind erosion of dusts and soils, anthropogenic fugitive dusts, and emissions from automobiles, power plants, coke ovens, municipal waste incinerators, and metal smelting operations [5]. Ambient air manganese concentrations are typically quite low, ranging between 5 and 33 ng Mn/m^3 [9]. Significant occupational manganese exposure (≥0.2 mg Mn/m^3) can occur in some workers involved in ferroalloy production, iron and steel foundries, and welding [9].

Workers exposed to high atmospheric manganese concentrations frequently demonstrate an increased incidence of cough and other signs associated with bronchitis [10,11]. Acute inhalation of air with extremely high manganese concentrations (≥1 mg Mn/m^3) can result in pneumonitis [12]. Although manganese-induced pneumonitis has been recognized since the mid-1940's, histological characterization of the pulmonary response remains incomplete. Most experimental exposures in laboratory animals have shown only minor lung pathology despite the administration of high doses of manganese oxides by intratracheal instillation or inhalation [13-18]. Far less is known about the potential respiratory effects induced by exposure to other inorganic forms of manganese. Manganese chloride instillation into rabbits failed to induce significant pulmonary pathology [19]. Dorman et al. [20] showed that subchronic exposure of rats to manganese sulfate ($MnSO_4$) was associated with rhinitis in the anterior part of the nose. To our knowledge, histologic assessment of pulmonary changes occurring in association with subchronic inhalation of $MnSO_4$ has not been performed and is the subject of our study. Herein, we report that subchronic high-dose inhalation exposure of nonhuman primates to $MnSO_4$ resulted in mild subacute bronchiolitis, alveolar duct inflammation, and proliferation of bronchus-associated lymphoid tissue (BALT), in the absence of rhinitis or other forms of nasal pathology.

Methods

Chemicals

Manganese (II) sulfate monohydrate ($MnSO_4 \cdot H_2O$) was obtained from Aldrich Chemical Company, Inc. (Milwaukee, WI).

Animals

This study was conducted under federal guidelines for the care and use of laboratory animals [21] and was approved by the CIIT Centers for Health Research (CIIT) Institutional Animal Care and Use Committee. Additional endpoints evaluated in this study, but not presented in the present manuscript, included determination of manganese concentrations in additional tissues and magnetic resonance imaging (MRI) of the brain. We chose to use rhesus monkeys since they are extensively used in toxicology studies, manganese-exposed monkeys develop distribution patterns for this metal within the brain that mimic those seen in heavily exposed people [22], and there are anatomically-based simulation models for air flow in the macaque upper and lower respiratory tracts [23,24]. Thirty-six male rhesus monkeys purchased from Covance Research Products, Inc. (Alice, TX) were used in this study. Monkeys were 17 to 22 months old at the time of their arrival at CIIT. Animals were screened for the nasal parasite *Anatrichosoma spp*. herpes B, simian immunodeficiency virus, simian respiratory virus, pulmonary acariasis, and tuberculosis, and were subjected to a thorough clinical examination including an evaluation of pre-exposure blood samples for routine hematology and clinical chemistry. The results of these evaluations were within normal limits.

Assignment of animals to treatment cohorts considered the age of the animal. Assignment occurred so that the animals were between 20 and 24 months of age at the start of the inhalation exposure. Randomization of animals to treatment groups occurred prior to the start of the inhalation exposure and was based upon a weight randomization procedure. Animals were acclimated to the facility for at least 43 days prior to the start of the first inhalation exposure. Additional endpoints evaluated in this study, but not presented in the present manuscript, included magnetic resonance imaging (MRI) of the brain, post-exposure clinical chemistry and hematological evaluations, and determination of tissue manganese

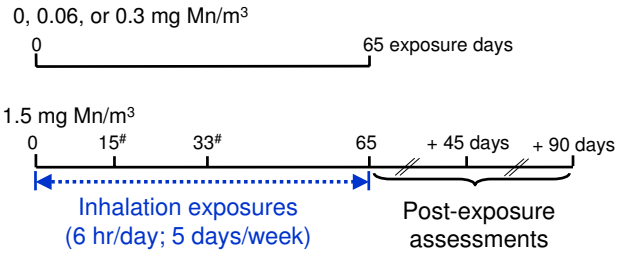

Figure 1
Experimental design overview. Group size equals 4 monkeys per exposure group, with the exception of the 0 and 0.06 mg Mn/m³ exposure groups (n = 6 monkeys/exposure concentration). Lung manganese concentrations and respiratory histologic changes were evaluated after 15, 33, or 65 exposure days or 45 or 90 days after the 65th exposure day. #Denotes animals assigned to cohort 2.

concentrations in the central nervous system and other organs.

Animal Husbandry

Animal rooms were maintained at daily temperatures of 22 ± 4°C, relative humidity of 30–70%, and an air flow rate sufficient to provide 10–15 air changes per hour. Lighting was controlled by automatic controls (lights on approximately 0600–1800). All exposures were conducted during the animal's light cycle (approximately from 0800 to 1400). All animals were housed in animal rooms or exposure chambers within CIIT's animal facility. This facility is accredited by the Association for Assessment and Accreditation of Laboratory Animal Care, International. A certified primate chow (# 5048) diet from Purina Mills (St. Louis, MO) was fed twice-a-day (total daily amount fed was approximately 4% of the animal's body weight). Dietary supplements were also used as part of CIIT's nonhuman primate enrichment program. These supplements included fruits (e.g., oranges, raisins, apples), vegetables (e.g., carrots), and treats (e.g., honey, candies, cereal, fruit juices) purchased from a local grocery store. Reverse osmosis purified water was available *ad libitum*. During non-exposure periods, domiciliary stainless steel cages (0.4 m^2 × 0.8 m tall) suitable for housing macaque monkeys (Lab Products, Inc.; Seaford, DE) were used to individually house monkeys. On each exposure day, animals were transferred to 0.2 m^2 × 0.6 m tall stainless steel cages (Lab Products, Inc.; Seaford, DE) that were designed to fit within the 8-m^3 inhalation chambers. Animals were moved back to their domiciliary cages after the end of each 6-hr exposure.

Manganese Exposures

$MnSO_4$ aerosol concentrations of 0.18, 0.92, and 4.62 mg $MnSO_4/m^3$, corresponding to 0.06, 0.3, and 1.5 mg Mn/m^3, were generated for this study. Control animals were exposed to filtered air. Animal exposures were conducted as described in Figure 1. Four 8-m^3 stainless steel and glass inhalation exposure chambers with glass doors and windows for animal observation were used. Animal position within the inhalation chambers was rotated weekly to minimize the impact of any undetected differences in the environment or in the $MnSO_4$ exposure concentrations. Air flow through the 8-m^3 inhalation chamber was typically maintained at a rate sufficient to provide at least 12 air changes per hour. Airflow through each chamber was monitored continuously during each exposure and recorded every 30 minutes. Temperature and relative humidity inside each inhalation chamber were recorded every 30 minutes during each 6-hr exposure. The average chamber temperature and relative humidity during the 6-hr exposure period were maintained at 18–26°C and 50 ± 20%, respectively. Methods describing the generation of the $MnSO_4$ atmosphere with a dry powder generator (Wright Dust Feeder, Model WDF-II, BGI, Inc., Waltham, MA) and the characterization of the subsequent aerosol have been previously described [25]. $MnSO_4$ was packed in separate dry powder generator cups at pressures between 2000 and 3000 psi (Model 3912, Carver Inc., Wabash, IN) using a hydraulic press (Model C, Carver Inc., Menomonee Falls, WI).

Necropsy Procedures

Necropsies were performed the day following the last inhalation exposure (i.e., 12–18 hr after termination of the final inhalation exposure). Food was withheld overnight prior to necropsy. Monkeys were anesthetized with ketamine (20 mg/kg, IM, Fort Dodge Animal Health, Fort Dodge, IA) and euthanized with pentobarbital (80–150 mg/kg, IV, Henry Schein Inc., Port Washington, NY) followed by exsanguination. Following euthanasia, the lungs and other thoracic organs were removed, weighed, and inspected for gross lesions. The left primary bronchus was ligated and the left lung separated for determination of tissue manganese concentration. The right lung and trachea were then inflated with 10% neutral-buffered formalin using 30-cm of hydrostatic pressure [26]. The olfactory epithelium was excised for chemical analysis and the remaining nasal tissues, including the nasopharynx and larynx, were stored in 10% neutral-buffered formalin. The larynx samples were decalcified in 10% formic acid (Fisher Scientific International, Inc., Hampton, NH) for two days. Cranial tissues were decalcified in RDO® (Apex Engineering Products Corporation, Plainfield, IL) for up to 6 days. Following decalcification, tissues were washed in running tap water for at least 6 hr. Following fixation (and decalcification when appropriate), representative

Table 1: Characteristics of manganese aerosols generated for whole-body exposures in this study (means ± SD)

	Nominal $MnSO_4$ exposure concentration (mg/m^3)			
	0.18	0.92	4.62[a]	4.62[b]
Actual exposure concentration (mg $MnSO_4/m^3$)[c]	0.19 ± 0.01	0.97 ± 0.06	4.55 ± 0.33	4.45 ± 0.35
Geometric mean diameter (μm)[d]	1.04	1.07	1.12	1.04
Geometric standard deviation (σ_g)[d]	1.51	1.54	1.58	1.50
Mass median aerodynamic diameter (μm)[e]	1.73	1.89	2.12	1.72

[a] Cohort 1
[b] Cohort 2
[c] Based on continuous chamber monitoring with a calibrated optical particle sensor (Real-Time Aerosol Sensors, Model RAM-S, MIE, Inc., Billerica, MA).
[d] Based on biweekly aerodynamic particle size spectrometry (Aerodynamic Particle Sizer, Model 3320, TSI, Inc., St. Paul, MN) measurements.
[e] Calculated value [56]

samples of the lung, trachea, larynx, oropharynx, tracheobronchial lymph nodes, and nose were collected from each animal. Tissue samples were trimmed, embedded in paraffin, and five-μm thick sections were cut and stained with hematoxylin and eosin for light microscopic evaluation. Histologic specimens were examined by an experienced veterinary pathologist (Howroyd).

Tissue manganese concentrations

Tissue samples collected for chemical analyses were stored in individual plastic containers, frozen in liquid nitrogen, and stored at approximately -80°C until chemical analyses were performed. Lung and olfactory epithelium manganese concentrations were determined by graphite furnace atomic absorption spectrometry using previously published methods [27].

Statistics

Tissue manganese concentrations were compared for the exposure and control groups by tests for homogeneity of variance (Levene's test), analysis of variance (ANOVA), and Dunnett's multiple comparison procedure for significant ANOVA. Histopathological findings were evaluated using a Chi-Square test. Statistical analyses were performed using SAS Statistical Software. A probability value of <0.01 was used for Levene's test, while <0.05 was used as the critical level of significance for all other statistical tests. Unless otherwise noted, data presented are mean values ± standard error of the mean (SEM).

Results

Test atmospheres

No significant differences in the test aerosol characteristics were observed between the two exposure cohorts (Table 1). Particles of unknown composition (arising from animal dander and other background sources) were present in the control chamber at an overall average concentration ± standard deviation (SD) of 0.004 ± 0.002 mg/m^3. The calculated mass median aerodynamic diameter (MMAD) for the particles in the control chamber was 3.9 μm.

Lung and olfactory epithelium manganese concentrations following $MnSO_4$ exposure

Lung and olfactory epithelium manganese concentrations are presented in Table 2. Animals exposed to $MnSO_4$ at ≥0.3 mg Mn/m^3 for 65 exposure days developed increased lung manganese concentrations. Animals exposed to $MnSO_4$ at ≥0.06 mg Mn/m^3 for 65 exposure days developed increased olfactory epithelium manganese concentrations. Increased lung and olfactory epithelium manganese concentrations developed within three weeks of exposure to $MnSO_4$ at 1.5 mg Mn/m^3. Within 45 days after completion of the 65-day inhalation exposure to $MnSO_4$ at 1.5 mg Mn/m^3 regimen, lung and olfactory epithelium manganese concentrations were not different from those seen in air-exposed controls.

Respiratory tract pathology following $MnSO_4$ exposure

Manganese exposure did not affect absolute or relative lung weights and did not result in coughing, dyspnea, or other respiratory signs (data not shown). High-dose exposure to $MnSO_4$ was associated with an increased incidence of minimal to mild subacute bronchiolitis (Table 3). These lesions consisted of infiltrates of lymphocytes, along with neutrophils and occasional eosinophils, primarily surrounding the terminal and respiratory bronchioles and/or alveolar ducts, but sometimes extending into the lamina propria (Figure 2). Macrophages with moderate amounts of pale-staining cytoplasm were occasionally observed in the adjacent airway lumen. Although the overlying epithelium generally appeared intact, because it is normally very thin at the level of the distal airways, it is difficult to confirm that epithelial integrity was unaffected. These changes appeared to be reversible upon cessation of $MnSO_4$ exposure. An increased incidence of enhanced proliferation of BALT in association with

Table 2: Olfactory epithelial and lung manganese concentrations in young monkeys following exposure to air or $MnSO_4$. Manganese concentrations were determined by graphite furnace atomic absorption spectrometry and are expressed as mean ± SEM μg Mn/g tissue wet weight. Young male rhesus monkeys (n = 4 except where noted) were exposed to either air or $MnSO_4$ 6 hours/day, 5 days/ week.

Tissue	$MnSO_4$ exposure concentration (mg Mn/m^3)	15	33	Exposure Day 65	65 [+45][a]	65 [+90][a]
Olfactory epithelium	0			0.42 ± 0.01[b]		
	0.06			1.22 ± 0.15*[b]		
	0.3			2.96 ± 0.46*		
	1.5	6.10 ± 0.39*	7.34 ± 0.70*	7.10 ± 2.01*	0.65 ± 0.04	0.69 ± 0.11
Lung	0			0.15 ± 0.03[b]		
	0.06			0.18 ± 0.01[b]		
	0.3			0.25 ± 0.02*		
	1.5	0.39 ± 0.06*	0.35 ± 0.02*	0.33 ± 0.04*	0.09 ± 0.01	0.06 ± 0.01

[a] Number in brackets indicates number of days post exposure assessment.
[b] n = 6.
* $p < 0.05$

Table 3: Incidence of $MnSO_4$-induced microscopic lesions observed in young male rhesus monkeys exposed to $MnSO_4$. Incidence is expressed as number affected/number examined.

Lesion	$MnSO_4$ exposure concentration (mg Mn/m^3)	15	33	Exposure Day 65	65 [+45][a]	65 [+90][a]
Subacute bronchiolitis/alveolar duct inflammation	0			0/6		
	0.06			0/6		
	0.3			1/4[b]		
	1.5	3/4*	4/4*	3/4*	0/4	1/4
Increased bronchus associated lymphoid tissue	0			0/6		
	0.06			0/6		
	0.3			1/4		
	1.5	2/4†	3/4*	1/4	2/4†	1/4

[a] Number in brackets indicates number of days post exposure assessment
[b] Subacute bronchiolitis was observed in one monkey; however, in this animal only, this lesion was observed in conjunction with aspirated food particles.
* $p < 0.05$ (Pearson's chi-square test)
† $p = 0.053$ (Pearson's chi-square test)

smaller (≤500 μm) airways also occurred in monkeys exposed to the highest $MnSO_4$ concentration (1.5 mg Mn/m^3) (Figure 3). Some BALT foci included germinal center formation. The incidence of increased BALT was highest in monkeys exposed to 1.5 mg $Mn/m^3$for 33 exposure days (Table 3) suggesting that BALT proliferation may subside even in the face of ongoing manganese exposure. Proliferation of BALT occurred in one animal exposed to $MnSO_4$ at 0.3 mg Mn/m^3; however, this increase was only minimal and was not statistically significant.

Several of the $MnSO_4$-exposed animals had minimal acute alveolitis. However, this finding was considered unlikely to be treatment-related since no statistically significant dose-response relationship was observed. Minimal changes consistent with chronic bronchiolitis were

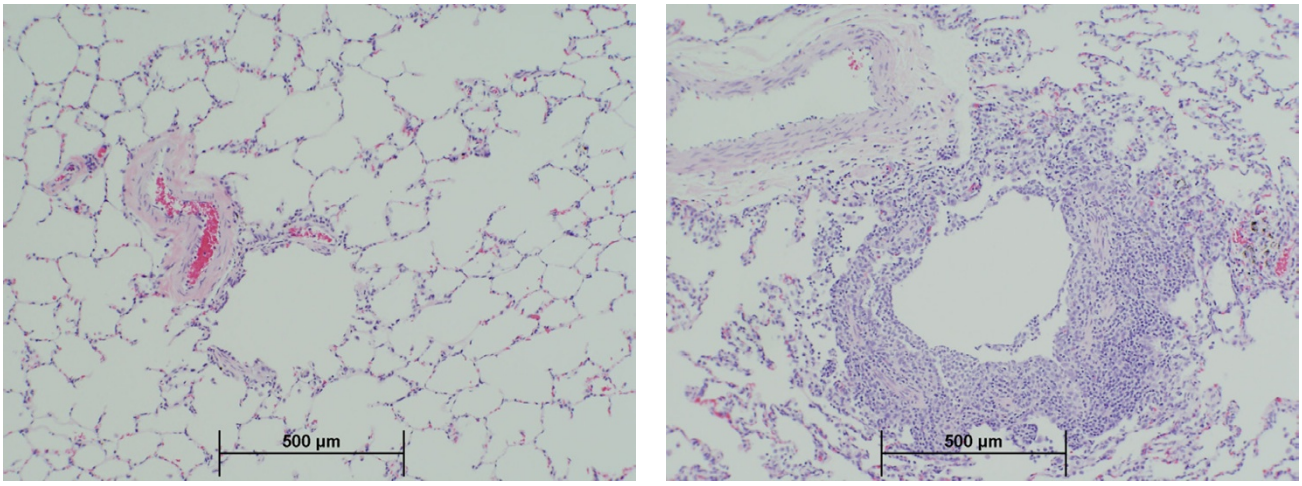

Figure 2
Bronchiolitis. Moderate subacute bronchiolitis in a monkey exposed to the highest (1.5 mg Mn/m^3) $MnSO_4$ exposure concentration for 15 exposure days (right). Normal appearing bronchioles present in an air-exposed control monkey (left). (10×)

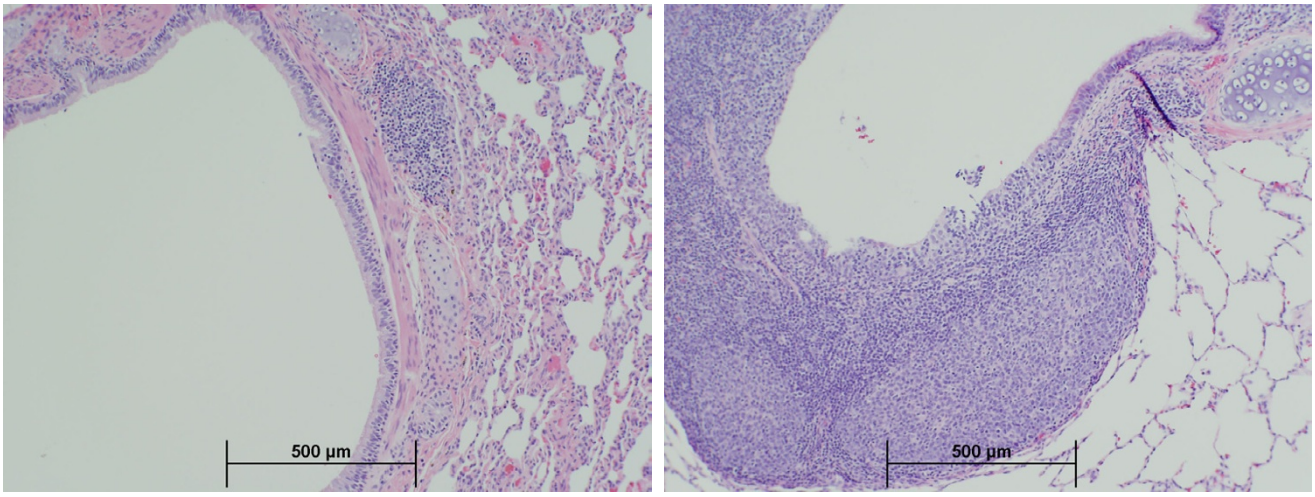

Figure 3
BALT proliferation. Peribronchial BALT proliferation in a monkey exposed to the highest (1.5 mg Mn/m^3) $MnSO_4$ exposure concentration for 65 exposure days (right). Normal appearing BALT present in an air-exposed control monkey (left). (4×)

observed in several control as well as $MnSO_4$-exposed animals. As such, these changes were not considered to be treatment-related. The majority of lung sections examined, including those taken from controls, had scattered deposits of brown-green pigment in the interstitial tissue. Such chronic bronchiolitic changes characterized by lung pigment deposits are commonly seen in monkeys with lung mites [28,29]. The most common lung mite is *Pneumonyssus simicola* and this agent occurs with nearly 100% incidence in rhesus monkeys [28,29]. Animals used on this study were treated with ivermectin prior to use; thus it is unlikely that superimposed active mite infection occurred. This conclusion is further supported by the absence of microscopic evidence of mites.

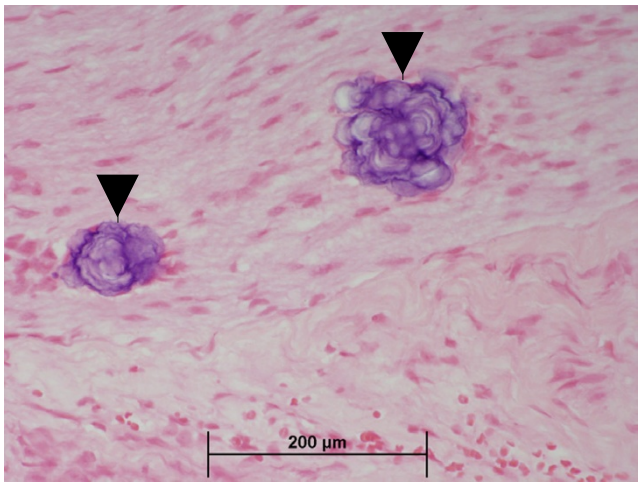

Figure 4
Basophilic foci in nerves. Basophilic foci (arrow) in nerves of olfactory mucosa from a monkey exposed to $MnSO_4$ at 0.06 mg Mn/m³, for 65 days (40×).

One animal from each of the 0.06 and 1.5 mg Mn/m³ exposure groups had minimal or mild, basophilic foci in the nerves of the nose. The spherical basophilic foci were approximately 40 µm in diameter and consisted of concentric lamellae (Figure 4). The foci were Periodic acid-Schiff stain positive but failed to stain with alizarin red, von Kossa's, or Perl's stains (for calcium or iron) and were not birefringent in polarized light (data not shown). Similar foci were present in the nasal epithelium of three other animals, including one control animal. Thus, it is unlikely that these foci were induced by $MnSO_4$ exposure. X-ray microanalysis of foci taken from the decalcified nasal epithelium of a single monkey from the 1.5 mg Mn/m³ exposure group showed the presence of sulfur but no other ions (data not shown). Thus, the basophilic foci noted in the nasal nerves were most likely glycoproteinaceous inclusion bodies (i.e., corpora amylacea) or psammoma bodies. Similar deposits have been observed in the olfactory nerves of untreated rhesus monkeys and rats (Howroyd, unpublished observations), in the olfactory tracts of humans [30], and in the brains of mice [31] and monkeys [32,33].

Discussion

Pulmonary inflammation is a common response to the inhalation of various types of particles including manganese [34]. In the present study, monkeys exposed to the highest $MnSO_4$ concentration (1.5 mg Mn/m³) developed subacute bronchiolitis and proliferation of BALT. Bronchiolitis included an infiltrate of acute inflammatory cells (neutrophils) in the peribronchiolar connective tissues in the centriacinar region. These lesions developed relatively rapidly as they were observed in monkeys exposed to $MnSO_4$ for only 15 exposure days. However, with ongoing $MnSO_4$ exposure, the bronchiolitic lesion progressed, affecting a larger percentage of respiratory bronchioles examined. Bronchiolitis resolved rapidly after cessation of $MnSO_4$ exposure and was absent 45 days after the end of the 13 week exposure to $MnSO_4$ at 1.5 mg Mn/m³.

Monkeys and human beings share similar lung anatomy [35], and their respiratory bronchioles and other small airways have similar sensitivity to inhaled toxicants such as cigarette smoke, coal dust, and ozone [36-38].

Following bronchiolitis, people are often noted to have increased wheeze, cough, and asthma, increased airway responsiveness, and reduced lung function due primarily to airflow obstruction [39]. In the present study, signs referable to the respiratory system were not recognized in the monkeys developing manganese-induced bronchiolitis. Although pulmonary function was not assessed in our study, reduced forced expiratory volume in one second ($FEV_{1)}$ and forced vital capacity (FVC) have been reported in workers that have been chronically exposed to high levels of manganese dust [10,40].

Particles deposited in the lung can be retained in the lung interstitium [41] or cleared via the mucociliary apparatus or through the lymphatic system [42]. Alternatively, particles may be transported from the lung via alveolar macrophages or neutrophils with subsequent accumulation in the BALT and tracheobronchial lymph node [42,43]. Thus, as a lymphoepithelial organ, the BALT is critical to the immune defense of the lung and to alveolar clearance of particles and lung pathogens. Proliferation of BALT has been observed in rodents following inhalation exposure to carbon black and silica [44,45]. There is evidence that BALT proliferation occurs in humans with panbronchiolitis, chronic hypersensitivity pneumonitis, and other chronic inflammatory airway disease [46,47]. Proliferative BALT lesions observed in these disease conditions are comparable to those observed in the $MnSO_4$-exposed monkeys, suggesting that BALT proliferation in the manganese-exposed monkeys may be related to the local airway immune response secondary to inflammation induced by $MnSO_4$.

Some agents that target the lung may also affect the upper airways as well. Our laboratory has recently reported that rats exposed subchronically to $MnSO_4$ (at 0.5 mg Mn/m³) develop a mild reversible inflammatory change consisting of pleocellular inflammatory infiltrates and fibrinonecrotic debris within the nasal respiratory epithelium [20]. These lesions occurred primarily in high airflow

regions and were consistent with mild irritation. In the present study, however, despite a 15-fold increase in nasal epithelial manganese concentrations, we did not observe any chemical-related nasal pathology in monkeys exposed to $MnSO_4$. Although nasal pathology did not occur, the fate of the manganese that is initially deposited in the nose and subsequently absorbed by the olfactory epithelium remains toxicologically important. Experiments from our laboratory have shown that manganese deposited on the olfactory epithelium can undergo transport along the olfactory nerve with subsequent delivery to the olfactory bulb [48].

Our interest in $MnSO_4$ stems from the use of manganese in the gasoline fuel additive methylcyclopentadienyl manganese tricarbonyl (MMT). Automobiles that use MMT in the fuel and are equipped with catalytic converters emit manganese primarily in the phosphate and sulfate forms with smaller amounts of manganese oxides also being discharged [49]. The manganese exposure concentrations used in this study bracket several human exposure scenarios. Prolonged human exposure to the highest $MnSO_4$ concentration used in this study (1.5 mg Mn/m^3) can occur among manganese miners and prolonged exposure is associated with frank neurotoxicity and respiratory disease [9]. Our mid-dose exposure concentration is analogous to the current 8-hr Threshold Limit Value (TLV) for inhaled manganese of 0.2 mg Mn/m^3 that has been established by the American Conference of Governmental Industrial Hygienists (ACGIH). Our lowest exposure concentration (0.06 mg Mn/m^3) is > 2,000-fold higher than typical air manganese concentrations observed in the ambient air including Canadian cities where MMT is extensively used in gasoline [9,50]. In the present study, exposure concentrations associated with increased lung manganese concentrations and lung pathology were respectively 1.5-and 7.5-fold higher than the current TLV.

The $MnSO_4$ particle size used in this study had an MMAD of 1.72 to 2.12 μm. Aerodynamic size is an important factor that influences particle deposition [51]. Several models based on airway geometry have been developed to describe particle deposition patterns in humans, monkeys, and rats [52,53]. The model of Asgharian and coworkers (1995) predicts a pulmonary deposition efficiency of an aerosol with a particle size of 1.5 μm of approximately 35% for humans and rhesus monkeys while the rat had much lower deposition efficiency (6%) due to higher nasal uptake [52]. The rate of particle clearance from the alveolar region also differs among species. Rodents clear particles from the lung more quickly than either monkeys or humans [54]. Anatomical differences between rodents and primates also affect particle deposition, retention, and clearance. Rodents lack respiratory bronchioles and have simple acini. Macaque monkeys and humans have larger alveoli and alveolar ducts than rats [55] and have similar numbers of respiratory bronchiole generations between the terminal bronchiole and the alveolar duct [35,56]. Our results may be especially important for human risk assessment owing to the fact that monkeys and human beings share similar lung anatomy (i.e., both species have extensive respiratory bronchioles comprised of bronchiolar epithelium and gas exchange epithelium) [35].

Conclusion

High-dose subchronic manganese sulfate inhalation is associated with increased lung manganese concentrations, mild subacute bronchiolitis, alveolar duct inflammation, and proliferation of bronchus-associated lymphoid tissue. Bronchiolitis and alveolar duct inflammatory changes were absent 45 days post-exposure, suggesting that these lesions are reversible upon cessation of subchronic high-dose manganese exposure. These small airway changes occurred in the absence of observable clinical signs. Subchronic exposure to manganese sulfate at exposure concentrations (≤0.3 mg Mn/m^3) similar to the current 8-hr occupational threshold limit value established for inhaled manganese was not associated with pulmonary or nasal pathology.

Competing interests

This publication is based on a study sponsored and funded by Afton Chemical Corporation in satisfaction of registration requirements arising under Section 211(a) and (b) of the Clean Air Act and corresponding regulations at 40 C. F. R. Subsections 79.50 *et seq*.

Authors' contributions

DCD conceived of the study, was the principal investigator and participated in all phases of the study, and drafted the manuscript. MFS participated in the design, coordination, and conduct of the study. EAG participated in and supervised the necropsy and preparation of histology specimens. BAW designed the exposure generation system and characterization of the aerosol. PCH was the study pathologist and conducted the histopathological evaluation of tissues. All authors contributed to, read, and approved the final manuscript.

Acknowledgements

The authors would like to thank Marianne Marshall, Carl Parkinson, Paul Ross and the staff of the CIIT animal care facility for their contributions. We also thank Drs. Jamie Bonner, Jan Dye, Jeff Everitt, Owen Moss, and Elizabeth Roberts for their critical review of this manuscript.

References

1. De Vuyst P, Camus P: **The past and present of pneumoconioses.** *Curr Opin Pulm Med* 2000, **6:**151-156.
2. Kelleher P, Pacheco K, Newman LS: **Inorganic dust pneumonias: the metal-related parenchymal disorders.** *Environ Health Perspect* 2000, **108(Suppl 4):**685-696.

3. Pope CA 3rd: **What do epidemiologic findings tell us about health effects of environmental aerosols?** *J Aerosol Med* 2000, **13:**335-354.
4. Schwartz J: **Air pollution and daily mortality: a review and meta analysis.** *Environ Res* 1994, **64:**36-52.
5. United States Environmental Protection Agency(U.S. EPA): *Air Quality Criteria for Particulate Matter. EPA/600/P-95/001 Volume 2*. Washington DC: Office of Research and Development; 1996.
6. Chapman RS, Watkinson WP, Dreher KL, Costa DL: **Ambient particulate matter and respiratory and cardiovascular illness in adults: particle-borne transition metals and the heart-lung axis.** *Environ Toxicol Pharmacol* 1997, **4:**331-338.
7. Costa DL, Dreher KL: **Bioavailable transition metals in particulate matter mediate cardiopulmonary injury in healthy and compromised animal models.** *Environ Health Perspect* 1997, **105(Suppl 5):**1053-1060.
8. Gavett SH, Madison SL, Dreher KL, Winsett DW, McGee JK, Costa DL: **Metal and sulfate composition of residual oil fly ash determines airway hyperreactivity and lung injury in rats.** *Environ Res* 1997, **72:**162-172.
9. Agency for Toxic Substances and Disease Registry (ATSDR): *Toxicological Profile for Manganese* Atlanta, GA: US Department of Health and Human Services; 2000.
10. Roels H, Lauwerys R, Buchet JP, Genet P, Sarhan MJ, Hanotiau I, deFays M, Bernard A, Stanescu D: **Epidemiological survey among workers exposed to manganese: effects on lung, central nervous system, and some biological indices.** *Am J Ind Med* 1987, **11:**307-327.
11. Saric M: **Occupational and environmental exposures and nonspecific lung disease – a review of selected studies.** *Isr J Med Sci* 1992, **28:**509-512.
12. Lloyd Davies TA, Harding HE: **Manganese pneumonitis. Further clinical and experimental observations.** *Br J Ind Med* 1949, **6:**82-90.
13. Adkins B Jr, Luginbuhl GH, Gardner DE: **Acute exposure of laboratory mice to manganese oxide.** *Am Ind Hyg Assoc J* 1980, **41:**494-500.
14. Bergstrom R: **Acute pulmonary toxicity of manganese dioxide.** *Scand J Work Environ Health* 1977, **3(Suppl 1):**1-41.
15. Shanker R, Dogra RK, Sahu AP, Zaidi SH: **Experimental manganese lymphadenopathy in guinea pigs.** *Arch Toxicol* 1976, **36:**151-157.
16. Singh J, Kaw JL, Zaidi SH: **Early biochemical response of pulmonary tissue to manganese dioxide.** *Toxicology* 1977, **8:**177-184.
17. Ulrich CE, Rinehart W, Brandt M: **Evaluation of the chronic inhalation toxicity of a manganese oxide aerosol. III. Pulmonary function, electromyograms, limb tremor, and tissue manganese data.** *Am Ind Hyg Assoc J* 1979, **40:**349-353.
18. Zaidi SH, Dogra RK, Shanker R, Chandra SV: **Experimental infective manganese pneumoconiosis in guinea pigs.** *Environ Res* 1973, **6:**287-297.
19. Camner P, Curstedt T, Jarstrand C, Johannsson A, Robertson B, Wiernik A: **Rabbit lung after inhalation of manganese chloride: a comparison with the effects of chlorides of nickel, cadmium, cobalt, and copper.** *Environ Res* 1985, **38:**301-309.
20. Dorman DC, McManus BE, Parkinson CU, Manuel CA, McElveen AM, Everitt JI: **Nasal toxicity of manganese sulfate and manganese phosphate in young male rats following subchronic (13-week) inhalation exposure.** *Inhal Toxicol* 2004, **16:**481-488.
21. National Research Council: *Guide for the Care and Use of Laboratory Animals* Washington DC: National Academy Press; 1996.
22. Newland MC: **Animal models of manganese's neurotoxicity.** *Neurotoxicology* 1999, **20:**415-432.
23. Kepler GM, Richardson RB, Morgan KT, Kimbell JS: **Computer simulation of inspiratory nasal airflow and inhaled gas uptake in a rhesus monkey.** *Toxicol Appl Pharmacol* 1998, **150:**1-11.
24. Martonen TB, Katz IM, Musante CJ: **A nonhuman primate aerosol deposition model for toxicological and pharmaceutical studies.** *Inhal Toxicol* 2001, **13:**307-324.
25. Dorman DC, Struve MF, James RA, Marshall MW, Parkinson CU, Wong BA: **Influence of particle solubility on the delivery of inhaled manganese to the rat brain: manganese sulfate and manganese tetroxide pharmacokinetics following repeated (14-day) exposure.** *Toxicol Appl Pharmacol* 2001, **170:**79-87.
26. Mellick PW, Dungworth DL, Schwartz LW, Tyler WS: **Short term morphologic effects of high ambient levels of ozone on lungs of rhesus monkeys.** *Lab Invest* 1977, **36:**82-90.
27. Dorman DC, McManus BE, Marshall MW, James RA, Struve MF: **Old age and gender influence the pharmacokinetics of inhaled manganese sulfate and manganese phosphate in rats.** *Toxicol Appl Pharmacol* 2004, **197:**113-124.
28. Brack M: **Histochemistry of the lung mite pigment in infections of *Pneumonyssus sp.* in nonhuman primates.** *Parasitology* 1972, **64:**47-52.
29. Hull WB: **Respiratory mite parasites in nonhuman primates.** *Lab Anim Care* 1970, **20:**402-406.
30. Fuller GN, Burger PC: **Central nervous system.** In *Histology for Pathologists* 2nd edition. Edited by: Sternberg SS. Philadelphia: Lippincott Williams & Wilkins; 1997:243-282.
31. Morgan KT, Johnson BP, Frith CH, Townsend J: **An ultrastructural study of spontaneous mineralization in the brains of aging mice.** *Acta Neuropathol* 1982, **58:**120-124.
32. Kast A, Peil H, Weisse I: **Calcified foci at the junction between adrenal cortex and medulla of rhesus monkeys.** *Lab Anim* 1994, **28:**80-89.
33. Wadsworth PF, Jones HB, Cavanagh JB: **The topography, structure and incidence of mineralized bodies in the basal ganglia of the brain of cynomolgus monkeys (Macaca fascicularis).** *Lab Anim* 1995, **29:**276-281.
34. Donaldson K, Tran CL: **Inflammation caused by particles and fibers.** *Inhal Toxicol* 2002, **14:**5-27.
35. Tyler NK, Plopper CG: **Morphology of the distal conducting airways in rhesus monkey lungs.** *Anat Rec* 1985, **211:**295-303.
36. Heppleston AG: **The pathological anatomy of simple pneumoconiosis in coal workers.** *J Pathol Bact* 1953, **66:**235-246.
37. Hyde DM, Hubbard WC, Wong V, Wu R, Pinkerton K, Ploppper CG: **Ozone-induced acute tracheobronchial epithelial injury: relationship to granulocyte emigration in the lung.** *Am J Respir Cell Mol Biol* 1992, **6:**481-497.
38. Niewoehner DE, Kleinerman J, Rice DB: **Pathologic changes in the peripheral airways of young cigarette smokers.** *N Engl J Med* 1974, **291:**755-758.
39. Ryu JH, Myers JL, Swensen SJ: **Bronchiolar disorders.** *Am J Respir Crit Care Med* 2003, **168:**1277-1292.
40. Boojar MM, Goodarzi F: **A longitudinal follow-up of pulmonary function and respiratory symptoms in workers exposed to manganese.** *J Occup Environ Med* 2002, **44:**282-290.
41. Nikula KJ, Vallyathan V, Green FH, Hahn FF: **Influence of exposure concentration or dose on the distribution of particulate material in rat and human lungs.** *Environ Health Perspect* 2001, **109:**311-318.
42. Harmsen AG, Mason MJ, Muggenburg BA, Gillett NA, Jarpe MA, Bice DE: **Migration of neutrophils from lung to tracheobronchial lymph node.** *J Leukoc Biol* 1987, **41:**95-103.
43. Lee KP, Kelly DP: **Translocation of particle-laden alveolar macrophages and intra-alveolar granuloma formation in rats exposed to Ludox colloidal amorphous silica by inhalation.** *Toxicology* 1993, **77:**205-222.
44. Henderson RF, Driscoll KE, Harkema JR, Lindenschmidt RC, Chang IY, Maples KR, Barr EB: **A comparison of the inflammatory response of the lung to inhaled versus instilled particles in F344 rats.** *Fundam Appl Toxicol* 1995, **24:**183-197.
45. Hiramatsu K, Azuma A, Kudoh S, Desaki M, Takizawa H, Sugawara I: **Inhalation of diesel exhaust for three months affects major cytokine expression and induces bronchus-associated lymphoid tissue formation in murine lungs.** *Exp Lung Res* 2003, **29:**607-622.
46. Sato A, Chida K, Iwata M, Hayakawa H: **Study of bronchus-associated lymphoid tissue in patients with diffuse panbronchiolitis.** *Am Rev Respir Dis* 1992, **146:**473-478.
47. Suda T, Chida K, Hayakawa H, Imokawa S, Iwata M, Nakamura S, Sato A: **Development of bronchus-associated lymphoid tissue in chronic hypersensitivity pneumonitis.** *Chest* 1999, **115:**357-363.
48. Brenneman KA, Wong BA, Bucellato MA, Costa ER, Gross EA, Dorman DC: **Direct olfactory transport of inhaled manganese ($^{54}MnCl_2$) to the rat brain: Toxicokinetic investigations in a unilateral nasal occlusion model.** *Toxicol Appl Pharmacol* 2000, **169:**238-248.

49. Molders N, Schilling PJ, Wong J, Roos JW, Smith IL: **X-ray fluorescence mapping and micro-XANES spectroscopic characterization of exhaust particulates emitted from auto engines burning MMT-added gasoline.** *Environ Sci Technol* 2001, **35:**3122-3129.
50. Pellizzari ED, Clayton CA, Rodes C, Mason RE, Piper LL, Fort B, Pfeifer G, Lynam D: **Particulate matter and manganese exposures in Toronto, Canada.** *Atmos Environ* 1999, **33:**721-734.
51. Schlesinger RB: **Deposition and clearance of inhaled particles.** In *Concepts in Inhalation Toxicology* Edited by: McClellan RO, Henderson RF. Taylor and Francis, Washington, DC; 1995:191-224.
52. Asgharian B, Wood R, Schlesinger RB: **Empirical modeling of particle deposition in the alveolar region in the lungs: A basis for interspecies extrapolation.** *Fundam Appl Toxicol* 1995, **27:**232-238.
53. Snipes MB: **Long-term retention and clearance of particles inhaled by mammalian species.** *Crit Rev Toxicol* 1989, **20:**175-211.
54. Mercer RR, Crapo JD: **Structure of the gas exchange region of the lungs determined by three dimensional reconstruction.** In *Toxicology of the Lung* New York:Raven Press; 1988:43-70.
55. Tyler WS: **Small airways and terminal units: comparative subgross anatomy of lungs.** *Am Rev Respir Dis* 1983, **128:**S32-S36.
56. Hinds WC: *Aerosol Technology* 2nd edition. New York: John Wiley and Sons; 1999.

ATTACHMENT B

Summary of Relevant Toxicity Studies

Current, Peer-reviewed Short-term Toxicity Data for Setting Guidance Levels

Study	Type	Mn Compound	Particle Size (µm)	Exposure Type	Species Used in Study	Mn Exposure Concentration	Study/Exposure Details	Primary Endpoints	Additional Observations	Comments
Dorman et al. (2005)	Primary	MnSO4	1.72-2.12	Whole body	Male rhesus monkeys (4 or 6/group)	0 or 1.5 mg Mn/m3	Subacute study: 6 hr/day, 5 days/wk, for 15 exposure days (90 hours total)	Significant,mild subacute bronchiolitis, increase in bronchus-associated lymphoid tissue (BALT)	Histologic changes to the respiratory system & lung Mn concentrations were determined. No signs of clinical toxicity, including neurotoxicity, were observed in the animals	Based on this study, TCEQ identified 1.5 mg Mn/m3 as a LOAEL for subacute exposure
							Subacute study: 6 hr/day, 5 days/wk, for 33 exposure days (198 hour total)	Significant bronchiolitis impacting more of the respiratory bronchioles & alveolar duct inflammatory alterations & alveolar duct inflammation, as well as increased Mn lung		--
					Male rhesus monkeys (4-6/group)	0, 0.06, 0.3, or 1.5 mg Mn/m3	Subchronic study: 6 hours/day, 5 days/week, for 65 exposure days (390 hours total)	Increased lung Mn concentrations in monkeys exposed to 0.3 or 1.5 mg Mn/m3 for 65 days & alveolar duct inflammation, as well as increased Mn lung concentrations (seen at exposures for ≥15 days). However, all observed changes were reversible and not seen at 45 days post-exposure		--
					Male rhesus monkeys (8)	1.5 mg Mn/m3	Subchronic study: 6 hours/day, 5 days/week, for 65 exposure days (390 hours total); plus 45 or 90 days for recovery)			--
McGough and Jardine (2017)	Primary	MnCl2	Not provided	Nose-only	Sprague Dawley rats (10/group/sex)	0, 2.2, 8.7 or 13.1 mg Mn/m3	Initial range finding study; planned for 9 weeks but stopped at 3 weeks due to frank toxicity at 13.1 mg Mn/m3	Overt toxicity	--	--
			2.32-2.57		Sprague Dawley F0 and F1 rats (24-28 /sex/group); F2 rats (details not provided)	0, 2.2, 4.4 or 8.7 mg Mn/m3	2-generation reproductive toxicity guideline study; F0 & F1: before mating (for 10 and 11 weeks, respectively), during mating, pregnancy and lactation (males: 6 hours/day, 7 days/week; 17 weeks [714 hours total]; females: no dose GD 20/21; 1 hour/day during days 1-2 of lactation; 2 hours/day during days 3-4 of lactation; 6 hours/day otherwise) F2: exposed throughout gestation until lactation day 21	No effects observed in the F2 rats; although mild respiratory effects occurred in the F0 rats at 4.4 & 8.8 mg Mn/m3. No reproductive effects occurred. The mild respiratory effects were attributed to irritation caused by Cl2 and slower lung clearance of Mn+2	Various reproductive/ developmental & toxicological endpoints were assessed, including growth, fertility, estrous cycles, survival, respiratory effects	Although this study does not provide acute exposure data, it addresses one of the data gaps identified by ATSDR when it set the chronic MRL in 2012. Specifically, it supports the lack of reproductive & developmental toxicity at exposures higher than the subacute LOAEL from Dorman et al. (2005)
Saputra et al. (2016)	Primary	MnCl2	1.2	Nose-only	Male Sprague-Dawley rats (12/group)	0 or 17 mg Mn/m3	4 hours/day, 5 days/week for 3 weeks (60 hours total)	Mild lung effects (minimal infiltration of inflammatory cells in respiratory bronchioles), altered expression of dopamine in the brain & significantly higher Mn levels in the striatum, cerebellum, prefrontal cortex, olfactory bulb, lung & other tissues	The Mn-exposed group had no motor effects, no brain histopathological changes, no brain neuronal changes & no body weight differences	LOAEL from this study was 17 mg/m3
HaMai et al. (2006)	Primary	MnSO4	0.55	Nose-only	Sprague–Dawley rats (3-5/group)	0 or 0.71 mg Mn/m3	Prenatal group: exposed pregnant females 2 hours/day on GDs 9 & 10 (4 hours total) Adulthood group: exposed 2 hours/day starting at 6 weeks after birth for 10 days (20 hours total) Prenatal + Adulthood group: exposed 2 hours/day on GDs 9 & 10, & 6 weeks of age for 10 days (24 hours total)	While no overt toxicity was observed, in the Adult group, mRNA levels of amyloid precursor protein (APP), cyclooxygenase-2 (COX-2), neuronal nitric oxide synthase (nNOS), glial fibrillary acidic protein (GFAP), & transformation growth factor beta (TGF-β) were significantly decreased The other two groups showed lesser decreases in mRNA levels for these genes. Animals in the Prenatal group had significant decreases in mRNA levels of all but TGF-β; rats in the Prenatal + Adult group had significant decreases in mRNA levels of COX-2, nNOS & TGF-β	Overall, brief Mn prenatal exposure to Mn lessened the response of several genes associated with inflammation or oxidative stress to additional Mn exposure	Subacute exposure to 0.71 mg Mn/m3 during gestation and adulthood altered the transcription of certain genes, but did not result in biologically adverse effects. ATSDR considers these results as a NOAEL
Erikson et al. (2005)	Primary	MnSO4	1.03-1.07	Whole body	CD rats (10 rats/group/sex)	0, 0.05, 0.5, or 1 mg Mn/m3	Exposed 28 days before breeding & ≤14 days during mating (F0 generation) (7 days/week, 6 hours/day; up to 252 total hours) Pregnant females exposed GD 0-GD 19, but not when delivery was anticipated (after GD 19) Pups & nursing dams exposed to MnSO4 during PND 1–PND 18 (222 total hours) Animals allowed 3 weeks of recovery	Oxidative stress measurements were determined in 5 brain regions. While total glutathione (GSH) levels were unchanged, GSH levels were significantly lower in the cerebella of F1 males At the highest concentration (1 mg Mn/m3), glutamine synthetase (GS) mRNA was decreased in F1 female striata & increased in F1 male olfactory bulb and hypothalamus. Metallothionein (MT) was unchanged at 1 mg Mn/m3, 0.5 mg Mn/m3 led to decreased MT in F1 female olfactory bulbs and F1 male hypothalami & hippocampi At the lowest dose (0.05 mg Mn/m3) F1 males had decreased MT mRNA in the striatum, hippocampus & hypothalamus		Upon subchronic exposure to 0.05-1 mg Mn/m3, changes in biomarkers of oxidative stress following in utero & neonatal inhalation exposure to manganese persisted even after 3 weeks of recovery, although brain Mn levels returned to normal

Current, Peer-reviewed Short-term Toxicity Data for Setting Guidance Levels

Study	Type	Mn Compound	Particle Size (µm)	Exposure Type	Species Used in Study	Mn Exposure Concentration	Study/Exposure Details	Primary Endpoints	Additional Observations	Comments
Taylor et al. (2006)	Review (evaluated 7 studies: Erikson et al. 2004, 2005, 2006; Dorman et al. 2001, 2004, 2005a; & Dobson et al. 2003)	MnSO4 for 6 studies; manganese phosphate in Dorman et al. (2001)	Not provided	Not provided	Neonatal & adult rats (males & females) & male senescent rats	Across the studies, rats were exposed for 14 to 90 days, PND 19 or 45 (following exposure during gestation & lactation until PND 18), at concentrations ranging from 0.01–3 mg Mn/m3 Concentrations used were considered sufficient to cause Mn to accumulate in tissue		Measurements of oxidative stress included alterations in total GSH, MT mRNA, GS protein & RNA in the hypothalamus, hippocampus, striatum, olfactory bulb & cerebellum		Oxidative stress does not appear to be a substantial component of Mn-induced neurotoxicity, & although there is evidence of oxidative stress in some areas of the brain, evidence is inconsistent

ATTACHMENT C

Schroeter et al. (2012) and Gentry et al. (2017)

TOXICOLOGICAL SCIENCES **129(2)**, 432–446 (2012)
doi:10.1093/toxsci/kfs212
Advance Access publication June 21, 2012

Application of a Multi-Route Physiologically Based Pharmacokinetic Model for Manganese to Evaluate Dose-Dependent Neurological Effects in Monkeys

Jeffry D. Schroeter,*[,1] David C. Dorman,† Miyoung Yoon,* Andy Nong,* Michael D. Taylor,‡ Melvin E. Andersen,* and Harvey J. Clewell III*

*The Hamner Institutes for Health Sciences, Research Triangle Park, North Carolina; †College of Veterinary Medicine, North Carolina State University, Raleigh, North Carolina; and ‡Afton Chemical Corp., Richmond, Virginia

[1]To whom correspondence should be addressed at Applied Research Associates, Inc., 8537 Six Forks Road, Suite 600, Raleigh, NC 27615. Fax: (919) 582-3301. E-mail: jschroeter@ara.com.

Received March 23, 2012; accepted June 4, 2012

Manganese (Mn) is an essential element that is neurotoxic under certain exposure conditions. Monkeys and humans exposed to Mn develop similar neurological effects; thus, an improved understanding of the dose-response relationship seen in nonhuman primates could inform the human health risk assessment for this essential metal. A previous analysis of this dose-response relationship in experimental animals (Gwiazda, R., Lucchini, R., and Smith, D., 2007, Adequacy and consistency of animal studies to evaluate the neurotoxicity of chronic low-level manganese exposure in humans, *J. Toxicol. Environ. Health Part A* 70, 594–605.) relied on estimates of cumulative intake of Mn as the sole measure for comparison across studies with different doses, durations, and exposure routes. In this study, a physiologically based pharmacokinetic model that accurately accounts for the dose dependencies of Mn distribution was used to estimate increases in brain Mn concentrations in monkeys following Mn exposure. Experimental studies evaluated in the analysis included exposures by inhalation, oral, iv, ip, and sc dose routes, and spanned durations ranging from several weeks to over 2 years. This analysis confirms that the dose-response relationship for the neurotoxic effects of Mn in monkeys is independent of exposure route and supports the use of target tissue Mn concentration or cumulative target tissue Mn as the appropriate dose metric for these comparisons. These results also provide strong evidence of a dose-dependent transition in the mode of action for the neurological effects of Mn that needs to be considered in risk assessments for this essential metal.

Key Words: **manganese; neurotoxicity; dose response; physiologically based pharmacokinetic modeling.**

Manganese (Mn) is an essential nutrient that is required for many physiological functions. Mn occurs naturally in soil, water, and air, leading to a widespread presence in the environment. The primary source of Mn exposure is through the diet. Adult dietary intake in people has been estimated to range from 1 to 10 mg Mn/day with only a small fraction (1–5%) absorbed by the gastrointestinal (GI) tract (Aschner *et al.*, 2005; ATSDR, 2000). Homeostatic controls regulate intestinal absorption and biliary excretion to ensure adequate and stable tissue Mn concentrations and to prevent Mn deficiency or toxicity despite mild fluctuations in daily exposure levels.

As with other essential elements, Mn may induce toxicity under certain high-dose exposure conditions. Adverse neurological, reproductive, and respiratory effects characterize Mn toxicity in humans. Mn-induced neurotoxicity is of particular concern and is considered one of the most sensitive endpoints (Aschner *et al.*, 2005). Early manifestations of Mn overexposure include fatigue, headache, muscle cramps, loss of appetite, apathy, insomnia, and diminished libido. As overexposure continues and the disease progresses, patients may develop prolonged muscle contractions (dystonia), decreased muscle movement (hypokinesia), rigidity, and muscle tremors (Pal *et al.*, 1999). Structural changes in the globus pallidus of Mn-exposed people indicate that this brain region is a target site for Mn accumulation and effects (Perl and Olanow, 2007). Individuals with chronic Mn neurotoxicity resemble patients with Parkinson's disease; however, unlike in Parkinson's disease, the substantia nigra is largely spared and dopamine levels remain generally unaffected during Mn neurotoxicity (Guilarte, 2010).

Mn-induced neurological effects have been reported from studies of occupational exposure to high inhaled (> 0.2 mg/m^3) Mn concentrations (Myers *et al.*, 2003; Roels *et al.*, 1987), environmental studies of residents near ferroalloy plants (Lucchini *et al.*, 2007), individuals exposed to Mn-laden drinking water (Bouchard *et al.*, 2011; Kawamura *et al.*, 1941; Kondakis *et al.*, 1989), and from people with prolonged use of total parenteral nutrition formulations that contain Mn

(Alves *et al.*, 1997; Fell *et al.*, 1996). These observations suggest that brain Mn concentration is the critical determinant for Mn neurotoxicity, regardless of exposure route. This is an important distinction to consider when assessing long-term health risks from chronic, low-level environmental Mn exposure.

Studies on Mn neurotoxicity have been conducted in rodents and nonhuman primates using various exposure routes and a wide range of doses and durations. Gwiazda *et al.* (2007) conducted a review of subchronic to chronic rodent and nonhuman primate studies to determine whether a consistent dose-response relationship existed among different studies. One goal of Gwiazda *et al.*'s work was to determine whether animal studies could be used to evaluate the neurotoxicity of chronic low-level Mn exposures in humans. They estimated internal cumulative Mn dose as "the total amount of Mn that was taken up into the circulatory system by the time the endpoint was detected." The range of exposures associated with adverse changes was profound (over two orders of magnitude) in the animal studies evaluated by Gwiazda *et al.*, leading them to conclude that most existing animal studies might be of limited relevance for the risk assessment of chronic low-level Mn exposure to humans.

Since Gwiazda *et al.*'s study was published, several physiologically based pharmacokinetic (PBPK) models for Mn have been reported (Nong *et al.*, 2009; Schroeter *et al.*, 2011; Yoon *et al.*, 2011). These PBPK models effectively simulate Mn tissue kinetics from inhaled, oral, and parenteral Mn intake (Andersen *et al.*, 2010). This multi–dose route capability is achieved by incorporating homeostatic control processes, saturable tissue binding capacities, and preferential fluxes in various tissue regions (see Taylor *et al.*, 2012 for review). PBPK models have been widely used in risk assessment of chemical compounds to support extrapolation across species, high to low doses, and across exposure routes and to allow for calculation of target tissue dose, which is more biologically relevant than administered dose, exposure concentration, or estimated systemic dose as a metric for predicting toxic outcomes.

The purpose of this study was to apply PBPK modeling approaches to a subset of the studies initially identified by Gwiazda *et al.* (2007). We focused our attention on work performed in nonhuman primates because unlike rodents, Mn-exposed monkeys develop regionally selective increases in brain Mn concentrations (Aschner *et al.*, 2005; Dorman *et al.*, 2006b; Eriksson *et al.*, 1992b; Newland *et al.*, 1989) and behavioral effects similar to those seen in Mn-affected humans (Olanow *et al.*, 1996). To this end, we used a PBPK model developed specifically for rhesus monkeys (Schroeter *et al.*, 2011) to simulate the exposure scenarios from each study and to predict the corresponding increases in brain Mn concentrations for various dose routes, exposure concentrations, and durations.

MATERIALS AND METHODS

Study Selection

The 15 nonhuman primate studies identified by Gwiazda *et al.* (2007) were used as a starting point for this analysis. Three of the studies identified by Gwiazda used cebus monkeys (*Cebus* spp.) or squirrel monkeys (*Saimiri sciureus*) (Neff *et al.*, 1969; Newland and Weiss, 1992; Ulrich *et al.*, 1979). These studies were excluded from our analysis because the PBPK models were developed and calibrated using pharmacokinetic data obtained in rhesus monkeys (*Macaca mulatta*) or phylogenetically similar macaque relatives. A fourth excluded study (Van Bogaert and Dallemagne, 1946) used macaques but included an inhalation coexposure to sodium perchlorate, thus confounding our interpretation of the reported clinical signs. In addition to the studies identified by Gwiazda, we also included two recent studies (Dorman *et al.*, 2006a; Guilarte *et al.*, 2006) and the report by Coulston and Griffin (1976). The study by Chandra *et al.* (1979) was also included for model calibration although clinical effects were not reported. In the end, 15 studies were identified in our analysis (summarized in Table 1). Exposure routes for these studies included inhalation, oral delivery, and iv, ip, sc, and im injection. Different forms of Mn were used in the exposures and included both soluble (e.g., $MnCl_2$ and $MnSO_4$) and relatively insoluble (e.g., MnO_2 and Mn_3O_4) forms of Mn. These studies also included a wide range of Mn dose levels, dose frequencies, and exposure durations.

Assessment of Clinical Signs

Clinical signs were evaluated using modifications of clinical sign scales developed for monkeys with 1-methyl-4-phenyl-1,2,3,6-tetrahydropyridine–induced parkinsonism (Imbert *et al.*, 2000; Kurlan *et al.*, 1991). Evaluations were based upon the original data and descriptions as published in the studies included in this review (Table 1). Scoring of clinical signs was performed by a veterinarian with expertise in neurotoxicology (David D. Dorman). The following effect categories and severity scoring system were used to assess the monkey studies:

Coordination
- 0—normal
- 1—very slight to no loss of balance
- 2—moderate lapses in balance
- 3—frequent and major lapses in balance

Bradykinesia
- 0—normal speed and facility of movement
- 1—mild (25–50%) reduction
- 2—moderate (51–75%) reduction
- 3—severe (> 75%) reduction

Rigidity/Gait disorders
- 0—normal
- 1—walks slowly and with difficulty
- 2—markedly impaired; ambulate slowly +/– effort
- 3—severe decrease in ability to ambulate

Postural instability
- 0—absent
- 1—minor
- 2—marked

Muscle tremors
- 0—absent
- 1—mild
- 2—moderate
- 3—severe

Other neurological clinical signs (included CNS excitation and hyperactivity)
- 0—none
- 1—mild
- 2—moderate
- 3—severe

TABLE 1
Summary of Mn Exposure Studies in Rhesus Monkeys

Study	Mn form	Dose route	Body weight (kg)	Dosing regimen
Chandra *et al.* (1979)	$MnCl_2$	oral	5	5.6 mg/kg Mn in $MnCl_2$ solution given once daily for 18 months
Gupta *et al.* (1980)	$MnCl_2$	oral	5–6	7.0 mg/kg Mn in $MnCl_2$ solution given once daily for 18 months
Van Bogaert and Dallemagne (1946)	$MnSO_4$	oral	2.85	1.3–6.3 mg/kg Mn in $MnSO_4$ solution given once daily for 292 days
Mella (1924)	$MnCl_2$	ip	5[a]	0.5–2.2 mg/kg Mn given every other day for up to 14 months
Olanow *et al.* (1996)	$MnCl_2$	iv	12–18	2.8–4.0 mg/kg Mn given by iv injection 7 times at ~1-week intervals
Guilarte *et al.* (2006)/Schneider *et al.* (2006)	$MnSO_4$	iv	6.5	3.6–5.4 mg/kg Mn injected weekly for approximately 40 weeks
Suzuki *et al.* (1975)	MnO_2	sc	3.5–4.5	Up to 158 mg/kg Mn injected once a week for 9 weeks
Eriksson *et al.* (1987)	MnO_2	sc	3.5–4.5	Approximately 112 mg/kg Mn injected on 18 occasions over 5 months
Eriksson *et al.* (1992a)	MnO_2	sc	4.5–6.0	38 mg/kg Mn injected on 13 occasions over 26 months
Eriksson *et al.* (1992b)	MnO_2	sc	4–5	89 mg/kg Mn injected on 11 occasions over 4 months
Pentschew *et al.* (1963)	MnO_2	im	5[a]	Single doses of 252 and 441 mg/kg Mn injected 2 months apart
Bird *et al.* (1984)	MnO_2	inhalation	2–3	Exposure to 30 mg Mn/m^3 for 6 h/day, 5 days/week for 2 years
Nishiyama *et al.* (1977)	MnO_2	inhalation	3–4	Exposure to 0.7 or 3.0 mg Mn/m^3 for 22 h/day, 7 days/week for 10 months
Coulston and Griffin (1976)	Mn_3O_4	inhalation	2.75–6.5	Exposure to 0.1 mg Mn/m^3 for 23 h/day, 7 days/week for up to 15 months or to 5.0 mg Mn/m^3 for 23 h/day, 7 days/week for 23 weeks
Dorman *et al.* (2006)	$MnSO_4$	inhalation	2.5	Exposure to 0.06, 0.3, or 1.5 mg Mn/m^3 for 6 h/day, 5 days/week for 90 days

[a]Body weights were not reported in the study, so a 5 kg body weight for an adult rhesus monkey was assumed for model simulations.

The severity scores for the categories listed above were summed to obtain a final severity score for each dose group in the studies listed in Table 1. The minimum possible score was 0 (no effect) and the maximum possible score was 17. If a sufficient description of a change in clinical signs was reported during the course of the exposure, then severity scores at multiple time points were used in the analysis.

Mn PBPK Model

The Mn PBPK model for rhesus monkeys was previously described in detail (Nong *et al.*, 2009; Schroeter *et al.*, 2011), so only a brief description is given of some of the important aspects of the model. The PBPK model contained compartments for the liver, lung, nasal cavity, bone, blood, and brain regions (Fig. 1). All other body tissues were combined into a single compartment. The brain was divided into compartments representing blood, globus pallidus, cerebellum, olfactory bulb, and pituitary gland. The globus pallidus, cerebellum, and pituitary gland were included because they accumulate Mn to varying degrees during inhalation exposure. The olfactory bulb was included because it receives direct transport from olfactory epithelium during Mn inhalation (Aschner *et al.*, 2005; Dorman *et al.*, 2006a,b).

Tissue Mn concentrations represent the sum of free Mn and bound forms within the tissues. Free Mn circulates in the blood throughout the body; the bound form is stored in tissue constituents. Tissue binding is a reversible, saturable process that likely represents incorporation of specific macromolecular Mn stores. The incorporation of Mn into tissue constituents is governed by tissue-specific association and dissociation rate constants (k_a and k_d). The distribution between bound and free Mn is determined by the dissociation binding ratio (k_d/k_a) and the tissue-specific maximum binding capacity (B_{max}), which regulates the storage capacity of bound Mn in each tissue. Saturation of the binding capacity with increased exposure leads to increases in free Mn and subsequent increases in total tissue Mn. Following cessation of exposure, free Mn is rapidly cleared from the body and tissue Mn concentrations return to their basal levels.

The differential rise in free Mn concentration in brain regions was described with tissue-specific diffusion rate constants (k_{in} and k_{out}) to describe diffusion-limited flux between brain blood and brain tissues. The influx rates for the globus pallidus and pituitary regions were dose dependent in order to accurately describe changes in Mn concentration in these brain regions with increased Mn exposure. Increases in free Mn concentration in brain regions depend on asymmetric diffusional clearance rates, binding rate constants, and the binding capacity of each tissue. Tissue Mn binding capacity and diffusion parameters were calibrated by Schroeter *et al.* (2011) to the pharmacokinetic data from Mn-exposed monkeys in Dorman *et al.* (2006a) to simulate the rise in tissue Mn levels following the onset of inhalation exposure, followed by a return to basal levels after the exposure period. These parameters were unchanged for all simulations in this study.

A series of gut compartments were included in the PBPK model to track Mn absorption by the GI tract (Fig. 1). For dietary Mn, a small fraction (F_{dietup}) was absorbed by the GI tract and directed to the liver for systemic circulation. The remaining fraction of Mn in the gut lumen ($1-F_{dietup}$) was either transiently stored in gut epithelial cells (F_{ent}) or transferred to the lower GI tract lumen ($1-F_{ent}$) and excreted through the feces. Mn transfer from the gut lumen to the portal blood was reflected by the rate constant k_{GI}. Mn transfer from the gut epithelium to the lower GI tract occurred by sloughing of enterocytes from the epithelial layer (k_{ent}). The stored Mn in enterocytes was not available to the systemic circulation due to rapid enterocyte turnover and was excreted into feces.

The elimination of Mn from the body occurs via biliary excretion in the liver. Biliary excretion was governed by the rate constant, k_{bile}, which was induced by blood concentration to reflect the dose-dependent behavior of Mn elimination (Nong *et al.*, 2009):

$$k_{bile} = k_{bile0} \cdot \left(1 + \frac{k_{bmax} \cdot C_{art}^{n}}{k_{b50}^{n} + C_{art}^{n}}\right),$$

where k_{bile0} is the basal biliary excretion rate constant, k_{bmax} is the maximal increase in the excretion rate constant, k_{b50} is the arterial concentration at half the induced level of Mn in the arterial blood (C_{art}), and n is the slope factor. Arterial blood concentration (C_{art}) was used as a surrogate for free liver Mn concentration because Mn blood levels were directly measured in exposed monkeys (Dorman *et al.*, 2006a).

As described in Schroeter *et al.* (2011), fractional dietary absorption (F_{dietup} = 0.0021) and the biliary excretion rate constant (k_{bilec} = 0.051) were calibrated by fitting basal Mn tissue concentrations to tissue levels from the

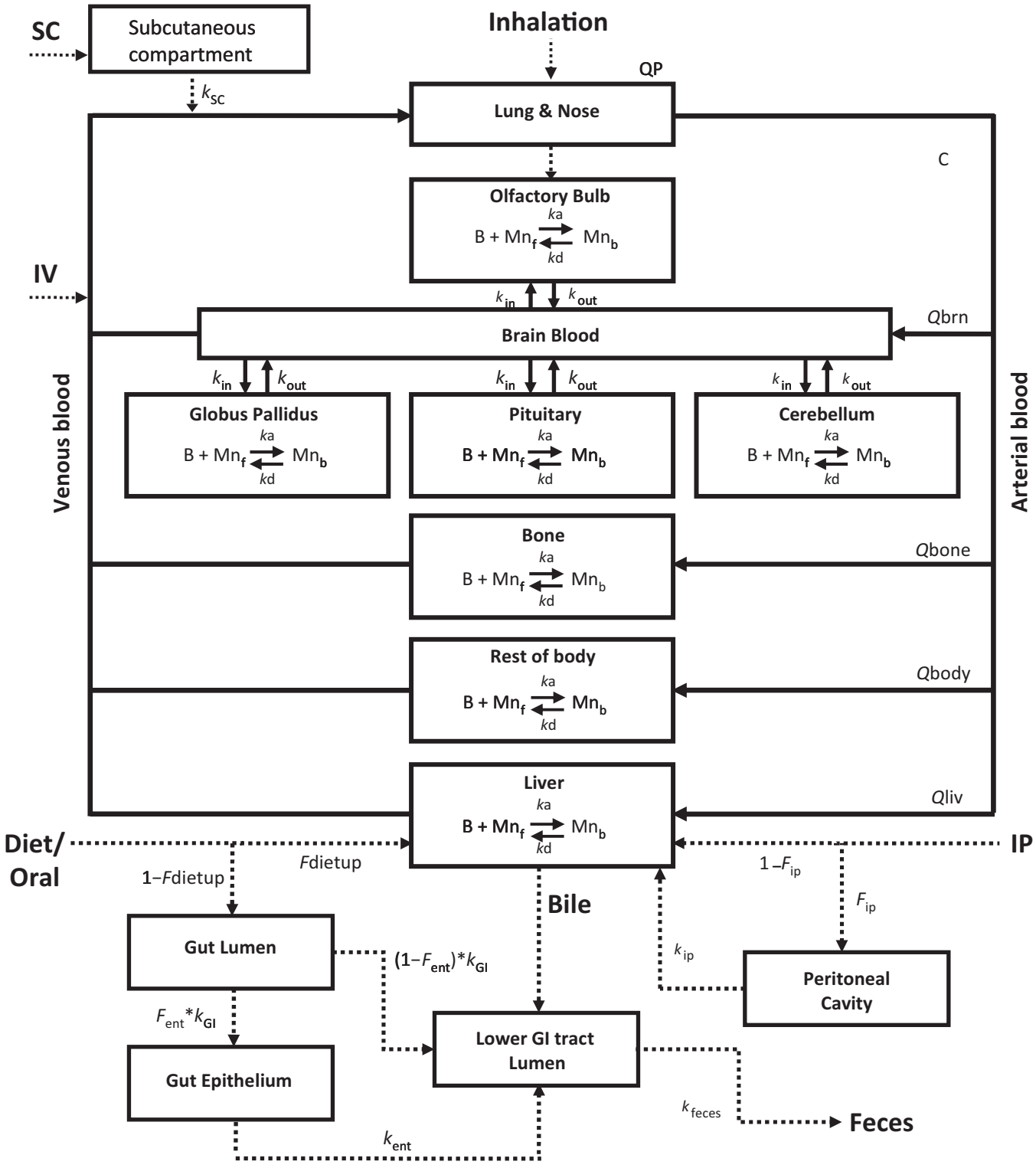

FIG. 1. Schematic of the Mn PBPK model for nonhuman primates. The PBPK model can accommodate the following Mn exposure routes: inhalation, diet/oral, ip, iv, and sc. Tissue-specific binding processes were controlled by association and dissociation parameters (k_a and k_d) and the binding capacity (B_{tissue}). Diffusion rate constants (k_{in} and k_{out}) control increases in free Mn in brain regions. Q_{tissue} parameters refer to tissue blood flow rates.

control monkeys in Dorman *et al.* (2006a). Parameters governing GI absorption of Mn were calibrated using clearance data of oral doses of ^{54}Mn (Furchner *et al.*, 1966). Biliary induction parameters were originally estimated by Nong *et al.* (2009) for low-dose Mn inhalation exposures (Dorman *et al.*, 2006a), where a maximum induction factor of k_{bmax} = 2.5 was sufficient to describe the increase in biliary excretion following Mn exposure. However, most of the studies that were considered in this analysis used much higher Mn doses, so a larger maximal induction factor was needed to simulate increased biliary excretion rates following increased Mn intake. For all of the simulations in this study, the parameter k_{bmax} was increased to 20.0 and the other parameters in the biliary induction equation were modified accordingly (k_{b50} = 0.105, n = 2.1) to remain consistent with the low-dose behavior described by Nong *et al.* (2009). Studies in rats have shown that the biliary excretion of Mn is saturable, indicating a carrier-mediated transport mechanism (Ballatori *et al.*, 1987; Klaassen, 1974). To date, the transport protein(s) responsible for transporting Mn from hepatocytes into bile remain unknown. Because of known interaction between Mn and iron, it is plausible that Mn may share iron efflux transporters including ferroportin (Fpn1/Slc40a1), divalent metal transporter-1 (DMT-1), or copper ATPase (Atp7a or Atp7b) (Abboud and Haile, 2000; Goss *et al.*, 2008). The eightfold increase in k_{bmax} is consistent with studies evaluating Atp7a and DMT-1 hepatic expression in a rodent model of iron deficiency (which mimics Mn toxicity) (Jiang *et al.*, 2011).

Simulation of Mn Exposure Routes

The Mn PBPK model included the exposure routes that have been used in experimental studies (Table 1). For all exposures, the nominal dose used in modeling simulations was calculated from the Mn atomic weight fraction in the administered solution (or exposure concentration). Typical commercial diets provided to research monkeys contain 70 to 100 ppm Mn (Knapka *et al.*, 1995). All simulations were, therefore, conducted with monkeys maintained on an 80 ppm diet, simulated as a continuous dietary exposure. The one exception was the study by Dorman *et al.* (2006a), in which a 133 ppm diet was specified. Simulated exposures followed the dosing schedules precisely as described in the studies (e.g., dosing every day, every other day, once a week, etc.). All model parameters governing internal Mn kinetics, such as diffusion constants, biliary induction parameters, and GI absorption constants, remained unchanged for all of the simulations in this study, regardless of exposure route.

Oral exposure. Oral Mn exposures were given once daily in either $MnCl_2$ or $MnSO_4$ solutions (Chandra *et al.*, 1979; Gupta *et al.*, 1980; Van Bogaert and Dallemagne, 1946). For PBPK model simulations, these exposures were treated as a daily bolus dose and intestinal absorption was modeled in the same way as dietary Mn exposure. Even though GI absorption of Mn may decrease with time in reaction to increased oral dosage levels, uncertainties surrounding the timing and magnitude of this change led us to keep F_{dietup} constant. This decision also reflected the desire to maintain the most conservative scenario by assuming that F_{dietup} did not decrease with increased Mn oral doses.

Intraperitoneal injection. Following the dosing schedule given by Mella (1924), which was the only study in this analysis to use the ip route, injections of $MnCl_2$ solution were given every other day with gradually increased dosage levels. Injection of Mn solution by the ip route was simulated by assuming that the majority of the ip dose was directly absorbed in the liver and a small fraction (F_{ip}) was absorbed into the peritoneal cavity for slow release into the liver (Fig. 1). The rate constant k_{ip} governs the movement of Mn from the peritoneal cavity to the liver. The parameters F_{ip} =0.03 and $k_{ip} = 1.0 \times 10^{-7}$ h^{-1} were previously calibrated to the whole-body elimination data of ^{54}Mn given by ip injection (Dastur *et al.*, 1971), as described by Schroeter *et al.* (2011). These parameters were unchanged for simulations of the Mella study.

Intravenous injection. Dosing for iv studies was typically once per week (Guilarte *et al.*, 2006; Olanow *et al.*, 1996) although longer durations between injections were sometimes needed depending on the state of the animal. For model simulations, the iv dose was input directly into venous blood (Fig. 1).

sc injection. Studies on sc administration used MnO_2 powder mixed with saline, olive oil, or water for injection into sc tissue (Eriksson *et al.*, 1987, 1992a,b; Suzuki *et al.*, 1975). For model simulations, the entire Mn dose from the sc injection went into a compartment representing sc tissue (Fig. 1). Mn delivery by im injection (Pentschew *et al.*, 1963) was treated the same as a sc injection. The rate constant k_{sc} = 0.0007 h^{-1}, which governs the release of Mn from the sc tissue into the venous blood, and the bioavailability of MnO_2 at the injection site (42%) were calibrated by fitting model predictions of globus pallidus Mn concentrations to the data from Suzuki *et al.* (1975) and Eriksson *et al.* (1987), where globus pallidus Mn concentrations were measured at multiple time points following sc Mn injections. These model parameters were kept constant for all sc exposure simulations.

Inhalation exposure. Inhalation exposures were simulated using the exposure concentrations and schedules (e.g., days/week, hours/day) used in the experimental procedures (Bird *et al.*, 1984; Coulston and Griffin, 1976; Dorman *et al.*, 2006a; Nishiyama *et al.*, 1977). Respiratory tract deposition was estimated for inhalation of $MnSO_4$ particles with a mass median aerodynamic diameter of 2.0 µm, a geometric SD of 1.5 and a particle density of 2.95 g/cm^3 (Dorman *et al.*, 2006a). Lung and nasal deposition efficiencies for these aerosol particles were estimated to be 40 and 27%, respectively (Schroeter *et al.*, 2011). No distinction was made between deposition on tracheobronchial or pulmonary airways due to uncertainties regarding clearance and absorption rates from these lung regions. Nasal deposition was further partitioned onto respiratory and olfactory epithelium according to an airflow allocation of 91 and 9%, respectively (Kepler *et al.*, 1998). For model simulations of the Dorman study, deposited Mn from $MnSO_4$ particles was rapidly absorbed from lung tissues and nasal respiratory epithelium into the systemic circulation or transported from nasal olfactory epithelium to the olfactory bulb. For simulations of other studies that used MnO_2 and Mn_3O_4 (Bird *et al.*, 1984; Coulston and Griffin, 1976; Nishiyama *et al.*, 1977), lung deposition was decreased to account for different particle size fractions and reduced bioavailability of less soluble Mn forms in lung tissues (Table 3).

Dose Metrics

PBPK model simulations were run from the beginning of the exposure period (time = 0) until exposures stopped or clinical outcomes were observed (time = T), as reported in each study. Simulations were run using AcslX version 3.0 (Aegis Technologies Group, Inc., Huntsville, AL). For each simulation, time-course profiles of tissue Mn concentrations following Mn exposure were evaluated. Mn concentrations in the globus pallidus were considered for the dose-response analysis because it is the likely target tissue for Mn-induced motor effects and is a conservative surrogate for other potential target brain regions that do not accumulate Mn as readily. The following three dose metrics for globus pallidus Mn concentration ($C_{gp}(t)$) were used to correlate with observed clinical effects in monkeys:

$$\text{Peak concentration} = \max\left\{C_{gp}(t)\right\}\Big|_{t=0,T}$$

$$\text{Area under the curve (AUC)} = \int_0^T C_{gp}(t)dt$$

$$\text{Average concentration} = \frac{1}{T}\cdot\int_0^T C_{gp}(t)dt\ .$$

Categorical Regression

A regression analysis was performed using the U.S. EPA CatReg software (available for download at www.epa.gov/ncea). CatReg fits a cumulative probability distribution using the method of maximum likelihood estimation to estimate the probability of a specific severity level (i.e., a category) at any specified dose. The dose can be defined using any relevant dose metric. The dose-response behavior was evaluated by plotting the severity scores for each dose group from the Mn exposure studies versus the corresponding dose metrics of peak concentration, average concentration, and AUC in the globus pallidus from the PBPK model simulations.

RESULTS

Clinical Observations

In general, studies performed prior to the 1990s had limited histological, neurochemical, or neuropathological assessments. These studies generally relied on very high-dose Mn exposures, and monkeys often developed postural instability, increased excitability, hypoactivity, falling, muscular rigidity, intention and/or action tremors, and ataxia. Studies using lower Mn doses were often associated with hypoactivity, loss of fine motor control, action tremor, or deficits in working memory. The severity scores applied to each dose group in each of the studies are shown in Table 2. Using this scoring system, the maximum summed severity score in this analysis was 9. With the exception of the inhalation exposures, most studies either used one monkey in each dose group or reported effects for individual monkeys.

PBPK Model Simulations

Three studies used the oral route to deliver a Mn solution given as a bolus dose once daily. In the study by Chandra *et al.* (1979), brain Mn concentrations were reported in monkeys following an 18-month exposure period. Increases of 173 and 24% above control levels were reported in the midbrain region and cerebellum, respectively. Model predictions for this scenario yielded maximum tissue Mn concentrations of 138 and 57% for the globus pallidus and cerebellum, respectively. The study by Gupta *et al.* (1980) used an identical exposure scenario except that slightly higher Mn doses were used (7.0 vs. 5.6 mg/kg in Chandra *et al.* (1979)) and clinical observations were reported at the end of the exposure period. In the study by Van Bogaert and Dallemagne (1946), oral doses were also administered daily but were varied during the exposure period. The PBPK model simulation of this exposure is shown in Figure 2. Globus pallidus Mn concentrations were observed to fluctuate with the daily dosing regimen and also increased with higher Mn doses. A maximum globus pallidus concentration of 1.5 µg/g was predicted at the highest oral dose of 6.3 mg/kg. Although the oral doses were high in these studies, only a small fraction was predicted to be absorbed into the systemic circulation from the GI tract, resulting in moderate increases in brain Mn concentrations.

In the study by Mella (1924), monkeys were injected by the ip route every other day with progressively higher Mn doses. The predicted globus pallidus Mn concentration for monkey no. 6 from Mella (1924) is shown in Figure 3. The initial ip dose of Mn was 0.9 mg/kg and continued for 96 days, followed by doses of 1.8 mg/kg for 48 days and 2.2 mg/kg for 22 days. The maximum predicted globus pallidus Mn concentration of 31.5 µg/g occurred during the highest dosing period. Predicted brain Mn concentrations exhibited a wide fluctuation between doses due to rapid systemic delivery from ip injection. This was followed by rapid clearance of Mn from the body after the ip injection.

Simulation of Mn globus pallidus concentration following exposure by iv injection is shown in Figure 4. In this exposure (monkey no. 2 in Olanow *et al.*, 1996), the monkey was injected once per week with variable Mn doses of 2.8–3.6 mg/kg. Extremely high brain Mn concentrations (> 50 µg/g) were predicted due to the high Mn doses and rapid delivery to tissues following direct systemic exposure from iv injection. These rapid increases in tissue Mn concentrations were followed by returns to near basal levels after several days. Similar behavior was observed in the other exposed monkeys from the Olanow study and in the iv exposures from Guilarte *et al.* (2006).

Studies that used sc injection for Mn delivery typically used much higher Mn doses (Table 1) to overcome the poor bioavailability and absorption of the insoluble MnO_2 form. Simulations of the two dose levels in Suzuki *et al.* (1975) and the single dose level in Eriksson *et al.* (1987) are shown in Figure 5. Globus pallidus Mn concentrations from the other sc studies (Eriksson *et al.*, 1992a,b; Pentschew *et al.*, 1963) displayed similar kinetic behavior, including a rapid rise in brain Mn concentrations immediately following injection followed by a slow decline to near basal levels that in some instances took over one year. Compared with ip and iv exposures, brain Mn concentrations from sc exposures remained elevated for much longer periods of time, which may be due to slow absorption of relatively insoluble Mn particles at the injection sites, as was reported by Eriksson *et al.* (1987). The model did underpredict globus pallidus concentration 1 year following the last sc exposure in Eriksson *et al.* (1987); however, because the focus of this analysis was on a comparison of brain Mn concentrations with clinical effects observed during the exposure period or shortly thereafter, parameters governing transfer from the sc compartment were selected to calibrate simulation results closer to the end of the exposure period. This underprediction could also be due to liver impairment following high-dose Mn exposure, which would reduce biliary excretion and lead to higher tissue Mn concentrations. This effect was not included in the model due to a lack of quantitative information regarding changes in hepatobiliary excretion rates following Mn exposure.

Inhalation exposure studies used several different forms of Mn (MnO_2, Mn_3O_4, and $MnSO_4$) of varying degrees of solubility (Bird *et al.*, 1984; Coulston and Griffin, 1976; Dorman *et al.*, 2006a; Nishiyama *et al.*, 1977). Model parameters were calibrated by Schroeter *et al.* (2011) to the time-course data from Dorman *et al.* (2006a) for a 90-day exposure to a $MnSO_4$ atmosphere containing 1.5 mg Mn/m^3 to simulate a rapid rise in brain Mn concentrations during the 90-day exposure followed by a return to near basal levels during the 90 days following cessation of exposure (Fig. 6). To account for differences in lung deposition and absorption due to the different particle densities, particle sizes, and solubilities of the Mn aerosols used in the other studies, a Deposition Adjustment Factor (DAF) was applied to the lung deposition fraction of Mn oxide particles to

TABLE 2
Severity Scores Applied to Clinical Effects Observed in Mn Exposure Studies in Monkeys

				Observation						
Study	Dose route	Monkey ID	Time until effect (days)	Coordination	Bradykinesia/ Gross motor skills	Rigidity/Gait disorders	Postural instability	Muscle tremors	Other clinical signs	Sum
Gupta *et al.* (1980)	oral	Group I	540	2		1				3
Van Bogaert and Dallemagne (1946)	oral	1	292							0
Mella (1924)	ip	3	253	2					1	3
			255	2		1			1	4
			275	2		1		1		4
		4	370	2					1	3
			429	2		1			1	4
			444	2		2		1		5
			473	2		3		2	2	9
		5	196	1		1			1	3
			204	1		1			2	4
		6	110	1						1
			112	1					1	2
			144	1					2	3
Olanow *et al.* (1996)	iv	1	10		2	2	1		2	7
		2	12		2	2	1		1	6
		3	49							0
Guilarte *et al.* (2006)	iv	Group 1	140	1						1
			196	1	1					2
Suzuki *et al.* (1975)	sc	1	14					1		1
			42		2			1		3
		2	21					1		1
			28	2				1	1	4
			42	2		2		1	2	7
		3	49						1	1
			56	2		2			2	6
		4	35	2					1	3
			56	2		2			2	6
		5	49					1		1
		6	42					1		1
			56					1	1	2
			63	2		2			2	6
Eriksson *et al.* (1987)	sc	1	90	1		1			1	3
			150	1	2	2				5
			210	1	2	2		1	1	7
		2	90	1	2	2		2		7
			150	2	2	2		2		8
		3 and 4	150	2	2	2				6
Eriksson *et al.* (1992a)	sc	1	189							0
		2	189		1					1
Eriksson *et al.* (1992b)	sc	1 and 2	120	1	2	2				5
Pentschew *et al.* (1963)	im	1	270				2		2	4
			435	2		2	2		2	8
Bird *et al.* (1984)	inhalation	Group 1	730							0
Nishiyama *et al.* (1977)	inhalation	A	90	1	1			1		3
		B	300							0
Coulston and Griffin (1976)	inhalation	Low dose	450							0
		High dose	161							0
Dorman *et al.* (2006)	inhalation	Low, mid, and high exposure groups	90							0

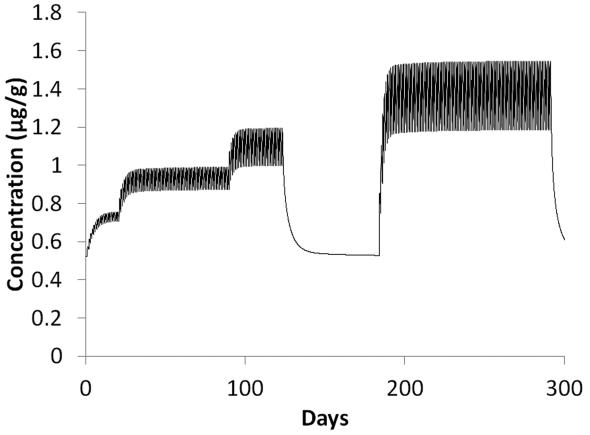

FIG. 2. PBPK model simulation of the globus pallidus Mn concentration with the dosing schedule from Van Bogaert and Dallemagne (1946). Oral Mn doses were given once daily: day 1–20: 1.3 mg/kg/day; day 21–89: 2.5 mg/kg/day; day 89–123: 3.8 mg/kg/day; day 124–183: 0 mg/kg/day; day 184–291: 6.3 mg/kg/day.

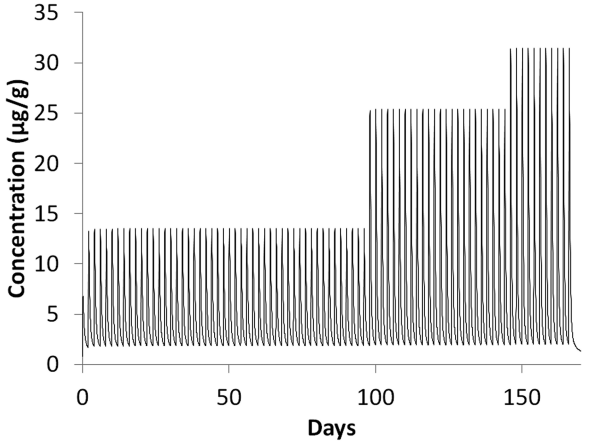

FIG. 3. Predicted Mn globus pallidus concentrations in monkey no. 6 from Mella (1924) subject to ip injection of Mn every other day. Dosing schedule: day 1–96: 0.9 mg/kg; day 97–144: 1.8 mg/kg; day 145–166: 2.2 mg/kg.

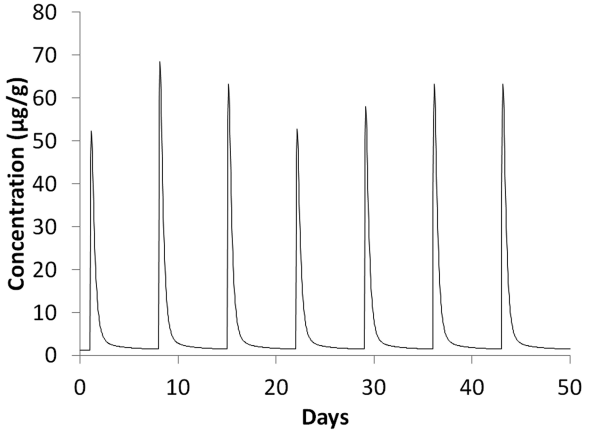

FIG. 4. Predicted Mn globus pallidus concentration in a monkey exposed by iv injection according to the dosing schedule from Olanow *et al.* (1996). The monkey was injected once a week with 2.8–3.6 mg/kg Mn.

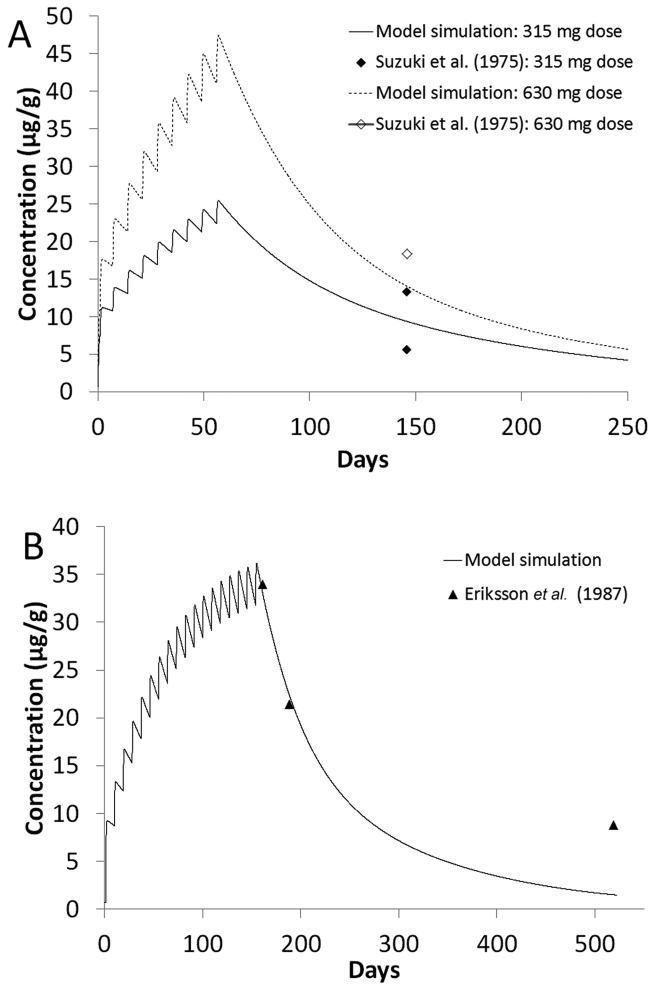

FIG. 5. Simulated globus pallidus concentrations in monkeys exposed by sc injection: (A) Monkeys were injected once a week for 9 weeks with 315 or 630 mg Mn/injection (Suzuki *et al.*, 1975); (B) Monkeys were injected on 18 occasions over 5 months with 444 mg Mn/injection (Eriksson *et al.*, 1987). The curves are model simulations, and the data points are measured globus pallidus concentrations from individual animals from Suzuki *et al.* (1975) and Eriksson *et al.* (1987).

account for their reduced bioavailability (Table 3). The DAF was calibrated based on measured end-of-exposure globus pallidus Mn concentrations. Simulations of the exposures from the Nishiyama *et al.* (1977) study are shown in Figure 6B. As with the Dorman simulations, brain Mn concentrations were predicted to rise during the exposure event and decrease once exposures stopped, although the predicted daily fluctuations from the Nishiyama simulations were less than those from the Dorman simulations due to the reduced bioavailability of the deposited Mn oxide particles in the lung. Even though the exposure concentration of 3.0 mg/m^3 was higher in the Nishiyama study, brain Mn concentrations were lower than in the Dorman study due to the lower solubility of MnO_2. Model simulations of the Bird *et al.* (1984) and Coulston and Griffin (1976) studies showed similar behavior.

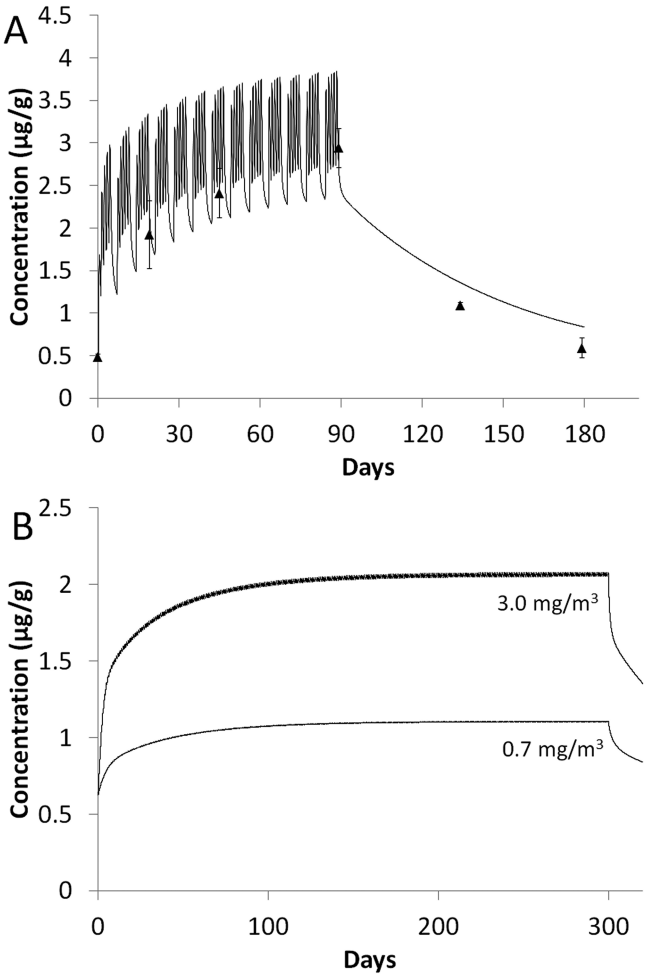

FIG. 6. Predicted globus pallidus concentrations in monkeys exposed by inhalation: (A) the exposure scenario from Dorman *et al.* (2006a): exposure to $MnSO_4$ at 1.5 mg Mn/m³ for 6 h/day, 5 days/week for 90 days; (B) the exposure scenario from Nishiyama *et al.* (1977): exposure to MnO_2 at 0.7 or 3.0 mg Mn/m³ for 22 h/day, 7 days/week for 10 months.

Dose-Response Analysis

The peak concentration, AUC (which represents cumulative internal dose), and average concentration for globus pallidus Mn concentrations during the exposure periods were computed from the PBPK model simulations for all of the dose groups from the Mn exposure studies included in this review. Severity scores applied to each dose group were plotted against all three dose metrics (Fig. 7). A steep dose-response behavior was observed when severity scores were plotted against peak globus pallidus Mn concentration (Fig. 7A). A visible pattern of increased severity was observed for peak concentrations greater than ~7 µg/g. When plotted against AUC, the progression of severity scores with exposure duration can be clearly observed (Fig. 7B). With the exception of a few dose groups (Nishiyama *et al.*, 1977; Olanow *et al.*, 1996), the severity scores started to increase for AUC values > 6000 (µg/g)-h. Although the dose-response behavior for all dose metrics exhibited significant scatter, the dose-response behavior for average concentration was not as evident, with increased severity scores for globus pallidus Mn concentrations between 4 and 30 µg/g (Fig. 7C).

A CatReg analysis was performed using the severity scores for the dose metrics of Mn peak concentration and AUC in the globus pallidus following Mn exposure. The dose metric of average globus pallidus Mn concentration was not considered for the regression analysis because the severity scores did not display a clear dose-dependent increase with concentration. Because the CatReg software limits severity scores to four categories, the severity scores summarized in Table 2 were combined to generate new severity scores for the regression analysis: 0:0, 1:1–3, 2:4–6, 3:7–9. These data were log transformed prior to the regression analysis. For the CatReg analysis, the p value was < 0.05 for both cases of peak concentration and AUC, indicating that the model fits were acceptable. R^2 values were 0.20 and 0.16 for the dose metrics of peak concentration and AUC, respectively, indicating that a small amount (20 and 16%) of

TABLE 3
Summary of Aerosol Parameters and Lung Deposition Factors Used for the Simulation of Mn Inhalation Exposures

Study	Mn form	Particle size	Density (g/cm³)	Exposure concentration (mg Mn/m³)	Deposition adjustment factor	Reported increase in globus pallidus Mn concentration (%)	Predicted increase in globus pallidus Mn concentration (%)
Dorman *et al.* (2006a)	$MnSO_4$	MMAD = 2.0 µm, GSD = 1.5	2.95	1.5	1.0[a]	513	471
Bird *et al.* (1984)	MnO_2	< 5 µm	5.0	30	0.0028[b]	79	80
Nishiyama *et al.* (1977)	MnO_2	< 2 µm	5.0	0.7	0.03[b]	133[c]	83
				3.0		183[c]	250
Coulston and Griffin (1976)	Mn_3O_4	< 6 µm	4.9	0.1	0.4[b]	122[c]	107
				5.0		Not reported	990

[a]The Dorman *et al.* (2006a) study was used to estimate model parameters, so there was no need to further adjust lung deposition.
[b]Deposition adjustment factors were calibrated to reported globus pallidus Mn concentrations from the respective study.
[c]Mn concentrations were reported in the basal ganglia. These values were used as surrogates for globus pallidus Mn concentrations.

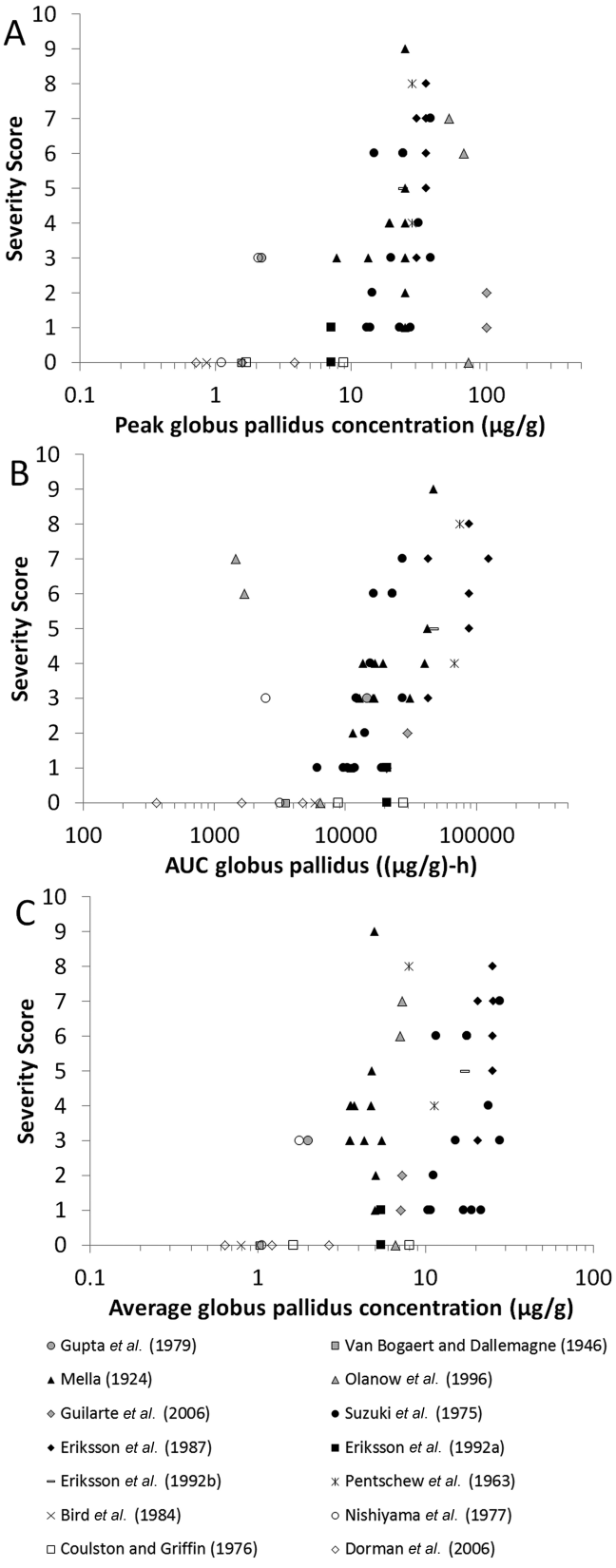

FIG. 7. Dose-response relationship for the Mn exposure studies using various dose metrics in the globus pallidus: (A) peak concentration, (B) area under the concentration curve (AUC), and (C) average concentration.

TABLE 4
Results of the CatReg Analysis of Severity Scores for the Dose Metrics of Peak Concentration and AUC from the PBPK Model Simulations. ERD_{10}, ERD_{20}, and ERD_{30} Correspond to 10, 20, and 30% Extra Risk, Respectively, of the Corresponding Severity Score

Severity score	ERD_{10}	ERD_{20}	ERD_{30}
Peak concentration (µg/g)			
1	0.8	1.4	2.0
2	5.5	9.6	13.9
3	18.1	31.6	45.9
AUC ((µg/g)-h)			
1	813.1	1477.7	2198.2
2	4860.7	8834.5	13141.7
3	20283.9	36866.5	54840.2

the variability in the data was accounted for with the regression curve. The low R^2 values are likely due to the fact that most studies reported incidence fractions of 0 or 1 because only one animal was typically used in each dose group.

CatReg was also used to provide a maximum likelihood estimate of the peak globus pallidus Mn concentrations and AUC values that would result in 10, 20, and 30% extra risk (denoted as ERD_{10}, ERD_{20}, and ERD_{30}, respectively) of attaining severity grades 1, 2, and 3 (Table 4). For example, the estimated 10% extra risk of attaining a severity score of 1, as informed by the severity scores applied to each dose group, was achieved with a peak globus pallidus Mn concentration of 0.8 µg/g or an AUC value of 813.1 µg/g-h.

DISCUSSION

An improved understanding of the dose-response relationships between Mn exposure, abnormally increased tissue Mn concentrations, and the development of neurotoxicity and other adverse clinical effects is a critical issue for Mn risk assessment. Many studies have been conducted to examine Mn-induced neurotoxicity in nonhuman primates. Most of these studies used elevated Mn doses, parenteral exposures, and variable dosing scenarios, making it difficult to extrapolate high-dose effects to potential responses from chronic low-dose inhalation exposure. There is also significant variability across studies regarding the onset and severity of neurotoxic effects. This variability is primarily due to the use of different forms of Mn and different exposure routes, leading to differences in Mn absorption, elimination, and tissue accumulation. Although it is difficult to extrapolate results from an individual study that may have only relied on several animals each acutely exposed to high Mn doses, a meta-analysis that utilizes a consistent measure of internal dose can reveal a clearer understanding of the dose-response behavior of Mn.

The analysis by Gwiazda *et al.* (2007) considered multiple studies on Mn neurotoxicity in Mn-exposed nonhuman

primates to see whether there was a consistent dose-response relationship. In their analysis, internal cumulative Mn dose was estimated from the nominal dose provided in the reviewed study (corrected for the weight fraction of Mn in the compound administered), the measured or estimated daily consumption of the exposure media, treatment duration, estimated fraction of Mn absorbed into the bloodstream, and the body weight of the animal. For the nonhuman primate studies, Gwiazda assumed Mn uptake rates of 3% for oral exposures and 100% for all other exposure routes. They reported that the cumulative Mn dose at which adverse effects were detected in monkeys was dependent on the chemical species of Mn administered. Adverse effects also demonstrated a dose dependency. For example, in monkeys, motor deficits and/or effects on the globus pallidus were seen at relatively low cumulative doses (between 20 and 70 mg Mn/kg). More profound effects and involvement of additional brain regions (e.g., caudate and putamen) were noted at higher cumulative exposure doses (> 260 mg Mn/kg). The range of exposures associated with adverse changes was over two orders of magnitude in the animal studies, which led Gwiazda *et al.* (2007) to conclude that most existing animal model studies might be of limited relevance for the risk assessment of chronic low-level Mn exposure to humans. Newland (1999) also reviewed the progressive effects of Mn exposure with increased dose from several studies, where dose was defined as the "cumulative dose of Mn in mg of Mn/kg body mass that had been administered when the sign appeared." He concluded that there is considerable variability across studies in the latency to onset of neurotoxic effects associated with Mn.

Although these earlier reviews of Mn neurotoxicity estimated cumulative Mn dose, they did not take into account internal Mn kinetics, solubility differences among the sulfate, phosphate, and oxide forms of Mn used in different studies, dose-dependent biliary excretion, or increases in Mn concentrations within brain regions (e.g., the globus pallidus) that are target tissues for Mn neurotoxicity. In the present analysis, PBPK model simulations were used to estimate toxicologically relevant internal measures of Mn accumulation within the globus pallidus: peak concentration, average concentration, and cumulative internal dose (AUC) during the Mn exposure period. Rodent studies were not described in this evaluation because, unlike nonhuman primates, they lack behavioral similarities to humans and are less sensitive to Mn than are humans and nonhuman primates (Guilarte, 2010).

The PBPK model for Mn dosimetry was derived from a rich pharmacokinetic data set in rhesus monkeys exposed to Mn by inhalation (Dorman *et al.*, 2006a). Additional exposure routes in the model (oral, ip, iv, and sc) were validated using ^{54}Mn clearance data, which showed differences in elimination rates depending on exposure route, but with all tracer studies displaying a biphasic elimination (Schroeter *et al.*, 2011). Because tracer studies reflect the overall kinetics of Mn in the body, this gives us significant confidence that the model captured the main dose-dependent characteristics of Mn uptake, elimination, and distribution in monkeys. By accounting for dose-route differences in Mn absorption and elimination, we were able to estimate common dose metrics among the many Mn exposure studies that have been conducted in nonhuman primates, regardless of the exposure route, solubility, or dosing schedule used in the animal studies.

The PBPK model structure used in this study was originally developed to describe Mn tissue dosimetry in rats subject to dietary and inhalation exposure (Nong *et al.*, 2008). This model structure was subsequently extended to monkeys and humans with additional exposure routes added as needed to accommodate various experimental methods used to administer Mn and ^{54}Mn (Nong *et al.*, 2009; Schroeter *et al.*, 2011). These modeling efforts helped inform key processes involved in Mn kinetics, including saturable tissue binding, asymmetric flux into brain regions, and dose-dependent biliary excretion that allow tissue Mn concentrations to remain fairly constant during low levels of exposure and to rise rapidly during high-dose episodes, as was observed in animals. The models have also been recently used to guide a tissue dose–based risk assessment approach and to study Mn tissue accumulation in sensitive subpopulations (Andersen *et al.*, 2010; Taylor *et al.*, 2012). The ability of the PBPK models to consistently describe Mn kinetics across multiple species and exposure routes indicates that the models have accurately captured the dose-dependent characteristics of Mn disposition. For this study, several parameters governing portal-of-entry effects were estimated to accurately simulate the delivery of Mn to the systemic circulation from multiple exposure routes. However, the parameters governing internal Mn kinetics, such as diffusion rate constants and tissue binding parameters, were unchanged for all simulations regardless of exposure route. Once further biochemical details for tissue binding, membrane transport, and Mn retention in enterocytes (to name a few examples) become available, then these parameters can be appropriately refined in the model. Slight reparameterization of other rate constants may then be necessary to maintain the same quality as the current model-fit with pharmacokinetic data in animals because, as pointed out by Schroeter *et al.* (2011), model simulations are sensitive to some parameters such as the biliary excretion and diffusion rate constants.

This analysis depended not only on an accurate estimation of tissue Mn concentrations following Mn exposure but also on a consistent application of severity scores to multiple studies from numerous investigators over a wide period of time. Our clinical understanding of neurochemical changes associated with Mn neurotoxicity has undergone significant revisions during the past decade as single photon emission computed tomography and positron emission tomography studies have been used. In addition, some studies performed in monkeys have assessed dopamine, γ-aminobutyric acid, and other neurotransmitters in Mn-exposed monkeys. Guilarte (2010) performed a thorough review of the available human and nonhuman primate Mn neurotoxicity data and concluded that there

is overwhelming evidence showing that Mn-induced neurological signs do not involve degeneration of midbrain dopamine neurons. Moreover, handling of brain tissue samples in some early neurochemistry studies (e.g., Neff *et al.*, 1969) was of concern because tissue samples from control and Mn-treated animals were subjected to different storage times and conditions (Guilarte, 2010). Thus, unlike Gwiazda *et al.* (2007), we did not focus on brain dopamine changes as an endpoint of interest in this re-evaluation because too few contemporary studies would support this analysis.

Clinical evaluations, including an assessment of animal behavior, are a key component in neurotoxicity testing (Tilson and Moser, 1992). One challenge associated with this study is the confidence we have in the ability of the original study investigators to assess clinical signs in Mn-exposed monkeys. The *a priori* use of a scoring system is known to improve the ability to detect subclinical disease in animals. Among the studies we reviewed, only the one performed by Guilarte *et al.* (2006) fully described their observational methods and provided a scoring scale. Guilarte rated a variety of behaviors using a scale developed for a monkey model of parkinsonism (Schneider and Kovelowski, 1990). Each item was rated as 0 (normal), 1 (mild), 2 (moderate), or 3 (severe) with disability (up to a maximum score) and dystonia/dyskinesia (maximum score of 21) being assessed individually. Guilarte also used an automated system to assess gross motor activity and a separate test apparatus to assess fine motor skills in their Mn-exposed animals. Guilarte *et al.* (2006) reported that behavioral rating scores in Mn-exposed monkeys increased slightly as the exposure duration progressed. Throughout the course of the study, animals appeared grossly normal and detected changes were considered very subtle (we rated these effects as mild with affected animals receiving a score of 2/17 in our scoring system).

Our data analysis is further complicated by the lack of detailed reporting of when clinical signs emerged (often given in weeks or months rather than days). For example, on the one hand, Mella (1924) provided a detailed account of clinical signs associated with Mn exposure every other day during the exposure period, whereas the study by Gupta *et al.* (1980) merely reported that clinical signs were evident after 18 months of exposure. In the latter case, because no other information was given regarding the onset of effects, we had to assume that they began at 18 months. Another confounder that should be recognized is that many of the studies fail to describe whether or not animal selection was randomized (unlikely given the extremely small numbers of animals used) or whether the person performing the animal observations were blinded to treatment groups. As in human studies, failure to control for these confounders often leads to an overestimate of the effect seen in animals (Bebarta *et al.*, 2003).

Our data analysis method also warrants examination. The clinical scoring system we used develops categorical data. The analysis of such categorical data has been less robustly explored in neurotoxicology (Markgraf *et al.*, 2010). We utilized a descriptive approach that relied on the experience of the evaluator (David D. Dorman) to assess whether the reported clinical signs were abnormal and consistent with Mn neurotoxicity. Markgraf *et al.* (2010) compared the use of an experienced behavioral toxicologist to more routine statistical approaches in interpreting rodent functional observational battery data. Similar to our methods, the behavioral toxicologist evaluating the data sets in the Markgraf study was not blinded prior to evaluation. Markgraf found that professional judgments and statistical approaches yielded similar estimates of an individual study no-effect level.

Despite the use of different Mn forms, multiple exposure routes, a wide range of dose levels, and possible inconsistencies among studies regarding the reporting of Mn-induced effects, a clear dose-response behavior was observed when severity scores were analyzed versus the PBPK model–derived dose metrics of peak concentration and cumulative dose (AUC) in the globus pallidus region. This analysis can help inform threshold levels for dose-dependent transitions in effects from Mn exposure. The fact that peak concentration demonstrated a sharp transition in effects indicates the existence of a threshold brain Mn concentration for Mn-induced effects. For example, from the CatReg analysis, a 10% extra risk for a mild response (severity level 1) occurred at a peak concentration of 0.8 μg/g (Table 4). This value is 81% higher than the average basal Mn concentration in the globus pallidus from these studies. A rapid increase in severity score was observed for peak Mn concentrations > 7 μg/g. Likewise, when plotted against AUC, an increase in severity with cumulative dose was also observed, indicating a progression of effects with increasing dose and exposure duration.

Although most of the data points followed a sigmoidal dose-response curve, there were several exceptions, which were expected given the wide range of experimental conditions used in the studies. For example, for peak globus pallidus concentration (Fig. 7A), the results from the Gupta *et al.* (1980) study (oral dosing) and from the high-dose group (3.0 mg/m^3 inhalation exposure concentration) of the Nishiyama *et al.* (1977) study displayed mild clinical effects at lower peak brain concentrations (~2 μg/g). The Nishiyama study was the only inhalation exposure study in this analysis to observe Mn-induced clinical effects, despite other inhalation studies using higher exposure concentrations or having higher estimated brain Mn concentrations. Some possible reasons for these discrepancies are that brain Mn concentrations were reported by Nishiyama as μg Mn per g dry tissue weight in the basal ganglia region. To be consistent with model predictions, these values were reduced by 80% (Molokhia and Smith, 1967) to convert to wet weight. It is also possible that basal ganglia Mn concentrations are not a suitable surrogate for globus pallidus Mn concentrations, as the basal ganglia includes other brain regions in addition to the globus pallidus. The Gupta study observed mild effects after oral Mn dosing, whereas the study by Van Bogaert and Dallemagne (1946) did not report any effects after similar

oral dosing schedules. The peak concentration predicted for the Gupta study was slightly greater than that for the Van Bogaert and Dallemagne (1946) study, but when the data points were plotted versus AUC, both points fell in line with other studies, indicating the importance of accounting for exposure duration as a predictor of toxicity. These discrepancies may also be due to differences in Mn absorption among individuals or may reflect a dose-dependent transition region where some animals begin to show effects whereas others do not.

Another aberration in the dose-response curve for peak concentration occurred from one of the animals in the Olanow *et al.* (1996) study, where globus pallidus Mn concentrations were predicted to be almost 90 µg/g, yet no clinical effects were observed. This contrasts with two other animals from the same study that received slightly lower Mn doses yet demonstrated severe clinical effects. Olanow attributed this to individual variability to Mn intoxication. Simulations of the Guilarte *et al.* (2006) study also predicted high brain Mn concentrations following iv injection of Mn, yet only mild effects were observed. Model predictions for high-dose Mn iv injections demonstrated rapid increases in tissue Mn concentrations immediately following the injection, followed by rapid decreases in the days following injection. This behavior led to lower AUC values compared with sc injections, where much slower decreases in tissue Mn concentrations were predicted. There was no data available to validate the rise in tissue Mn concentrations following iv injection. Model predictions could possibly be improved if data existed for brain Mn concentrations at several time points following iv injection. Although Guilarte *et al.* (2006) reported globus pallidus Mn concentrations in iv-injected monkeys, measurements were taken 33 days after the last Mn injection and therefore were of limited use for validating peak tissue concentrations that occur soon after injection.

Finally, we offer one additional comment regarding the interpretation of the dose-response data. Cumulative dose (AUC) correlated with toxicity at the high-exposure situations considered in this analysis. This conclusion does not imply that equivalent cumulative doses experienced over a much longer duration (e.g., 70 years) at lower daily doses would generate neurological effects. This current analysis clearly showed that the tissue concentration correlated with neurological responses. In the case of inhalation, the PBPK models demonstrate that at or below an identifiable dose-dependent transition point for tissue accumulation (exposures of approximately 0.01 mg/m^3), tissue Mn does not increase significantly above background concentrations because of natural homeostatic mechanisms (Andersen *et al.*, 2010; Schroeter *et al.*, 2011). Our analysis, then, indicates that neurological responses in rhesus monkeys correlate well with integrated tissue exposure (i.e., AUC) above a limiting globus pallidus concentration of about 7 µg/g (see Figure 7A).

An approach to risk assessment for inhaled Mn has been suggested that considers increases in target tissue dose above background tissue levels (Andersen *et al.*, 2010). The dose-response behavior presented here lends validity to this approach by evaluating internal measures of dose in the central nervous system that relate to Mn toxicity. Homeostatic controls maintain relatively stable Mn tissue concentrations by regulating intestinal absorption and biliary excretion. Toxicity results when these homeostatic controls are overwhelmed under conditions of excessive exposure, which was common in many of the high-dose studies examined in this study. This analysis clearly demonstrates that the dose response for the neurotoxic effects of Mn is independent of exposure route and supports the use of peak or cumulative tissue Mn concentrations as appropriate dose metrics. This analysis also provides evidence of a dose-dependent transition in the mode of action for the neurological effects of Mn that should be considered in risk assessments for this essential metal.

FUNDING

This work was sponsored in part by the University of Ottawa. The development of the PBPK models used in this publication was sponsored by Afton Chemical Corporation in satisfaction of registration requirements arising under Section 211(a) and (b) of the Clean Air Act and corresponding regulations at 40 C. F. R. Subsections 79.50 et seq.

ACKNOWLEDGMENTS

The authors gratefully acknowledge Drs Harry Roels and Daniel Krewski for helpful conversations regarding this analysis.

REFERENCES

Abboud, S., and Haile, D. J. (2000). A novel mammalian iron-regulated protein involved in intracellular iron metabolism. *J. Biol. Chem.* **275,** 19906–19912.

Agency for Toxic Substances Disease Registry (ATSDR). (2000). *Toxicological Profile for Manganese*. U.S. Department for Health and Human Services, Public Health Service, Atlanta, GA.

Alves, G., Thiebot, J., Tracqui, A., Delangre, T., Guedon, C., and Lerebours, E. (1997). Neurologic disorders due to brain manganese deposition in a jaundiced patient receiving long-term parenteral nutrition. *J. Parenter. Enteral Nutr.* **21,** 41–45.

Andersen, M. E., Dorman, D. C., Clewell, H. J., 3rd, Taylor, M. D., and Nong, A. (2010). Multi-dose-route, multi-species pharmacokinetic models for manganese and their use in risk assessment. *J. Toxicol. Environ. Health Part A* **73,** 217–234.

Aschner, M., Erikson, K. M., and Dorman, D. C. (2005). Manganese dosimetry: Species differences and implications for neurotoxicity. *Crit. Rev. Toxicol.* **35,** 1–32.

Ballatori, N., Miles, E., and Clarkson, T. W. (1987). Homeostatic control of manganese excretion in the neonatal rat. *Am. J. Physiol.* **252**(5 Pt 2), R842–R847.

Bebarta, V., Luyten, D., and Heard, K. (2003). Emergency medicine animal research: Does use of randomization and blinding affect the results? *Acad. Emerg. Med.* **10,** 684–687.

Bird, E. D., Anton, A. H., and Bullock, B. (1984). The effect of manganese inhalation on basal ganglia dopamine concentrations in rhesus monkey. *Neurotoxicology* **5,** 59–65.

Bouchard, M. F., Sauvé, S., Barbeau, B., Legrand, M., Brodeur, M. È., Bouffard, T., Limoges, E., Bellinger, D. C., and Mergler, D. (2011). Intellectual impairment in school-age children exposed to manganese from drinking water. *Environ. Health Perspect.* **119,** 138–143.

Chandra, S. V., Srivastava, R. S., and Shukla, G. S. (1979). Regional distribution of metals and biogenic amines in the brain of monkeys exposed to manganese. *Toxicol. Lett.* **4,** 189–192.

Coulston, F., and Griffin, T. (1976). *Inhalation Toxicology of Airborne Particulate Manganese in Rhesus Monkeys. EPA Contract 68-02-0710*. Institute of Comparative and Human Toxicology, Albany Medical College, and New Mexico International Center of Environmental Safety, Holloman Air Force Base, New Mexico.

Dastur, D. K., Manghani, D. K., and Raghavendran, K. V. (1971). Distribution and fate of 54Mn in the monkey: Studies of different parts of the central nervous system and other organs. *J. Clin. Invest.* **50,** 9–20.

Dorman, D. C., Struve, M. F., Marshall, M. W., Parkinson, C. U., James, R. A., and Wong, B. A. (2006a). Tissue manganese concentrations in young male rhesus monkeys following subchronic manganese sulfate inhalation. *Toxicol. Sci.* **92,** 201–210.

Dorman, D. C., Struve, M. F., Wong, B. A., Dye, J. A., and Robertson, I. D. (2006b). Correlation of brain magnetic resonance imaging changes with pallidal manganese concentrations in rhesus monkeys following subchronic manganese inhalation. *Toxicol. Sci.* **92,** 219–227.

Eriksson, H., Gillberg, P. G., Aquilonius, S. M., Hedström, K. G., and Heilbronn, E. (1992a). Receptor alterations in manganese intoxicated monkeys. *Arch. Toxicol.* **66,** 359–364.

Eriksson, H., Tedroff, J., Thuomas, K. A., Aquilonius, S. M., Hartvig, P., Fasth, K. J., Bjurling, P., Långström, B., Hedström, K. G., and Heilbronn, E. (1992b). Manganese induced brain lesions in Macaca fascicularis as revealed by positron emission tomography and magnetic resonance imaging. *Arch. Toxicol.* **66,** 403–407.

Eriksson, H., Mägiste, K., Plantin, L. O., Fonnum, F., Hedström, K. G., Theodorsson-Norheim, E., Kristensson, K., Stålberg, E., and Heilbronn, E. (1987). Effects of manganese oxide on monkeys as revealed by a combined neurochemical, histological and neurophysiological evaluation. *Arch. Toxicol.* **61,** 46–52.

Fell, J. M., Reynolds, A. P., Meadows, N., Khan, K., Long, S. G., Quaghebeur, G., Taylor, W. J., and Milla, P. J. (1996). Manganese toxicity in children receiving long-term parenteral nutrition. *Lancet* **347,** 1218–1221.

Furchner, J. E., Richmond, C. R., and Drake, G. A. (1966). Comparative metabolism of radionuclides in mammals. 3. Retention of manganese-54 in the mouse, rat, monkey and dog. *Health Phys.* **12,** 1415–1423.

Goss, J. A., Barshes, N. R., Karpen, S. J., Gao, F. Q., and Wyllie, S. (2008). Liver ischemia and ischemia-reperfusion induces and traffics the multi-specific metal transporter Atp7b to bile duct canaliculi: Possible preferential transport of iron into bile. *Biol. Trace Elem. Res.* **122,** 26–41.

Guilarte, T. R. (2010). Manganese and Parkinson's disease: A critical review and new findings. *Environ. Health Perspect.* **118,** 1071–1080.

Guilarte, T. R., Chen, M. K., McGlothan, J. L., Verina, T., Wong, D. F., Zhou, Y., Alexander, M., Rohde, C. A., Syversen, T., Decamp, E., *et al.* (2006). Nigrostriatal dopamine system dysfunction and subtle motor deficits in manganese-exposed non-human primates. *Exp. Neurol.* **202,** 381–390.

Gupta, S. K., Murthy, R. C., and Chandra, S. V. (1980). Neuromelanin in manganese-exposed primates. *Toxicol. Lett.* **6,** 17–20.

Gwiazda, R., Lucchini, R., and Smith, D. (2007). Adequacy and consistency of animal studies to evaluate the neurotoxicity of chronic low-level manganese exposure in humans. *J. Toxicol. Environ. Health Part A* **70,** 594–605.

Imbert, C., Bezard, E., Guitraud, S., Boraud, T., and Gross, C. E. (2000). Comparison of eight clinical rating scales used for the assessment of MPTP-induced parkinsonism in the Macaque monkey. *J. Neurosci. Methods* **96,** 71–76.

Jiang, L., Ranganathan, P., Lu, Y., Kim, C., and Collins, J. F. (2011). Exploration of the copper-related compensatory response in the Belgrade rat model of genetic iron deficiency. *Am. J. Physiol. Gastrointest. Liver Physiol.* **301,** G877–G886.

Kawamura, R., Ikuta, H., Fukuzumi, S., Yamada, R., Tsubaki, S., Kodama, T., and Kurata, S. (1941). Intoxication by manganese in well water. *Arch. Exp. Med.* **18,** 145–169.

Kepler, G. M., Richardson, R. B., Morgan, K. T., and Kimbell, J. S. (1998). Computer simulation of inspiratory nasal airflow and inhaled gas uptake in a rhesus monkey. *Toxicol. Appl. Pharmacol.* **150,** 1–11.

Klaassen, C. D. (1974). Biliary excretion of manganese in rats, rabbits, and dogs. *Toxicol. Appl. Pharmacol.* **29,** 458–468.

Knapka, J. J., Barnard, D. E., Bayne, K. A. L., Lewis, S. M., Marriott, B. M., and Oftedal, O. T. (1995). Nutrition. In *Nonhuman Primates in Biomedical Research: Biology and Management* (B. T. Bennett, C. R. Abee, and R. Henrickson, Eds.), pp 211–248. Academic Press, New York, NY.

Kondakis, X. G., Makris, N., Leotsinidis, M., Prinou, M., and Papapetropoulos, T. (1989). Possible health effects of high manganese concentration in drinking water. *Arch. Environ. Health* **44,** 175–178.

Kurlan, R., Kim, M. H., and Gash, D. M. (1991). Oral levodopa dose-response study in MPTP-induced hemiparkinsonian monkeys: Assessment with a new rating scale for monkey parkinsonism. *Mov. Disord.* **6,** 111–118.

Lucchini, R. G., Albini, E., Benedetti, L., Borghesi, S., Coccaglio, R., Malara, E. C., Parrinello, G., Garattini, S., Resola, S., and Alessio, L. (2007). High prevalence of Parkinsonian disorders associated to manganese exposure in the vicinities of ferroalloy industries. *Am. J. Ind. Med.* **50,** 788–800.

Markgraf, C. G., Cirino, M., and Meredith, J. (2010). Comparison of methods for analysis of functional observation battery (FOB) data. *J. Pharmacol. Toxicol. Methods* **62,** 89–94.

Mella, H. (1924). The experimental production of basal ganglion symptomatology in macacus rhesus. *Arch. Neurol. Psychiat.* **11,** 405–417.

Molokhia, M. M., and Smith, H. (1967). Trace elements in the lung. *Arch. Environ. Health* **15,** 745–750.

Myers, J. E., Thompson, M. L., Ramushu, S., Young, T., Jeebhay, M. F., London, L., Esswein, E., Renton, K., Spies, A., Boulle, A., *et al.* (2003). The nervous system effects of occupational exposure on workers in a South African manganese smelter. *Neurotoxicology* **24,** 885–894.

Neff, N. H., Barrett, R. E., and Costa, E. (1969). Selective depletion of caudate nucleus dopamine and serotonin during chronic manganese dioxide administration to squirrel monkeys. *Experientia* **25,** 1140–1141.

Newland, M. C. (1999). Animal models of manganese's neurotoxicity. *Neurotoxicology* **20,** 415–432.

Newland, M. C., and Weiss, B. (1992). Persistent effects of manganese on effortful responding and their relationship to manganese accumulation in the primate globus pallidus. *Toxicol. Appl. Pharmacol.* **113,** 87–97.

Newland, M. C., Ceckler, T. L., Kordower, J. H., and Weiss, B. (1989). Visualizing manganese in the primate basal ganglia with magnetic resonance imaging. *Exp. Neurol.* **106,** 251–258.

Nishiyama, K., Suzuki, Y., Fujii, N., Yano, H., Ohnishi, K., and Miyai, T. (1977). Biochemical changes and manganese distribution in monkeys exposed to manganese dioxide dust. *Tokushima J. Exp. Med.* **24,** 137–145.

Nong, A., Taylor, M. D., Clewell, H. J., 3rd, Dorman, D. C., and Andersen, M. E. (2009). Manganese tissue dosimetry in rats and monkeys: Accounting for dietary and inhaled Mn with physiologically based pharmacokinetic modeling. *Toxicol. Sci.* **108,** 22–34.

Nong, A., Teeguarden, J. G., Clewell, H. J., 3rd, Dorman, D. C., and Andersen, M. E. (2008). Pharmacokinetic modeling of manganese in the rat IV: Assessing factors that contribute to brain accumulation during inhalation exposure. *J. Toxicol. Environ. Health Part A* **71,** 413–426.

Olanow, C. W., Good, P. F., Shinotoh, H., Hewitt, K. A., Vingerhoets, F., Snow, B. J., Beal, M. F., Calne, D. B., and Perl, D. P. (1996). Manganese

intoxication in the rhesus monkey: A clinical, imaging, pathologic, and biochemical study. *Neurology* **46,** 492–498.

Pal, P. K., Samii, A., and Calne, D. B. (1999). Manganese neurotoxicity: A review of clinical features, imaging and pathology. *Neurotoxicology* **20,** 227–238.

Pentschew, A., Ebner, F. F., and Kovatch, R. M. (1963). Experimental manganese encephalopathy in monkeys. A preliminary report. *J. Neuropathol. Exp. Neurol.* **22,** 488–499.

Perl, D. P., and Olanow, C. W. (2007). The neuropathology of manganese-induced Parkinsonism. *J. Neuropathol. Exp. Neurol.* **66,** 675–682.

Roels, H., Lauwerys, R., Buchet, J. P., Genet, P., Sarhan, M. J., Hanotiau, I., de Fays, M., Bernard, A., and Stanescu, D. (1987). Epidemiological survey among workers exposed to manganese: Effects on lung, central nervous system, and some biological indices. *Am. J. Ind. Med.* **11,** 307–327.

Schneider, J. S., Decamp, E., Koser, A. J., Fritz, S., Gonczi, H., Syversen, T., and Guilarte, T. R. (2006). Effects of chronic manganese exposure on cognitive and motor functioning in non-human primates. *Brain Res.* **1118,** 222–231.

Schneider, J. S., and Kovelowski, C. J., 2nd. (1990). Chronic exposure to low doses of MPTP. I. Cognitive deficits in motor asymptomatic monkeys. *Brain Res.* **519,** 122–128.

Schroeter, J. D., Nong, A., Yoon, M., Taylor, M. D., Dorman, D. C., Andersen, M. E., and Clewell, H. J., 3rd. (2011). Analysis of manganese tracer kinetics and target tissue dosimetry in monkeys and humans with multi-route physiologically based pharmacokinetic models. *Toxicol. Sci.* **120,** 481–498.

Suzuki, Y., Mouri, T., Suzuki, Y., Nishiyama, K., and Fujii, N. (1975). Study of subacute toxicity of manganese dioxide in monkeys. *Tokushima J. Exp. Med.* **22,** 5–10.

Taylor, M. D., Clewell, H. J., 3rd, Andersen, M. E., Schroeter, J. D., Yoon, M., Keene, A. M., and Dorman, D. C. (2012). Update on a pharmacokinetic-centric alternative tier II program for MMT-part II: Physiologically based pharmacokinetic modeling and manganese risk assessment. *J. Toxicol.* Article ID 791431.

Tilson, H. A., and Moser, V. C. (1992). Comparison of screening approaches. *Neurotoxicology* **13,** 1–13.

Ulrich, C. E., Rinehart, W., Busey, W., and Dorato, M. A. (1979). Evaluation of the chronic inhalation toxicity of a manganese oxide aerosol. II. Clinical observations, hematology, clinical chemistry and histopathology. *Am. Ind. Hyg. Assoc. J.* **40,** 322–329.

Van Bogaert, L., and Dallemagne, M. J. (1946). Approches experimentales des troubles nerveux du manganisme. *Monatisshrift. Psychiat. Neurol.* **111/112,** 61–89.

Yoon, M., Schroeter, J. D., Nong, A., Taylor, M. D., Dorman, D. C., Andersen, M. E., and Clewell, H. J., 3rd. (2011). Physiologically based pharmacokinetic modeling of fetal and neonatal manganese exposure in humans: Describing manganese homeostasis during development. *Toxicol. Sci.* **122,** 297–316.

Toxicology and Applied Pharmacology 322 (2017) 27–40

Contents lists available at ScienceDirect

Toxicology and Applied Pharmacology

journal homepage: www.elsevier.com/locate/taap

A tissue dose-based comparative exposure assessment of manganese using physiologically based pharmacokinetic modeling—The importance of homeostatic control for an essential metal

P. Robinan Gentry [a,*], Cynthia Van Landingham [a], William G. Fuller [a], Sandra I. Sulsky [b], Tracy B. Greene [a], Harvey J. Clewell III [c], Melvin E. Andersen [c], Harry A. Roels [d], Michael D. Taylor [e], Athena M. Keene [f]

[a] Ramboll Environ US Corporation, 3701 Armand St., Monroe, LA 71201, United States
[b] Ramboll Environ US Corporation, Amherst, MA, United States
[c] ScitoVation, RTP, NC, United States
[d] Université Catholique de Louvain, Brussels, Belgium
[e] NIPERA, Durham, NC, United States
[f] Afton Chemical Corporation, Richmond, VA, United States

ARTICLE INFO

Article history:
Received 28 October 2016
Revised 17 February 2017
Accepted 20 February 2017
Available online 22 February 2017

Keywords:
Margin of safety
MOS
Manganese
PBPK
Pharmacokinetics

ABSTRACT

A physiologically-based pharmacokinetic (PBPK) model (Schroeter et al., 2011) was applied to simulate target tissue manganese (Mn) concentrations following occupational and environmental exposures. These estimates of target tissue Mn concentrations were compared to determine margins of safety (MOS) and to evaluate the biological relevance of applying safety factors to derive acceptable Mn air concentrations. Mn blood concentrations measured in occupational studies permitted verification of the human PBPK models, increasing confidence in the resulting estimates. Mn exposure was determined based on measured ambient air Mn concentrations and dietary data in Canada and the United States (US). Incorporating dietary and inhalation exposures into the models indicated that increases in target tissue concentrations above endogenous levels only begin to occur when humans are exposed to levels of Mn in ambient air (i.e. >10 μg/m^3) that are far higher than those currently measured in Canada or the US. A MOS greater than three orders of magnitude was observed, indicating that current Mn air concentrations are far below concentrations that would be required to produce the target tissue Mn concentrations associated with subclinical neurological effects. This application of PBPK modeling for an essential element clearly demonstrates that the conventional application of default factors to "convert" an occupational exposure to an equivalent continuous environmental exposure, followed by the application of safety factors, is not appropriate in the case of Mn. PBPK modeling demonstrates that the relationship between ambient Mn exposures and dose-to-target tissue is not linear due to normal tissue background levels and homeostatic controls.

1. Introduction

Manganese (Mn) is an essential element required as a cofactor for many enzymes with key biological functions, yet studies demonstrate that adverse health effects occur following exposure to high concentrations. Manganese exposure can occur through the diet; releases from industrial sources such as ferroalloy production plants, iron and steel foundries, alkaline battery manufacture, power plants, and coke ovens; and other sources. Long-term exposures to high concentrations of Mn are neurotoxic, leading to deficits in neuromotor and cognitive domains (Guilarte, 2010, 2013; Roels et al., 2012).

Although risk assessments for Mn have attempted to quantitatively estimate potential toxicity from inhalation exposures including those in the ambient environment, many of these assessments rely largely on the results from occupational cohorts where exposures may be many orders of magnitude higher than ambient air exposures of the general population. Using external concentration as the "dose metric" may not adequately address nonlinearities in complex biological processes (e.g. absorption, metabolism), resulting in target tissue concentrations that are not linearly correlated with external concentrations. Accounting for these nonlinearities is especially important for chemicals that are essential elements, whereby individuals already have substantial background tissue levels resulting from typical dietary intake.

In evaluating target tissue dosimetry following chemical exposures, the application of physiologically-based pharmacokinetic (PBPK) models has been suggested as a valuable tool. These models provide a

* Corresponding author.
E-mail address: rgentry@ramboll.com (P.R. Gentry).

http://dx.doi.org/10.1016/j.taap.2017.02.015

method for integrating toxicological and pharmacokinetic data and provide valuable alternatives to using external exposures in risk assessment (Barton and Clewell, 2000; Clewell and Andersen, 1985; Clewell et al., 1995). Use of PBPK modeling is the preferred approach for estimating internal doses of chemical substances for route and species extrapolation, preferably at the target tissue, that would then be used in dose-response modeling for deriving acceptable regulatory levels (USEPA, 2005, 2006). PBPK models also offer advantages for extrapolation across large differences in exposure concentrations, such as those that exist when attempting to compare the potential for health effects at Mn concentrations from occupational studies to those following exposure to lower ambient air concentrations (Andersen et al., 1999). This investigation relies upon a published human PBPK model developed by Schroeter et al. (2011) to evaluate target tissue concentrations following reported occupational exposures, as well as measured ambient air concentrations of Mn and the potential for health effects.

Traditional approaches to risk assessment for noncancer toxicants use a threshold approach where safety factors are applied to the highest concentration of the toxic agent that does not elicit toxicity (the no observed adverse effect level [NOAEL] or a benchmark dose [BMD]) to estimate an acceptable exposure concentration where even sensitive subpopulations will be protected. Evaluating the "margin of safety" (MOS) is an alternative approach where the maximum amount of exposure producing no measurable adverse effect is divided by the actual amount of human exposure in a population to understand the magnitude of the difference between actual exposures and concentrations associated with potential for health effects. By examining the target tissue Mn concentrations associated with occupational air exposure concentrations for which adverse changes in one or more specific physiological functions have been reported, comparisons can be made to target tissue exposures expected following exposure to Mn from ambient air. The MOS thus reveals how much of an increase in the ambient Mn air concentrations would be required to produce target tissue levels at or near the range where adverse impacts might be expected to occur.

The approach applied in this assessment is grounded in the synthesis of all available data and information on biological mechanisms, examines the application of PBPK models in risk assessment, and provides a comparison to the traditional risk assessment approach that incorporates default adjustments. Our investigation demonstrates that use of a MOS approach for an essential nutrient such as Mn allows for a harmonized biologically-based approach to risk assessment that is more specific to the chemical of interest than the traditional approach that relies on safety factors. Toward this goal, we applied a human adult PBPK model for Mn (Schroeter et al., 2011) to investigate: 1) target tissue and corresponding air concentrations of Mn below which subclinical neurological effects would not be expected to occur, based on observations reported in workers in occupational studies; 2) target tissue concentrations corresponding to ambient air concentrations of Mn; and 3) the range of air concentrations associated with increases of Mn above background levels in the target tissue.

2. Materials and methods

Epidemiological, toxicological, and pharmacokinetic studies of Mn and exposure studies of the levels of Mn in the environment have been conducted, some of which have been reported in the published literature. However, all of these studies have been conducted independently of one another. The approach presented here allows for the integration of epidemiological, toxicological, and exposure data in a quantitative manner, along with pharmacokinetic data to lay the foundation for a new approach to dose-response and exposure analyses for Mn – the estimation of target tissue concentrations.

Epidemiological and toxicological studies that provided quantitative exposure and response data were selected. The epidemiological/toxicological/exposure data were evaluated to determine if the quantitative information could be used in combination with published PBPK models to estimate target tissue concentrations of Mn and at what target tissue concentrations potential health effects would be expected. In addition, data sources from both Canada and the United States (US) were surveyed to provide data that would allow for the estimation of potential exposure to Mn in both the diet and ambient air. Potential exposure from ingestion of drinking water containing Mn was not considered.

2.1. Selection of epidemiological data

Literature involving occupational studies of workers exposed to Mn was identified through searches of PubMed and Google Scholar, as well as review of the citations/reference lists in the studies identified. The identified studies were reviewed to determine if sufficient quantitative information on Mn exposures were provided in order to allow modeling of tissue Mn concentrations in exposed workers. Ideally, the most useful epidemiological studies would include the following: 1) a well-defined exposed population with little or no exposure to other neurotoxicants, 2) a well-defined and appropriate comparison group, 3) objective measures of neurological deficits (e.g. as opposed to self-reported symptoms or measured effects of unknown clinical importance), 4) estimates of personal exposure to respirable fractions of Mn, and 5) neurological measures collected for the same individuals. At a minimum, studies needed to provide quantitative exposure estimates for respirable Mn and objective measures of neurological deficits. The level of detail necessary to model tissue concentrations of Mn requires individual exposure and response data; however, this is often absent from published studies. Therefore, the raw data was relied upon when available.

2.2. Exposure to manganese from ambient air[1]

Air monitoring data were obtained from publicly available databases in both Canada and the US for the years 1991 through 2014, inclusively, to allow estimation of potential Mn concentrations in the ambient air. Sources of air monitoring data were the Canadian National Air Pollution Surveillance Network (NAPS, 2015) and the US Technology Transfer Network Air Quality System (USEPA, 2015). Total suspended particles (TSP) and particulate matter (PM) with aerodynamic diameter less than or equal to 10 μm (PM_{10}), 2.5 μm ($PM_{2.5}$), and between 10 and 2.5 μm ($PM_{10-2.5}$) were measured at these monitoring networks. The Canadian monitoring stations reported Mn concentrations from either $PM_{2.5}$ or $PM_{10-2.5}$, while the US stations generally reported Mn concentrations from TSP, PM_{10}, and/or $PM_{2.5}$, with a small number also reporting $PM_{10-2.5}$. All available Mn measurements from 1991 to 2014 were used to estimate the mean concentration and 95% lower and upper confidence limits (95% CLs) of Mn in ambient air as presented in the Supplemental information. For the purpose of this study, respirable PM was defined as particulate matter ≤10 μm. Estimates of mean concentrations of Mn from respirable particles were calculated as the sum of PM_{10} and $PM_{10-2.5}$ for Canadian data, and PM_{10} for US data. In all cases, the estimated 95% CLs assumed a normal distribution of the data.

2.3. Exposure to manganese the diet[2]

Estimated daily dietary intake of Mn for Canadians was obtained from tables provided by Health Canada (2011). Values reported in microgram per kilogram (μg/kg) body weight/day were converted to total daily intake using comparable body weight data for each age and gender category from US Department of Health and Human Service's 2009–2012 National Health and Nutrition Examination Surveys (NHANES) (CDC, 2010, 2012). Estimated daily dietary intake of Mn for the US population was obtained from NHANES. Two sets of data (NHANES 2009–2010 and NHANES 2011–2012) were combined for

[1] See discussion presented in Supplemental information.
[2] See discussion presented in Supplemental information.

this analysis and the body weights were adjusted so that the combination provided a nationally representative sample of dietary intake (CDC, 2006, 2007). The amount of Mn in the food items consumed was determined using the United States Department of Agriculture (USDA) Food and Nutrient Database for Dietary Studies (FNNDS) (USDA, 2012), and the USDA National Nutrient Database for Standard Reference, SR27 (USDA, 2014). The FNNDS database provides the "recipes" which break down the food items in the NHANES database into the individual items in the SR27 database. The SR27 database provides the amount of Mn (in units of mg/100 g) for each food item in a recipe.

Using data from the three databases (NHANES, FNNDS, and SR27), estimates of the amount of Mn consumed daily in the diet were determined for specific age groups and gender combinations. Intake from both food and nutritional supplements was based on data from the NHANES dietary intake interview and the data on supplements provided by the CDC in NHANES 2009–2012.

2.4. Application of the human PBPK Mn model

The development of the current human PBPK model for Mn compounds (Schroeter et al., 2011) builds upon previous models (Andersen et al., 2010; Leavens et al., 2007; Nong et al., 2008, 2009; Teeguarden et al., 2007a, 2007b, 2007c; Yoon et al., 2009a, 2009b, 2011). These models characterize the movement of Mn compounds in the body following intake by oral or inhalation routes, as well as target tissue concentrations of Mn in selected regions of the brain. The Schroeter et al. (2011) model also incorporates direct transport of Mn to the brain via the olfactory nerve (Leavens et al., 2007; Nong et al., 2008, 2009). They build upon integration of pharmacokinetic data for various Mn compounds in rats, monkeys, and humans (Dorman et al., 2012; Taylor et al., 2012), considering the significant physiological and biochemical differences between species (Schroeter et al., 2011).

The Schroeter et al. (2011) human PBPK model was the primary model used for this investigation. This PBPK model has the capability of simulating concurrent exposure to dietary and inhaled Mn. The structure for this model relies on the structure initially developed for the rat and the monkey (Nong et al., 2009). This structure was extended to humans to predict dietary and inhalation exposure conditions, with human tracer studies relied upon for verification. Information for the characterization of the kinetics of Mn in humans was based on ^{54}Mn clearance studies in monkeys and humans (Dastur et al., 1971; Davidsson et al., 1988; Dorman et al., 2006a; Furchner et al., 1966; Mahoney and Small, 1968; Mena et al., 1967; Newland et al., 1987). Clearance behavior of Mn displayed biphasic kinetics, dose-dependent differences in elimination, and dependence on total Mn body burden, either from Mn in the diet or supplemental Mn exposures. The Schroeter et al. (2011) model has adequately simulated the results from ^{54}Mn tracer kinetics from oral and inhalation exposures and also for multiple water-soluble Mn compounds (i.e. Mn sulfate [$MnSO_4$], Mn (II) chloride [$MnCl_2$]) administered by intraperitoneal, intravenous, or subcutaneous administration.

The results of the extensive modeling effort by Schroeter et al. (2011) identified that one of the primary species differences that affect Mn kinetics is dietary exposure. Because Mn is an essential nutrient, dose-dependent biological processes that regulate absorption, tissue storage, and elimination must be considered, with a focus on those external exposures that alter uptake processes in the gut. The current models (Nong et al., 2008, 2009; Schroeter et al., 2011, 2012; Yoon et al., 2009a, 2009b, 2011) have characterized these processes, specifically changes in intestinal absorption and biliary elimination, capturing the homeostatic controls that regulate Mn body burden.

In the Schroeter et al. (2011) model, estimation of the deposition of Mn particles in the lung was conducted using the Multiple-Path Particle Dosimetry Model (MPPD model) particle deposition software; (copyright Applied Reseach Associates Inc., Albuquerque, NM), which considered species-specific lung geometries, ventilatory rates and particle properties. Data for $MnSO_4$, which is a more bioavailable compound than other forms of manganese (i.e. Mn dioxide [MnO_2], Mn [III] phosphate), were relied upon for characterizing lung deposition, and hence, subsequent systemic distribution in the human model based on the available studies for characterizing lung deposition in the monkey (Aschner and Aschner, 2005; Bush et al., 1995; Dorman et al., 2006a, 2006b; Schroeter et al., 2008). The use of the sulfate form assumes the highest absorption and distribution of manganese in the tissues as other forms have lower absorption and are likely to result in lower tissue concentrations (Dorman et al., 2001; Vitarella et al., 2000).

Information regarding the particle size for the distribution of total dust particles of Mn measured in the occupational studies is necessary to incorporate into the MPPD model to estimate the deposition fractions that are used in the PBPK model. However, data on the mean or median particle diameter for the occupational Mn measurements were not provided in the published studies (Gibbs et al., 1999; Lucchini et al., 1999; Myers et al., 2003a; Roels et al., 1987a, 1987b, 1992). The most detailed information characterizing particle size distributions of total Mn in occupational settings were measured using personal air monitors. Therefore, these data were focused upon initially for simulations.

Information on the particle size distribution from measurements of Mn dust gathered at a large alkaline battery plant from 1987 to 1995 (Roels et al., 1992, 1999) was obtained from the author. This database represents approximately 1500 air sampling results (total and respirable dust), and demonstrates a bimodal distribution for the airborne Mn particles with one peak observed at 6.0–6.5 μm, characteristic of respirable particles, and a second peak >8.5 μm, characteristic of the non-respirable fraction. Because no additional information was available on the size distribution of the respirable concentration of Mn dust from any other occupational studies, the median particle diameter for respirable dust was assumed to be approximately 6 μm in diameter. USEPA (1993) notes a similar median diameter cut point for the respirable dust fraction of 5 μm based on information provided by Roels et al. (1992) and Roels (1993). Since information was not available regarding median particle size for the respirable and non-respirable fraction from other Mn-associated occupational cohorts, a Monte Carlo analysis using personal exposure measures from the one occupational cohort study with particle size distribution data available (Roels et al., 1999) was conducted to estimate a potential geometric standard deviation (GSD) that would encompass the respirable range of particles (defined as <10 μm), as well as each of the bimodal distribution peaks. These data (Roels et al., 1999) displayed a respirable particle size distribution with peaks at 5.0 μm (d_{50}) and 7.1 μm (d_{100}). This analysis predicts a median particle size of 6.0 μm (GSD 3.4 μm). While this represents a large variation in the potential particle size distribution, a median particle diameter of 6 μm (GSD 3.4 μm) for simulating occupational exposures was used in the MPPD model.

Additional simulations were conducted to evaluate the potential effect of the assumptions of particle diameter and GSD on the PBPK model estimates of target tissue concentration (e.g. Mn concentration in the globus pallidus) (Table 1). The model was allowed to simulate exposure concentrations ranging from 21 to 1317 micrograms per cubic meter (μg/m^3) corresponding to the exposure range for respirable Mn dust in alkaline battery plant workers (Roels et al., 1992). The mass media aerosol diameter (MMAD) varied from 3 to 9 μm with GSD values of 1.5 μm or 3.4 μm. At the lower concentrations of particles (<100 μg/m^3), relatively little change in target tissue concentration was predicted. At the highest concentration (1317 μg/m^3), the variation in target tissue concentration ranged from 7% less to 6% more than the value estimated using the MMAD of 6 μm (GSD 3.4 μm) for simulating occupational exposures.

2.5. Comparison with results from analyses in nonhuman primates

An analysis similar to that presented here was conducted by Schroeter et al. (2012) using manganese neurotoxicity studies

Table 1
PBPK-predicted concentration in the globus pallidus (μg Mn/g of tissue) after occupational exposure (8 h/day, 5 days/week) for 1 year in a 77.7 kg man with a dietary intake of 3 mg Mn/day.

μg Mn/m^3 respirable dust	MMAD = 3, GSD = 3.4, head 54.2%, lungs 14.3%	MMAD = 6, GSD = 3.4, head 69.8%, lungs 13.5%	MMAD = 9, GSD = 3.4, head 78.8%, lungs 13.1%	MMAD = 3, GSD = 1.5, head 54.9%, lungs 23.5%	MMAD = 6, GSD = 1.5, head 81.3%, lungs 15.1%	MMAD = 9, GSD = 1.5, head 91.3%, lungs 7.3%
0	0.39					
21	0.45	0.46	0.46	0.45	0.46	0.47
46	0.50	0.52	0.52	0.51	0.53	0.53
65	0.53	0.55	0.56	0.55	0.57	0.57
104	0.59	0.61	0.63	0.61	0.63	0.63
163	0.65	0.68	0.70	0.68	0.71	0.70
179	0.67	0.70	0.71	0.70	0.72	0.72
201	0.69	0.72	0.73	0.72	0.74	0.74
243	0.72	0.75	0.77	0.75	0.78	0.78
244	0.72	0.75	0.77	0.75	0.78	0.78
265	0.74	0.77	0.79	0.77	0.80	0.80
314	0.77	0.80	0.82	0.80	0.83	0.83
319	0.77	0.81	0.83	0.81	0.84	0.84
468	0.85	0.89	0.92	0.89	0.93	0.93
499	0.87	0.91	0.93	0.91	0.95	0.95
530	0.88	0.93	0.95	0.93	0.97	0.96
613	0.92	0.97	0.99	0.97	1.01	1.01
634	0.93	0.98	1.00	0.98	1.02	1.02
796	0.99	1.05	1.08	1.05	1.10	1.10
907	1.04	1.10	1.14	1.10	1.16	1.15
1201	1.14	1.23	1.27	1.23	1.30	1.29
1317	1.19	1.27	1.33	1.28	1.36	1.35

MMAD: mass media aerosol diameter.
GSD: geometric standard deviation.
Head: percentage of Mn deposited in the head (nasal cavities and brain) as estimated by the MPPD model.
Lungs: percentage of Mn deposited in the lungs (tracheobronchial and pulmonary regions) as estimated by the MPPD model.

conducted in monkeys. Gwiazda et al. (2007) had conducted a review of subchronic to chronic rodent and nonhuman primate studies to determine whether a consistent dose-response relationship existed among different studies. The goal of the Gwiazda et al. (2007) review was to determine whether animal studies could be used to evaluate the neurotoxicity of chronic low-level manganese exposures in humans.

Since the completion of the Gwiazda et al. (2007) review and with the development of recent PBPK models (Nong et al., 2009; Schroeter et al., 2011; Yoon et al., 2011), it is now possible to estimate the target tissue concentrations that would be associated with exposures to manganese in rat or monkey studies. Schroeter et al. (2012) focused on applying PBPK modeling approaches to a subset of the monkey studies identified by Gwiazda et al. (2007). Unlike rats, monkeys develop regionally selective increases in brain manganese concentrations (Dorman et al., 2006a, 2006b; Newland et al., 1987, 1989; Eriksson et al., 1992; Aschner and Aschner, 2005) and behavioral effects similar to those reported for manganese affected humans (Olanow et al., 1996). Using a PBPK model for Rhesus monkeys, Schroeter et al. (2012) simulated exposure scenarios from each monkey study reported by Gwiazda et al. (2007) and predicted the corresponding concentrations in the brain for various dose routes, exposure concentrations and durations. The observed responses were categorized using a clinical scoring system for dose-response analysis. We also compared results from this earlier analysis in monkeys to the current analyses relying on occupational studies.

2.6. Statistical analysis approach

A no-statistical-significance-of-trend (NOSTASOT) approach was used to estimate the NOAEL in target tissue (Tukey et al., 1985), using the data that indicated whether each individual had an adverse neurological test response combined with the PBPK model estimated Mn target tissue concentrations. The data separated into two groups (exposed to respirable Mn dust or unexposed), and the exposed group was sorted lowest to highest by the PBPK model predicted concentration of Mn in the globus pallidus. A Fisher's exact test was used to compare the combined incidence rate of abnormal scores for eye-hand coordination or the hand steadiness test between the exposed and unexposed groups. If there was a significant difference in incidence of an abnormal score between the exposed and unexposed group, the test was repeated after removing the subject(s) from the exposed group with the highest concentration of Mn in the globus pallidus. This process continued until a Fisher's exact test comparing the prevalence rate of abnormal neurological test response in the remaining exposed group to the prevalence rate in the unexposed group was not statistically significant. Removing the highest exposed individuals until a point was reached of no statistical significance allowed for the identification of a target tissue concentration NOAEL.

A second approach using the Tukey et al. (1985) NOSTASOT to derive a NOAEL used the Cochran-Armitage trend test (Armitage, 1955; Cochran, 1954). As with the method described above using the Fisher's exact test, this approach involves repeated application of a test for a significant dose-response trend grouping only by the PBPK model predicted concentration of Mn in the globus pallidus. If there is a significant difference in the complete data set, the test is repeated after removing the highest dose group. This procedure is repeated until the trend test is no longer statistically significant.

3. Results

3.1. Relevant epidemiological data

Twenty-one occupational studies with Mn exposure were initially identified (Bast-Pettersen et al., 2004; Bouchard et al., 2007a, 2007b; Deschamps et al., 2001; Fittro et al., 1992; Gibbs et al., 1999; Health Canada, 2010; Lee et al., 2003; Lees-Haley et al., 2006; Lucchini et al., 1995, 1997, 1999; Mergler et al., 1994; Myers et al., 2003a, 2003b, 2003c; Roels et al., 1987a, 1987b, 1992, 1999; Young et al., 2005). Emphasis was placed on occupational studies because these studies have provided the basis for current regulatory recommendations regarding inhalation exposure to Mn compounds (USEPA, 1998). Fourteen were selected for detailed review (Bast-Pettersen et al., 2004; Bouchard et al., 2007a, 2007b; Deschamps et al., 2001; Gibbs et al., 1999; Lucchini et al., 1999; Mergler et al., 1994; Myers et al., 2003a, 2003b, 2003c;

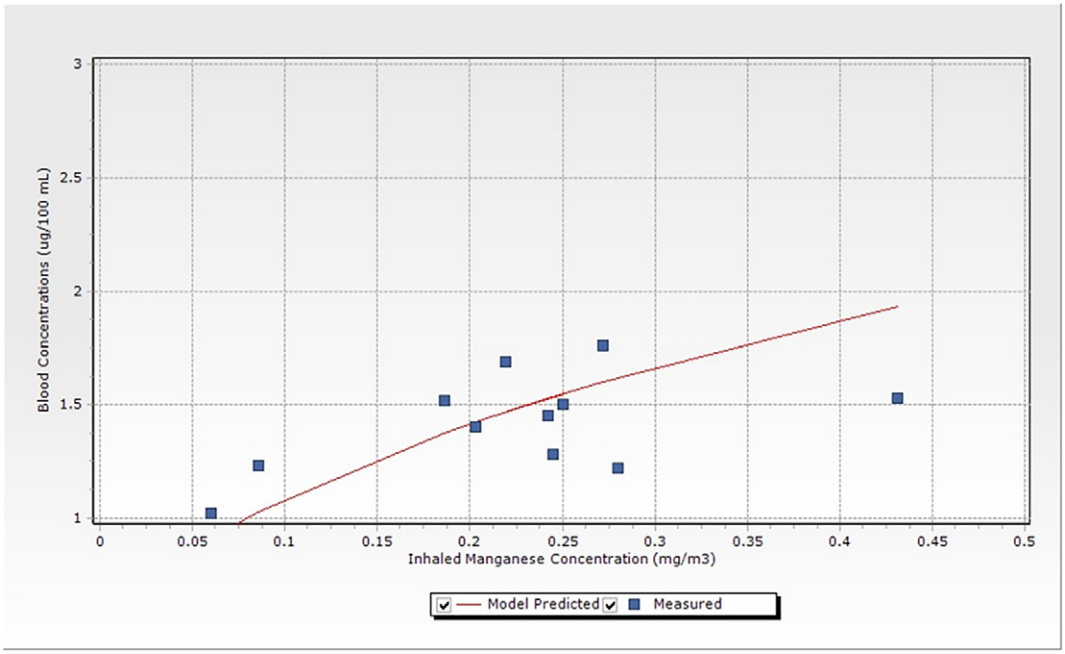

Fig. 1. Data from Roels et al. (1987a)—respirable Mn vs. blood concentrations at start of work week.

Roels et al., 1987a, 1987b, 1992, 1999; Young et al., 2005) that reported having the data necessary for quantitative exposure estimates and objective measures of neurological effects. Full individual exposure and response data were available for three of these studies (Bast-Pettersen et al., 2004; Roels et al., 1992, 1999[3]) and partial exposure and response data were available in seven studies (Bouchard et al., 2007a, 2007b; Gibbs et al., 1999[3]; Mergler et al., 1994; Myers et al., 2003a, 2003b; Young et al., 2005). Published studies provided data that were used in verifying the PBPK model and/or estimating Mn target tissue levels (Lucchini et al., 1999; Myers et al., 2003a; Roels et al., 1987a).

3.2. Exposure to manganese from ambient air and the diet

The estimated background air mean Mn concentrations and 95% confidence limits (CLs) for each country and respirable PM size (<10 μm) are 0.013 μg/m^3 (CL 0.012–0.013 μg/m^3) in Canada and 0.014 μg/m^3 (CL 0.013–0.016 μg/m^3) in the US (see Supplemental information). The estimated respirable ambient air concentration of Mn used in our PBPK models ranged from 0.01–0.02 μg/m^3.

For occupational exposure modeling, the dietary exposure was 3 mg Mn per day based on average dietary intakes of Mn for Canadian and US populations (see Supplemental information). This value could be an underestimate of the mean dietary intake of adults in both the US and Canada as values of Mn from the dietary data reported in NHANES ranged up to >20 mg/day from diet alone (CDC, 2012) and to values >60 mg/day when supplements were also considered (Supplemental Table S4).

3.3. Verification of the human PBPK Mn model

The Mn PBPK models were developed using tissue and whole body concentration data, but due to their physiological structure, the models also can predict blood concentrations. To demonstrate that the simulated Mn blood concentrations from our PBPK model were consistent with those measured in occupational studies, available blood concentrations (Roels et al., 1987a) were compared to blood Mn concentrations simulated with the adult human PBPK model (Schroeter et al., 2011). Since specific information on particle size distribution for this cohort was not available, the median particle size and GSD from a later study (Roels et al., 1992) were applied and exposure was simulated for 8 h/day, 5 days/week. As occupational exposure is not continuous and "steady state" would not be achieved, the model was run until the pattern of blood concentrations observed reached a constant, recurrent pattern, referred to as "periodicity". Estimates of the blood concentration at the beginning and end of the work week were determined for comparison to the published data (Roels et al., 1987a).

The results of the PBPK modeling were similar in trends with the available Mn blood concentrations (Roels et al., 1987a), whether it was assumed that the blood samples were drawn from the workers at the beginning or the end of the work week (Figs. 1, 2). The model was applied without incorporation of available information on variability of physiological parameters, and thus does not reflect individual variability observed from individual blood measurements. However, the model simulation is consistent with the available measured Mn blood concentrations, particularly for individuals with lower exposures, a point that is critical for the evaluation of ambient exposures.

The PBPK model-predicted results from another study (Myers et al., 2003c) are shown along with the measured blood data (Figs. 3, 4). The simulations were compared with the blood draws at either the start or the end of the work week.

The data from a study measuring Mn blood concentrations in a group of ferroalloy workers (Lucchini et al., 1999) was also considered for comparison with the PBPK model. However, there were both internal (Lucchini et al., 1999) and external (Health Canada, 2010) inconsistencies related to estimating the fraction of inhaled Mn in the respirable range. In the publication (Lucchini et al., 1999), the authors reported that the respiratory fraction of Mn (as MnO_2 and Mn_3O_4) ranged from 40 to 60%. However, comparison of the values reported in the publication for total Mn dust (5–1490 μg/m^3; geometric mean 54.25 μg/m^3; arithmetic mean 175.59 μg/m^3) to respirable dust (1–670 μg/m^3; geometric mean 17.18 μg/m^3; arithmetic mean 67.08 μg/m^3) suggests a lower respirable fraction, 20–40%. Examination of individual data by Health Canada (2010), presenting the range, median, and mean concentrations across all job categories for total and respirable dust, suggests that only a limited number of "intermittent" samples of respirable Mn were taken. Health Canada (2010) relied upon these data to estimate the average respirable concentrations (ARE) over the duration of the

[3] Roels et al. (1992, 1999) and Gibbs et al. (1999) data were supplemented by raw data from authors.

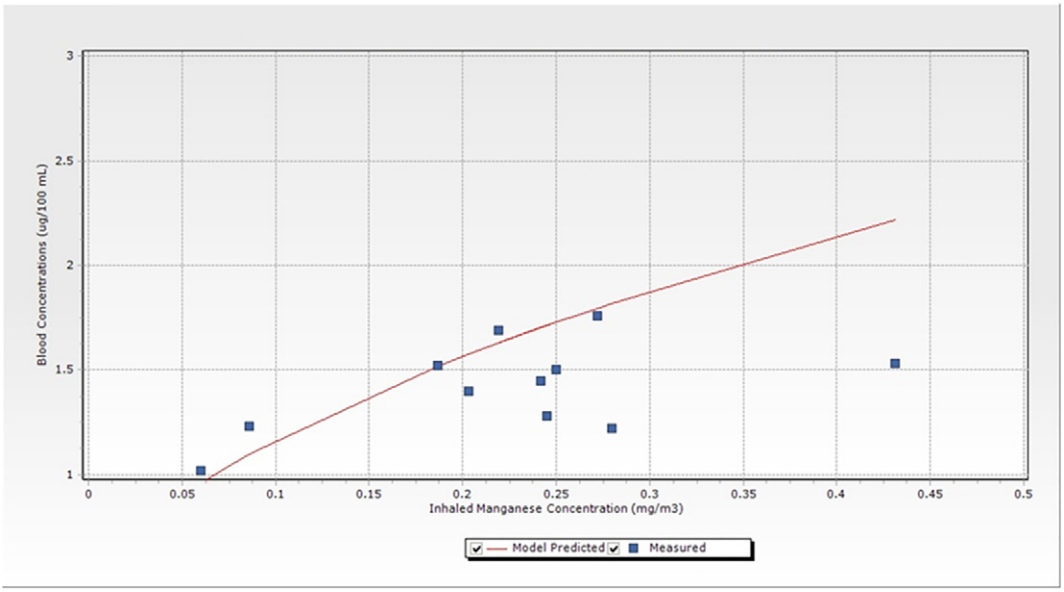

Fig. 2. Data from Roels et al. (1987a)—respirable Mn vs. blood concentrations at end of work week.

work history for each subject and over a shorter 5 year period (ARE5). Comparing the Health Canada (2010) estimates of ARE (1.21 to 285.16 μg/m^3, arithmetic mean of 70.92) or ARE5 (1.1 to 145.43 μg/m^3, arithmetic mean of 41.79) to the total dust concentrations reported by Lucchini et al. (1999) suggested that the respirable fraction of Mn could range from approximately 10–25% of the total concentration.

The estimates of the respirable fraction of Mn have a significant effect on predicted Mn blood concentrations from the Lucchini et al. (1999) study (Fig. 5). Using 20–60% as the respirable fraction gives a better match for expected blood Mn concentrations associated with total Mn dust concentrations of <0.2 mg/m^3. For total Mn dust concentrations >0.2 mg/m^3, however, model results are more consistent with a 20% respirable fraction. This outcome illustrates how different assumptions made for the respirable fraction affects model results for Mn in target tissue. Thus, the use of dose metrics from this study (Lucchini et al., 1999) for the evaluation of Mn target tissue concentrations associated with potential adverse effects carries a high degree of uncertainty.

Since a strong agreement between model estimates and measured blood Mn concentrations is found in two of the three available occupational studies that report blood concentrations (Myers et al., 2003a; Roels et al., 1987a), the confidence in the model using data from these studies is higher. While the data necessary to validate the target tissue concentration of concern (i.e. increases of Mn in selected regions of the brain) are not available, the ability to simulate the available Mn blood concentrations measured in workers, as well as the available

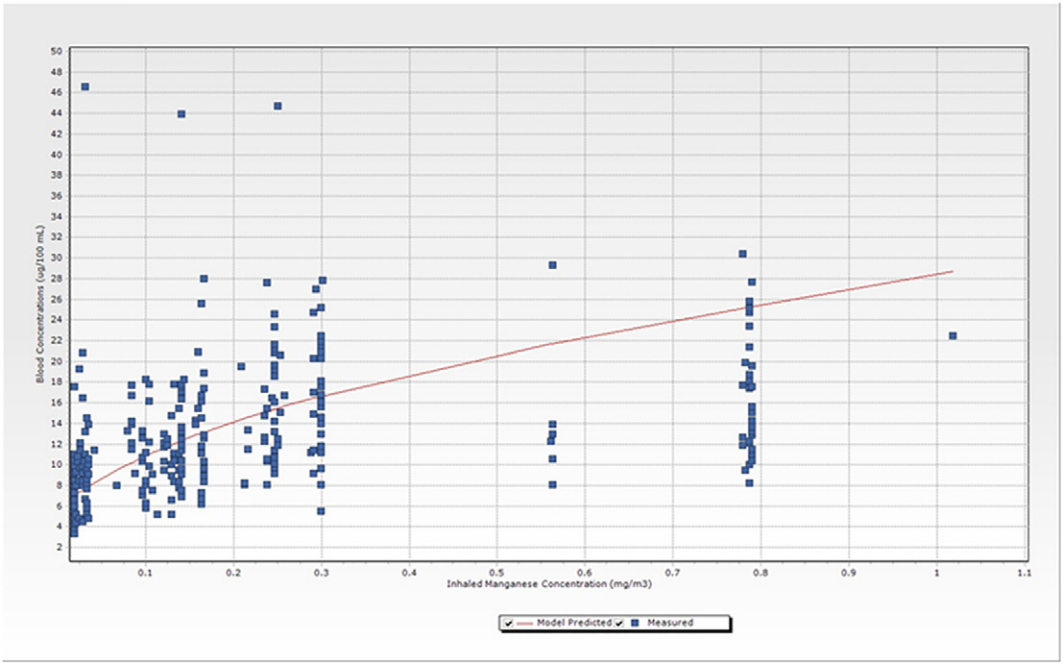

Fig. 3. Data from Myers et al. (2003a)—respirable Mn vs. modeled blood concentration at start of work week.

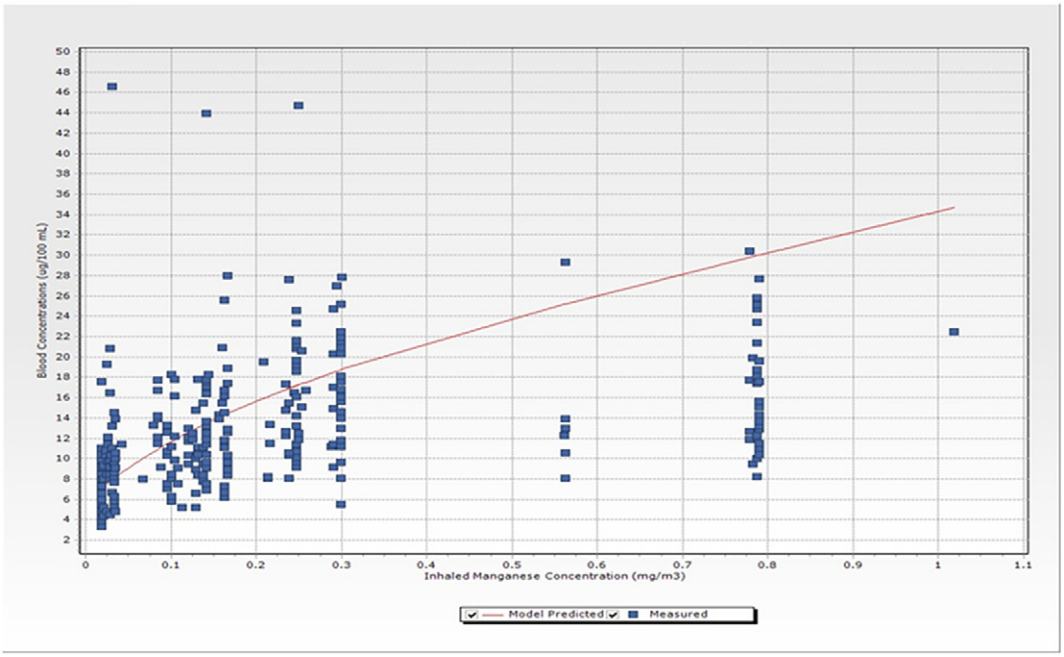

Fig. 4. Data from Myers et al. (2003a)—respirable Mn vs. modeled blood concentrations at end of work week.

data from human tracer studies, provides additional confidence in the estimates provided by the PBPK model. Further confidence comes from the ability of the primate model to accurately predict target tissue concentrations over an even greater range of dose-routes, including intravenous, intraperitoneal, and subcutaneous, in addition to inhalation and oral (Schroeter et al., 2012).

3.4. Application of the human PBPK Mn model

Based on the changes in specific, subclinical neurological effects associated with Mn air concentrations reported in several occupational studies, the increase of Mn in the globus pallidus of the brain can be viewed as the relevant target tissue for neurological effects (Guilarte, 2010; Health Canada, 2010). Thus, the PBPK model can be used to derive a "target tissue NOAEL" by applying the model to simulate the concentration of Mn expected in the globus pallidus following exposures at the highest air concentrations reported to have no effect on neurological function.

Exposure information and individual dichotomized data (response/no response) were available for each subject in a study of workers exposed to Mn oxide dust in a dry alkaline battery factory (Roels et al., 1992). This study evaluated the prevalence of neuropsychological symptoms and neurofunctional performance, thus allowing several types of analyses to be conducted to estimate a potential Mn target tissue NOAEL. The PBPK model was applied using data from this study (Roels et al., 1992), simulating the available respirable air concentrations for each individual and assuming 8 h/day, 5 day/week inhalation exposure. The target tissue concentrations (i.e. μg Mn/g tissue in the

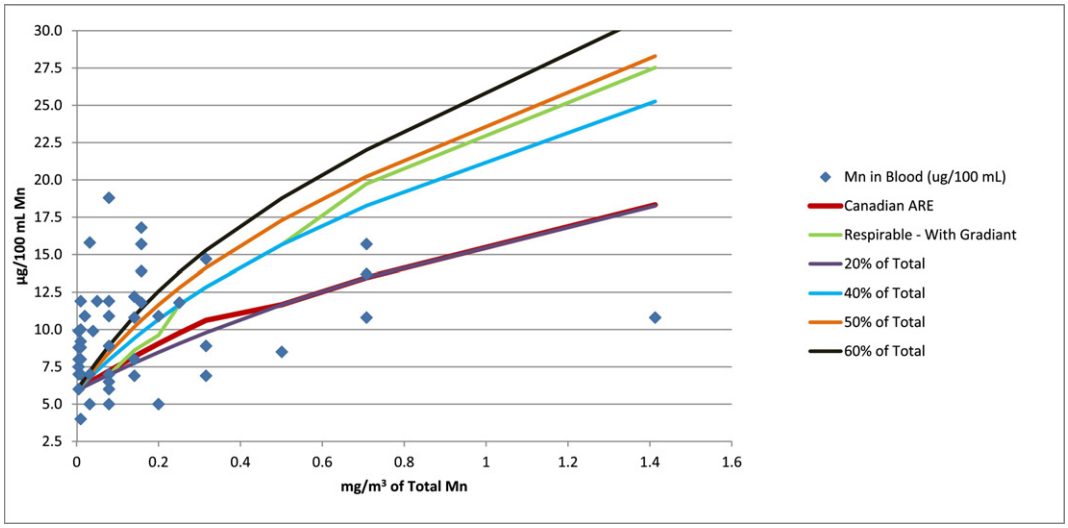

Fig. 5. Data from Lucchini et al. (1999)—impact of respirable fraction of Mn on blood concentration estimates.

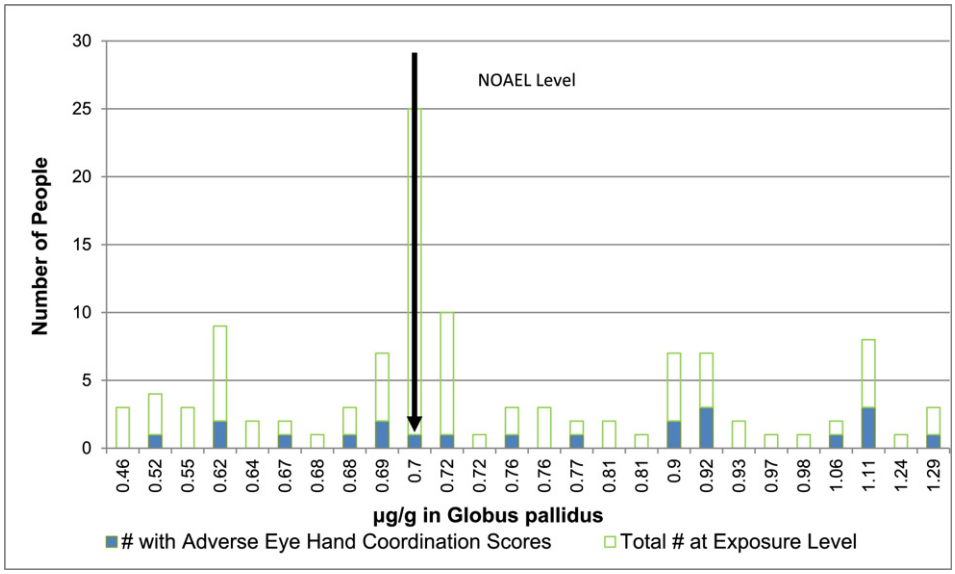

Fig. 6. Data from Roels et al. (1992)—individuals with adverse eye-hand coordination scores vs. globus pallidus Mn concentrations at end of work week.

globus pallidus) were estimated for each individual and used to determine a potential Mn target tissue NOAEL.

No-statistical-significance-of-trend (NOSTASOT) approach with a Fisher's exact test predicts a target tissue (Mn concentration in the globus pallidus) NOAEL of 0.7 µg/g using the prevalence rate of abnormal eye-hand coordination, (Fig. 6) and a target tissue NOAEL of 0.9 µg/g using the adverse effect endpoint of abnormal hand steadiness (Fig. 7). Applying the NOSTASOT statistical approach using trend tests to the data from the Roels et al. (1992) study, using eye-hand coordination data grouped into the same seven exposure groups (Table 2) determined by ATSDR (2012), yields a NOAEL corresponding to the exposure group with respirable continuous Mn concentrations of 100–199 µg/m^3 consistent with the ATSDR (2012) BMDL of 142 µg/m^3, with a corresponding PBPK modeled target Mn tissue concentration of 0.7 µg/g. These two different statistical evaluations provided similar results.

Other epidemiological studies identified through literature searching reported no statistically significant abnormal neurofunctional test results following Mn exposure in occupational cohorts, even in the highest exposure groups (Myers et al., 2003a; Gibbs et al., 1999). One study (Myers et al., 2003a) evaluated nervous system effects in a large cohort of South African mineworkers exposed to concentrations of Mn in the workplace. Only total dust Mn concentrations were reported, so it was assumed that the respirable fraction of the total dust Mn also changed as the concentration increased. The range of total dust Mn (digitized from Fig. 3 of Myers et al., 2003a) was 58 µg/m^3–5088 µg/m^3. Due to the shallow rise in the blood levels associated with the rise in the total dust, it appeared that the percentage of respirable dust declined with increasing total dust. Three different fractions were assumed for converting the total dust to respirable dust. For values of 58–<500 µg/m^3 of total dust, the assumed percentage of respirable dust was 33%. For values of 500–<1000 µg/m^3 of total dust, the assumed percentage of respirable dust was 25% and for concentrations of total Mn dust of ≥1000 µg/m^3, the respirable fraction was assumed to be 20% of the total dust. These assumptions result in a range of respirable concentrations of Mn dust of 19–1018 µg/m^3. Since this study did not report any neurological effects associated with any

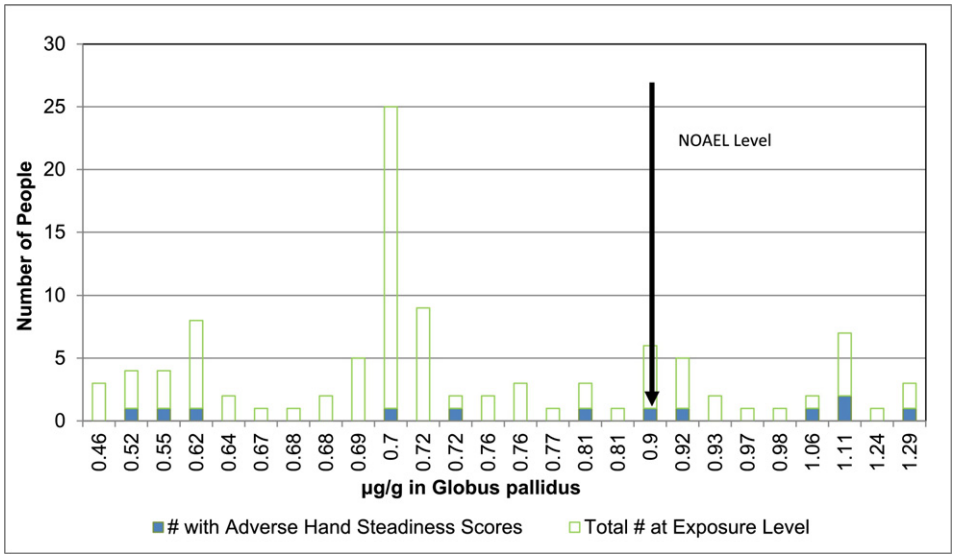

Fig. 7. Data from Roels et al. (1992)—individuals with adverse hand steadiness scores vs. globus pallidus concentrations of Mn at end of work week.

Table 2
Grouped prevalence data for abnormal eye-hand coordination scores in workers exposed to respirable manganese.

Group	Range of respirable manganese exposure concentrations (μg Mn/m^3)	Average respirable manganese exposure concentrations (μg Mn/m^3)	# of workers with abnormal eye-hand coordination scores	Total number of workers in exposure group
1	Control	0	5	101
2	1.0–99	33	1	7
3	**100–199**	**174**	**6**	**39**
4	200–299	224	4	28
5	300–399	307	2	3
6	400–499	451	4	9
7	>500 (523–650)	564	4	6

Source: ATSDR, 2012, based on Roels et al., 1992. The $BMDL_{10}$ used in the MRL derivation is 142 μg/m^3 (ATSDR, 2012).
Bolded data are those corresponding to the NOAEL.

exposure groups, the highest respirable concentration could be considered a NOAEL. Based on these assumptions, the PBPK model was run resulting in estimates of approximately 1 μg/g tissue in the globus pallidus, which could be considered the NOAEL. Similarly, a study in which a population of US workers exposed to low levels of Mn dust were evaluated for subclinical neurological effects (Gibbs et al., 1999) reported no significant effects on neurofunctional performance at monthly average respirable Mn air concentrations as high as 328 μg/m^3. Therefore, the highest air concentration reported for this study could be considered a NOAEL and the PBPK model, assuming an occupational exposure scenario (8 h/day, 5 days/week), provides an estimate of a Mn target tissue NOAEL of approximately 0.8 μg/g.

In conducting the PBPK modeling simulations of the occupational exposures, it was assumed that there was no significant contribution to internal dose resulting from the ingestion of non-respirable particulates.

3.5. Comparison with results from analyses in nonhuman primates

The results from the Schroeter et al. (2012) analysis suggested a clear dose-response behavior of effects versus peak and cumulative dose area under the curve (AUC) in the globus pallidus region of the brain. Using a CatReg analysis, a 10% extra risk for a mild response, which would be comparable to subclinical effects such as those measured in human occupational studies, occurred at a peak concentration of 0.8 μg/g manganese in the globus pallidus estimated using the PBPK model. This is consistent with the target tissue NOAELs 0.7 μg/g Mn (eye-hand coordination) to 0.9 μg/g Mn (hand steadiness scores) estimated in the current analysis.

3.6. Estimation of target tissue levels based on ambient air monitoring

Evaluation of the available air monitoring data from both Canada and the US (see Supplemental information) indicate that the 95% upper confidence limit (UCL) on the mean ambient respirable Mn air concentrations are approximately 0.01–0.02 μg/m^3. The concentration of Mn in the globus pallidus associated with this ambient air concentration was estimated using the median diameter of Mn-containing particles based on the relationship between the amount of Mn measured in filters with a 2.5 μm cut-point and a cut-point between 2.5 and 10 μm. Values of 1.5 and 2.5 μm were used for the median particle size diameters with a standard deviation of 1.5.

The PBPK model was applied assuming continuous exposure concentrations of 0.01–0.02 μg/m^3 for 10 years to ensure that the target tissue concentrations achieved steady state. The modeling results indicated that this was achieved within 100 days for dietary exposure alone. The model estimated a target tissue concentration of Mn of 0.4 μg/g with only dietary exposure. For occupational exposure, comparable patterns of tissue concentration (considering that occupational exposure is not continuous) were achieved within 200 days. In addition, in order to determine the ambient air concentrations that would be needed to result in target tissue concentrations similar to those reported for the target tissue NOAEL from occupational studies, the PBPK model was applied assuming continuous exposure, increasing the concentration of respirable Mn until a target tissue concentration of approximately 1 μg/g globus pallidus was achieved (Table 3, Fig. 8). This would be an exposure to respirable dust of at least 150 μg/m^3.

3.7. Estimation of margins of safety based on target tissue concentrations

To develop a MOS, the continuous ambient air concentration associated with target tissue NOAELs from Roels et al. (1992) (0.7 μg/g Mn for eye-hand coordination; 0.9 μg/g Mn for hand steadiness scores) was compared to the 95% UCL on the mean on the ambient air concentration (0.01 to 0.02 μg/m^3). Based on the results of PBPK modeling, continuous exposure to an ambient air concentration of 50 μg/m^3 would be associated with a target tissue concentration of approximately 0.7 μg/g Mn (Table 3), while continuous exposure to an ambient air concentration of 120 μg/m^3 would be associated with a target tissue concentration of approximately 0.9 μg/g Mn. Based on these results, the MOS would be approximately 2500–5000 (calculated as 50 μg/m^3 divided by 0.02 μg/m^3 or 0.01 μg/m^3). For the target NOAEL based on results from neuropsychological testing to measure hand steadiness, the MOS would be approximately 6000–12,000 (calculated as 120 μg/m^3 divided by 0.02 μg/m^3 or 0.01 μg/m^3).

In all of the current regulatory assessments, application of adjustment factors have been applied to "convert" an occupational air concentration to an ambient air concentration and then safety factors have been applied. These approaches implicitly assume that any effect is linearly related to the external air concentration. However, the results of this analysis demonstrate that target tissue concentrations are not linearly associated with external air concentrations due to homeostatic

Table 3
Ambient respirable Mn concentrations vs. PBPK estimates of Mn concentration in globus pallidus.

μg/m^3 respirable dust	Total μg/g in globus pallidus
0.01	0.39
0.1	0.39
1	0.41
10	0.50
20	0.57
30	0.63
40	0.67
50	0.71
60	0.74
70	0.77
80	0.80
90	0.83
100	0.85
110	0.87
120	0.89
130	0.91
140	0.93
150	0.95

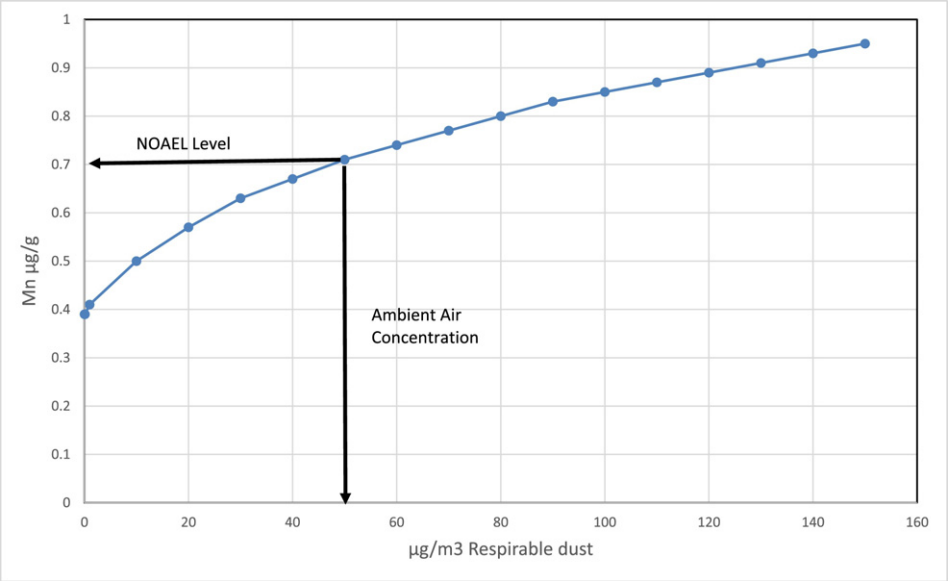

Fig. 8. Predicted total Mn (µg/g) in the globus pallidus from exposure to varying amounts of respirable Mn dust.

mechanisms that maintain target tissue levels within a certain range of exposure. With the application of the PBPK model, Table 4 demonstrates that decreasing an ambient air concentration by safety factors of 10 does not result in corresponding decreases in the target tissue concentrations.

4. Discussion

Current regulatory assessments for Mn rely on occupational studies to provide a point of departure (POD), which would be adjusted by safety factors to derive an acceptable Mn ambient air concentration. However, an approach that relies on the application of safety factors is only biologically reasonable if reductions in acceptable air Mn concentrations are associated with reductions in the concentration of Mn in target tissues. Incorporating PBPK modeling into the safety assessment for Mn allows consideration of available quantitative data, rather than applying default uncertainty or safety factors for this essential element.

Application of the PBPK model to estimate Mn concentrations in target tissues following occupational inhalation exposure demonstrated that there will not necessarily be linear decreases in target tissue Mn with decreasing Mn air concentrations. When the external Mn air concentration is below the concentration that would result in an increase in target tissue concentrations above background Mn, these air concentrations would not be associated with health effects. Decreases in concentrations assumed with the use of additional safety factors would not result in lower target tissue Mn concentrations (Table 4).

One uncertainty noted for the current analysis is the potential contribution from ingestion of Mn resulting from the non-respirable fraction of Mn in the occupational studies. The current analysis only incorporates the contribution from inhalation of respirable particles. The concentrations and particle sizes reported for the available occupational studies suggest there could be non-respirable Mn inhaled and removed from the respiratory tract via mucociliary processes and then swallowed, resulting in the potential for swallowed particles to contribute to target tissue concentrations. Inclusion of this additional contribution to estimated target tissue concentrations would result in an increase in the target tissue concentration associated with the NOAEL, so would only increase the MOS. Using information from Roels et al. (1992), inhalation exposure of workers to 1 Mn mg/m^3 total dust (80% is non-respirable) would result in approximately 8 mg Mn available for potential transfer to the gastrointestinal tract (assuming 10 m^3 of air inhaled for an 8 h workday). PBPK model-predicted concentrations in the globus pallidus following exposure to various dietary levels (Fig. 9a) indicate that the contribution due to swallowing the non-respirable fraction of inhaled particles could increase the target tissue concentration by approximately a factor of 2. The contribution from diet of 8 mg/day only results in approximately 0.65 µg/g Mn in striatum/globus pallidus which, if considered, could potentially increase the NOAEL from 0.7 µg/g Mn to approximately 1.4 µg/g Mn or a factor of 2.

In addition, while the current study does not directly assess potentially sensitive subpopulations (e.g. susceptibility in fetal or neonatal children), Yoon et al. (2011) developed a PBPK model to integrate the available information on Mn kinetics during gestation and lactation in

Table 4
Target tissue concentrations of Mn associated with Mn ambient air concentrations derived from applying adjustment factors to NOAEL values.

Study	NOAEL concentration of Mn in the target tissue, globus pallidus (µg/g)	Ambient air concentration (µg Mn/m^3)	After applying adjustment factors of:					
			10		100		1000	
			Ambient air concentration (µg/m^3)	Mn conc. in the globus pallidus (µg/g)	Ambient air concentration (µg/m^3)	Mn conc. in the globus pallidus (µg/g)	Ambient air concentration (µg/m^3)	Mn conc. in the globus pallidus (µg/g)
Roels et al. (1992)	0.7	47	4.7	0.5	0.47	0.4	0.047	0.4
	0.9	124	12.4	0.5	1.24	0.4	0.124	0.4
Myers et al. (2003a)	1	157	15.7	0.6	1.57	0.4	0.157	0.4
Gibbs et al. (1999)	0.8	80	8	0.5	0.8	0.4	0.08	0.4

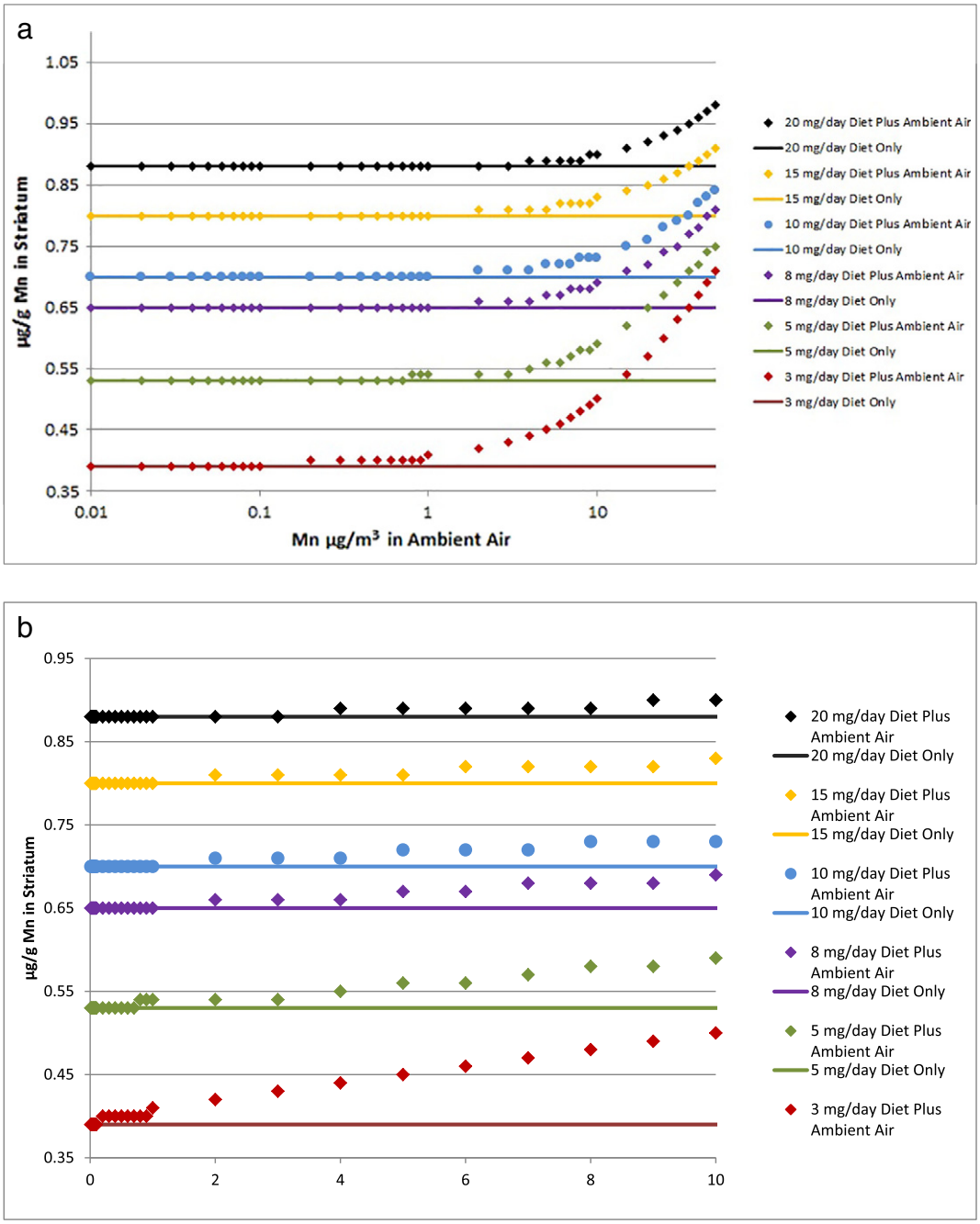

Fig. 9. a. Model-predicted concentration of Mn (μg/g) in the globus pallidus (striatum) from exposure to various daily dietary Mn levels, or dietary Mn daily intake plus various ambient air levels of respirable Mn. Figure is based on a 70 kg human with exposure for 10 years at the indicated dietary intake. b. Model-predicted concentration of Mn (μg/g) in the globus pallidus (striatum) from exposure to various daily dietary Mn levels, or dietary daily intake plus low ambient air levels of respirable Mn. Figure is based on a 70 kg human with exposure for 10 years at the indicated dietary intake.

an attempt to describe homeostatic controls of Mn during human development when challenged with overexposure to Mn. Mn plays a central role in normal prenatal and neonatal development and its deficiency may cause developmental deficits, such as abnormal brain function (Yoon et al., 2011). These life-stage PBPK models showed that adult males achieved a higher daily dose-to-target tissue than fetal, neonatal, pregnant, and non-pregnant female life-stages (Yoon et al., 2011). Based on these pharmacokinetic results, early life stages would be expected to have lower target tissue concentrations, therefore, no sensitive subpopulation adjustment would be necessary when basing risk assessments on occupational studies of adult males exposed to Mn (Taylor et al., 2012).

The potential variability in dietary intake of Mn on target tissue concentrations also needs to be considered when assessing the effects of inhaled Mn. A sensitivity analysis was conducted to determine the parameters that have the most significant impact on the estimation of Mn tissue concentrations in the globus pallidus when the human PBPK model was developed (Schroeter et al., 2011). At low Mn concentrations, the parameters having the largest impact were the influx and efflux diffusion rate constants into the brain, changes in dietary absorption and biliary excretion. Model predictions became less sensitive to dietary absorption and biliary excretion with increasing Mn inhalation exposure concentrations, because brain Mn levels were driven more by inhalation than diet. This observation demonstrates the importance

of any assumptions regarding dietary intake/absorption and biliary excretion in the estimation of changes in target tissue concentrations based on the contribution of inhalation exposure, as well as setting a target tissue NOAEL in occupational studies.

An average dietary intake of 3 mg/day Mn (slightly higher than the "adequate intake" level Aschner and Aschner, 2005), was applied in the human PBPK model for the current study. However, data from both the US (CDC, 2010, 2012) and Canada (Health Canada, 2011) indicate that average dietary intake of Mn varies from 2–>6 mg/day in adults depending on the age range, with maximum intake up to 60–75 mg/day for individuals taking dietary supplements. These dietary intake values can significantly change the baseline target tissue concentration (Fig. 9a), particularly when considering the low Mn concentrations anticipated in ambient air (Fig. 9b). Analyses reported by Schroeter et al. (2011) demonstrated that PBPK model predictions became less sensitive to dietary absorption and biliary excretion with increasing Mn inhalation exposure concentrations, because brain Mn levels were driven more by inhalation than diet at higher air concentrations. Thus, dietary intake, rather than Mn air concentration, may be a dominant factor in determining target tissue concentration following exposure to low air concentrations, and thus, a likely determining factor in human variability of background Mn tissue concentrations.

Multiple occupational studies were evaluated using the human PBPK model for Mn to estimate tissue concentrations from corresponding air concentrations to derive the air concentrations associated with NOAELs. Two studies were negative for health outcomes (Gibbs et al., 1999; Myers et al., 2003a), so the highest Mn air concentrations from these studies were used. All of the estimates of Mn target tissue concentrations were 0.7–1.0 μg/g with corresponding air concentrations based on a typical workday of 200 μg/m^3–1000 μg/m^3. The PBPK model was also used to estimate the continuous inhalation exposure expected to cause these Mn target tissue concentrations. The modeled air concentrations of 50 μg/m^3–>150 μg/m^3 are compared to measured ambient Mn concentrations for Canada and the US to derive a MOS. The estimated MOS of 2500–12,000 suggest how much of an increase in ambient concentrations would be required to produce target tissue concentrations associated with the NOAEL for subclinical neurological effects.

The PBPK model for Mn may also be used to estimate inhaled concentrations required to cause increases in target tissues above background. This point of inflection falls in the ambient air range from 1 to 10 μg Mn/m^3 (Table 3). The model may also be used to estimate the target tissue concentration and corresponding air concentration corresponding to a NOAEL. Our simulations show that tissue concentration at the point of inflection is substantially below target tissue Mn associated with changes in subclinical neurological test results in occupational exposures (Roels et al., 1992). For instance, a recent study in welders indicated that plasma Mn (P-Mn) does not increase until the respirable Mn levels reach 10 μg/m^3 (Hoet et al., 2012). This observation, combined with the results of the current analysis, suggest that a Mn TLV-TWA larger than the currently recommended value of 20 μg/m^3 for respirable dust (ACGIH, 2012) could be relied upon and still be health protective.

In summary, the results of studies on Mn pharmacokinetics demonstrate that homeostatic mechanisms regulate the levels of Mn in the body from inhalation. Increases in target tissues above background occur only when humans (regardless of their age or gender) are exposed to air Mn concentrations far higher than those historically or currently measured in Canada or the US. These findings suggest that regulatory air Mn guidelines are extremely conservative and that the application of standard safety factors may not represent alterations in tissue delivery of Mn due to the nonlinearities in biological processes.

The current human PBPK models (Schroeter et al., 2011; Yoon et al., 2011) are calibrated for adults or infants during gestation and lactation, and have not been extended to specifically address potential differences in children. Therefore, development of a model with pharmacokinetic values specific to children would be of value in addressing the need for an uncertainty factor to extrapolate from adults to children. However, it is expected that children will display similar pharmacokinetics to adults—with significant background tissue levels of Mn that change very little with exposures until reaching 10 μg/m^3. Questions regarding the potential for Mn to affect brain development and cognitive function might be addressed by extension of the model during gestation and lactation to evaluate potential changes in the cerebral cortex as the target tissue. Nonetheless, the globus pallidus is the most sensitive brain region regarding Mn accumulation, and is thus likely an appropriate surrogate for tissue level changes in the frontal cortex (Dorman et al., 2006a, 2006b). While the results of PBPK modeling have indicated critical parameters in estimating Mn target tissue concentrations, a Monte Carlo analysis for selected parameters in the PBPK model, in particular dietary variability among children and adults, would help refine the model estimates and more clearly evaluate the contribution of such factors as dietary exposure versus inhalation exposure in the low exposure regions.

Funding

This publication and work is based on studies sponsored and funded by Afton Chemical Corporation in satisfaction of registration requirements arising under Section 211(a) and (b) of the Clean Air Act and corresponding regulations at 40 CFR Substance 79.50 et seq.

Conflict of interest statement

The authors declare that there are no conflicts of interest and have read and understood the Conflict of Interest Policy from for the Journal.

Transparency document

The Transparency document associated with this article can be found, in online version.

Acknowledgements

We would like to acknowledge Dr. Debra Kaden's insight and assistance in the development of this manuscript.

Appendix A. Supplementary data

Information on the determination of the amount of Mn consumed by an individual in their diet and through the use of supplements is presented as supplementary data. Additionally, the determination of the ambient air concentration of Mn inhaled by an individual is also presented as supplementary material. This information is published online. Supplementary data associated with this article can be found in the online version, at 10.1016/j.taap.2017.02.015.

References

ACGIH, 2012. Threshold Limit Values for Chemical Substances and Physical Agents and Biological Exposure Indices. American Conference of Governmental Industrial Hygienists, Cincinnati.

Andersen, M.E., Gearhart, J.M., Clewell III, H.J., 1999. Pharmacokinetic data needs to support risk assessments for inhaled and ingested manganese. Neurotoxicology 20 (2–3), 161–172.

Andersen, M.E., Dorman, D.C., Clewell 3rd, H.J., Taylor, M.D., Nong, A., 2010. Multi-dose-route, multi-species pharmacokinetic models for manganese and their use in risk assessment. J. Toxicol. Environ. Health 73 (2), 217–234.

Armitage, P., 1955. Tests for linear trends in proportions and frequencies. Biometrics 11 (3), 375–386.

Aschner, J.L., Aschner, M., 2005. Nutritional aspects of manganese homeostasis. Mol. Asp. Med. 26 (4–5), 353–362.

ATSDR, 2012. Toxicological Profile for Manganese. Agency for Toxic Substances and Disease Registry, U.S. Department of Health and Human Services September 2012. http://www.atsdr.cdc.gov/ToxProfiles/tp151.pdf.

Barton, H.A., Clewell 3rd., H.J., 2000. Evaluating noncancer effects of trichloroethylene: dosimetry, mode of action, and risk assessment. Environ. Health Perspect. 108 (Suppl. 2), 323–334.
Bast-Pettersen, R., Ellingsen, D.G., Hetland, S.M., Thomassen, Y., 2004. Neuropsychological function in manganese alloy plant workers. Int. Arch. Occup. Environ. Health 77 (4), 277–287.
Bouchard, M., Mergler, D., Baldwin, M., Panisset, M., Bowler, R., Roels, H.A., 2007a. Neurobehavioral functioning after cessation of manganese exposure: a follow-up after 14 years. Am. J. Ind. Med. 50 (11), 831–840.
Bouchard, M., Mergler, D., Baldwin, M., Panisset, M., Roels, H.A., 2007b. Neuropsychiatric symptoms and past manganese exposure in a ferro-alloy plant. Neurotoxicology 28 (2), 290–297.
Bush, V.J., Moyer, T.P., Batts, K.P., Parisi, J.E., 1995. Essential and toxic element concentrations in fresh and formalin-fixed human autopsy tissues. Clin. Chem. 41 (2), 284–294.
CDC, 2006. National Center for Health Statistics (NCHS). National Health and Nutrition Examination Survey. Analytic and Reporting Guidelines. The National Health and Nutrition Examination Survey (NHANES). U.S. Department of Health and Human Services, Centers for Disease Control and Prevention, Hyattsville, MD September, 2006. Available at: http://www.cdc.gov/nchs/nhanes/nhanes_questionnaires.htm.
CDC, 2007. National Center for Health Statistics (NCHS). National Health and Nutrition Examination Survey Data. U.S. Department of Health and Human Services, Centers for Disease Control and Prevention, Hyattsville, MD 2003–2006. Available at: http://www.cdc.gov/nchs/nhanes/nhanes_questionnaires.htm.
CDC, 2010. National Center for Health Statistics (NCHS). National Health and Nutrition Examination Survey Data. U.S. Department of Health and Human Services, Centers for Disease Control and Prevention, Hyattsville, MD Demographics Data 2009–2010. Available at: http://www.cdc.gov/nchs/nhanes/nhanes_questionnaires.htm.
CDC, 2012. National Center for Health Statistics (NCHS). National Health and Nutrition Examination Survey Data. U.S. Department of Health and Human Services, Centers for Disease Control and Prevention, Hyattsville, MD Demographics Data 2011–2012. Available at: http://www.cdc.gov/nchs/nhanes/nhanes_questionnaires.htm.
Clewell 3rd, H.J., Andersen, M.E., 1985. Risk assessment extrapolations and physiological modeling. Toxicol. Ind. Health 1 (4), 111–131.
Clewell, H.J., Gentry, P.R., Gearhart, J.M., Allen, B.C., Andersen, M.E., 1995. Considering pharmacokinetic and mechanistic information in cancer risk assessments for environmental contaminants: examples with vinyl chloride and trichloroethylene. Chemosphere 31 (1), 2561–2578.
Cochran, W., 1954. Some methods for strengthening the common X^2 tests. Biometrics 10 (4), 417–451.
Dastur, D.K., Manghani, D.K., Raghavendran, K.V., 1971. Distribution and fate of Mn in the monkey: studies of different parts of the central nervous system and other organs. J. Clin. Invest. 50 (1), 9–20.
Davidsson, L., Cederblad, A., Hagebo, E., Lonnerdal, B., Sandstrom, B., 1988. Intrinisic and extrinsic labeling for studies of manganese absorption in humans. J. Nutr. 118 (12), 1517–1521.
Deschamps, F.J., Guillaumot, M., Raux, S., 2001. Neurological effects in workers exposed to manganese. J. Occup. Environ. Med. 43 (2), 127–132.
Dorman, D.C., Struve, M.F., James, R.A., Marshall, M.W., Parkinson, C.U., Wong, B.A., 2001. Influence of particle solubility on the delivery of inhaled manganese to the rat brain: manganese sulfate and manganese tetroxide pharmacokinetics following repeated (14-day) exposure. Toxicol. Appl. Pharmacol. 170 (2), 79–87.
Dorman, D.C., Struve, M.F., Marshall, M.W., Parkinson, C.U., James, R.A., Wong, B.A., 2006a. Tissue manganese concentrations in young male rhesus monkeys following subchronic manganese sulfate inhalation. Toxicol. Sci. 92 (1), 201–210.
Dorman, D.C., Struve, M.F., Wong, B.A., Dye, J.A., Robertson, I.D., 2006b. Correlation of brain magnetic resonance imaging changes with pallidal manganese concentrations in rhesus monkeys following subchronic manganese inhalation. Toxicol. Sci. 92 (1), 219–227.
Dorman, D.C., Andersen, M.E., Roper, J.M., Taylor, M.D., 2012. Update on a pharmacokinetic-centric Alternative Tier II Program for MMT—part I: program implementation and lessons learned. J. Toxicol. 2012, 946742.
Eriksson, H., Tedroff, J., Thuomas, K.A., Aquilonius, S.M., Hartvig, P., Fasth, K.J., Bjurling, P., Langström, B., Hedström, K.G., Heilbronin, E., 1992. Manganese induced brain lesions in *Macaca fascicularis* as revealed by positron emission tomography and magnetic resonance imaging. Arch. Toxicol. 66 (6), 403–407.
Fittro, K.P., Bolla, K.I., Heller, J.R., Meyd, C.J., 1992. The Milan Automated Neurobehavioral System. Age, sex, and education differences. J. Occup. Med. 34 (9), 918–922.
Furchner, J.E., Richmond, C.R., Drake, G.A., 1966. Comparative metabolism of radionuclides in mammals. III. Retention of manganese-54 in the mouse, rat, monkey, and dog. Health Phys. 12 (10), 673–675.
Gibbs, J.P., Crump, K.S., Houck, D.P., Warren, P.A., Mosley, W.S., 1999. Focused medical surveillance: a search for subclinical movement disorders in a cohort of U.S. workers exposed to low levels of manganese dust. Neurotoxicology 20 (2–3), 299–313.
Guilarte, T.R., 2010. Manganese and Parkinson's disease: a critical review and new findings. Environ. Health Perspect. 118 (8), 1071–1080.
Guilarte, T.R., 2013. Manganese neurotoxicity: new perspectives from behavioral, neuroimaging, and neuropathological studies in humans and non-human primates. Front. Aging Neurosci. 5, 1–10 Article 23.
Gwiazda, R., Lucchini, R., Smith, D., 2007. Adequacy and consistency of animal studies to evaluate the neurotoxicity of chronic low-level manganese exposure in humans. J. Toxicol. Environ. Health A 70 (7), 594–605.
Health Canada, 2010. Human Health Risk Assessment for Inhaled Manganese. Prepared by: Water, Air and Climate Change Bureau Healthy Environments and Consumer Safety Branch.
Health Canada, 2011. Trace Elements Table: Average Dietary Intakes (μg/kg bw/day) of Trace Elements for Canadians in Different Age/Sex Groups for Total Diet Study in 2007. (Last Updated: January 31, 2011. Available at: http://www.hc-sc.gc.ca/fn-an/surveill/total-diet/intake-apport/index-eng.php?_sm_au_=iVV4Z1Wr62nQvSP6. Accessed September 2015).
Hoet, P., Vanmarcke, E., Geens, T., Deumer, G., Haufroid, V., Roels, H.A., 2012. Manganese in plasma: a promising biomarker of exposure to Mn in welders. A pilot study. Toxicol. Lett. 213 (1), 69–74.
Leavens, T.L., Rao, D., Andersen, M.E., Dorman, D.C., 2007. Evaluating transport of manganese from olfactory mucosa to striatum by pharmacokinetic modeling. Toxicol. Sci. 97 (2), 265–278.
Lee, W.Y., Iannucci-Berger, W.A., Eitzer, B.D., White, J.C., Mattina, M.I., 2003. Plant uptake and translocation of air-borne chlordane and comparison with the soil-to-plant route. Chemosphere 53 (2), 111–121.
Lees-Haley, P.R., Rohling, M.L., Langhinrichsen-Rohling, J., 2006. A meta-analysis of the neuropsychological effects of occupational exposure to manganese. Clin. Neuropsychol. 20 (1), 90–107.
Lucchini, R., Selis, L., Folli, D., Apostoli, P., Vanoni, O., Iregren, A., Alessio, L., 1995. Neurobehavioral effects of manganese in workers from a ferroalloy plant after temporary cessation of exposure. Scand. J. Work Environ. Health 21 (2), 143–149.
Lucchini, R., Bergamaschi, E., Smargiassi, A., Festa, D., Apostoli, P., 1997. Motor function, olfactory threshold, and hematological indices in manganese-exposed ferroalloy workers. Environ. Res. 73 (1–2), 175–180.
Lucchini, R., Apostoli, P., Perrone, C., Placidi, D., Albini, E., Migliorati, P., Mergler, D., Sassine, M.P., Palmi, S., Alessio, L., 1999. Long term exposure to "low levels" of manganese oxides and neurofunctional changes in ferroalloy workers. Neurotoxicology 20 (2–3), 287–298.
Mahoney, J.P., Small, W.J., 1968. Studies on manganese III. The biological half-life of radiomanganese in man and factors which affect this half-life. J. Clin. Invest. 47 (3), 643–653.
Mena, I., Marin, O., Fuenzalida, S., Cotzias, G.C., 1967. Chronic manganese poisoning: clinical picture and manganese turnover. Neurology 17 (2), 128–136.
Mergler, D., Huel, G., Bowler, R., Iregren, A., Belanger, S., Baldwin, M., Tardif, R., Smargiassi, A., Martin, L., 1994. Nervous system dysfunction among workers with long-term exposure to manganese. Environ. Res. 64 (2), 151–180.
Myers, J.E., Thompson, M.L., Naik, I., Theodorou, P., Esswein, E., Tassell, H., Daya, A., Renton, K., Spies, A., Paicker, J., Young, T., Jeebhay, M., Ramushu, S., London, L., Rees, D.J., 2003a. The utility of biological monitoring for manganese in ferroalloy smelter workers in South Africa. Neurotoxicology 24 (6), 875–883.
Myers, J.E., Thompson, M.L., Ramushu, S., Young, T., Jeebhay, M.F., London, L., Esswein, E., Renton, K., Spies, A., Boulle, A., Naik, I., Iregren, A., Rees, D.J., 2003b. The nervous system effects of occupational exposure on workers in a South African manganese smelter. Neurotoxicology 24 (6), 885–894.
Myers, J.E., teWaterNaude, J., Fourie, M., Zogoe, H.B., Naik, I., Theodorou, P., Tassel, H., Daya, A., Thompson, M.L., 2003c. Nervous system effects of occupational manganese exposure on South African manganese mineworkers. Neurotoxicology 24 (4–5), 649–656.
NAPS, 2015. National Air Pollution Surveillance Network. (Available at: http://www.ec.gc.ca/natchem/default.asp?lang=en&n=EE0E2169-1. Last accessed September 2015).
Newland, M.C., Cox, C., Hamada, R., Oberdorster, G., Weiss, B., 1987. The clearance of manganese chloride in the primate. Fundam. Appl. Toxicol. 9 (2), 314–328.
Newland, M.C., Cecklet, T.L., Kordower, J.H., Weiss, B., 1989. Visualizing manganese in the primate basal ganglia with magnetic resonance imaging. Exp. Neurol. 106 (3), 251–258.
Nong, A., Teeguarden, J.G., Clewell 3rd, H.J., Dorman, D.C., Andersen, M.E., 2008. Pharmacokinetic modeling of manganese in the rat. IV: assessing factors that contribute to brain accumulation during inhalation exposure. J. Toxicol. Environ. Health 71 (7), 413–426.
Nong, A., Taylor, M.D., Clewell 3rd, H.J., Dorman, D.C., Andersen, M.E., 2009. Manganese tissue dosimetry in rats and monkeys: accounting for dietary and inhaled Mn with physiologically based pharmacokinetic modeling. Toxicol. Sci. 108 (1), 22–34.
Olanow, C.W., Good, P.F., Shinotoh, H., Hewitt, K.A., Vingerhoets, F., Snow, B.J., Beal, M.F., Caine, D.B., Perl, D.P., 1996. Manganese intoxication in the rhesus monkey: a clinical, imaging, pathologic, and biochemical study. Neurology 46 (2), 492–498.
Roels, H., 1993. Correspondence from H. Roels, Faculte de Medecine, Unite de Toxicologie et Medecine du Travail, Catholique Universite de Louvain, Clos Chapelle-aux-Champs 30, BTE 3054, 1200 Bruxelles, Belgium, to J. Michael Davis, Environmental Criteria and Assessment Office (MD-52). U.S. EPA, Research Triangle Park, NC 27711 (October 19. As cited in USEPA 1993).
Roels, H., Lauwerys, R., Genet, P., Sarhan, M.J., de Fays, M., Hanotiau, I., Buchet, J.P., 1987a. Relationship between external and internal parameters of exposure to manganese in workers from a manganese oxide and salt producing plant. Am. J. Ind. Med. 11 (3), 297–305.
Roels, H., Lauwerys, R., Buchet, J.P., Genet, P., Sarhan, M.J., Hanotiau, I., de Fays, M., Bernard, A., Stanescu, D., 1987b. Epidemiological survey among workers exposed to manganese: effects on lung, central nervous system, and some biological indices. Am. J. Ind. Med. 11 (3), 307–327.
Roels, H.A., Ghyselen, P., Buchet, J.P., Ceulemans, E., Lauwerys, R.R., 1992. Assessment of the permissible exposure level to manganese in workers exposed to manganese dioxide dust. Br. J. Ind. Med. 49 (1), 25–34.
Roels, H.A., Ortega Eslava, M.I., Ceulemans, E., Robert, A., Lison, D., 1999. Prospective study on the reversibility of neurobehavioral effects in workers exposed to manganese dioxide. Neurotoxicology 20 (2–3), 255–271.
Roels, H.A., Bowler, R.M., Kim, Y., Claus Henn, B., Mergler, D., Hoet, P., Gocheva, V.V., Bellinger, D.C., Wright, R.O., Harris, M.G., Chang, Y., Bouchard, M.F., Rioias-Rodriguez, H., Menezes-Filho, J.A., Tellez-Rojo, M.M., 2012. Manganese exposure and cognitive deficites: a growing concern for manganese neurotoxicity. Neurotoxicology 33 (4), 872–880.

Schroeter, J.D., Kimbell, J.S., Gross, E.A., Willson, G.A., Dorman, D.C., Tan, Y.M., Clewell III, H.J., 2008. Application of physiological computational fluid dynamics models to predict interspecies nasal dosimetry of inhaled acrolein. Inhal. Toxicol. 20 (3), 227–243.

Schroeter, J.D., Nong, A., Yoon, M., Taylor, M.D., Dorman, D.C., Andersen, M.E., Clewell 3rd, H.J., 2011. Analysis of manganese tracer kinetics and target tissue dosimetry in monkeys and humans with multi-route physiologically based pharmacokinetic models. Toxicol. Sci. 120 (2), 481–498.

Schroeter, J.D., Dorman, D.C., Yoon, M., Nong, A., Taylor, M.D., Andersen, M.E., Clewell 3rd., H.J., 2012. Application of a multi-route physiologically based pharmacokinetic model for manganese to evaluate dose-dependent neurological effects in monkeys. Toxicol. Sci. 129 (2), 432–446.

Taylor, M.D., Clewell 3rd, H.J., Andersen, M.E., Schroeter, J.D., Yoon, M., Keene, A.M., Dorman, D.C., 2012. Update on a pharmacokinetic-centric Alternative Tier II Program for MMT—part II: physiologically based pharmacokinetic modeling and manganese risk assessment. J. Toxicol. 2012, 791431.

Teeguarden, J.G., Dorman, D.C., Covington, T.R., Clewell 3rd, H.J., Andersen, M.E., 2007a. Pharmacokinetic modeling of manganese. I. Dose dependencies of uptake and elimination. J. Toxicol. Environ. Health 70 (18), 1493–1504.

Teeguarden, J.G., Dorman, D.C., Nong, A., Covington, T.R., Clewell 3rd, H.J., Andersen, M.E., 2007b. Pharmacokinetic modeling of manganese. II. Hepatic processing after ingestion and inhalation. J. Toxicol. Environ. Health 70 (18), 1505–1514.

Teeguarden, J.G., Gearhart, J., Clewell 3rd, H.J., Covington, T.R., Nong, A., Andersen, M.E., 2007c. Pharmacokinetic modeling of manganese. III. Physiological approaches accounting for background and tracer kinetics. J. Toxicol. Environ. Health 70 (18), 1515–1526.

Tukey, J.W., Ciminera, J.L., Heyse, J.F., 1985. Testing the statistical certainty of a response to increasing doses of a drug. Biometrics 41 (1), 295–301.

USDA, 2012. USDA Food and Nutrient Database for Dietary Studies 2011–2012. Food Surveys Research Group Home Page. U.S. Department of Agriculture, Agricultural Research Service Available at: http://www.ars.usda.gov/ba/bhnrc/fsrg.

USDA, 2014. USDA National Nutrient Database for Standard Reference, Release 27. (Version Current: August 2014. Available at: http://www.ars.usda.gov/ba/bhnrc/ndl. Accessed September 2015).

USEPA, 1993. Manganese (CASRN 7439-96-5). Inhalation RfC Assessment. United States Environmental Protection Agency (Available at: http://www.epa.gov/iris/subst/0373.htm. Last Accessed April, 2016).

USEPA, 1998. Integrated Risk Information System (IRIS): Manganese (CASRN 7439-96-5). United States Environmental Protection Agency Available at: http://cfpub.epa.gov/ncea/iris/index.cfm?fuseaction=iris.showQuickView&substance_nmbr=0373.

USEPA, 2005. Guidelines for Carcinogen Risk Assessment. Risk Assessment Forum. United States Environmental Protection Agency, Washington, D.C. (EPA/630/P-03/001F).

USEPA, 2006. Approaches for the Application of Physciologically Based Pharmacokinetic (PBPK) Models and Supporting Data in Risk Assessment. National Center for Enviromental Assessment, Office of Research and Development, United States Environmental Protection Agency, Washington, D.C. (EPA/600/R-05/043F).

USEPA, 2015. Technology Transfer Network (TTN) Air Quality System (AQS) Data Mart. United States Environmental Protection Agency Available at: https://aqs.epa.gov/aqsweb/documents/data_mart_welcome.html.

Vitarella, D., Moss, O., Dorman, D.C., 2000. Pulmonary clearance of manganese phosphate, manganese sulfate, and manganese tetraoxide by CD rats following intratracheal instillation. Inhal. Toxicol. 12 (10), 941–957.

Yoon, M., Nong, A., Clewell 3rd, H.J., Taylor, M.D., Dorman, D.C., Andersen, M.E., 2009a. Evaluating placental transfer and tissue concentrations of manganese in the pregnant rat and fetuses after inhalation exposures with a PBPK model. Toxicol. Sci. 112 (1), 44–58.

Yoon, M., Nong, A., Clewell 3rd, H.J., Taylor, M.D., Dorman, D.C., Andersen, M.E., 2009b. Lactational transfer of manganese in rats: predicting manganese tissue concentration in the dam and pups from inhalation exposure with a pharmacokinetic model. Toxicol. Sci. 112 (1), 23–43.

Yoon, M., Schroeter, J.D., Nong, A., Taylor, M.D., Dorman, D.C., Andersen, M.E., Clewell 3rd., H.J., 2011. Physiologically based pharmacokinetic modeling of fetal and neonatal manganese exposure in humans: describing manganese homeostasis during development. Toxicol. Sci. 122 (2), 297–316.

Young, T., Myers, J.E., Thompson, M.L., 2005. The nervous system effects of occupational exposure to manganese—measured as respirable dust—in a South African manganese smelter. Neurotoxicology 26 (6), 993–1000.

ATTACHMENT D

Schroeter et al. (2011)
Yoon et al. (2019)
Campbell et al. (2022)

TOXICOLOGICAL SCIENCES **120(2)**, 481–498 (2011)
doi:10.1093/toxsci/kfq389
Advance Access publication December 27, 2010

Analysis of Manganese Tracer Kinetics and Target Tissue Dosimetry in Monkeys and Humans with Multi-Route Physiologically Based Pharmacokinetic Models

Jeffry D. Schroeter,*,[1] Andy Nong,* Miyoung Yoon,* Michael D. Taylor,† David C. Dorman,‡ Melvin E. Andersen,* and Harvey J. Clewell, III*

*The Hamner Institutes for Health Sciences, Research Triangle Park, North Carolina 27709-2137; †Afton Chemical Corp., Richmond, Virginia 23219; and ‡College of Veterinary Medicine, North Carolina State University, Raleigh, North Carolina 27606

[1]To whom correspondence should be addressed at The Hamner Institutes for Health Sciences, 6 Davis Drive, Research Triangle Park, NC 27709-2137. Fax: (919) 558-1300. E-mail: jschroeter@thehamner.org.

Received October 18, 2010; accepted December 10, 2010

Manganese (Mn) is an essential nutrient with the capacity for toxicity from excessive exposure. Accumulation of Mn in the striatum, globus pallidus, and other midbrain regions is associated with neurotoxicity following high-dose Mn inhalation. Physiologically based pharmacokinetic (PBPK) models for ingested and inhaled Mn in rats and nonhuman primates were previously developed. The models contained saturable Mn tissue-binding capacities, preferential fluxes of Mn in specific tissues, and homeostatic control processes such as inducible biliary excretion of Mn. In this study, a nonhuman primate model was scaled to humans and was further extended to include iv, ip, and sc exposure routes so that past studies regarding radiolabeled carrier-free $^{54}MnCl_2$ tracer kinetics could be evaluated. Simulation results accurately recapitulated the biphasic elimination behavior for all exposure routes. The PBPK models also provided consistent cross-species descriptions of Mn tracer kinetics across multiple exposure routes. These results indicate that PBPK models can accurately simulate the overall kinetic behavior of Mn and predict conditions where exposures will increase free Mn in various tissues throughout the body. Simulations with the human model indicate that globus pallidus Mn concentrations are unaffected by air concentrations < 10 $\mu g/m^3$ Mn. The use of this human Mn PBPK model can become a key component of future human health risk assessment of Mn, allowing the consideration of various exposure routes, natural tissue background levels, and homeostatic controls to explore exposure conditions that lead to increased target tissue levels resulting from Mn overexposure.

Key Words: **manganese; PBPK; inhalation exposure; risk assessment; neurotoxicity; pharmacokinetics.**

The essential trace element manganese (Mn) is found in all human tissues and is required for numerous physiological processes, including protein and carbohydrate metabolism, immune system function, and bone growth. The primary source of Mn exposure is through the diet, with adult human consumption ranging from 1 to 10 mg Mn/day, of which approximately 1–5% is absorbed by the gastrointestinal (GI) tract (Aschner *et al.*, 2005; ATSDR, 2000; Freeland-Graves, 1994). Homeostatic controls tightly restrict Mn absorption and regulate Mn excretion to maintain stable tissue levels despite fluctuations in daily Mn dietary exposure.

Neurotoxicity can occur when Mn intake exceeds elimination resulting in Mn accumulation in midbrain regions that influence motor control such as the globus pallidus, striatum, and substantia nigra (Dorman *et al.*, 2006b; Yamada *et al.*, 1986). Similar neurological responses have been linked to prolonged high-dose Mn inhalation (Pal *et al.*, 1999) or drinking water ingestion (Kawamura *et al.*, 1941), impaired Mn clearance because of liver dysfunction (Spahr *et al.*, 1996), and long-term parenteral nutrition (Fell *et al.*, 1996). To understand the risk to humans from excessive Mn exposure, it is important to determine the exposure conditions that result in Mn concentrations in the brain that are increased significantly compared with brain Mn concentrations arising from normal dietary intake (Andersen *et al.*, 1999).

Inhalation has historically been the exposure route of most concern for Mn because inhaled Mn particles that deposit on lung epithelium bypass uptake control in the GI tract and liver and directly enter the systemic circulation. Prolonged exposure to high levels (> 1 mg/m^3) of Mn-laden dusts in occupational settings such as mining can result in severe Mn-induced neurotoxicity, including the onset of manganism, an extrapyramidal movement disorder that is similar but clinically distinguishable from Parkinson's disease (Aschner *et al.*, 2005; Pal *et al.*, 1999). Neurological effects of a subclinical nature have been reported in workers with chronic inhalation to lower concentrations (0.5–1.0 mg/m^3) of Mn in the workplace (Iregren, 1990; Lucchini *et al.*, 1995, 1999; Mergler *et al.*, 1994; Myers *et al.*, 2003; Roels, *et al.*, 1987, 1992, 1999; Young *et al.*, 2005). Other studies have indicated that

environmental exposures may also be associated with subtle, subclinical neurological changes in the general population (Finkelstein and Jerrett, 2007; Lucchini *et al*., 2007; Mergler *et al*., 1999; Rodriguez-Agudelo *et al*., 2006).

Concerns regarding chronic low-level Mn inhalation exposure have led to the development of an extensive Mn pharmacokinetic data set and physiologically based pharmacokinetic (PBPK) models. This series of pharmacokinetic modeling studies described Mn kinetics using compartmental models (Teeguarden *et al*., 2007a,b,c), PBPK models of adult rats and monkeys (Nong *et al*., 2008, 2009), and PBPK models of gestation and lactation in rats (Yoon *et al*., 2009a,b). The first Mn compartmental pharmacokinetic models used linear exchange rates to simulate Mn tissue kinetics under normal and deficient dietary conditions but were unable to capture the rapid rise in tissue Mn concentrations seen during inhalation exposure to high Mn concentrations. An enhanced model structure allowed tissue compartments to retain fairly constant Mn levels during normal dietary intake and included saturable Mn tissue stores that increased rapidly under inhalation exposure conditions (Nong *et al*., 2009). These PBPK modeling efforts produced a consistent description of Mn tissue kinetics in rats and monkeys following dietary and inhalation exposures (Andersen *et al*., 2010).

In the current study, the previous PBPK model for rats and monkeys (Nong *et al*., 2009) was extended to humans to predict inhalation exposure conditions that result in increased brain Mn concentrations. In addition, multiple exposure routes were examined, including iv, ip, and sc injection, to simulate distribution and elimination of the radioisotope ^{54}Mn. The addition of these exposure routes allowed analysis of studies that have been conducted to analyze tracer kinetics of ^{54}Mn in nonhuman primates and human volunteers. These studies are important to consider because activity of the soluble, carrier-free ^{54}Mn (given as $^{54}MnCl_2$) implicitly reflects the overall kinetics of Mn in the body.

MATERIALS AND METHODS

PBPK model structure. The PBPK model structure contained compartments for the liver, lung, nasal cavity, bone, blood, cerebellum, olfactory bulb, globus pallidus, and pituitary gland (Fig. 1). Remaining body tissues were combined into a single compartment. The same model structure was used for monkeys and humans. A thorough description of the model parameters and underlying equations are given in Nong *et al.* (2008, 2009). The model simulates concurrent exposure to dietary and inhaled Mn and also simulates ^{54}Mn tracer kinetics from oral and inhalation exposure and by ip, iv, and sc administration.

Inhalation exposure was to $MnSO_4$ particles, which are highly soluble in mucus and tissue (Vitarella *et al*., 2000). Aerosol parameters for $MnSO_4$ consisted of a mass median aerodynamic diameter of 2.0 μm, a geometric SD of 1.5 and a particle density of 2.95 g/cm^3 (Dorman *et al*., 2006a). Fractional deposition of inhaled $MnSO_4$ particles in the respiratory tract was calculated using the Multiple-Path Particle Dosimetry model (MPPD version 2.0; Anjilvel and Asgharian, 1995; Asgharian *et al*., 2001; available at http://www.thehamner.org). Nasal deposition estimates from the MPPD model were partitioned onto the respiratory and olfactory epithelium based on species-dependent airflow allocation (Kepler *et al*., 1998; Schroeter *et al*., 2010). Deposited Mn was assumed to be rapidly absorbed from lung tissues and nasal respiratory epithelium into the systemic circulation or transported from the nasal olfactory epithelium to the olfactory bulb.

Absorption of Mn by the GI tract is dose dependent. As dietary Mn levels increase, GI absorption decreases and biliary excretion increases (Dorman *et al*., 2001b; Teeguarden *et al*., 2007b). These homeostatic controls are overwhelmed when Mn exposure is high, leading to increases in free Mn tissue levels. The fraction of Mn absorbed by the GI tract (Fdietup) and the biliary excretion rate constant (kbilec) were calibrated based on steady-state tissue concentrations and ^{54}Mn whole-body elimination curves. Induction of biliary elimination of Mn was included to describe increased bile elimination that was directly observed in higher exposure concentrations in monkeys (Nong *et al*., 2009). The biliary elimination rate constant was dependent on blood Mn concentration:

$$k_{\text{bile}} = k_{\text{bile0}}\left(1 + \frac{k_{\text{bmax}} C_{\text{art}}^{n}}{k_{\text{b50}}^{n} + C_{\text{art}}^{n}}\right), \quad (1)$$

where k_{bile0} is the basal biliary excretion rate constant, k_{bmax} is the maximal increase in the excretion rate constant, k_{b50} is the arterial concentration at half the induced level of Mn in the arterial blood (C_{art}), and n is the slope factor. C_{art} was used as a surrogate for free Mn liver concentrations, the presumed driver for Mn excretion, because Mn blood levels were directly measured in monkeys (Dorman *et al*., 2006a; Nong *et al*., 2009).

A simplified GI tract was used in the Mn PBPK model by Nong *et al.* (2009) because there was no need to track unabsorbed or absorbed Mn after it was excreted in the bile. Modifications were made to this GI structure to include fecal excretion (to be consistent with the data from Newland *et al*., 1987) and simulate tracer kinetics of ^{54}Mn administered orally in monkeys and humans. A series of gut compartments were added that were consistent with the physiology of Mn absorption by the GI tract (Fig. 1). Fdietup represents the fraction of dietary Mn that was absorbed in the GI tract and was available to the systemic circulation. This process was described as a direct transfer from the gut lumen to the liver. The remaining fraction of Mn (1 − Fdietup) in the gut lumen was absorbed by the gut epithelium and stored in enterocytes or transferred to the lower GI tract lumen and excreted through the feces. $F_{\text{ent}} \times k_{\text{GI}}$ represents the storage rate constant of the enterocytes in the gut epithelium, where F_{ent} is the fraction stored by the enterocytes and k_{GI} is the rate constant for movement from the gut lumen. Mn transfer from the gut epithelium to the lower GI tract was by sloughing of enterocytes (k_{ent}) from the epithelial layer. The stored Mn in enterocytes was eventually excreted into feces without entering the systemic circulation because of enterocyte turnover. Mn elimination from the body through the feces was governed by the rate constant k_{feces}.

The following biologically informed assumptions were made concerning distribution of absorbed Mn. All tissues contain both free and bound Mn. Free Mn circulates in the blood throughout the body. Bound Mn is stored in tissue constituents where it participates in various physiological functions. Mn binding is a reversible, saturable process described by tissue-specific association (k_{a}) and dissociation (k_{d}) rate constants. The distribution between bound and free Mn is determined by the dissociation binding ratio ($k_{\text{d}}/k_{\text{a}}$). The maximal binding capacity (B_{max}) constrains the levels of bound Mn in each tissue; saturation of the binding capacity with increasing exposure concentration leads to increases in concentrations of free Mn in each tissue. The rate of change of free Mn in each tissue depends on their respective binding rate constants and maximal binding capacity.

Certain brain regions in monkeys exposed to higher doses of Mn by inhalation have preferential increases in tissue Mn (Dorman *et al*., 2006a). Selective increases in brain Mn in some tissues following inhalation exposure could not be accurately simulated using only dissociation processes. Differential increases in free Mn in the four brain regions (globus pallidus, pituitary, cerebellum, and olfactory bulb) were described by asymmetric diffusion rate constants from tissue blood into tissue and back (k_{in} and k_{out}). In addition, the globus pallidus and pituitary influx rates were modified by introducing a concentration-dependent influx rate constant (Nong *et al*., 2009):

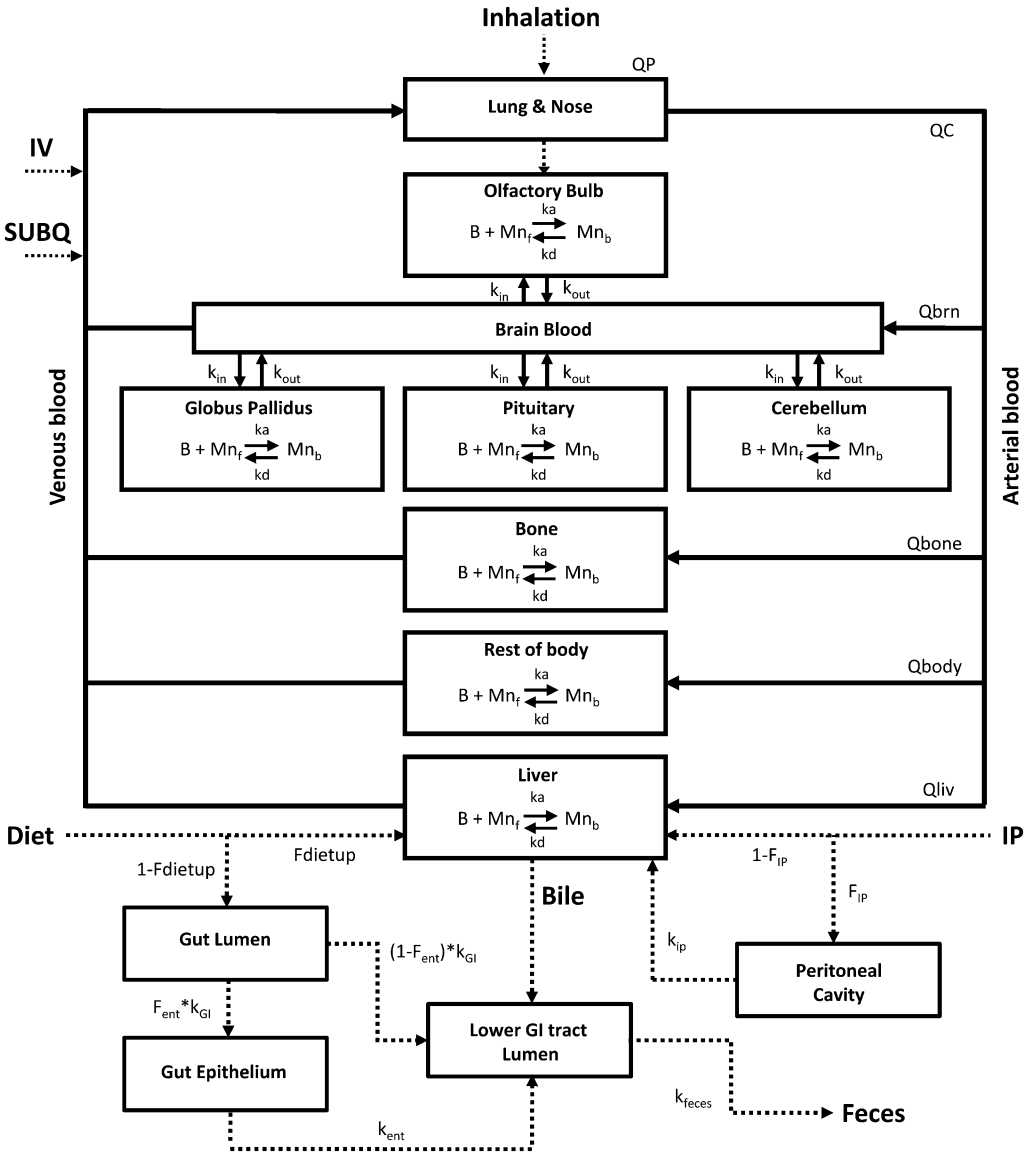

FIG. 1. The PBPK model structure describing Mn tissue kinetics in adult monkeys and humans. In each tissue compartment, the amount of bound Mn is in equilibrium with the assumed binding capacity (B_{tissue}) and free Mn. Tissue-binding processes were controlled by association and dissociation rate constants (k_a and k_d). Free Mn moves in the blood throughout the body and is stored in each tissue as bound Mn. Influx and efflux diffusion rate constants (k_{in} and k_{out}) control preferential increases in free Mn in brain regions. Q_P, Q_C, and Q_{tissue} refer to pulmonary ventilation, cardiac output, and tissue blood flows.

$$k_{\text{in}} = k_{\text{in0}}\left(1 + \frac{k_{\text{in max}}\,A_{\text{free},t}}{k_{\text{in50}} + A_{\text{free},t}}\right), \tag{2}$$

where k_{in0} is the basal influx rate constant, k_{inmax} is the maximal influx rate, k_{in50} is the affinity rate constant, and A_{free} is the amount of free Mn in the respective brain region. Defining an increase in tissue influx rate constant as free Mn increases was needed to describe changes in Mn concentrations in these brain regions that could not be sufficiently described by association and dissociation rate constants. The rate of change of free Mn in brain regions depends on diffusional clearance into and out of the tissues and on the binding rate constants and binding capacity in each tissue.

In addition to dietary and inhalation exposure routes, model components were included to account for administration of ^{54}Mn by ip, iv, and sc injection (Fig. 1). Iv and sc injections were input directly into the venous blood; ip injections were simulated by placing the majority of the injected dose directly into the liver, consistent with uptake by the highly vascularized GI tissue. A small fraction of the ip dose (F_{IP}) was absorbed into the peritoneal cavity where it was slowly released (k_{IP}) into the liver.

Monkey model parameterization. Physiological and anatomical parameters for the monkey PBPK model were obtained from Davies and Morris (1993), Dorman *et al.* (2006a), and Nong *et al.* (2009) (Table 1). A body weight of 2.5 kg was used in the monkey inhalation exposure simulations to be consistent with body weights reported by Dorman *et al.* (2006a). Basal Mn tissue levels (Table 2) were set to tissue measurements in control monkeys fed a commercial diet containing 133 ppm Mn (Dorman *et al.*, 2006a) by adjusting the parameters governing dietary absorption (Fdietup) and biliary elimination (kbilec) (Table 3). Nasal and lung deposition fractions for the monkey were scaled from the rat by nasal epithelial surface area and pulmonary ventilation, respectively. As reported by Nong *et al.* (2009), Mn nasal and lung deposition values were 40 and 27%, respectively. Nasal deposition was further divided

TABLE 1
Physiological Parameters for Monkeys and Humans

Parameter	Monkey	Human	Units
Body weight[a] (kg)	2.5	70	kg
Tissue volumes (as fraction of body weight)			
Blood[a,b]	0.0734	0.079	
Bone[a,b]	0.12	0.12	
Brain[a,b]	0.036	0.02	
Cerebellum[a]	0.08	0.08	
Olfactory bulb[a]	0.0006	0.0006	
Globus Pallidus[a]	0.0015	0.0015	
Pituitary[a]	0.0013	0.0013	
Liver[a,b]	0.027	0.026	
Lung[a,b]	0.008	0.008	
Remaining body	Difference[g]		
Surface area of nasal respiratory epithelium[c,d]	15.6	9.81	$cm^2/kg^{0.75}$
Surface area of nasal olfactory epithelium[c,d]	1.6	0.52	$cm^2/kg^{0.75}$
Average nasal tissue thickness[e]	375	375	μm
Cardiac output[a,b]	19.5	13.0	l/h/kg
Pulmonary ventilation[a,b]	30.0	18.0	l/h/kg
Tissue blood flow (as fraction of cardiac output)			
Bone[a,b]	0.042	0.042	
Brain[a,b]	0.065	0.114	
Liver[a,b]	0.194	0.227	
Nose[f]	0.01	0.01	
Remaining body	Difference[g]		

[a]Monkey values are from Davies and Morris (1993) or Dorman *et al.* (2006a).
[b]Human values are from Brown *et al.* (1997).
[c]Monkey values are from Menache *et al.* (1997).
[d]Human values are from Schroeter *et al.* (2008).
[e]Values are from Conolly *et al.* (2000).
[f]From Frederick *et al.* (1998).
[g]Difference = 1.0 − (sum of listed compartment).

into respiratory and olfactory deposition according to an airflow allocation of 9% olfactory and 91% respiratory (Kepler *et al.*, 1998).

Dissociation rate constants (k_a and k_d), tissue binding capacities (B_{max}), and diffusion parameters (k_{in} and k_{out}) in each tissue compartment were calibrated to the pharmacokinetic data from Dorman *et al.* (2006a). In that study, monkeys were exposed by inhalation to $MnSO_4$ exposure atmospheres for 90 days (6 h/day, 5 days/week) at concentrations of 0, 0.06, 0.3, or 1.5 mg Mn/m^3. Tissues were collected on the day following the last Mn exposure to determine tissue Mn concentrations. Dissociation rate constants and maximal binding capacities were adjusted so that each brain region contained approximately 60% bound Mn under dietary exposure only (i.e., with no inhalation). These parameters reflect a change in bound Mn fraction from that reported by Nong *et al.* (2009) (approximately 20% bound Mn) to provide a more consistent description of Mn binding in brain regions across animal species. Diffusion parameters were then adjusted to simulate the rise in brain Mn tissue levels following the onset of inhalation exposure and the subsequent decrease in Mn brain tissue concentrations following the end-of-the exposure period. Further refinements to brain kinetics in the globus pallidus and pituitary regions were included by adding the dose-dependent influx term so that simulations accurately predicted the rise in Mn tissue levels in these regions. Tissue binding and diffusion parameters are listed in Table 4.

Human model parameterization. Physiological parameters in the human PBPK model were either scaled from the monkey or were obtained from the literature (Brown *et al.*, 1997) (Table 1). An average body weight of 70 kg was used in all simulations. Human basal Mn tissue levels were obtained from autopsy reports (Table 2). Dietary intake was set at 3 mg/day Mn, a value slightly higher than the adequate intake level (Aschner and Aschner, 2005). Dietary absorption (Fdietup) and biliary excretion (kbilec) were calibrated to whole-body elimination kinetics from iv tracer doses of ^{54}Mn (Table 3) (Mahoney and Small, 1968; Mena *et al.*, 1967).

Human respiratory tract deposition of $MnSO_4$ particles was estimated with MPPD using standard ventilatory parameters for resting nasal breathing in adults: 12 breaths per minute and a tidal volume of 625 ml. Nasal and lung deposition were estimated to be 37.6 and 25%, respectively. Deposition on human olfactory epithelium was assumed to be 5% of total nasal deposition based on olfactory airflow allocation (Schroeter *et al.*, 2010).

Interspecies scaling from monkeys to humans was based on allometric scaling for flows ($BW^{0.75}$) and volumes body weight (BW). For the initial human model parameterization, diffusion rate constants for brain compartments

TABLE 2
Basal Tissue Mn Concentrations in Monkeys and Humans

Tissue	Mn concentration (μg Mn/g tissue wet weight) Monkey[a]	Human	References for human values
Liver	2.49	1.2	Sumino *et al.* (1975)
Lung	0.15	0.22	Sumino *et al.* (1975)
Bone	0.08	0.074	Sumino *et al.* (1975)
Blood	0.01	0.064	Sumino *et al.* (1975)
Cerebellum	0.44	0.33	Aschner *et al.* (2005) and Bush *et al.* (1995)[b]
Globus pallidus	0.48	0.39	Aschner *et al.* (2005), Bush *et al.* (1995)[b], and Tracqui *et al.* (1995)
Olfactory bulb	0.31	0.67	Bonilla *et al.* (1982)[b]
Pituitary	0.84	0.46	Thorlacius-Ussing *et al.* (1988)[b]

[a]From Dorman *et al.* (2006a).
[b]Mn tissue concentrations in these references were reported as micrograms of Mn per gram dry tissue weight and were reduced by 80% to convert to wet tissue weight (Molokhia, 1967).

TABLE 3
Dietary Absorption and Biliary Elimination Parameters in Monkeys and Humans

Parameter	Description	Monkey	Human	Units
Fdietup	Fractional gut absorption	0.0021[a]	0.06[b]	
kbilec	Biliary excretion rate constant[c]	0.051	0.051	l/h/kg
k_{bmax}	Maximal biliary excretion rate constant[d]	2.5	2.5	l/h
k_{b50}	Affinity rate constant[d]	0.027	0.027	μg/ml
n	Slope factor[d]	3	3	
k_{GI}	Transfer rate from gut lumen	0.6[e]	0.026[f]	/h
F_{ENT}	Fractional enterocyte storage	0.011[e]	0.005[f]	
k_{ENT}	Enterocyte sloughing rate	0.0022[e]	0.0022[f]	/h

[a]Calibrated with a 133-ppm Mn diet to the data from Dorman *et al.* (2006a).
[b]Calibrated using a 3 mg/day Mn diet to the data from Mahoney and Small (1968) and Mena *et al.* (1967).
[c]kbile is allometrically scaled (kbile = kbilec × $BW^{0.75}$).
[d]see Equation 1.
[e]Calibrated to the data from Furchner *et al.* (1966).
[f]Calibrated to the data from Davidsson *et al.* (1988).

were scaled from the monkey as $BW^{-0.25}$ because they represent clearance terms divided by tissue volume. Tissue binding capacity (B_{max}) was scaled by tissue volume. Association and dissociation rate constants (k_a and k_d) were modified from monkey values to yield a higher bound fraction in human brain regions (80% bound Mn under dietary exposure only) compared with that in monkeys. This reflects the greater bound Mn storage requirements associated with lower Mn dietary intake in humans. Inhalation exposure simulations were also conducted assuming a 60% bound Mn fraction in humans to test the sensitivity of this assumption. Since there are further physiological and biochemical differences between monkeys and humans that affect Mn uptake and storage, a direct scaling of parameters between species did not adequately describe steady-state Mn tissue levels. Although parameters were retained across species to the extent possible, additional refinements to model parameters were employed to maintain basal tissue levels with only dietary Mn exposure (i.e., no inhalation). The final dissociation rate constants, maximal binding capacities, and diffusion parameters for the human model are listed in Table 4.

Inhalation exposure simulations. Mn inhalation exposure was simulated in monkeys for 90 days (6 h/day, 5 days/week) to be consistent with the study by Dorman *et al.* (2006a). Mn inhalation exposures in humans were simulated for 90 days (8 h/day, 5 days/week), unless otherwise noted.

RESULTS

^{54}Mn Tracer Kinetics in Monkeys

The Mn PBPK model simulated ^{54}Mn tracer kinetics in monkeys exposed by ip, iv, and sc injection and by oral and inhalation routes. Exposure routes were selected based on whole-body elimination or fecal excretion data available from ^{54}Mn tracer kinetic studies in monkeys. Fractional dietary absorption (Fdietup) and biliary excretion (kbilec) were adjusted for each exposure scenario to account for the different Mn diets and body weights used in each study (Table 5). These parameters were calibrated to maintain the basal tissue Mn levels reported by Dorman *et al.* (2006a) prior to exposure and to fit whole-body retention or fecal excretion data of ^{54}Mn. All the other parameters in the PBPK model were unchanged to maintain a consistent description of Mn tissue kinetics regardless of exposure route.

In the study by Dastur *et al.* (1971), 12 rhesus monkeys with an average body weight of 2.5 kg were administered an ip dose of 200 μCi of carrier-free $^{54}MnCl_2$ solution. Whole-body activity of ^{54}Mn was reported up to 278 days postexposure. The amount of Mn in the diet was not stated, so an 80-ppm Mn diet was used to be consistent with other published studies (Furchner *et al.*, 1966). Because this was lower than the 133-ppm Mn diet used by Dorman *et al.* (2006a) for model calibration, Fdietup was increased to 0.00345 to calibrate steady-state tissue Mn levels. Rapid elimination of ^{54}Mn from the body was observed in the first 50 days following ip injection. This phase was followed by a slow phase of

TABLE 4
Tissue Mn Binding Capacity and Diffusion Parameters for Monkeys and Humans

	Binding			Diffusion			
	B_{max}(μg/g tissue)	k_a (/μg/h)	k_d (/h)	k_{in} (/h/kg)	k_{out} (/h/kg)	k_{inmax}	k_{in50} (μg)
Monkey[a]							
Brain							
Cerebellum	550	0.001	0.0014	4.3	0.08		
Olfactory bulb	700	0.3	0.005	2.9	11.0		
Globus pallidus	600	0.2	0.0056	0.16	0.3	7.9	0.16
Pituitary	2000	0.3	0.036	0.129	0.2	10.0	0.2
Liver	4000	0.0011	0.0004				
Lung	2700	0.01	0.038				
Bone	600	0.00464	0.024				
Remaining body	200	0.0093	0.0045				
Human[b]							
Brain							
Cerebellum	370	0.001	0.003	2.4	0.08		
Olfactory bulb	620	0.35	0.005	3.0	7.5		
Globus pallidus	500	0.2	0.02	0.08	0.4	4.6	0.16
Pituitary	620	0.3	0.036	0.079	0.3	3.5	0.2
Liver	1245	0.0011	0.00048				
Lung	460	0.01	0.038				
Bone	78	0.00464	0.024				
Remaining body	84	0.0093	0.0045				

[a]Kinetic parameters for the monkey model were calibrated to the pharmacokinetic data from Dorman *et al.* (2006a).
[b]Kinetic parameters for the human model were adjusted from the monkey parameters to maintain the basal tissue levels in Table 2 with no Mn inhalation.

elimination for the remaining time. The parameters $F_{IP} = 0.03$ and $k_{IP} = 1.0 \times 10^{-7}$/h were calibrated to the whole-body elimination data to simulate the slow release of ^{54}Mn from the peritoneal cavity to the liver. With these adjustments to specific parameters, model simulations were consistent with the nonlinear kinetics of ^{54}Mn observed by ip administration (Fig. 2A).

In the study by Furchner *et al.* (1966), 0.6 μCi of carrier-free $^{54}MnCl_2$ was administered iv to three rhesus monkeys with an average body weight of 8.5 kg. The monkeys were maintained on a commercial diet containing 80 ppm Mn. Whole-body ^{54}Mn activity was measured for 290 days. Fdietup was reduced to 0.0017 to account for the higher levels of Mn ingested by the larger monkeys and to maintain stable background Mn tissue levels. After 300 days, whole-body retention after ip and iv administration were very similar, but initial clearance was much faster after ip dosing (Figs. 2A and 2B).

Furchner *et al.* (1966) also orally dosed three rhesus monkeys with 0.6 μCi of carrier-free $^{54}MnCl_2$. These monkeys had an average body weight of 7 kg and were also maintained on an 80-ppm Mn commercial diet. Whole-body activity of ^{54}Mn was measured for 23 days postexposure. Parameters governing GI absorption (k_{GI}, F_{ENT}, and k_{ENT}) were calibrated based on the oral ^{54}Mn tracer data. Fdietup was set to 0.002 to maintain consistent background Mn tissue levels. Rapid elimination of ^{54}Mn was observed in the first 5 days following oral administration of Mn that was not taken up systemically followed by a slow elimination phase for the remaining time period (Fig. 2C).

In the study by Newland *et al.* (1987), one monkey (*Macaca nemistrina*, 5 kg) received a 6-week continuous infusion of ^{54}Mn through two sc osmotic pumps implanted between the shoulder blades. Each solution contained 200 μCi ^{54}Mn and 400 mg Mn in an $MnCl_2$ solution. As noted by the authors, there was leakage at the osmotic pump implant sites, so the reported doses represent an estimate of the maximum dose as calculated from the pumping rate, and the actual dose received by the monkey could have been lower. For PBPK model simulations, the maximal dose as reported by Newland *et al.* (1987) was used. Fecal ^{54}Mn activity was measured for approximately 160 days. Fecal ^{54}Mn concentrations were elevated during the exposure period and were relatively constant. A rapid decrease in fecal ^{54}Mn concentration was observed immediately following removal of the sc pumps (Fig. 3A). This rapid elimination phase was followed by a slow elimination phase for the remaining observation period. Rapid clearance of ^{54}Mn following sc exposure appears to be because of dose rate differences and not to the route of administration. Because the osmotic pump solution contained a high concentration of carrier (400 mg of Mn), the kinetics are not equivalent to carrier-free radiotracer kinetics.

Newland *et al.* (1987) exposed two anesthetized monkeys (*Macaca fascicularis*, 2.5 and 3.1 kg) to a nebulized aerosol of $^{54}MnCl_2$ for 30 min through a tracheal tube. Each monkey was

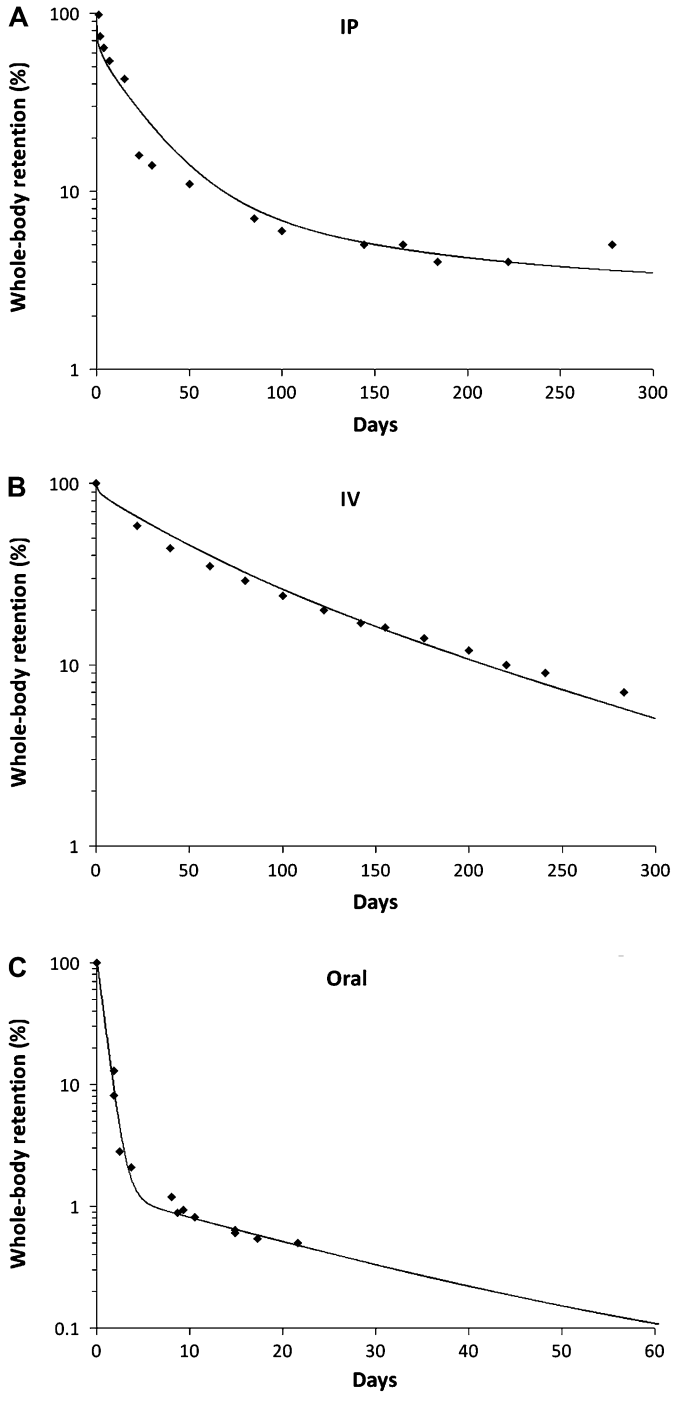

FIG. 2. Simulated whole-body retention of ^{54}Mn in monkeys compared with experimental data using different exposure routes: (A) monkeys were exposed by ip injection to 200 μCi $^{54}MnCl_2$ (Dastur *et al.*, 1971); Fdietup = 0.00345, kbilec = 0.051; (B) monkeys were exposed by iv administration to 0.6 μCi $^{54}MnCl_2$ (Furchner *et al.*, 1966); Fdietup = 0.0017, kbilec = 0.051; (C) monkeys were orally dosed with 0.6 μCi of $^{54}MnCl_2$ (Furchner *et al.*, 1966); Fdietup = 0.002, kbilec = 0.051. The curves represent model simulations and the symbols are retention data from individual monkeys.

exposed to a different aerosol with different specific activities. Fecal gamma activity was reported for approximately 250 days. The lung dose for each aerosol was estimated to be 16% by Newland *et al.* (1987). Calibrated dietary parameters in the PBPK model were Fdietup = 0.001 and kbilec = 0.015 to fit background Mn tissue levels and obtain fecal elimination rates consistent with the data. Fecal Mn declined rapidly in the first few days following exposure, followed by a slow decline for the remaining time period (Fig. 3B).

^{54}Mn Tracer Kinetics in Humans

^{54}Mn tracer kinetics were also available for humans given an iv dose of $^{54}MnCl_2$. In the study by Mahoney and Small (1968), three normal subjects (identified in Fig. 4 by their initials: HM, MM, and CH) were given an iv dose of 2.5 μCi of ^{54}Mn. Whole-body retention of ^{54}Mn was measured for 60 days. No information was given in the study regarding the subjects' gender, body weight, or diet. In another study by Mena *et al.* (1967), eight healthy medical personnel were injected with an iv dose of 20 μCi ^{54}Mn, and whole-body retention was measured for 30 days. Observations of whole-body clearance of ^{54}Mn from both studies were consistent (Fig. 4), with all subjects showing a gradual decrease in ^{54}Mn retention from near 100% at day 1 to about 40% on day 30. Additionally, whole-body retention in the three subjects in the study of Mahoney and Small (1968) decreased to 20–30% by day 60. Clearance curves revealed a fast elimination component in the first few days followed by a slow elimination component for the remaining time period, consistent with ^{54}Mn clearance observations in nonhuman primates and other species. Dietary absorption and biliary excretion rate constants in the human model were calibrated to the whole-body retention data from these two studies. The biliary excretion rate constant (*k*bilec = 0.051) and biliary induction parameters were identical to those used for the monkey. Fractional dietary absorption was higher in humans (*Fdietup* = 0.06) than in monkeys because of the lower amount of Mn in the human diet. Model simulations recapitulated the decrease in human whole-body retention of ^{54}Mn observed over the 60-day time frame (Fig. 4).

To study dose-dependent effects of Mn intake on ^{54}Mn clearance rates, Mahoney and Small (1968) also analyzed whole-body retention of ^{54}Mn in subjects receiving supplemental Mn. One subject (subject JM) was on a voluntary reduced calorie diet (800 calories per day) for 6 months prior to the start of the study. This subject was given an iv dose of 2.5 μCi of ^{54}Mn at the start of the study, and whole-body retention was measured periodically. The reduced calorie diet was continued throughout the observation period. Sixty days after the ^{54}Mn injection, the subject began to ingest 800 mg/day of

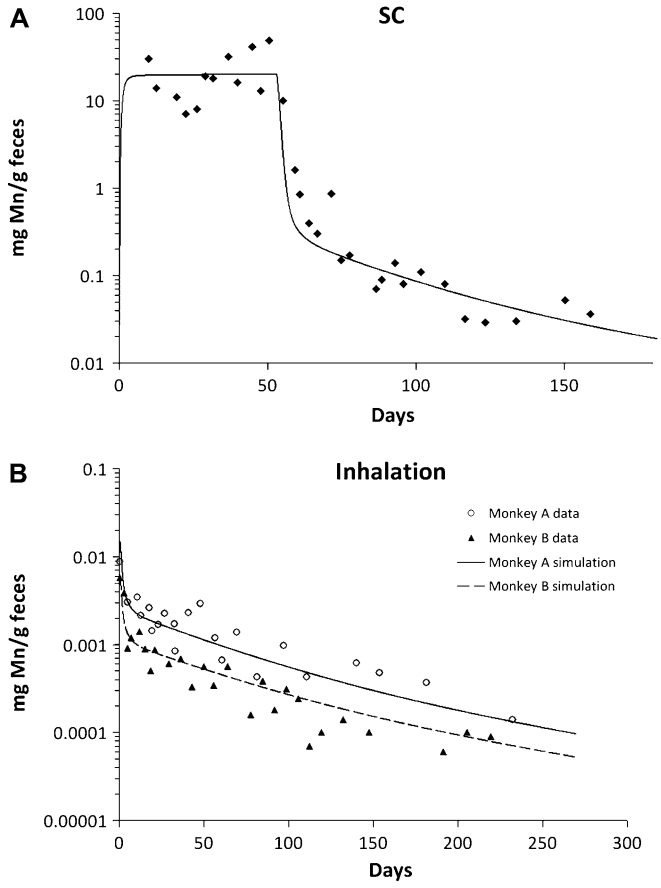

FIG. 3. Simulated fecal excretion of ^{54}Mn in monkeys compared with the experimental data from Newland *et al.* (1987): (A) one monkey was injected sc with 200 μCi ^{54}Mn and 400 mg Mn in an $MnCl_2$ solution; Fdietup = 0.0025, kbilec = 0.051; (B) two monkeys were exposed by inhalation to a nebulized aerosol of $^{54}MnCl_2$; Fdietup = 0.001, kbilec = 0.015. The curves represent model simulations and the symbols are fecal excretion data from individual monkeys.

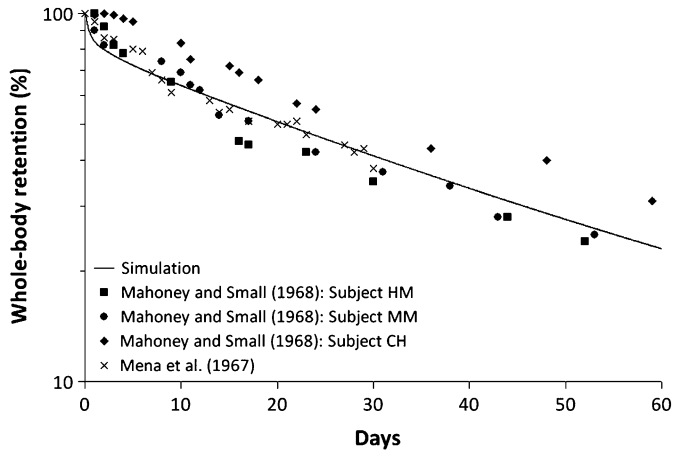

FIG. 4. Comparison of simulated whole-body retention in humans given an iv dose of ^{54}Mn with the whole-body retention data of Mahoney and Small (1968) and Mena *et al.* (1967). The curve represents the model simulation; the symbols for the study of Mahoney and Small (1968) are retention data for individual subjects; and the symbols for the study of Mena *et al.* (1967) represent average retention from eight subjects. Fdietup = 0.06, kbilec = 0.051.

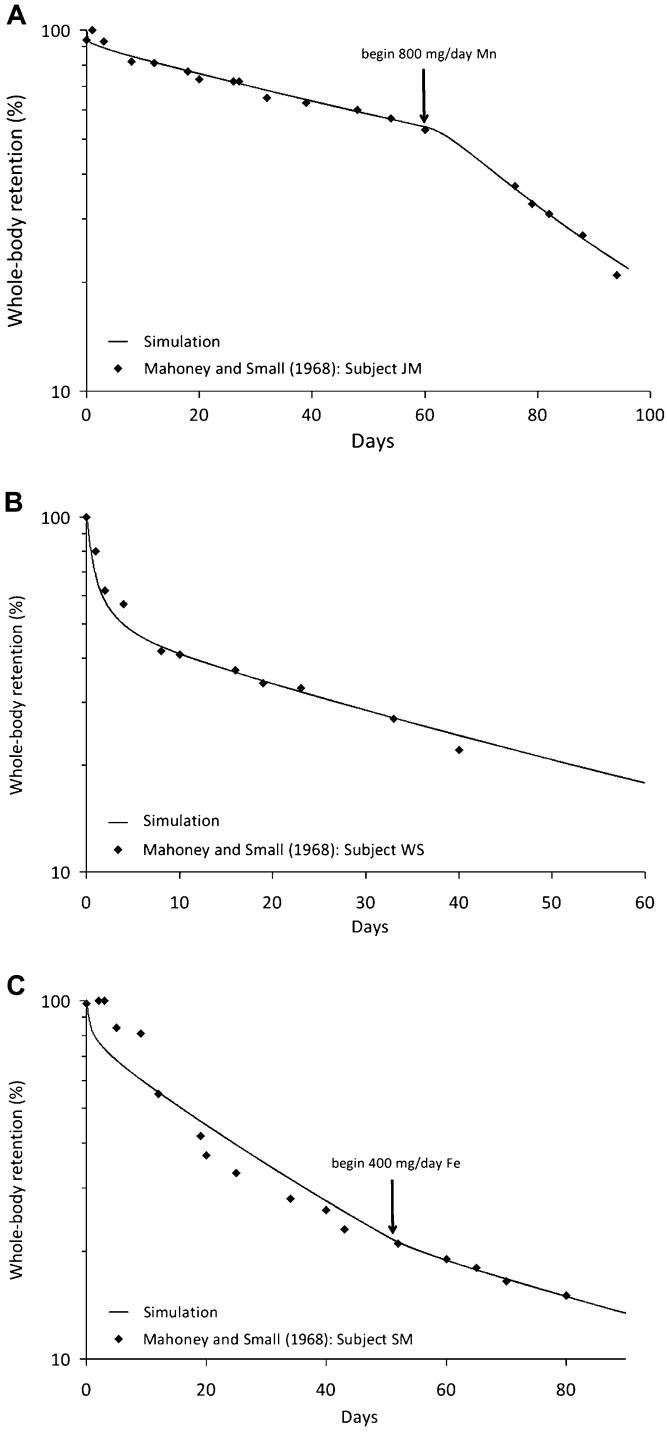

FIG. 5. Comparison of simulated whole-body retention of ^{54}Mn in human volunteers given supplemental Mn or Fe compared with the experimental data from Mahoney and Small (1968): (A) subject JM was on a reduced calorie diet and began to ingest 800 mg/day Mn on day 60 of the study; (B) subject WS was preloaded with 300 mg/day Mn 10 days prior to the start of the study; (C) subject SM had an iron deficiency and began to ingest 400 mg/day Fe on day 50. The condition of each subject was accommodated in the PBPK model by adjusting Mn dietary absorption (Fdietup). The curves represent model simulations and the symbols are retention data from individual subjects.

Mn as an $MnCl_2$ solution. Whole-body retention measurements of ^{54}Mn continued for another 25 days to examine the effect of the "flushing dose" of ingested Mn on ^{54}Mn clearance (Fig. 5A). Before the high Mn dose was ingested, whole-body retention was higher in the reduced calorie subject than in the normal subjects because of decreased biliary elimination from the presumably lower Mn in the calorie-restricted diet. At day 30, retention in the subject on the reduced calorie diet was about 65% compared with about 40% in normal subjects. After the high Mn ingestion period began, a rapid increase in ^{54}Mn clearance was observed. For the PBPK model simulations, the reduced calorie diet was simulated by assuming 1 mg Mn/day in the diet. As a result of the reduced calorie diet, Mn dietary absorption increased. Fdietup was increased slightly to 0.062 to fit the whole-body retention data until day 60. Once the flushing Mn dose was ingested, Fdietup was reduced to 0.00046 to account for decreased GI absorption of these high Mn oral doses. With these changes in dietary absorption corresponding to the different amounts of Mn ingested, the PBPK model simulations were consistent with ^{54}Mn whole-body retention data for this subject (Fig. 5A).

To examine another high-dose Mn scenario, another subject (subject WS) in the study of Mahoney and Small (1968) that was on a normal diet was preloaded for 10 days prior to iv injection of ^{54}Mn by ingesting 300 mg Mn/day as an $MnCl_2$ solution. This dosing schedule continued throughout the experiment for an additional 40 days. The disappearance of ^{54}Mn from the body was much more rapid in the subject preloaded with Mn than in normal subjects (Fig. 5B). Ten days after the ^{54}Mn iv injection, approximately 40% remained in the body compared with about 70% in normal subjects. For the model simulations, Mn dietary absorption was reduced by 28% per day for 15 days beginning at the start of the high-dose Mn ingestion. After 15 days, Fdietup was then kept constant at its reduced value of 0.00043 for the remainder of the exposure period. This adjustment accounts for the slow decrease in dietary absorption of Mn from moderately high doses over extended time periods (Fig. 5B).

Mahoney and Small (1968) also investigated ^{54}Mn retention in a mildly iron-deficient subject and found that ^{54}Mn clearance was faster in the iron-deficient subject than in normal subjects (Fig. 5C). Fifty days after ^{54}Mn administration, iron therapy was initiated with 400 mg/day Fe. This immediately decreased the elimination rate of ^{54}Mn from the body. Model simulations recapitulated whole-body retention in this subject by increasing Mn absorption (Fdietup = 0.075) during the iron-deficient phase and decreasing Mn absorption (Fdietup = 0.035) after the initiation of iron therapy (Fig. 5C). This behavior was consistent with previous findings where decreased Mn absorption was observed with high iron intake (Davis *et al.*, 1992; Finley, 1999). The interaction of Mn and Fe absorption is likely because of the fact that both metals share common uptake and storage transporters such as divalent metal transporter-1 and transferrin, so increases in the dietary

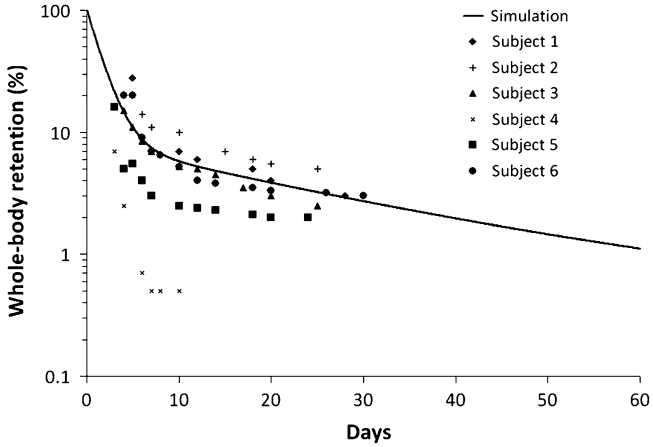

FIG. 6. Comparison of simulated whole-body retention of ^{54}Mn in humans with the experimental data from Davidsson *et al.* (1988), where female volunteers ingested a meal labeled with ^{54}Mn. The curve represents a model simulation and the data symbols are from individual subjects. Fdietup = 0.12, kbilec = 0.102.

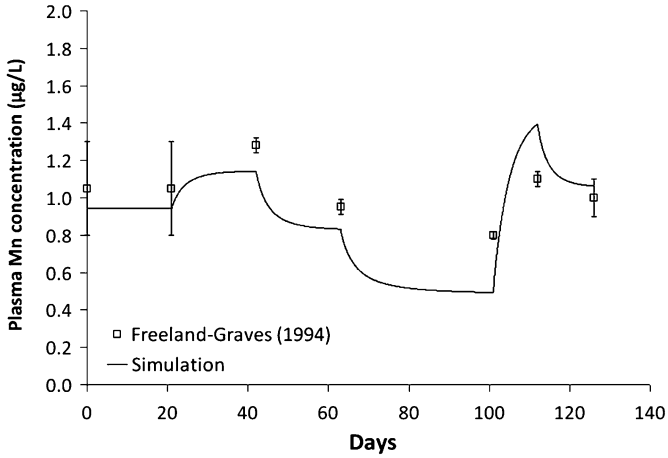

FIG. 7. Comparison of simulated plasma Mn concentrations with the experimental data from Freeland-Graves (1994). Simulated plasma Mn concentrations were calculated as 20% of simulated blood Mn concentrations. The data points represent the average plasma Mn concentration from five healthy men consuming diets containing different levels of dietary Mn (mean ± SD)—Days 1–21: 2.36, Days 22–42: 2.89, Days 42–63: 2.06, Days 64–101: 1.21, Days 102–112: 3.79, Days 113–125: 2.65 mg Mn/day. Fdietup = 0.06, kbilec = 0.051.

concentration of one element inhibit absorption and transport of the other (Fitsanakis *et al.*, 2010).

Oral Mn exposures were used to calibrate GI parameters in the PBPK model (Table 4). In the study by Davidsson *et al.* (1988), whole-body retention of ^{54}Mn was measured in six women who ingested a meal labeled with 0.1 MBq ^{54}Mn (Fig. 6). A wide range of elimination rates was observed in the subjects, but all showed rapid elimination in the first 10 days followed by a slow phase of elimination for the remaining period (Fig. 6). The shape of the retention curve was similar to that observed in monkeys receiving an oral dose of $^{54}MnCl_2$ (Fig. 2). Fdietup and kbilec were increased twofold for this simulation to account for increased Mn dietary absorption and biliary excretion in women (Aschner and Aschner, 2005). Simulated plasma Mn concentrations were also compared with plasma Mn measurements from men consuming different levels of dietary Mn (Freeland-Graves, 1994). Although the model predicted larger differences in plasma Mn concentration at the lowest and highest dietary levels, model simulations accurately captured the trend of plasma Mn levels caused by changes in dietary Mn exposure (Fig. 7).

Mn Inhalation Exposures in Monkeys and Humans

Basal tissue Mn levels were set to the measurements reported by Dorman *et al.* (2006a) for control monkeys on a 133-ppm Mn diet by adjusting dietary absorption and biliary excretion (Table 4). The monkey PBPK model parameters were first scaled from the rat values and were further calibrated to the pharmacokinetic data in Dorman *et al.* (2006a). Predicted brain tissue concentrations in monkeys were then compared with Mn concentrations observed in monkeys exposed for a 90-day period (Dorman *et al.*, 2006a). At an exposure concentration of 1.5 mg/m^3 Mn, predicted Mn tissue concentrations in the four brain regions (globus pallidus, pituitary, cerebellum, and olfactory bulb) were consistent with the rapid rise in tissue concentrations after the onset of high inhalation exposure followed by the decline to near basal levels in the 90 days following cessation of exposure (Fig. 8). Predicted time-dependent Mn tissue concentrations were also consistent with the rise in end-of-exposure brain tissue levels at different inhaled concentrations (Fig. 9). Predicted Mn tissue concentrations were similar to those reported by Nong *et al.* (2009) except that wider fluctuations in brain Mn concentrations during inhalation were observed because of the increase in magnitude of the diffusional rate constants.

In the human model, dietary absorption and biliary elimination were calibrated to ^{54}Mn whole-body retention data, as described previously (Table 3). Dissociation rate constants, maximal tissue binding, and diffusion rate constants were first scaled from the monkey and were then adjusted to fit the basal Mn tissue levels under dietary exposure only, assuming a 3 mg/day Mn diet (Table 4). Differences in parameter values between monkeys and humans are because of different basal Mn tissue levels between species (Table 2). Predicted brain Mn concentrations in humans were obtained for an inhalation exposure period of 90 days (8 h/day, 5 days/week) to simulate an occupational exposure and to be consistent with the inhalation exposure period used in the monkey simulations for direct comparison between species. Like monkeys, human brain Mn concentrations during this simulated exposure period exhibited a rapid rise in Mn tissue levels following the onset of exposure (Fig. 10). This was followed by a slower decline in human Mn tissue levels following the end of the exposure period. Simulated Mn

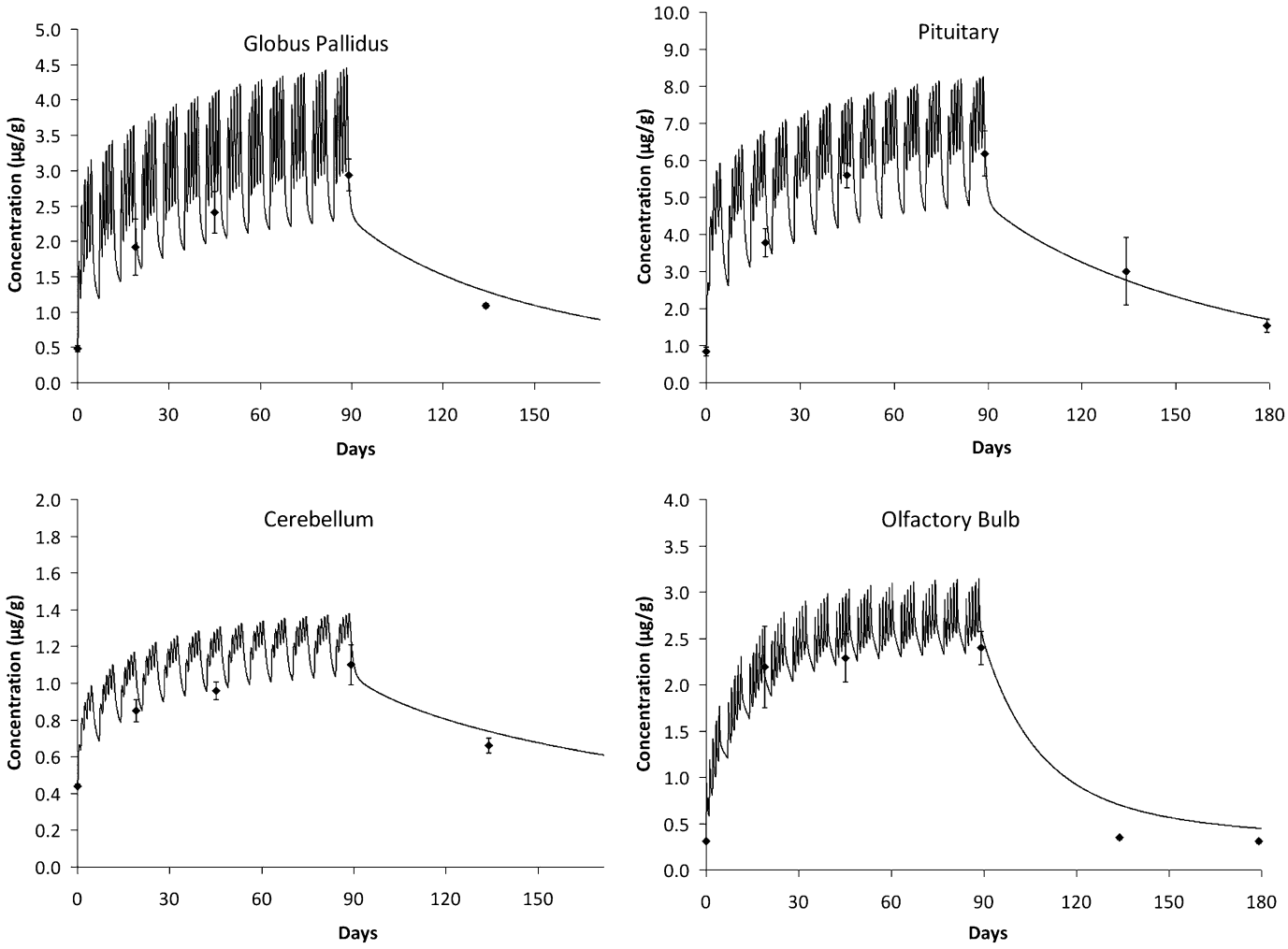

FIG. 8. Simulated brain tissue Mn levels in monkeys exposed by inhalation to 1.5 mg Mn/m^3 for 90 days (6 h/day, 5 days/week). The simulation results are compared with data from Dorman *et al.* (2006a). The curves are model simulations and symbols are means and SEs from four to six monkeys per exposure concentration.

concentrations in the human globus pallidus were also examined during a 90-day exposure to Mn concentrations of 0.01–5.0 mg/m^3 (Fig. 11). At the lowest exposure concentration (0.01 mg/m^3 Mn), the model predicted no appreciable increase (< 1%) in brain Mn concentrations above background levels that result from normal dietary exposure. At an exposure concentration of 0.1 mg/m^3, slight increases (~5%) in brain Mn concentration above background levels were observed during the inhalation exposure period. More significant (> 30%) increases in brain Mn concentrations were predicted at the higher exposure concentrations (> 1.0 mg/m^3).

Sensitivity Analysis

Sensitivity coefficients for predicted globus pallidus concentration from a 1% change in model parameter values were determined at inhalation exposure concentrations of 0.01, 0.1, and 1.0 mg/m^3 Mn in monkeys and humans (Table 6). Model predictions were most sensitive to the influx and efflux diffusion rate constants (k_{in} and k_{out}). Model predictions were also sensitive to dietary absorption (Fdietup) and biliary elimination (kbilec), although predictions became less sensitive with increasing exposure concentration as brain Mn levels were driven more by inhalation than diet. Sensitivity toward tissue-binding constants (B_{max}, k_a, and k_d) decreased as inhalation exposure concentration increased because of saturation of the tissue-binding capacity. Sensitivity of model predictions displayed similar trends in monkeys and humans and were consistent with sensitivity results in rats (Nong *et al.*, 2009). Sensitivity coefficients for other brain regions are presented in the Supplementary data

DISCUSSION

The PBPK model structure included commonly used exposure routes to take advantage of the multitude of ^{54}Mn

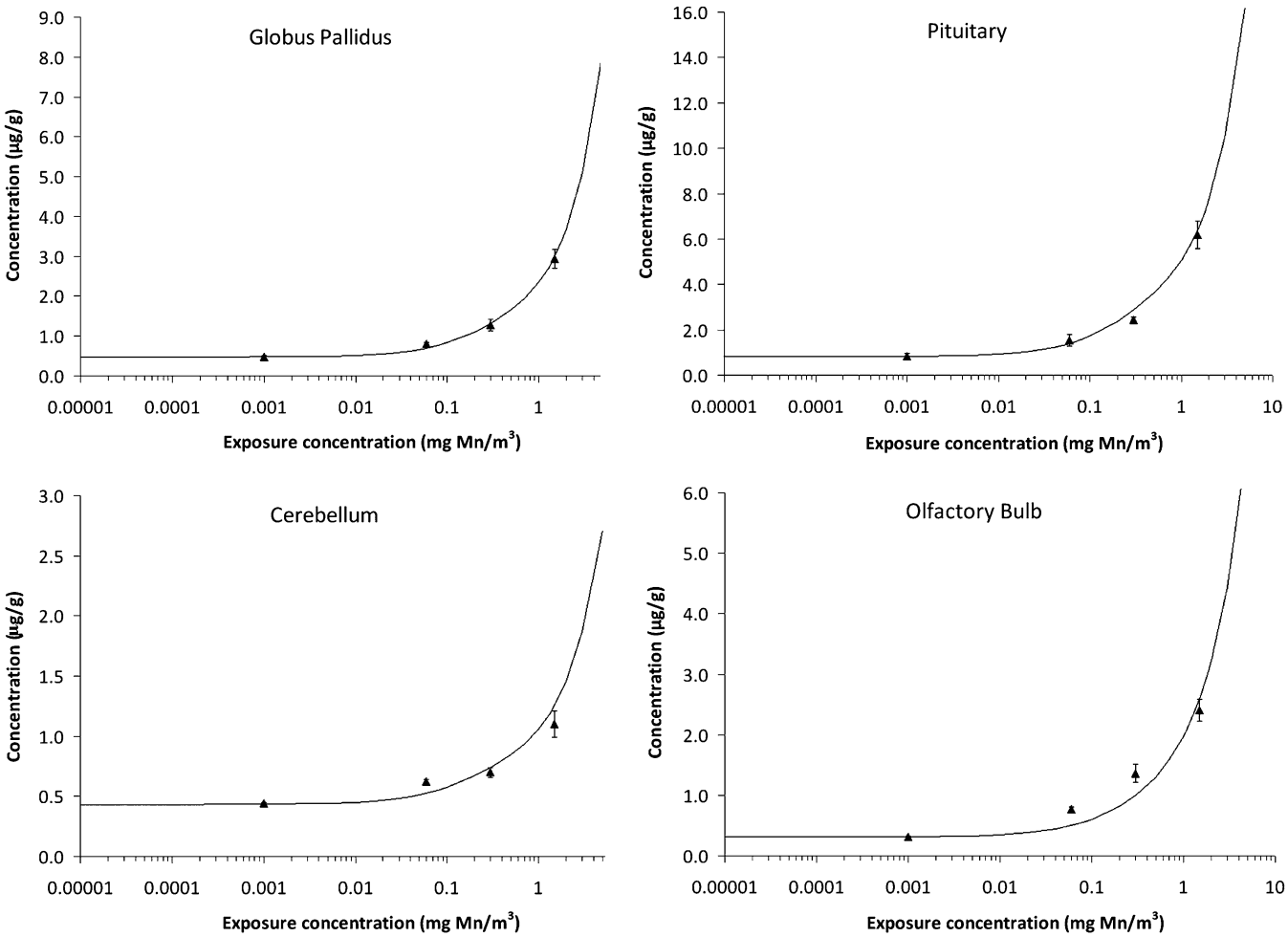

FIG. 9. Simulated end-of-exposure brain tissue Mn concentrations as a function of inhalation exposure concentration (milligrams of Mn per cubic meter). The simulation results are compared with data from Dorman *et al.* (2006a). Monkeys were exposed by inhalation for 90 days (6 h/day, 5 days/week). The curves are model simulations and symbols are means and SEs from four to six monkeys per exposure concentration.

clearance studies that have been conducted in monkeys and humans. A common feature from all these studies was that ^{54}Mn clearance from the body follows biphasic elimination, with a short "fast" elimination phase (with halftimes of around a few days) followed by a longer "slow" elimination phase. This elimination behavior was consistently observed with all exposure routes. The availability of tracer studies for multiple exposure routes permitted a comparison of dose route differences in elimination. The fastest clearance in monkeys and humans occurred from oral exposure, whereas the slowest clearance occurred following iv administration. Oral clearance has a component related to limited GI uptake and passage of 95–99% of the oral dose through the GI tract into feces. The ability of the models to accurately replicate the elimination phases observed in these tracer studies provides confidence that the PBPK model structure accurately depicts the key aspects of Mn pharmacokinetics in monkeys and humans, irrespective of exposure route.

Cotzias and Greenough (1958) and Dorman *et al.* (2001b) showed that ^{54}Mn clearance rates were affected by dietary Mn levels in mice and rats, respectively. Rats and mice given high Mn diets had significantly higher clearance rates when compared with animals kept on lower Mn diets. Similar findings were observed in humans by Mahoney and Small (1968), where a subject on a reduced calorie diet (which presumably resulted in lower Mn intake) had a much reduced elimination rate than subjects on a normal Mn diet. These effects arise from adaptive responses in Mn kinetics as oral doses vary. Model simulations reproduced the clearance rates of the individual on the reduced calorie diet by slightly increasing dietary absorption. The biliary excretion rate constant was reduced in the model simulations for this Mn-deficient individual because they also had decreased biliary elimination as evidenced by their reduced whole-body ^{54}Mn clearance rates.

The elimination kinetics of the ^{54}Mn tracer were influenced by the total administered Mn dose. Although elimination of

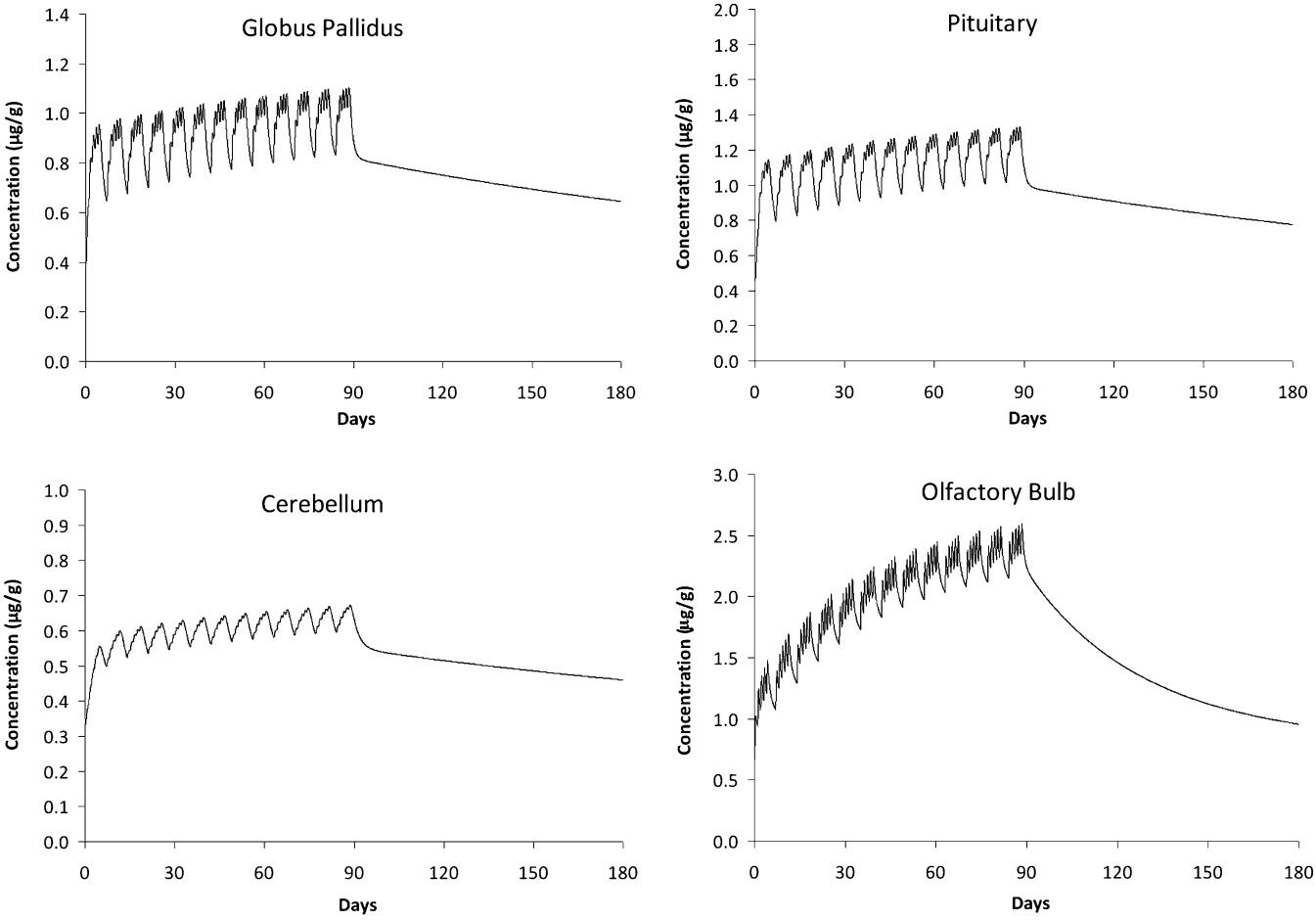

FIG. 10. Simulated brain tissue Mn levels in humans exposed by inhalation to 1.5 mg Mn/m^3 for 90 days (8 h/day, 5 days/week).

carrier-free ^{54}Mn exhibited similar behavior across dose routes and species, dose dependencies became more apparent when high levels of supplemental (carrier) Mn were added. In the study by Mahoney and Small (1968), subjects receiving 300–800 mg Mn/day had higher clearance rates than subjects on normal Mn diets alone. Similar observations were also made by Cotzias and Greenough (1958) who observed rapid ^{54}Mn clearance in mice receiving high doses of carrier Mn. These results were also consistent with those of Newland *et al.* (1987), where a monkey exposed to an sc tracer dose of ^{54}Mn with 400 mg of carrier Mn exhibited rapid clearance of the radiotracer. Clearance rates observed in this sc exposure were much faster than those seen following inhalation exposure (Newland *et al.*, 1987). Although Newland originally attributed these retention differences to a presumed slow-release Mn depot in the lung, it is more likely because of dose-dependent differences in Mn elimination caused by the large dose of carrier-free Mn. PBPK model simulations were able to accurately recapitulate all these dose-dependent scenarios by adjusting dietary absorption and controlling Mn tissue concentrations by dose-dependent inducible elimination rates.

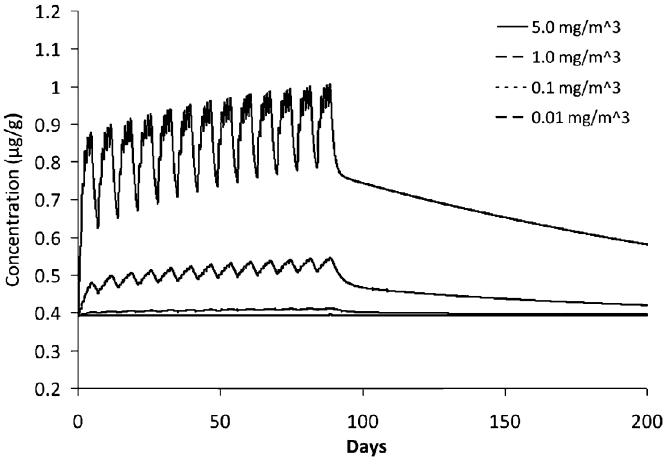

FIG. 11. Simulated human globus pallidus Mn concentrations during a 90-day exposure (8 h/day, 5 days/week) at various inhalation exposure concentrations.

Similar dose dependencies were observed in the case of inhalation exposure. Mena *et al.* (1967) examined clearance of an iv tracer dose of ^{54}Mn given to normal volunteers, healthy

Mn miners just removed from the mines, and in miners diagnosed with chronic Mn poisoning who had been removed from the mines several years prior to the study. Whole-body clearance of ^{54}Mn was faster in the active miners than in the other groups presumably because of their elevated Mn body burden. Although the miners diagnosed with Mn poisoning had also worked in the mines, they were removed from the Mn exposures long enough that tissue Mn levels had likely returned to near normal, and thus, they exhibited clearance rates similar to those reported in healthy individuals. This behavior was also demonstrated with the human PBPK model by comparing simulated clearance of ^{54}Mn in people exposed to different Mn exposure concentrations by inhalation (Fig. 12). In the model simulations, inhalation exposures started the day of the ^{54}Mn iv injection and lasted for 60 days (8 h/day, 5 days/week). Simulated exposure concentrations were 0, 0.01, 0.1, and 1.0 mg/m^3, spanning a range of concentrations that have been observed in human Mn exposure studies. At an exposure concentration of 0.01 mg/m^3, there was virtually no change in ^{54}Mn turnover from air-exposed controls. However, at the highest exposure concentration (1 mg/m^3), simulated ^{54}Mn elimination was rapidly increased because of the higher body burden and increased biliary excretion of Mn from the inhalation exposures. These predictions in humans were also consistent with the findings of Dorman *et al.* (2001a) who found that rats exposed by inhalation to high Mn concentrations (0.3 mg Mn/m^3) had faster ^{54}Mn clearance rates.

Tracer studies in rats, monkeys, and humans reveal similar findings: clearance behavior displays biphasic kinetics, there are dose route differences in elimination, and clearance rates depend on total Mn body burden either from Mn in diet or supplemental Mn exposures. Because tracer studies implicitly reflect the kinetics of Mn disposition, these studies reflect the dose dependencies of inducible biliary elimination on Mn levels in the body. The ability of the PBPK models to provide consistent multispecies descriptions of Mn tracer kinetics across multiple exposure routes indicates that the models have captured the dose-dependent characteristics of Mn disposition and can accurately predict conditions where exposures will increase free Mn in various tissues throughout the body above background levels from normal dietary exposure.

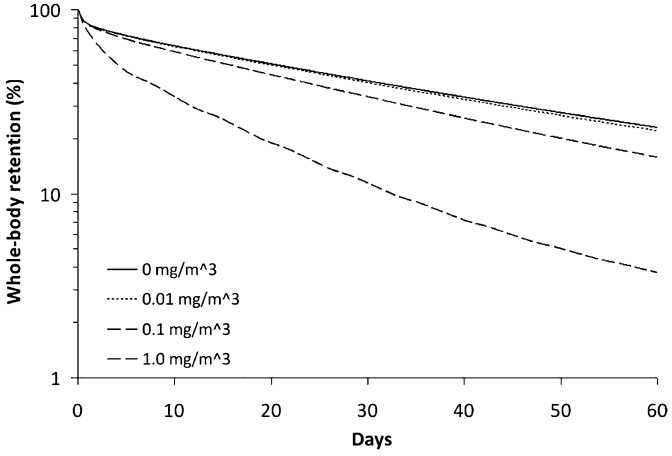

FIG. 12. Simulated effects of inhalation exposure to Mn particles on whole-body retention in humans given an iv dose of ^{54}Mn.

The ability of the human PBPK model to predict Mn tissue dosimetry based on pharmacokinetic data in laboratory animals depends on a consistent description of Mn kinetics across species. There are significant physiological and biochemical differences between rats, monkeys, and humans that had to be accounted for in the interspecies PBPK models, including tissue volumes, blood flows, pulmonary ventilation, and less well-understood processes regulating Mn uptake and storage. Direct allometric scaling of model parameters from the rat was often not adequate to describe Mn tissue kinetics in other species. However, the availability of Mn pharmacokinetic time courses in multiple species and ^{54}Mn clearance data in rats, monkeys, and humans allowed us to make further adjustments to model parameters beyond simple use of generic allometric scaling approaches to accurately describe Mn tissue dosimetry across multiple species. Although model parameters were changed beyond scaling, the underlying mechanisms governing Mn uptake and elimination (inducible biliary excretion, tissue-binding processes, and asymmetric diffusion fluxes) were preserved among species, providing confidence that a PBPK model with a consistent structure across species can accurately predict exposure conditions in humans that result in Mn tissue accumulation.

One of the primary species differences that affect Mn kinetics is diet. This difference is important to account for in the PBPK models because Mn is an essential nutrient. PBPK models for essential metals must account for dose-dependent biological processes that regulate absorption, tissue storage, and elimination. Concerns arise when exposure exceeds elimination capability. Laboratory animals are often maintained on diets that contain relatively high Mn concentrations, whereas the human diet is typically much lower in Mn (ranging from 1 to 10 mg/day). When Mn dietary intake is increased, homeostatic controls regulate Mn body burden by decreasing intestinal absorption and increasing biliary elimination. These processes were included in the PBPK model through use of the parameter Fdietup, which controls the amount absorbed by the GI tract, and kbilec, which is the biliary excretion rate constant induced by Mn blood concentration. With higher Mn exposure, blood Mn concentrations increase, resulting in increased biliary elimination. The maximum induction factor implemented in the model was 2.5-fold, which was reached at higher exposure concentrations (1.5 mg/m^3).

Lung dose is an important determinant for subsequent Mn tissue dosimetry calculations resulting from inhalation exposure. Pulmonary ventilation and lung airway structure differ significantly between species. Deposition estimates for Mn

particles incorporated species-specific lung geometries, ventilatory rates, and particle properties by use of particle deposition software (MPPD) to estimate regional respiratory tract deposition. Because the monkey lung morphology was not available in MPPD, surface area scaling from the rat was used to obtain monkey respiratory tract deposition estimates. Deposition estimates using this scaling procedure were consistent with those reported by Cheng *et al.* (2008), where deposition of aerosol droplets was measured in the upper respiratory tract and lungs of monkeys. $MnSO_4$ particles were used in this study because they were used in the monkey inhalation studies by Dorman *et al.* (2006a) and are more bioavailable than other less soluble forms (e.g., MnO_2 and $MnPO_4$). Adjustments can be made to lung absorption parameters based on solubility to predict pharmacokinetics and dosimetry of other forms of Mn.

Another important difference between species is in the olfactory region. Whereas the rat olfactory epithelium comprises almost 50% of the total nasal surface area, in monkeys and humans, it is about 9 and 5%, respectively. This difference will influence the amount of Mn delivered to the olfactory bulb via the olfactory pathway. Olfactory delivery did not make a significant contribution to striatal Mn levels in the rat (Leavens *et al.*, 2007), and magnetic resonance imaging in nonhuman primates showed no significant signal intensities in the tissues connecting the olfactory bulb and midbrain regions (Dorman *et al.*, 2006b). These studies indicate that similar kinetic mechanisms may be at work in humans for delivery of Mn to the olfactory bulb. Nonetheless, the current model structure included olfactory transport in monkeys and humans even though the contribution of this route to midbrain tissues is minimal.

As inhalation exposure concentration increases, homeostatic controls associated with biliary elimination are overwhelmed by increased input rates because of pulmonary Mn absorption. At higher inhaled concentrations (> 0.1 mg/m^3), binding capacities and biliary clearance processes become saturated, allowing free Mn to accumulate in the tissues (Fig. 13). Tissue-binding rate constants (k_a and k_d) and binding capacities (B_{max}) determine the ratios of bound versus free Mn in each tissue. The most toxicologically relevant metric for human Mn neurotoxicity is likely tissue concentration of free Mn in the globus pallidus and other midbrain regions. A comparison of rat, monkey, and human predictions of Mn concentrations in the globus pallidus (and rat striatum) reveals that all species exhibited similar behavior upon increasing levels of inhalation exposure (Fig. 14), although the magnitude increases in brain Mn concentrations were slightly different among species. Predicted human globus pallidus Mn concentrations were less than those predicted in monkeys at exposure concentrations > 0.1 mg/m^3 but were very similar to those seen in the rat striatum. The larger magnitude changes predicted in monkeys compared with humans at higher inhalation exposure concentrations may be because of saturation of Mn binding sites in the

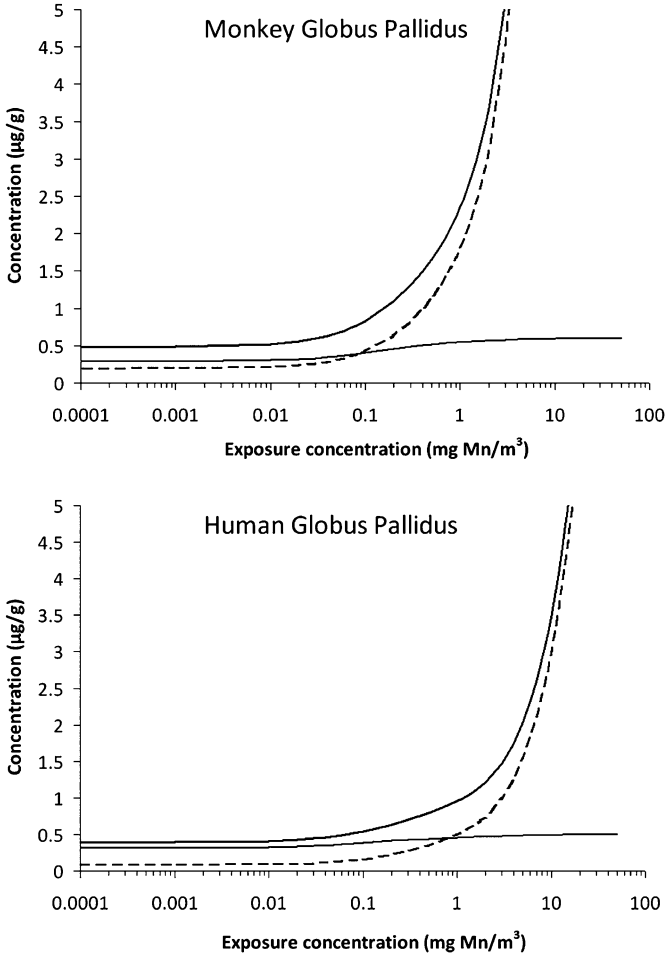

FIG. 13. Simulated end-of-exposure (90 days) Mn tissue concentrations of total (solid), free (dashed), and bound (gray) Mn in the monkey and human globus pallidus. The bound Mn fractions were 60 and 80% in the monkey and human, respectively, under normal dietary exposure.

monkey due to higher Mn concentrations in the diet. To test the sensitivity of Mn binding, further simulations were conducted assuming an equal bound Mn fraction (60% bound Mn fraction with no inhalation exposure) in humans and monkeys. Under these conditions, Mn globus pallidus concentrations in the human increased slightly faster than when an 80% bound fraction was used but still did not approach the levels observed in the monkey.

The human PBPK model can identify ranges of inhalation exposure concentrations where Mn levels in target tissues (specifically the globus pallidus) do not increase appreciably above background levels. Brain Mn concentrations begin to increase when subchronic (90 day) exposure concentrations rise to near 0.1 mg Mn/m^3 (Fig. 14). This was also evident in the time course predictions (Fig. 11), showing negligible increases in globus pallidus Mn concentration in humans subject to an inhalation exposure concentration of 0.01 mg/m^3 and tissue Mn levels increasing as exposure concentration increased. Predicted globus pallidus Mn concentrations

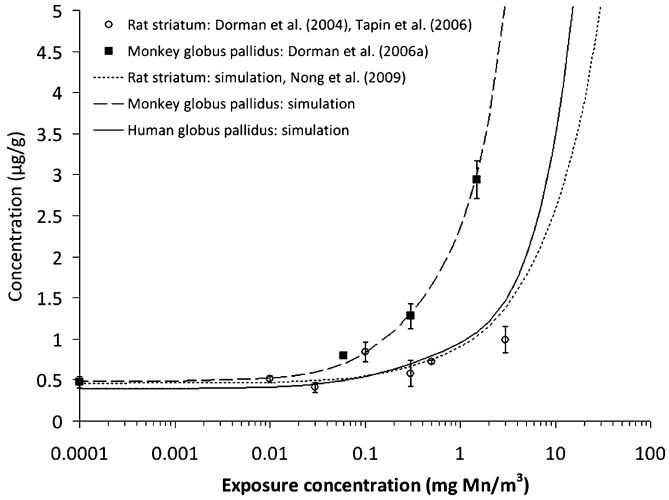

FIG. 14. Simulated end-of-exposure tissue Mn levels (total Mn) in the rat striatum and monkey and human globus pallidus. The simulated rat striatal Mn levels are from Nong *et al.* (2009) and are compared with data (mean ± SE) from Dorman *et al.* (2004) and Tapin *et al.* (2006). The simulated monkey globus pallidus Mn levels are compared with data from Dorman *et al.* (2006a). Rats and monkeys were exposed to 6 h/day, 5 days/week for 90 days. Humans were exposed to 8 h/day, 5 days/week for 90 days.

increased slightly (by about 5%) over background levels at an exposure concentration of 0.1 mg/m^3 and increased dramatically for higher exposure concentrations. These data are consistent with derivations of benchmark concentrations for subclinical neurological effects from occupational studies at concentrations of 0.2 mg/m^3 (Clewell *et al.*, 2003).

CONCLUSION

Risk assessments for Mn, as an essential element, should consider its essentiality as well as its toxicity. Homeostatic controls maintain relatively stable Mn tissue concentrations by regulating dietary absorption, compartmental transfer, and biliary excretion under low levels of Mn exposure. Toxicity may occur under conditions of excessive exposure when these homeostatic controls are overwhelmed. The PBPK models presented in this study account for background tissue levels associated with dietary exposure and simulate simultaneous exposure to Mn by ingestion and inhalation. Simulation results accurately recapitulated the rapid increase in tissue Mn from high inhalation concentrations and subsequent return to basal levels following inhalation exposures in monkeys and described clearance of tracer doses in monkeys and humans under normal dietary conditions and with supplemental Mn doses. The human model was validated against available Mn tracer data and was able to accurately capture Mn elimination dynamics following iv exposure to tracer Mn. Consistent interspecies descriptions of Mn kinetics show that the models can accurately predict exposure conditions that will result in increased tissue concentrations in humans and can be used in a dosimetry-based risk assessment (Andersen *et al.*, 1999) to identify exposure conditions that may lead to increased target tissue doses of this essential element.

TABLE 5
Dietary Absorption and Biliary Elimination Parameters Used in the Monkey ^{54}Mn Tracer Studies

Study	Body weight (kg)	Dose route	Mn diet (ppm)	Fdietup	kbilec (l/h/kg)
Dastur *et al.* (1971)	2.5	ip	80[a]	0.00345	0.051
Furchner *et al.* (1966)	8.5	iv	80	0.0017	0.051
Furchner *et al.* (1966)	7.0	Oral	80	0.002	0.051
Newland *et al.* (1987)	5.0	sc	80[a]	0.0025	0.050
Newland *et al.* (1987)	2.5–3.1	Inhalation	80[a]	0.001	0.015

[a]The Mn diet was not reported and was assumed to be 80 ppm for model simulations.

TABLE 6
Sensitivity Analysis of Peak Mn Concentration in the Globus Pallidus of Monkeys and Humans at Inhalation Exposure Concentrations of 0.01, 0.1, and 1.0 mg/m^3. Normalized Sensitivity Parameters Reflect a 1% Change in Model Parameters

	Sensitivity coefficient					
	Monkey			Human		
Model parameter	0.01	0.1	1.0	0.01	0.1	1.0
Fdietup	0.96	0.46	0.06	0.73	0.37	0.00
kbile	−0.96	−0.91	−0.68	−0.73	−0.37	−0.40
Q_{tissue}	0.00	0.00	−0.03	0.00	0.00	0.00
B_{max}	0.57	0.46	0.15	0.73	0.73	0.40
k_a	0.19	0.11	0.00	0.24	0.18	0.00
k_d	−0.38	−0.23	−0.03	−0.24	−0.18	−0.10
k_{in}	1.15	1.37	1.18	0.73	0.55	0.60
k_{out}	−1.34	−1.37	−1.05	−0.73	−0.55	−0.70
k_{inmax}	0.57	0.91	0.99	0.49	0.55	0.50
k_{in50}	−0.77	−0.68	−0.34	−0.24	−0.18	−0.10
FdepLU[a]	0.00	0.11	0.43	0.00	0.18	0.20
FdepNO[b]	0.00	0.00	0.03	0.00	0.00	0.00
FdepNR[c]	0.00	0.11	0.25	0.00	0.18	0.10
k_{GI}	0.00	0.00	0.00	0.00	0.00	0.00
F_{ent}	0.00	0.00	0.00	0.00	0.00	0.00
k_{ent}	0.00	0.00	0.00	0.00	0.00	0.00

[a]Fractional deposition on lung epithelium.
[b]Fractional deposition on nasal olfactory epithelium.
[c]Fractional deposition on nasal respiratory epithelium.

SUPPLEMENTARY DATA

Supplementary data are available online at http://toxsci.oxfordjournals.org/.

FUNDING

This publication and work is based on studies sponsored by Afton Chemical Corporation in satisfaction of registration requirements arising under Section 211(a) and (b) of the Clean Air Act and corresponding regulations at 40 CFR Substance 79.50 et seq.

REFERENCES

Agency for Toxic Substances Disease Registry (ATSDR). (2000). *Toxicological Profile for Manganese*. U.S. Department for Health and Human Services, Public Health Service, Atlanta, GA.

Andersen, M. E., Dorman, D. C., Clewell, H. J., III., Taylor, M. D., and Nong, A. (2010). Multi-dose-route, multi-species pharmacokinetic models for manganese and their use in risk assessment. *J. Toxicol. Environ. Health A* **73,** 217–234.

Andersen, M. E., Gearhart, J. M., and Clewell, H. J., III. (1999). Pharmacokinetic data needs to support risk assessments for inhaled and ingested manganese. *Neurotoxicology* **20,** 161–171.

Anjilvel, S., and Asgharian, B. (1995). A multiple-path model of particle deposition in the rat lung. *Fundam. Appl. Toxicol.* **28,** 41–50.

Aschner, J. L., and Aschner, M. (2005). Nutritional aspects of manganese homeostatis. *Mol. Aspects Med.* **26,** 353–362.

Aschner, M., Erikson, K. M., and Dorman, D. C. (2005). Manganese dosimetry: species differences and implications for neurotoxicity. *Crit. Rev. Toxicol.* **35,** 1–32.

Asgharian, B., Hofmann, W., and Bergmann, R. (2001). Particle deposition in a multiple-path model of the human lung. *Aerosol. Sci. Technol.* **34,** 332–339.

Bonilla, E., Salazar, E., Villasmil, J. J., and Villalobos, R. (1982). The regional distribution of manganese in the normal human brain. *Neurochem. Res.* **7,** 221–227.

Borg, D. C., and Cotzias, G. C. (1958). Manganese metabolism in man: rapid exchange of Mn^{56} with tissue as demonstrated by blood clearance and liver uptake. *J. Clin. Invest.* **37,** 1269–1278.

Brown, R. P., Delp, M. D., Lindstedt, S. L., Rhomberg, L. R., and Beliles, R. P. (1997). Physiological parameter values for physiologically based pharmacokinetic models. *Toxicol. Ind. Health* **13,** 407–484.

Bush, V. J., Moyer, T. P., Batts, K. P., and Parisi, J. E. (1995). Essential and toxic element concentrations in fresh and formalin-fixed human autopsy tissues. *Clin. Chem.* **41,** 284–294.

Cheng, Y. S., Irshad, H., Kuehl, P., Holmes, T. D., Sherwood, R., and Hobbs, C. H. (2008). Lung deposition of droplet aerosols in monkeys. *Inhal. Toxicol.* **20,** 1029–1036.

Clewell, H. J., Lawrence, G. A., Calne, D. B., and Crump, K. S. (2003). Determination of an occupational exposure guideline for manganese using the benchmark method. *Risk Analysis* **23,** 1031–1046.

Conolly, R. B., Lilly, P. D., and Kimbell, J. S. (2000). Simulation modeling of the tissue disposition of formaldehyde to predict nasal DNA-protein cross-links in Fischer 344 rats, rhesus monkeys, and humans. *Environ. Health Perspect.* **108**(Suppl. 5), 919–924.

Cotzias, G. C., and Greenough, J. J. (1958). The high specificity of the manganese pathway through the body. *J. Clin. Invest.* **37,** 1298–1305.

Dastur, D. K., Manghani, D. K., and Raghavendran, K. V. (1971). Distribution and fate of ^{54}Mn in the monkey: studies of different parts of the central nervous system and other organs. *J. Clin. Invest.* **50,** 9–20.

Davidsson, L., Cederblad, A., Hagebo, E., Lonnerdal, B., and Sandstrom, B. (1988). Intrinsic and extrinsic labeling for studies of manganese absorption in humans. *J. Nutr.* **118,** 1517–1521.

Davies, B., and Morris, T. (1993). Physiological parameters in laboratory animals and humans. *Pharm. Res.* **10,** 1093–1095.

Davis, C. D., Wolf, T. L., and Greger, J. L. (1992). Varying levels of manganese and iron affect absorption and gut endogenous losses of manganese by rats. *J. Nutr.* **122,** 1300–1308.

Dorman, D. C., McManus, B. E., Marshall, M. W., James, R. A., and Struve, M. F. (2004). Old age and gender influence the pharmacokinetics of inhaled manganese sulfate and manganese phosphate in rats. *Toxicol. Appl. Pharmacol.* **197,** 113–124.

Dorman, D. C., Struve, M. F., James, R. A., Marshall, M. W., Parkinson, C. U., and Wong, B. A. (2001a). Influence of particle solubility on the delivery of inhaled manganese to the rat brain: manganese sulfate and manganese tetroxide pharmacokinetics following repeated (14-day) exposure. *Toxicol. Appl. Pharmacol.* **170,** 79–87.

Dorman, D. C., Struve, M. F., James, R. A., McManus, B. E., Marshall, M. W., and Wong, B. A. (2001b). Influence of dietary manganese on the pharmacokinetics of inhaled manganese sulfate in male CD rats. *Toxicol. Sci.* **60,** 242–251.

Dorman, D. C., Struve, M. F., Marshall, M. W., Parkinson, C. U., James, A., and Wong, B. A. (2006a). Tissue manganese concentrations in young male rhesus monkeys following subchronic manganese sulfate inhalation. *Toxicol. Sci.* **92,** 201–210.

Dorman, D. C., Struve, M. F., Wong, B. A., Dye, J. A., and Robertson, I. D. (2006b). Correlation of brain magnetic resonance imaging changes with pallidal manganese concentrations in rhesus monkeys following subchronic manganese inhalation. *Toxicol. Sci.* **92,** 219–227.

Fell, J. M., Reynolds, A. P., Meadows, N., Khan, K., Long, S. G., Quaghebeur, G., Taylor, W. J., and Milla, P. J. (1996). Manganese toxicity in children receiving long-term parenteral nutrition. *Lancet* **347,** 1218–1221.

Finkelstein, M. M., and Jerrett, M. (2007). A study of the relationships between Parkinson's disease and markers of traffic-derived and environmental manganese air pollution in two Canadian cities. *Environ. Res.* **104,** 420–432.

Finley, J. W. (1999). Manganese absorption and retention by young women is associated with serum ferritin concentration. *Am. J. Clin. Nutr.* **70,** 37–43.

Finley, J. W., Johnson, P. E., and Johnson, L. K. (1994). Sex affects manganese absorption and retention by humans from a diet adequate in manganese. *Am. J. Clin. Nutr.* **60,** 949–955.

Fitsanakis, V. A., Zhang, N., Garcia, S., and Aschner, M. (2010). Manganese (Mn) and iron (Fe) interdependency of transport and regulation. *Neurotoxicol. Res.* **18,** 124–131.

Frederick, C. B., Bush, M. L., Lomax, L. B., Black, K. A., Finch, L., Kimbell, J. S., Morgan, K. T., Subramaniam, R. P., Morris, J. B., and Ultman, J. S. (1998). Application of a hybrid computational fluid dynamics and physiologically based inhalation model for interspecies dosimetry extrapolation of acidic vapors in the upper airways. *Toxicol. Appl. Pharmacol.* **152,** 211–231.

Freeland-Graves, J. (1994). Derivation of manganese safe and adequate daily dietary intakes. In *Risk Assessment of Essential Elements* (W. Mertz, C. O. Abernathy, and S. S. Olin, Eds.), pp. 237–252. ILSI Press, Washington, DC.

Furchner, J. E., Richmond, C. R., and Drake, G. A. (1966). Comparative metabolism of radionuclides in mammals. III. Retention of manganese-54 in the mouse, rat, monkey, and dog. *Health Phys.* **12,** 1415–1423.

Iregren, A. (1990). Psychological test performance in foundry workers exposed to low levels of manganese. *Neurotoxicol. Teratol.* **12,** 673–675.

Kawamura, R., Ikuta, H., Fukuzumi, S., Yamada, R., Tsubaki, S., Kodama, T., and Kurata, S. (1941). Intoxication by manganese in well water. *Arch. Exp. Med.* **18,** 145–169.

Kepler, G. M., Richardson, R. B., Morgan, K. T., and Kimbell, J. S. (1998). Computer simulation of inspiratory nasal airflow and inhaled gas uptake in a rhesus monkey. *Toxicol. Appl. Pharmacol.* **150,** 1–11.

Leavens, T. L., Rao, D., Andersen, M. E., and Dorman, D. C. (2007). Evaluating transport of manganese from olfactory mucosa to striatum by pharmacokinetic modeling. *Toxicol. Sci.* **97,** 265–278.

Lucchini, R., Apostoli, P., Perrone, C., Placidi, D., Albini, E., Migliorati, P., Mergler, D., Sassine, M. P., Palmi, S., and Alessio, L. (1999). Long-term exposure to "low levels" of manganese oxides and neurofunctional changes in ferroalloy workers. *Neurotoxicology* **20,** 287–297.

Lucchini, R., Selis, L., Folli, D., Apostoli, P., Mutti, A., Vanoni, O., Iregren, A., and Alessio, L. (1995). Neurobehavioral effects of manganese in workers from a ferroalloy plant after temporary cessation of exposure. *Scand. J. Work Environ. Health* **21,** 143–149.

Lucchini, R. G., Albini, E., Benedetti, L., Borghesi, S., Coccaglio, R., Malara, E. C., Parrinello, G., Garattini, S., Resola, S., and Alessio, L. (2007). High prevalence of Parkinsonian disorders associated to manganese exposure in the vicinities of ferroalloy industries. *Am. J. Ind. Med.* **50,** 788–800.

Mahoney, J. P., and Small, W. J. (1968). Studies on manganese III. The biological half-life of radiomanganese in man and factors which affect this half-life. *J. Clin. Invest.* **47,** 643–653.

Mena, I., Marin, O., Fuenzalida, S., and Cotzias, G. C. (1967). Chronic manganese poisoning: clinical picture and manganese turnover. *Neurology* **17,** 128–136.

Menache, M. G., Hanna, L. M., Gross, E. A., Lou, S. R., Zinreich, S. J., Leopold, D. A., Jarabek, A. M., and Miller, F. J. (1997). Upper respiratory tract surface areas and volumes of laboratory animals and humans: considerations for dosimetry models. *J. Toxicol. Environ. Health* **50,** 475–506.

Mergler, D., Baldwin, M., Belanger, S., Larribe, F., Beuter, A., Bowler, R., Panisset, M., Edwards, M., de Geoffroy, A., Sassine, M. P., *et al.* (1999). Manganese neurotoxicity, a continuum of dysfunction: Results from a community based study. *Neurotoxicology* **20,** 327–342.

Mergler, D., Huel, G., Bowler, R., Iregren, A., Belanger, S., Baldwin, M., Tardif, R., Smargiassi, A., and Martin, L. (1994). Nervous system dysfunction among workers with long-term exposure to manganese. *Environ. Res.* **64,** 151–180.

Molokhia, M. M. (1967). Trace elements in the lung. *Arch. Environ. Health* **15,** 745–750.

Myers, J. E., Thompson, M. L., Ramushu, S., Young, T., Jeebhay, M. F., London, L., Esswein, E., Renton, K., Spies, A., Boulle, A., *et al.* (2003). The nervous system effects of occupational exposure on workers in a South African manganese smelter. *Neurotoxicology* **24,** 885–894.

Newland, M. C., Cox, C., Hamada, R., Oberdorster, G., and Weiss, B. (1987). The clearance of manganese chloride in the primate. *Fundam. Appl. Toxicol.* **9,** 314–328.

Nong, A., Taylor, M. D., Clewell, H. J., III., Dorman, D. C., and Andersen, M. E. (2009). Manganese tissue dosimetry in rats and monkeys: accounting for dietary and inhaled Mn with physiologically based pharmacokinetic modeling. *Toxicol. Sci.* **108,** 22–34.

Nong, A., Teeguarden, J. G., Clewell, H. J., III., Dorman, D. C., and Andersen, M. E. (2008). Pharmacokinetic modeling of manganese in the rat IV: assessing factors that contribute to brain accumulation during inhalation exposure. *J. Toxicol. Environ. Health A* **71,** 413–426.

Pal, P. K., Samii, A., and Calne, D. B. (1999). Manganese neurotoxicity: a review of clinical features, imaging and pathology. *Neurotoxicology* **20,** 227–238.

Rodriguez-Agudelo, Y., Riojas-Rodriguez, H., Rios, C., Rosas, I., Sabido Pedraza, E., Miranda, J., Siebe, C., Texcalac, J. L., and Santos-Burgoa, C. (2006). Motor alterations associated with exposure to manganese in the environment in Mexico. *Sci. Total Environ.* **368,** 542–556.

Roels, H., Lauwerys, R., Buchet, J. P., Genet, P., Sarhan, M. J., Hanotiau, I., de Fays, M., Bernard, A., and Stanescu, D. (1987). Epidemiological survey among workers exposed to manganese: effects on lung, central nervous system, and some biological indices. *Am. J. Ind. Med.* **11,** 307–327.

Roels, H. A., Ghyselen, P., Buchet, J. P., Ceulemans, E., and Lauwerys, R. R. (1992). Assessment of the permissible exposure level to manganese in workers exposed to manganese dioxide dust. *Br. J. Ind. Med.* **49,** 25–34.

Roels, H. A., Ortega Eslava, M. I., Ceulemans, E., Robert, A., and Lison, D. (1999). Prospective study on the reversibility of neurobehavioral effects in workers exposed to manganese dioxide. *Neurotoxicology* **20,** 255–271.

Schroeter, J. D., Garcia, G. J. M., and Kimbell, J. S. (2010). A computational fluid dynamics approach to assess interhuman variability in hydrogen sulfide nasal dosimetry. *Inhal. Toxicol.* **22,** 277–286.

Schroeter, J. D., Kimbell, J. S., Gross, E. A., Willson, G. A., Dorman, D. C., Tan, Y. M., and Clewell, H. J., III. (2008). Application of physiological computational fluid dynamics models to predict interspecies nasal dosimetry of inhaled acrolein. *Inhal. Toxicol.* **20,** 227–243.

Spahr, L., Butterworth, R. F., Fontaine, S., Bui, L., Therrien, G., Milette, P. C., Lebrun, L. H., Zayed, J., Leblanc, A., and Pomier-Layrargues, G. (1996). Increased blood manganese in cirrhotic patients: relationship to pallidal magnetic resonance signal hyperintensity and neurological symptoms. *Hepatology* **24,** 1116–1120.

Sumino, K., Hayakawa, K., Shibata, T., and Kitamura, S. (1975). Heavy metals in normal Japanese tissues. *Arch. Environ. Health* **30,** 487–494.

Tapin, D., Kennedy, G., Lambert, J., and Zayed, J. (2006). Bioaccumulation and locomotor effects of manganese sulfate in Sprague-Dawley rats following subchronic (90 days) inhalation exposure. *Toxicol. Appl. Pharmacol.* **211,** 166–174.

Teeguarden, J. G., Dorman, D. C., Covington, T. R., Clewell, H. J., III., and Andersen, M. E. (2007a). Pharmacokinetic modeling of manganese. I. Dose dependencies of uptake and elimination. *J. Toxicol. Environ. Health A* **70,** 1493–1504.

Teeguarden, J. G., Dorman, D. C., Nong, A., Covington, T. R., Clewell, H. J., III., and Andersen, M. E. (2007b). Pharmacokinetic modeling of manganese. II. Hepatic processing after ingestion and inhalation. *J. Toxicol. Environ. Health A* **70,** 1505–1514.

Teeguarden, J. G., Gearhart, J., Clewell, H. J., III., Covington, T. R., Nong, A., and Andersen, M. E. (2007c). Pharmacokinetic modeling of manganese. III. Physiological approaches accounting for background and tracer kinetics. *J. Toxicol. Environ. Health A* **70,** 1515–1526.

Thorlacius-Ussing, O., Gregersen, M., and Hertel, N. (1988). The concentration of twelve elements in the anterior pituitary from human subjects and rats as measured by particle induced x-ray emission (PIXE). *Biol. Trace Element Res.* **16,** 189–202.

Tracqui, A., Tayot, J., Kintz, P., Alves, G., Bosque, M. A., and Mangin, P. (1995). Determination of manganese in human brain samples. *Forensic Sci. Int.* **76,** 199–203.

Vitarella, D., Moss, O., and Dorman, D. C. (2000). Pulmonary clearance of manganese phosphate, manganese sulfate, and manganese tetraoxide by CD rats following intratracheal instillation. *Inhal. Toxicol.* **12,** 941–957.

Yamada, M., Ohno, S., Okayasu, I., Okeda, R., Hatakeyama, S., Watanabe, H., Ushio, K., and Tsukagoshi, H. (1986). Chronic manganese poisoning: a neuropathological study with determination of manganese distribution in the brain. *Acta Neuropathol.* **70,** 273–278.

Yoon, M., Nong, A., Clewell, H. J., Taylor, M. D., Dorman, D. C., and Andersen, M. E. (2009a). Evaluating placental transfer and tissue

concentrations of manganese in the pregnant rat and fetuses after inhalation exposures with a PBPK model. *Toxicol. Sci.* **112,** 44–58.

Yoon, M., Nong, A., Clewell, H. J., Taylor, M. D., Dorman, D. C., and Andersen, M. E. (2009b). Lactational transfer of manganese in rats: predicting manganese tissue concentration in the dam and pups from inhalation exposure with a pharmacokinetic model. *Toxicol. Sci.* **112,** 23–43.

Young, T., Myers, J. E., and Thompson, M. L. (2005). The nervous system effects of occupational exposure to manganese—measured as respirable dust—in a South African manganese smelter. *Neurotoxicology* **26,** 993–1000.

Toxicology and Applied Pharmacology 372 (2019) 1–10

Contents lists available at ScienceDirect

Toxicology and Applied Pharmacology

journal homepage: www.elsevier.com/locate/taap

Updating physiologically based pharmacokinetic models for manganese by incorporating rapid association/dissociation processes in tissues

Miyoung Yoon[a,b,*], Alina Efremenko[a], Cynthia Van Landingham[c], P. Robinan Gentry[c], Athena M. Keene[d], Michael D. Taylor[e], Harvey J. Clewell[a,c], Melvin E. Andersen[a]

[a] ScitoVation, LLC, RTP, Cary, NC, USA
[b] Toxstrategies, Inc., Cary, NC, USA
[c] Ramboll, RTP, NC, USA
[d] Afton Chemical, Richmond, VA, USA
[e] NiPERA, RTP, NC, USA

ARTICLE INFO

Keywords:
Manganese
Essential metal
Metal transporters
Essential metal homeostasis
Dose-dependent kinetics

ABSTRACT

Previously, we developed a series of physiologically based pharmacokinetic (PBPK) models for manganese (Mn) in which saturable tissue binding and dose-dependent increases in biliary excretion captured key aspects of Mn homeostasis biology. These models reproduced the non-linear behavior of Mn kinetics in different tissues, accounting for dose-dependent changes in Mn kinetics. The original model construct had relatively slow association and dissociation rate constants for Mn binding in tissues. In this updated model, both rates of entry into tissue and the interaction of Mn with binding sites are rapid, and the step limiting Mn accumulation is the saturation of tissue binding sites. This binding reflects general cellular requirements for Mn with high affinity but rapid exchange between bound and free forms, which we captured using a dissociation constant (KD) of ~ 0.5 μM across tissues while maintaining different maximum binding capacities in each tissue. Variability in the binding capacities accounted for different background levels of Mn in particular tissues. This alternative structure successfully described Mn kinetics in tissues in adult rats exposed to Mn either in their diet or by inhalation, indicating that both the original and the present models capture the dose-dependent and tissue-specific kinetic behavior of Mn in adult rats. Although the published models that emphasize the role of smaller tissue binding rate constants in non-linear behaviors capture all relevant dose-dependent kinetic behaviors of this metal, increasing biological relevance of the model structure and parameters should provide greater confidence in applying the Mn PBPK models to risk assessment.

1. Introduction

Mn is an essential element and present in all tissues in significant concentrations. The best-known role of Mn in the body is as a redox-active cofactor in the cellular antioxidant defense enzymes such as Mn-superoxide dismutase (Aschner et al., 2007). Tissue Mn concentrations are maintained at a relatively constant level despite widely varying levels of Mn input from dietary intake ranging from 1 to 10 mg Mn per day in humans (ATSDR, 2013; Freeland-Graves, 1994). This tight control of body Mn is attributable to multiple homeostatic processes: 1) uptake in the gut, 2) storage and utilization in the tissue, and 3) biliary excretion (Aschner et al., 2005; Teeguarden et al., 2007). However, exposure to excessive Mn such as chronic inhalation of high doses Mn (over 1 mg Mn/m^3) can overwhelm the homeostasis leading to toxicity in the central nervous system (CNS) (Andersen et al., 2010; Roels et al., 1999). Other excessive exposure conditions such as long-term parenteral nutrition containing Mn and/or impaired Mn clearance due to liver dysfunction can also compromise homeostatic regulation of Mn and lead to elevated CNS target tissue concentration (Leyva-Illades et al., 2014; Santos et al., 2014).

A series of PBPK models has been developed for Mn considering both essentiality and toxicity to support a human health risk assessment of Mn exposure (Nong et al., 2009, Schroeter et al., 2011, Yoon et al., 2011). The models are intended to predict exposure conditions that would lead to toxicologically significant increases in Mn concentrations in the target tissue compared to the levels maintained with normal dietary intake. These models are based on the knowledge of the biological factors that control uptake, distribution, and clearance of Mn

* Corresponding author at: ToxStrategies, Inc., 1249 Kildaire Farm Road #134, Cary, North Carolina 27511, USA.
E-mail address: yoon.m.work@gmail.com (M. Yoon).

https://doi.org/10.1016/j.taap.2019.04.006
Received 11 December 2018; Received in revised form 2 April 2019; Accepted 6 April 2019
Available online 09 April 2019

and other essential trace metals that were available at the time of model development. To describe the dose-dependent pharmacokinetic behavior of Mn observed in multi-dose, multi-route and multi-species pharmacokinetic studies, it was necessary to describe Mn homeostasis as the underlying reason for those dose-dependent kinetics behavior (Andersen et al., 2010). The introduction of these biological processes was accomplished using the concept of saturable tissue binding and inducible biliary excretion.

The published models effectively reproduced the non-linear behavior of Mn kinetics in different tissues. However, the knowledge gained about Mn homeostasis in recent years indicates that metal homeostasis depends primarily on regulation of uptake into and efflux out of tissues via various cellular membrane metal transporters and less on avid binding of Mn within tissues (Aschner and Erikson, 2017; Chen et al., 2015). Recent studies have shown that several of the zinc transporter proteins are crucial in Mn homeostasis in addition to those already known such as the divalent metal transporter 1 (DMT1) and transferrin/transferrin receptor system. Notably, SLC30A10, SLC39A8 and SLC39A14 have shown to be pivotal in Mn clearance and maintenance of Mn homeostasis in vertebrates (Chen et al., 2015; Leyva-Illades et al., 2014; Lin et al., 2017; Tuschl et al., 2016). Compared to Mn importers, transporters for Mn efflux and the underlying mechanisms of Mn efflux and their role in maintaining Mn homeostasis in mammalian systems have been discovered only recently. Among those, SLC30A10 appear to be the most relevant Mn efflux transporters playing a role in mediating Mn efflux in neuronal systems (Chen et al., 2015; Hutchens et al., 2017; Leyva-Illades et al., 2014).

In this study, we evaluated an alternative model structure that is more consistent with the recent understanding of the biology of essential metal transport across the cell membrane through metal transporters rather than one relying on the description of tissue binding processes controlling elimination rates for Mn. While the published models have successfully served their roles in supporting internal exposure-based Mn risk assessment, the new model structure will facilitate the incorporation of data from emerging in vitro and in vivo models on Mn transport, enabling the mechanism-based refinement of the model structure, and should lead to increased confidence in model applications.

2. Materials and methods

2.1. Model structure

Two rat Mn PBPK models are compared in this study (Fig. 1). The published model (Nong et al., 2008) is referred as 'binding' or 'original' model, whereas the model newly introduced here is referred to as 'transporter', 'rapid binding/dissociation' or 'updated' model. Note that saturable tissue storage and asymmetric diffusion in and out of the tissue are key determinants of tissue Mn in both models (Fig. 1). Only the relative rates of these processes are different between the two models. Therefore, this update of the model can be viewed as a re-parameterization of the original model described in Nong et al. (2008).

2.1.1. Original model

The basic structure of the existing PBPK models describing Mn kinetics in multi-species with multi-exposure routes for rodents, primates and humans is based on the 'original' model developed in the rat (Nong et al., 2009). Most of the features in the Nong model were maintained in the updated model. Only the features that are notably different in the new model are detailed below. For other details of the published model, Nong et al. (2009) should be referred to.

Briefly, Mn is rapidly cleared into the tissues after entering the systemic circulation regardless of exposure routes. For brain, this clearance was described as an asymmetric bi-directional diffusion. The free Mn in systemic blood rapidly equilibrates with free Mn in the blood of the brain tissue. The flux between brain tissue-blood and brain tissue

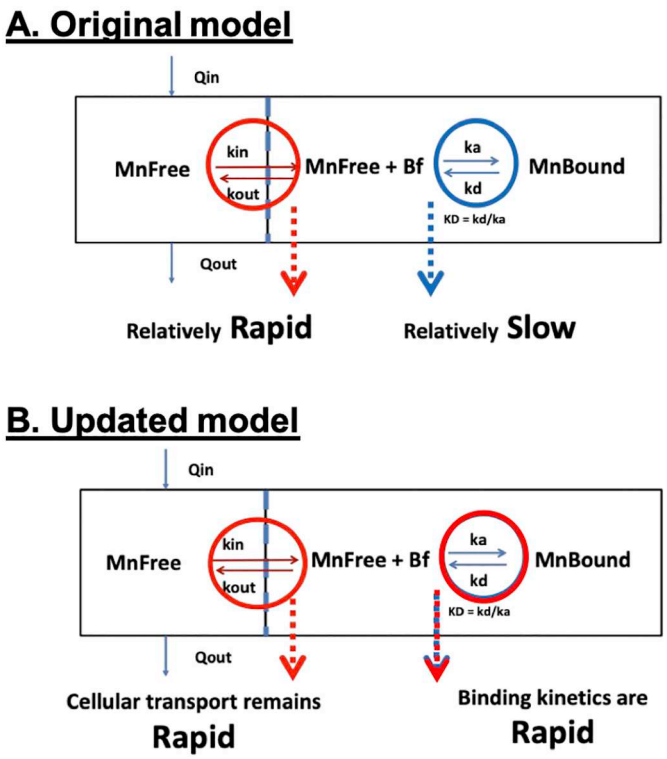

Fig. 1. Model structure: slow (A) versus rapid binding (B) reactions in tissues. The kin and kout represent diffusion rate constants for Mn influx and efflux, respectively, while the ka and kd represent association and dissociation rate constants.
Mn total = MnFree + MnBound, whereas Bmax = Bf + MnBound.
Bf represents binding sites that are available for binding, while Bmax represents the maximum binding capacity in a tissue.

is diffusion limited, the rate of which is determined by the diffusion rate constants, kin and kout, respectively. In the original model, the diffusion limitation in the brain was considered to reflect the role of blood-brain barrier in controlling Mn in and out fluxes.

The feature of asymmetrical diffusion was included in a brain region-specific fashion, a decision that was rationalized due to different requirements for basal manganese in different regions and differential distribution of transporters. The asymmetrical diffusion is necessary to describe the preferential uptake of Mn into the mid-brain seen with high levels of Mn exposure. For other tissues, a rapid and symmetrical flux of Mn between the systemic blood and tissue compartment was included using a partition coefficient, and thus, the tissue Mn in these other tissue compartments is primarily determined by the tissue binding characteristics.

Once distributed into the tissue, Mn is 'bound' to the cellular components that require Mn for a variety of biological functions, i.e., utilized in the cell. Bound Mn is not readily available to diffuse from tissue to blood. The 'binding' capacity, therefore, represents a total pool of accessible binding partners for manganese. The model structure does not attempt to differentiate between different enzymes, proteins, etc. with which Mn associates within tissues. The incorporation of Mn into these cellular proteins/tissue constituents and subsequent loss from those 'binding sites' back to blood are governed by three model parameters - maximum tissue binding capacity (Bmax) and tissue specific association and dissociation rate constants (ka and kd, respectively). Initial estimates of Bmax were based on the basal levels of manganese in various tissues.

The fraction bound (or fraction free) in the tissue varies dependent on the Mn content in diet at steady-state. At normal dietary intakes, the majority of Mn in the tissue will be associated with cellular

Table 1
Model parameters.

Nong model	Bmax[a] (uM)	KD (uM)	ka (/uM/h)	kd (/h)	Kin (ml/h)	Kout (ml/h)
Striatum	21	9.89	1.3	**0.001**	0.13	0.10
Cerebellum	19	0.01	70.2	**0.00013**	0.08	2.48
Olfactory blub	35	0.16	32.4	**0.0003**	0.02	0.19
Liver	43	0.07	14.6	**0.0111**	N/A	N/A
Bone	11	4.04	0.2	**0.0238**	N/A	N/A
Lung	270	43.17	5.4	**0.38**	N/A	N/A
Rest of body	4	0.03	0.5	**0.00454**	N/A	N/A

Updated model	Bmax[a] (uM)	KD (uM)	ka (/uM/h)	kd (/h)	Kin (ml/h)	Kout (ml/h)
Striatum	15	0.46	10	**4.6**	0.08	0.10
Cerebellum	9	0.37	10	**3.7**	0.08	0.44
Olfactory blub	4	0.46	10	**4.6**	0.08	0.05
Liver	46	0.46	10	**4.6**	3.95	36.9
Bone	20	0.46	10	**4.6**	0.01	0.63
Lung	15	0.46	10	**4.6**	0.77	16.1
Rest of body	4	0.37	10	**3.7**	0.01	1.33

Parameters used in the original model with small, fitted tissue dissociation rate constants (top) and the revised model that uses a common tissue equilibrium dissociation constant for Mn binding across tissues and more rapid Mn-dissociation rate constants (bottom). N/A denotes 'not applicable' as these parameters were not used, but the partition coefficients were used instead in the original model for these tissues. More rapid Mn-dissociation rate constants are used in the revised model than the original model are highlighted in bold.

[a] Tissue binding capacity is study specific, although the same values were used most of the studies. A few occasions they were varied from the listed Bmax values in this table to fit the observed basal tissue concentrations in the specific studies if necessary (see Table S1 in Supplementary materials for cerebellum, lung and liver).

constituents, i.e., 'bound'. With sufficiently high Mn in diet, the fraction of Mn in the tissue in a bound form, i.e., Mn_bound/(Mn_bound + Mn_free), would be lower than the same ratio in animals on a marginal Mn diet. The fraction bound expressed in this manner does not directly represent the actual occupancy of binding sites. In high-dose exposure, binding sites would be eventually saturated, and the fraction free could exceed the fraction bound. In such cases, free Mn – the form believed to be related to effects in target tissues – increases disproportionately compared to the increase in external dose.

Free Mn circulates in blood and is the form excreted into bile. The bound form is in the tissue and dissociates from the binding sites with a rate constant kd. A key factor differentiating the two models is the magnitude of kd: it was smaller in the original model and larger in the updated model.

2.1.2. The updated model

In the original model, dissociation of bound forms of Mn was slow (Table 1) and designed to be the limiting process for loss of Mn when body and tissue stores were reduced by alterations in intake or at the end of high dose exposures. In this updated model, the dissociation (and association) rate constants are much larger and tissue stores adjust more rapidly to alterations in Mn intake and total body burden.

These higher rates of tissue binding and the consistency of the dissociation equilibrium constant across tissues are more reflective of the biology of interactions of Mn with tissue proteins. The use of a common dissociation constant (KD) at 0.5 μM is more consistent with similarities in Mn utilization and requirements across tissue types and leads to maintenance of Mn in bound forms until the binding sites become saturated. The variability in the presumed binding capacities across tissues still accounts for different background levels of Mn in particular tissues as in the Nong et al. (2008) model, as they reflect differing degrees of Mn demands among different tissues. Using a KD of approximately 0.5 μM for all tissues, about 70% of Mn in tissues in the basal state is bound.

2.2. Model parameterization

All the physiological and chemical-specific parameters other than those updated (Table 1) were kept the same as the previously published binding model (Nong et al., 2008).

In our revised model, uptake of Mn to all the tissues, not just brain regions, is mediated by a tissue uptake rate constant rather than blood flow directly. This membrane transport is tissue dependent allowing differential increases in Mn in the target tissues after high-dose-rate exposures of Mn. Describing all transport as linear processes captured the kinetics both for steady-state and inhalation exposure conditions, i.e., there is no need to introduce dose-dependent transport rate constants across cellular membranes.

To convert parameter values from the original to the updated model, the following steps were taken. Briefly, the association rate constant (ka) was set at 10/μM/h to allow rapid complexing of Mn to binding partners in all the tissues. The corresponding dissociation rate constant (kd) was calculated to obtain a KD of around 0.5 μM in all the tissues. The uptake rate constant parameter (KinC) was set to give smaller uptake clearances (Kin in the unit of ml/h) for brain and bone (i.e., limited uptake), and higher uptake clearances for other tissues, in particular for liver (Table 1). Efflux parameters (KoutC) for each tissue were fitted to be consistent with the tissue concentrations both during steady-state conditions and during inhalation exposures that increase tissue Mn.

The new model could recapitulate dose-dependent increases in biliary excretion without biliary induction, and so the model structure was finalized as such.

2.3. Model evaluation and sensitivity analysis

2.3.1. Experimental data used for model evaluation

To compare the performance of the original and the updated models, three data sets from rat pharmacokinetic studies were used. They were collected both in steady-state dietary and inhalation exposure conditions and were used for model development and evaluation of the original model as well. A brief description of these studies is given below.

- *Steady-state dietary exposure study* - Rats were maintained on a diet containing Mn at 2, 10, and 100 ppm for over 11 weeks. Both tissue steady-state Mn concentrations and elimination kinetics for an intravenous tracer administration of $^{54}MnCl_2$ without inhalation exposure data were reported and used for model evaluation (Dorman et al., 2001a).
- *Fourteen-day inhalation study* – Rats were exposed to soluble $MnSO_4$ at concentrations of 0, 0.03, 0.3 or 3 mg Mn/m^3 for 14 consecutive days for 6 h/day in addition to a 125 ppm (approximately 100–150 ppm) dietary Mn exposure. Tissue concentrations of Mn as well as the ^{54}Mn tracer (which was administered at the end of the 14 day inhalation exposure) kinetics at the end of the 14 day exposure period from this study were used for model evaluation (Dorman et al., 2001b).
- *Ninety-day inhalation study* – Rats were fed a 10 ppm Mn diet and exposed via inhalation to $MnSO_4$ at concentrations of 0.1 or 0.5 mg/m^3 for 6 h/day and 5 days/week with weekends off, over a 90-day period. Tissue Mn concentrations were reported at 45- and 90-day after the cessation of the inhalation exposure (Dorman et al., 2004).

2.3.2. Sensitivity analysis

A sensitivity analysis of the original and the updated models was performed for 6 key model parameters, ones that had been shown to have a high sensitivity for striatal Mn in the original model (Nong et al., 2008). The 6 parameters included influx and efflux rates into and out of

the striatum (KINSTC and KOUTSTC), association and dissociation rate constants in the striatum (KAST and KDST), the biliary excretion rate constant (KBILEC), and the absorption fraction in the gut (FDIETUP). The relative importance of these parameters in determining the total Mn concentration in the brain striatum region (CTOTST) or the amount of remaining tracer Mn (ATOT54) in the whole body was evaluated as described in earlier studies (Nong et al., 2008; Yoon et al., 2011). The sensitivity coefficients of 0.1 or greater are reported.

2.4. Model simulations

All the model simulations were run using acslX (version 3.0.2.1; The Aegis Technologies Group, Inc., Huntsville, Alabama). Model fitting/parameter optimization was performed using the automated parameter optimization function in acslX based on NelderMead algorithm. The model code is available from the corresponding author upon request.

3. Results

3.1. Simulation of whole-body Mn tracer kinetics in steady-state and inhalation exposure

The time course of the intravenously injected ^{54}Mn elimination kinetics was determined in rats on three different diets, containing Mn at 2, 10 or 100 ppm, at steady-state (Dorman et al., 2001a). The simulation of the loss of ^{54}Mn from the body was fairly well described with either the original parameters or with the updated model structure (Fig. 2). A second tracer study was conducted in rats exposed to various concentrations of $MnCl_2$ by inhalation for 14 days in rats fed on an approximately 125 ppm diet (Dorman et al., 2001b). The tracer was administered intravenously at the end of the 14-day inhalation exposure; hence the tracer kinetics reflected how the total amount of Mn in the body changes immediately after the inhalation exposure stops. The updated model with rapid binding provided a slightly better fit to both the more rapid initial loss of Mn from the body and maintenance of tracer Mn at the later times at the three different dietary intakes (Fig. 4). As with diet alone, the rapid binding/dissociation model provided a more accurate description of the loss of tracer over time as the body returned to a basal condition after brief periods of high concentration exposure to Mn via tracer injection (Figs. 3 and 4).

3.2. Simulation of brain Mn kinetics in steady-state and inhalation exposure

The simulated striatum concentrations from both models were consistent with the observed total tissue Mn concentrations at steady state following administration of dietary Mn concentrations ranging from 2 to 100 ppm in the Dorman et al. (2001b) study (Fig. 5). Also, both models reproduced the observed striatum Mn concentrations at the end of the 14 day inhalation exposure (Fig. 5) reported in Dorman et al. (2001a). The updated model produced a more rapid rise in striatum Mn along with a greater daily fluctuation over the time course of the simulation. Similarly, the updated model performed marginally better in capturing the time profiles of striatum Mn after 90 day inhalation exposure (Fig. 5C). In particular, the updated model was able to better recapitulate a time profile of rapid elimination and return to steady state after the cessation of the last inhalation dosing as was shown with 0.5 mg Mn/m^3.

3.3. Comparison of the simulated Mn kinetics in free and bound Mn forms

Figs. 5 and C clearly showed that the updated model shows more extensive short-term excursions, although both models recapitulated the observed tissue concentrations during and at the end of inhalation exposure equally well. Updated model simulated striatum Mn kinetics in free vs. bound forms were plotted (Fig. 6) showing that striatum Mn time profiles are predominantly determined by the increase in free Mn in the updated model. This was also the case in the original model (Nong et al., 2009), although with much less short term excursions, particularly in the later refined original model (Nong et al., 2008) as is shown in Fig. 5-A.

3.4. Sensitivity analysis of binding and transporter model parameters

The results of the sensitivity analysis of the updated and the published original models performed for the 6 key model parameters that were shown to be highly influential to striatum Mn concentrations in the binding model were plotted for steady state (Fig. 7A), 14-day inhalation (Fig. 7B) and 90-day inhalation (Fig. 7C). In contrast to the earlier model sensitivity analysis, the updated model with more rapid binding and dissociation shows significant sensitivity for both the uptake and efflux rate constants in and out of the striatum, whereas with the original model, the striatum Mn concentration is sensitive to both transport and binding rates.

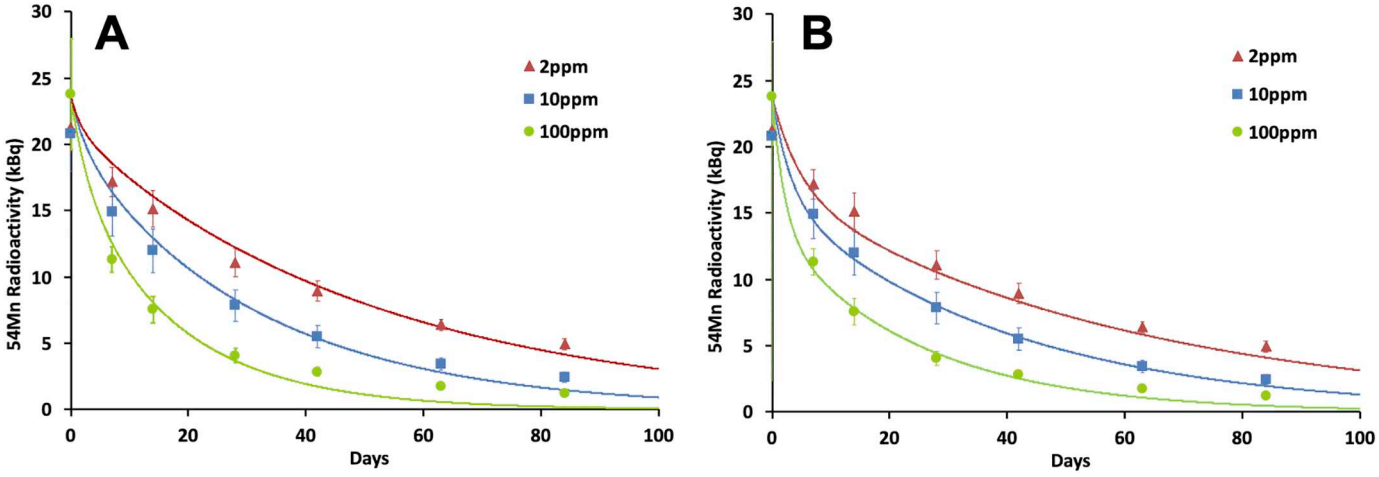

Fig. 2. Steady-state tracer kinetics. Symbols represent the mean ± SD from the data by Dorman et al. (2001a) of the individual animals, whereas the lines in corresponding colors represent model simulations using the published (A) or updated (B) model for ^{54}Mn tracer total body radioactivity in rats fed on a 2, 10 or 100 ppm Mn diet for 13 weeks in the same study. Intravenous injection of $^{54}MnCl_2$ was done following the 13-week diet, and the whole-body Mn radioactivity was measured for 10 weeks post-injection exposure.

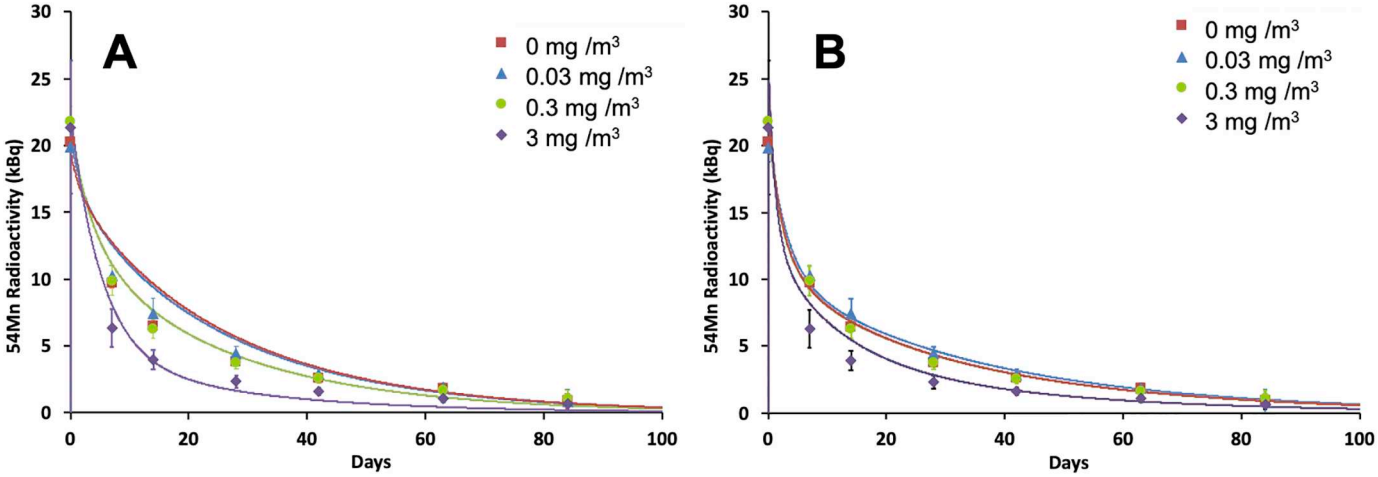

Fig. 3. 14 day inhalation tracer kinetics. Symbols represent the mean ± SD from the data by Dorman et al. (2001b), whereas the lines in corresponding colors represent model simulations using the published (A) or updated (B) model for ^{54}Mn tracer kinetics following a 14-d inhalation exposure at 0, 0.03, 0.3, or 3 mg Mn/m^3. The rats were fed on an approximately 125 ppm Mn diet prior to and during the 14-d inhalation exposure.

4. Discussion

Previously published PBPK models were developed based on the available knowledge of the biological determinants of the uptake, distribution, and clearance for Mn and included aspects of the factors important for the distribution of Mn as they were known at the time of model development (Nong et al., 2008; Schroeter et al., 2011; Yoon et al., 2011). Because of the limitations in the understanding of the biological steps involved in essential metal homeostasis, the parameters of these PBPK models did not necessarily have a one-to-one correspondence to specific biological and/or biochemical processes in Mn homeostasis and disposition in the body. In particular, the mechanism of cellular transport and utilization in different tissues under various exposure conditions had not been fully characterized when those models were being developed and when the structure of the initial models were finalized. As such, the primary goal in developing the previously published PBPK models was to have a model structure that captured the dose-dependent kinetics of Mn observed in rodents and, indirectly, provided confidence in utilizing a similar model structure for humans. Although the original model structure and parameters were based on particular assumptions about processes controlling Mn within tissues, they still allowed coherent integration of the known Mn biology at the time of model development, recapitulating the observed tissue Mn concentrations in various tissues within the body under various exposure conditions, and accounting for exposures that would lead to tissue overload and rapid increases in free Mn in tissues.

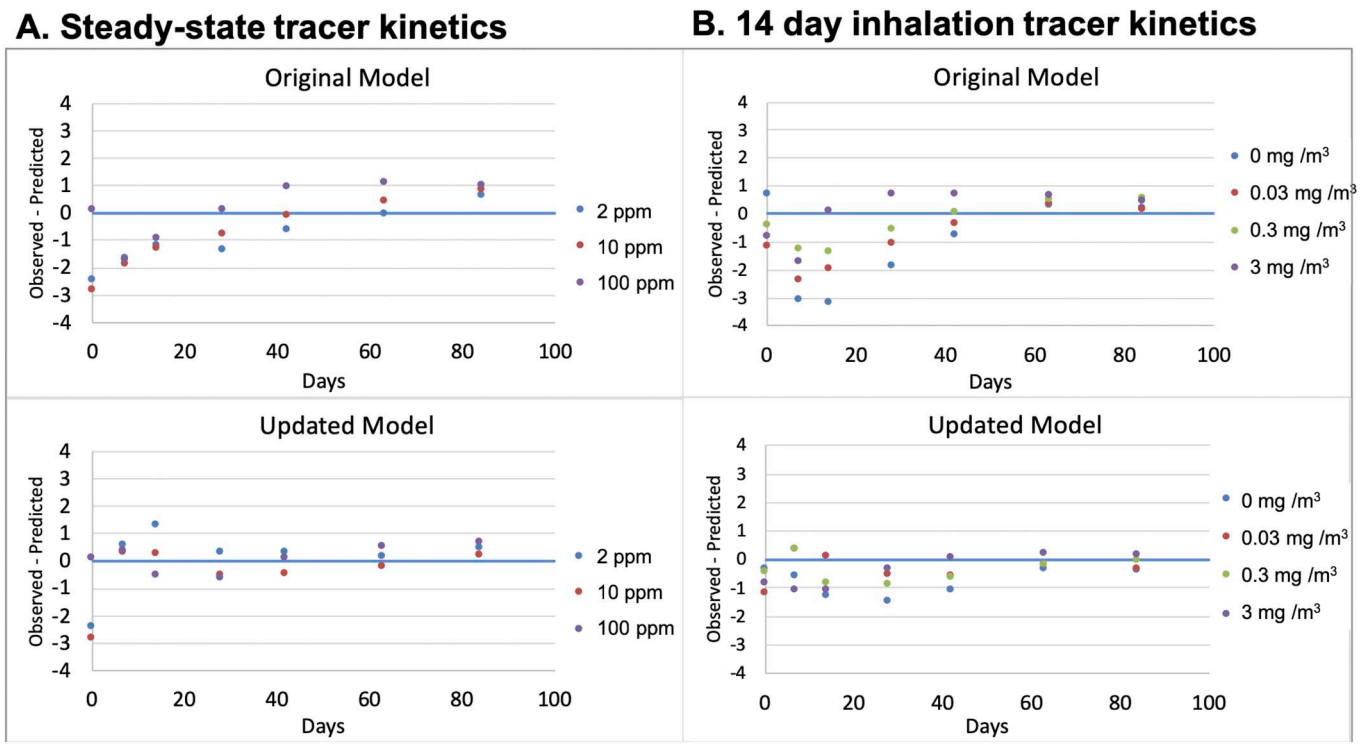

Fig. 4. Residual plots of the steady-state and 14 day inhalation tracer Mn kinetics. Residuals were calculated as the difference between the mean of the observed and predicted tracer levels at each time point reported in Figs. 2 and 3. Residual plots show that the updated model provides a somewhat better description of the time-course of the experimental data than the original model. The updated model also provides a higher likelihood than the original model (data not shown).

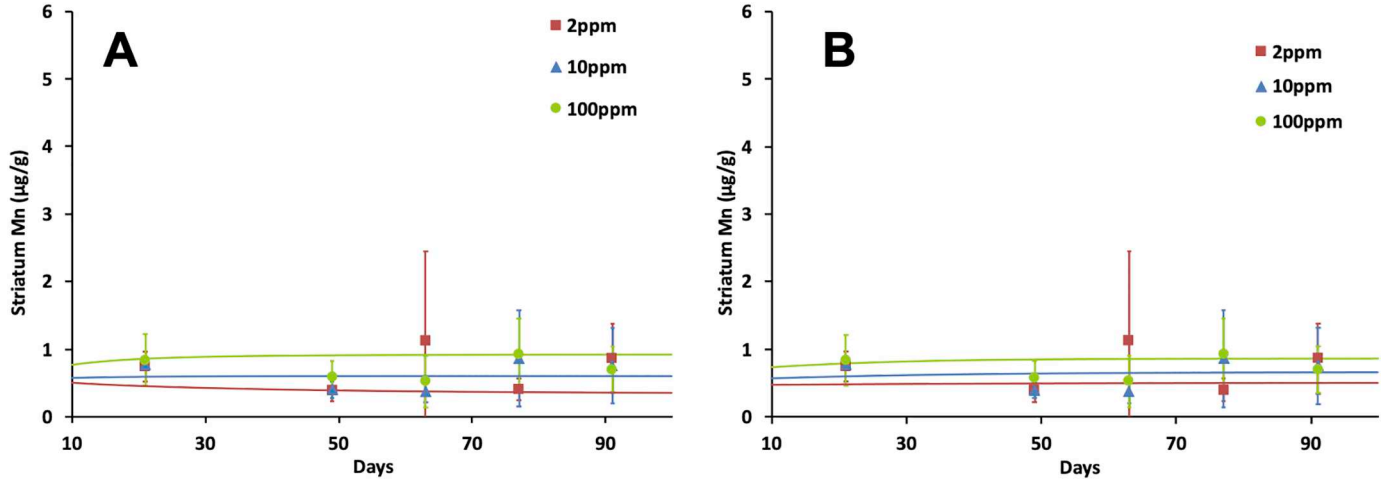

Fig. 5. A. Steady state brain striatum Mn concentration. Symbols represent the mean ± SD calculated from the data reported by Dorman et al. (2001b), whereas the lines represent model simulations using the published (A) or updated (B) model for striatum Mn concentrations in rats fed on 2, 10 or 100 ppm Mn diet for 13 weeks reported in the same study. Fig. 5B. 14 day inhalation brain striatum Mn concentration. Symbols represent the mean ± SD of the data reported by Dorman et al. (2001a), whereas the lines represent model simulations using the published (A) or updated (B) model for striatum Mn concentrations in rats exposed by inhalation to 0.03, 0.3 and 3 mg Mn/m^3 for 6 h/d for 14 consecutive days (Dorman et al., 2001a). Steady state conditions are achieved more quickly in the updated model. Fig. 5C. 90 day inhalation striatum Mn concentration. Symbols represent the mean ± SD of the data reported by Dorman et al. (2004), whereas the lines represent model simulations using the published (A & C) or updated (B & D) model for striatum Mn concentrations in rats during and following a 90-d inhalation exposure at 0.1 and 0.5 mg Mn/m^3. The rats were fed on a 10 ppm diet from 30 d prior to exposure, and then they were exposed for 13 weeks for 6 h/d, 5 d/week with weekends off.

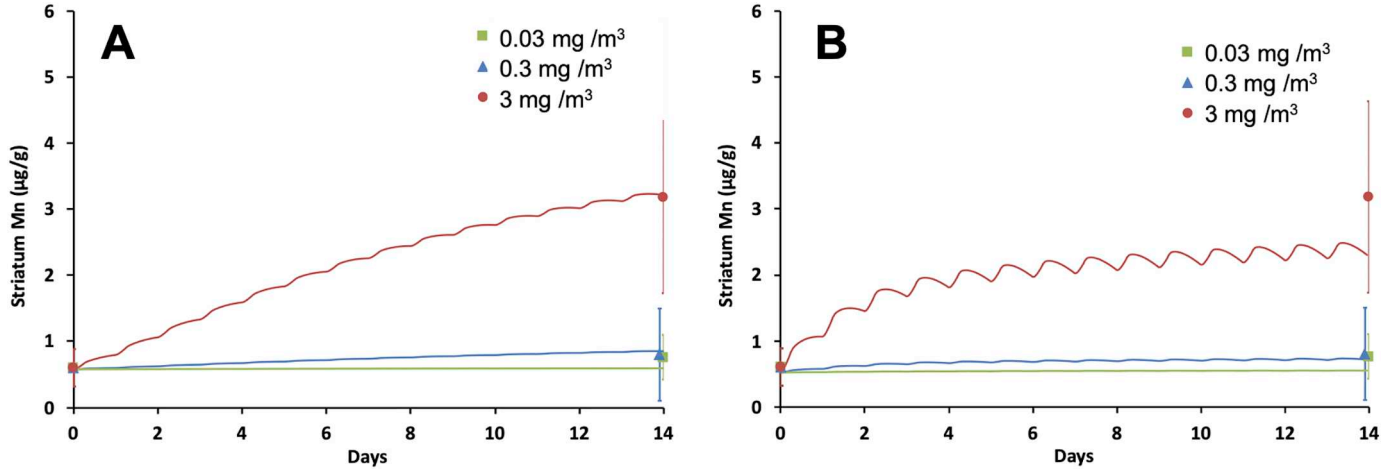

Fig. 5. (*continued*)

In both the original and this updated model structure, Mn time profiles in striatum after inhalation are predominantly determined by the increase in free Mn. As the free Mn, i.e., the form of Mn that is not associated with cellular macromolecules, is assumed to be responsible for Mn toxicity, this indicates that the predicted dose-response relationships from the two models would be similar. The processes accounting for the increase in free Mn with increasing tissue Mn differ in the original and this updated model. In the original models, slow dissociation rate constants provided the rate determining process for allowing Mn to exit the tissue. In this rapid equilibration model, the exchange between bound and free forms is rapid, and efflux rates from the tissues determine the rate at which free Mn leaves the tissues.

In the updated model, the KD values are similar among different tissues and consistent with similar utilization patterns for cellular Mn regardless of the tissue types. Differing amounts of Mn in various tissues -i.e., different levels of Mn containing macromolecules, lead to different background tissue Mn capacities in both models. While the KD in our updated model reflects a general binding affinity of multiple Mn-binding sites in tissues, there is little direct information about the amounts or affinity of these binding partners. Some experimental studies reported the cellular free Mn in rat hepatocytes at around 0.2 to 1 μM using the electron paramagnetic resonance analysis technique (Ash and Schramm, 1982; Powell and Brew, 1976). In addition, a few experimental studies reported dissociation constants for Mn binding/association to cellular macromolecules such as galactosyltransferase and Mn^{2+}-ATPase in a low micromolar range (Grisham and Mildvan, 1974; Powell and Brew, 1976). These estimates are in line with the physiological cellular concentration of free Mn and consistent with the KD we selected for our simulations.

Kinetics of Mn tracer in the whole body can be viewed as a reflection of free Mn behaviors under given exposure conditions, e.g., in the current study they were steady-state dietary or the end of inhalation exposure. Mn tracers are incorporated into cellular macromolecules, i.e., bound, and then released from those binding sites into the free form in the cell and subsequently exit the cells to blood for excretion to bile. The improvement with the updated model in providing better correspondence with tracer kinetics compared to the original model shows that the transients after changing exposure conditions need to be more rapid than allowed in the earlier description. The updated description also better captured the rapid clearance of circulating free Mn from

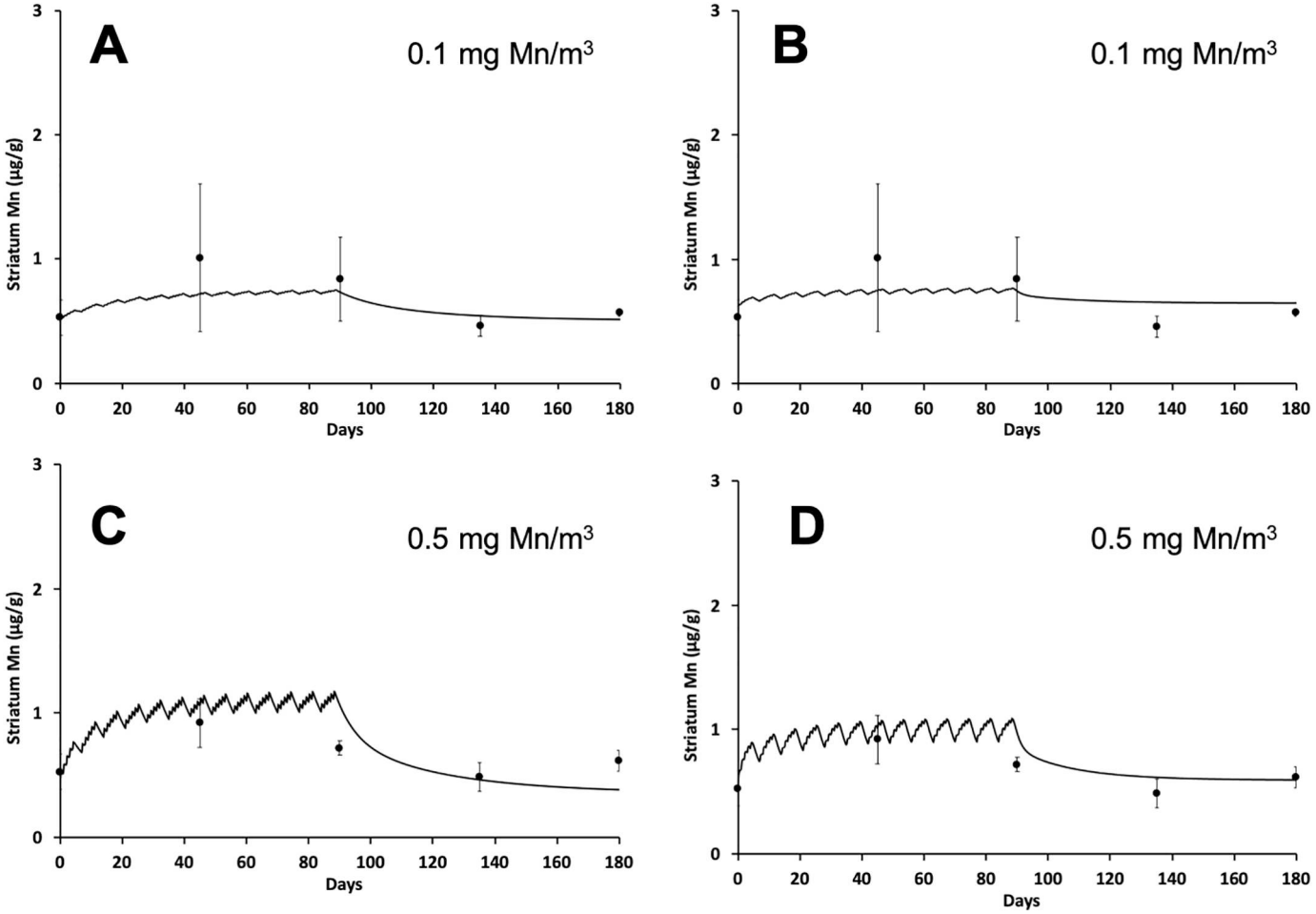

Fig. 5. (*continued*)

blood resulting from inhalation exposure, producing a more rapid rise in striatum Mn along with a greater daily fluctuation of total Mn in its time profile as well as a rapid return to the basal level at the cessation of the inhalation. Indeed, the updated model recapitulated the Mn elimination kinetics with changes in Mn intake much better that had been done previously.

The clear improvement in capturing Mn-transients, although either model recapitulates longer-exposure tissue dose-response, indicates that the updated tissue description may be particularly useful in investigating mechanisms of Mn toxicity in cell culture models and non-mammalian systems such as zebrafish or *C. elegans*. PK models can be used in these situations to describe Mn kinetics in the culture system itself, cellular loading and unloading of Mn from and to the media, which can then facilitate the extrapolation of in vitro mechanistic

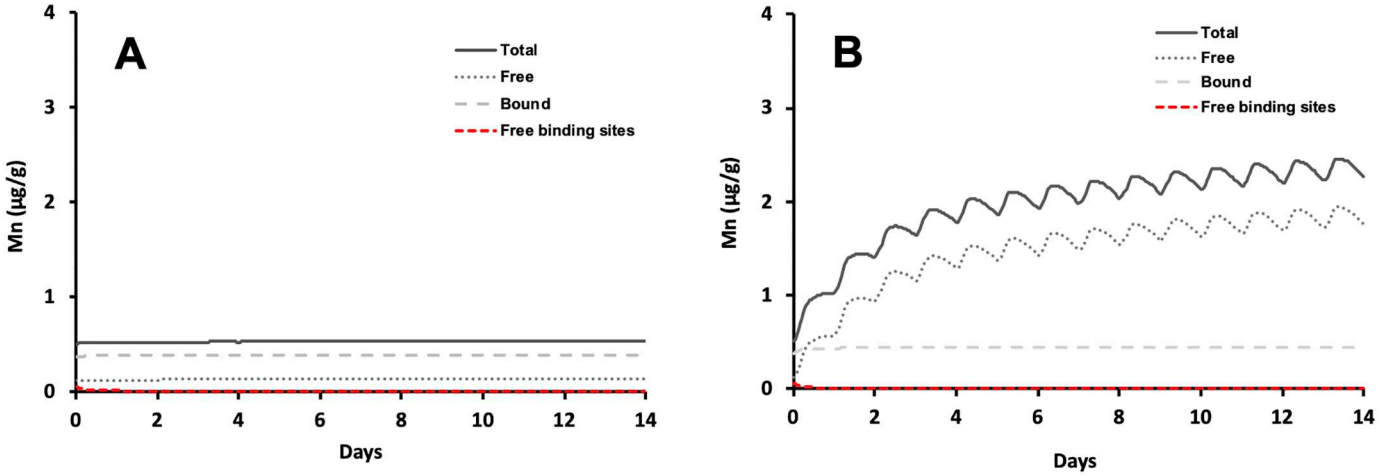

Fig. 6. Simulated brain striatum free and bound Mn kinetics. Striatum Mn kinetics in free vs. bound forms along with the remaining free binding site capacity were simulated using the updated model for the low concentration of 0.3 mg Mn/m^3 (A) and at high concentration of 3.0 mg Mn/m^3 (B) air Mn exposure for a 14-day period (Dorman et al., 2001a).

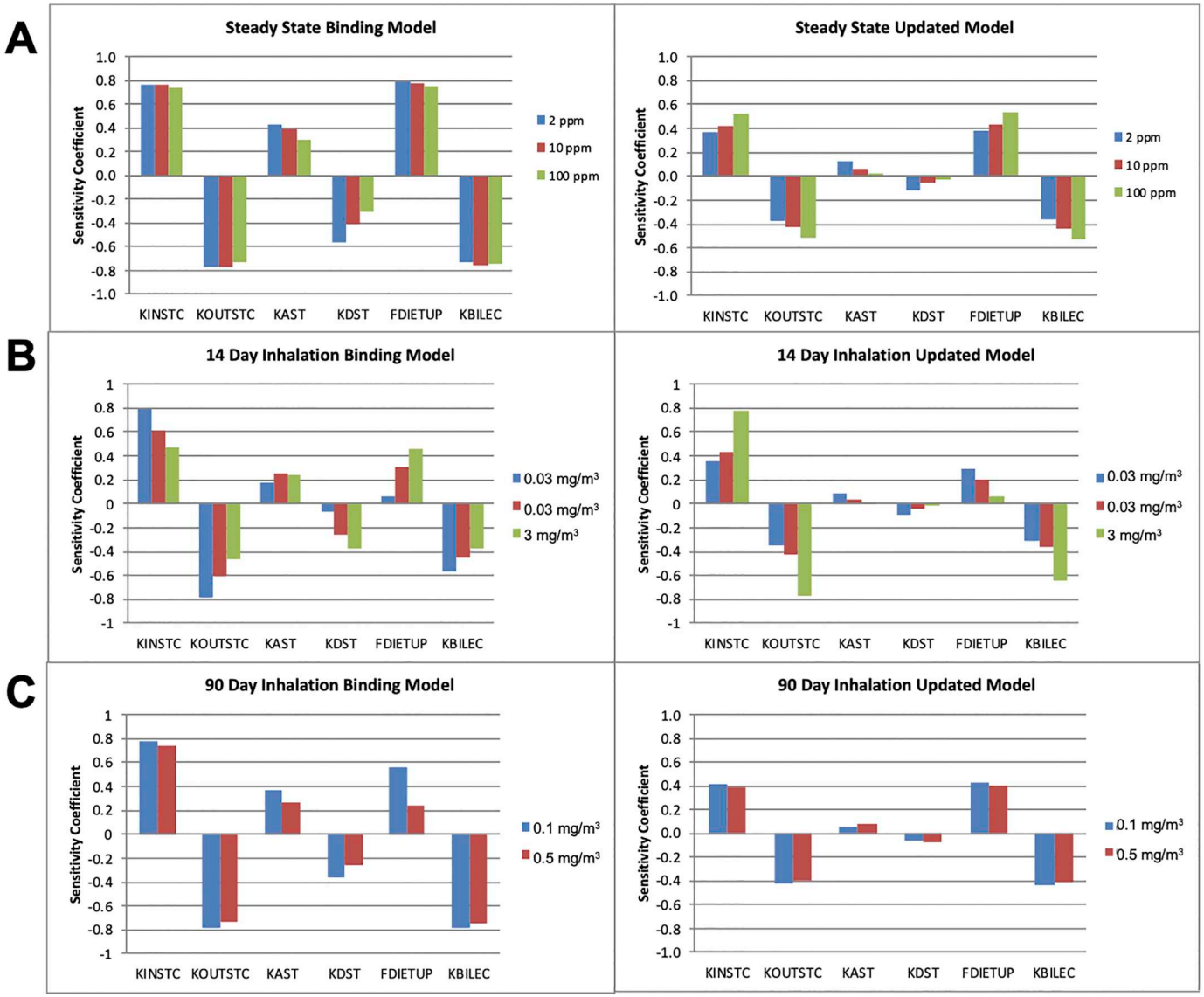

Fig. 7. Determinants of striatum Mn – comparison between the original vs. updated models. Sensitivity analysis was performed for 6 key parameters to test how sensitive the brain striatum Mn concentration is in response to a small change in each of these parameters. The resulting sensitivity coefficients are plotted here. Abbreviations for those 6 parameters are influx and efflux rates into and out of the striatum (KINSTC and KOUTSTC), association and dissociation rate constants in the striatum (KAST and KDST), the biliary excretion rate constant (KBILEC), and the absorption fraction in the gut (FDIETUP).

findings and dose-response relationships to corresponding in vivo conditions. For example, the new Mn model could provide a useful insight into the intracellular trafficking and efflux of Mn leading to better understanding of the concentration-dependent control of Mn transports via metal transporters at cellular surfaces as well as the intracellular movement of Mn in relation with cellular toxicity in in vitro models such as primary neuronal cells and model organisms such as *C. elegans* (Leyva-Illades et al., 2014; Lin et al., 2017).

With the rapid association/dissociation rates in this updated model, it was no longer necessary to include induction of the biliary excretion rate constant as body burdens of Mn increased (Fig. S1). The simulated dose-dependent rate of, or amount of, Mn excretion by the updated model remained comparable to that simulated by the original model indicating that in the new description, free Mn-dependent biliary excretion alone is sufficient to describe dose-dependent changes in Mn excretion via bile. This difference occurs because in the updated model, the saturation of binding sites throughout the body and more rapid increases in blood Mn drive the rate of biliary excretion rather than requiring enhancement of the rate constant to effectively provide a draw on tissue Mn in the face of the slow dissociation constant for tissue stores of Mn.

For the published models, the tissue binding and cellular transport parameters for rat striatum were allometrically scaled to monkey globus pallidus together with further optimization based on the available tissue time course data in monkeys (Nong et al., 2008; Schroeter et al., 2011). Inter-species extrapolation of the monkey pallidal parameters to those in humans was also based on the allometrical scaling along with the available human data (Schroeter et al., 2011; Yoon et al., 2011). Currently, we are investigating the feasibility of updating the monkey model with the rapid binding assumption as described in this study. Once successfully evaluated, inter-species extrapolation of the updated monkey model to human can be performed in a similar manner to the published models.

Since the motivation for recasting the Nong et al. (2008) model structure to this rapid association-dissociation model was the increasing appreciation of transporters in controlling metal kinetics and tissue accumulation, it is of interest to consider recent work on Mn-metal transporters and Mn toxicity in mice. Over the past two years research

has appeared evaluating the role of two Mn efflux transporters, SLC39A14 and SLC30A10. The work with both transporters used transgenic mice. With SLC39A14 (Xin et al., 2017), wild-type, whole body knock out (KO) and hepatocyte specific KOs were evaluated. For similar Mn intakes, the whole-body KO mice had 20 to 30-fold increases in blood and brain Mn compared to WT-mice. With the liver specific KOs, except for relatively small increase in liver itself, there was little change in Mn in other tissues. The study with SLC39A14 also evaluated the effect of the KO on other transporters, finding modest changes in another Mn-efflux transporter, SLC30A10, in several tissues.

A more extensive evaluation was reported with SLC30A10 (Taylor et al., 2019) using 5 strains of mice: WT, whole body KO, hepatocyte KO, endoderm specific KOs (i.e., KOs in both the liver and GI-tract), and pan-neuronal/glial KO. Whole body KOs increased brain Mn by about 20-fold and blood Mn by 20-to 25-fold. As with SLC39A14, liver specific KOs caused only small changes in blood and brain Mn. The endoderm specific KOs had increases in blood and brain Mn nearly as great as those seen in whole body KO mice. Surprisingly, the pan-neuronal/glial KOs had minimal increases in brain Mn compared to WT-mice.

The appearance of these new data sets on differential tissue Mn accumulation with manipulation of specific transporters represents an opportunity to further develop our restructured model with more explicit inclusion of transporter tissue distribution. As has been the practice with many other PBPK modeling programs, the ability to include different structural characteristics within models, in this case, different distributions and activities of transporters, together with different model structures, such as this rapid association-dissociation model, should provide important quantitative tests to what might remain qualitative conclusions about the influence of different tissue distributions of transporters on tissue accumulation of Mn.

Some of the observations with tissue specific KO mice are consistent with prior work from the nutritional literature on regulation of uptake with changing diets. Teeguarden et al. (2007) examined the uptake of Mn with increasing dietary Mn showing that the rate constant for uptake, a measure of the ability of Mn to move to the enterocyte and out was reduced 23-fold going from dietary intake of 0.49 to 73 ppm, while the rate of biliary excretion increased only by a factor of 4 (data from Malecki et al., 1996). These changes and other work showed that uptake from the gut to the circulation was under tight control. These processes indicated a primary role of enterocyte elimination of Mn in controlling the proportion retained from the diet rather than the biliary excretion after absorption. Clearly, the primacy of enterocyte function in controlling Mn homeostasis is also evident from these liver specific transporter KO mice. The role of biliary excretion is to move Mn into bile where it also is sensed by enterocytes. The most intriguing observation is the lack of brain accumulation in the pan-neuronal/glial KO mice. This behavior might indicate a role for SLC30A10 in intake as well as efflux at higher blood Mn or the presence of coordinate effects on expression of other efflux transporters in the SLC30A10 KO mice.

Our modeling efforts over the past decade have focused on uptake and distribution of Mn after inhalation exposures with animals or humans (Yoon et al., 2014). With inhalation, and uptake of Mn from the lungs, the control of uptake by enterocytes primarily affects the proportion Mn retained from the diet with the liver moving Mn from blood to the intestinal lumen. The increasing knowledge of tissue distribution and function in these transgenic mice coupled with species-specific PBPK modeling should be useful for informing risk assessments for both oral and inhalation exposures.

It also bears some emphasis that this recast rapid-association-dissociation PBPK model can be easily adapted to account for transporter distribution and for the characteristics of kinetic parameters of transporters in diverse tissues as such data become available. These models, as with those derived from the older model architecture, are also readily amenable to inclusion of life stage changes in the concentrations of transporters in animals and humans and for different life stages (Yoon et al., 2014).

5. Conclusion

Our alternative parameterization in an updated PBPK model successfully describes Mn kinetics in tissues in adult rats exposed to Mn both in their diet and by inhalation. The model structure with rapid binding was better in capturing transient dose dependent elimination processes of the tracer as dosing patterns and dose levels changed. However, the two model structures – with different kinetics of tissue binding – both capture the dose-dependent and tissue-specific kinetic behavior of Mn in adult rats for longer-term exposure conditions. The equivalent performance of the published and updated models in capturing the non-linear kinetics of Mn provides greater confidence in using the previously published Mn PBPK models in risk assessment, as updating the other published Mn models to incorporate the alternative parameterization is unlikely to lead to materially different outcomes when modeling changes in Mn concentration under different exposure conditions once steady-state is reached. The updated model has promise for extending the application of the Mn PBPK model to develop studies on mechanism-based toxicity testing approaches, in particular focusing on the target brain regions of mid-brain for Mn neurotoxicity such as striatum and globus pallidus (Aschner et al., 2005; Dorman et al., 2000), incorporate those new data on Mn transporters from non-animal and other emerging alternative models to the PBPK models for in vitro to in vivo extrapolation, and study periods of rapid changes in Mn exposures in various populations. Such abilities will also contribute to adding weight of evidence increasing confidence in model-based risk assessment.

Transparency document

The Transparency document associated to this article can be found, in the online version

Acknowledgements

This work is based on studies sponsored and funded by Afton Chemical Corporation in satisfaction of registration requirements arising under Section 211(a) and (b) of the Clean Air Act and corresponding regulations at 40 CFR Substance 79.50 et seq.

Appendix A. Supplementary data

Supplementary data to this article can be found online at https://doi.org/10.1016/j.taap.2019.04.006.

References

Andersen, M.E., Dorman, D.C., Clewell III, H.J., Taylor, M.D., Nong, A., 2010. Multi-dose-route, multi-species pharmacokinetic models for manganese and their use in risk assessment. J. Toxic. Environ. Health A 73 (2–3), 217–234.

Aschner, M., Erikson, K., 2017. Manganese. Adv. Nutr. 8, 520–521. https://doi.org/10.3945/an.117.015305.

Aschner, M., Erikson, K.M., Dorman, D.C., 2005. Manganese dosimetry: species differences and implications for neurotoxicity. Crit. Rev. Toxicol. 35 (1), 1–32.

Aschner, M., Guilarte, T.R., Schneider, J.S., Zheng, W., 2007. Manganese: recent advances in understanding its transport and neurotoxicity. Toxicol. Appl. Pharmacol. 221 (2), 131–147.

Ash, D.E., Schramm, V.L., 1982. Determination of free and bound manganese(II) in hepatocytes from fed and fasted rats. J. Biol. Chem. 257, 9261–9264.

ATSDR, 2013. Toxicological Profile for Manganese. U. S. Dep. Heal. Hum. Servhttps://doi.org/10.1155/2013/286524.

Chen, P., Chakraborty, S., Mukhopadhyay, S., Lee, E., Paoliello, M.M.B., Bowman, A.B., Aschner, M., 2015. Manganese homeostasis in the nervous system. J. Neurochem. 134, 601–610.

Dorman, D.C., Struve, M.F., Vitarella, D., Byerly, F.L., Goetz, J., Miller, R., 2000. Neurotoxicity of manganese chloride in neonatal and adult CD rats following subchronic (21-day) high-dose oral exposure. J. Appl. Toxicol. 20 (3), 179–187.

Dorman, D.C., Struve, M.F., James, R.A., McManus, B.E., Marshall, M.W., Wong, B.A., 2001a. Influence of dietary manganese on the pharmacokinetics of inhaled manganese sulfate in male CD rats. Toxicol. Sci. 60 (2), 242–251.

Dorman, D.C., Struve, M.F., James, R.A., Marshall, M.W., Parkinson, C.U., Wong, B.A.,

2001b. Influence of particle solubility on the delivery of inhaled manganese to the rat brain: manganese sulfate and manganese tetroxide pharmacokinetics following repeated (14-day) exposure. Toxicol. Appl. Pharmacol. 170 (2), 79–87.
Dorman, D.C., McManus, B.E., Marshall, M.W., James, R.A., Struve, M.F., 2004. Old age and gender influence the pharmacokinetics of inhaled manganese sulfate and manganese phosphate in rats. Toxicol. Appl. Pharmacol. 197 (2), 113–124.
Freeland-Graves, J., 1994. Derivation of manganese estimated safe and adequate daily dietary intakes. Risk Assess. Essential Elements 237–252.
Grisham, C.M., Mildvan, A.S., 1974. Magnetic resonance and kinetic studies of the mechanism of sodium and potassium ion-activated adenosine triphosphatase. J. Biol. Chem. 249 (10), 3187–3197.
Hutchens, S., Liu, C., Jursa, T., Shawlot, W., Chaffee, B.K., Yin, W., Gore, A.C., Aschner, M., Smith, D.R., Mukhopadhyay, S., 2017. Deficiency in the manganese efflux transporter SLC30A10 induces severe hypothyroidism in mice. J. Biol. Chem. jbc-M117.
Leyva-Illades, D., Chen, P., Zogzas, C.E., Hutchens, S., Mercado, J.M., Swaim, C.D., Morrisett, R.A., Bowman, A.B., Aschner, M., Mukhopadhyay, S., 2014. SLC30A10 is a cell surface-localized manganese efflux transporter, and parkinsonism-causing mutations block its intracellular trafficking and efflux activity. J. Neurosci. 34 (42), 14079–14095.
Lin, W., Vann, D.R., Doulias, P.T., Wang, T., Landesberg, G., Li, X., Ricciotti, E., Scalia, R., He, M., Hand, N.J., Rader, D.J., 2017. Hepatic metal ion transporter ZIP8 regulates manganese homeostasis and manganese-dependent enzyme activity. J. Clin. Invest. 127 (6), 2407–2417.
Malecki, E.A., Radzanowski, G.M., Radzanowski, T.J., Gallaher, D.D., Greger, J.L., 1996. Biliary manganese excretion in conscious rats is affected by acute and chronic manganese intake but not by dietary fat. J. Nutr. 126 (2), 489–498.
Nong, A., Taylor, M.D., Clewell III, H.J., Dorman, D.C., Andersen, M.E., 2009 Mar. Manganese tissue dosimetry in rats and monkeys: accounting for dietary and inhaled Mn with physiologically based pharmacokinetic modeling. Toxicol. Sci. 108 (1), 22–34. https://doi.org/10.1093/toxsci/kfn264.
Nong, A., Teeguarden, J.G., Clewell III, H.J., Dorman, D.C., Andersen, M.E., 2008. Pharmacokinetic modeling of manganese in the rat IV: assessing factors that contribute to brain accumulation during inhalation exposure. J. Toxic. Environ. Health A 71 (7), 413–426.
Powell, J.T., Brew, K., 1976. Metal ion activation of galactosyltransferase. J. Biol. Chem. 251 (12), 3645–3652.
Roels, H.A., Ortega Eslava, M.I., Ceulemans, E., Robert, A., Lison, D., 1999. Prospective study on the reversibility of neurobehavioral effects in workers exposed to manganese dioxide. Neurotoxicology 20, 255–271.
Santos, D., Batoreu, C., Mateus, L., Marreilha dos Santos, A.P., Aschner, M., 2014. Manganese in human parenteral nutrition: considerations for toxicity and biomonitoring. Neurotoxicology 43, 36–45.
Schroeter, J.D., Nong, A., Yoon, M., Taylor, M.D., Dorman, D.C., Andersen, M.E., Clewell 3rd, H.J., 2011. Analysis of manganese tracer kinetics and target tissue dosimetry in monkeys and humans with multi-route physiologically based pharmacokinetic models. Toxicol. Sci. 120, 481–498.
Taylor, C.A., Hutchens, S., Liu, C., Jursa, T., Shawlot, W., Aschner, M., Smith, D.R., Mukhopadhyay, S., 2019. SLC30A10 transporter in the digestive system regulates brain manganese under basal conditions while brain SLC30A10 protects against neurotoxicity. J. Biol. Chem. 294 (6), 1860–1876.
Teeguarden, J.G., Dorman, D.C., Covington, T.R., Clewell III, H.J., Andersen, M.E., 2007. Pharmacokinetic modeling of manganese. I. Dose dependencies of uptake and elimination. J. Toxic. Environ. Health A 70 (18), 1493–1504.
Tuschl, K., Meyer, E., Valdivia, L.E., Zhao, N., Dadswell, C., Abdul-Sada, A., Hung, C.Y., Simpson, M.A., Chong, W.K., Jacques, T.S., Woltjer, R.L., 2016. Mutations in SLC39A14 disrupt manganese homeostasis and cause childhood-onset parkinsonism–dystonia. Nat. Commun. 7, 11601.
Xin, Y., Gao, H., Wang, J., Qiang, Y., Imam, M.U., Li, Y., Wang, J., Zhang, R., Zhang, H., Yu, Y., Wang, H., 2017. Manganese transporter Slc39a14 deficiency revealed its key role in maintaining manganese homeostasis in mice. Cell Discov. 3, 17025.
Yoon, M., Schroeter, J.D., Nong, A., Taylor, M.D., Dorman, D.C., Andersen, M.E., Clewell III, H.J., 2011. Physiologically based pharmacokinetic modeling of fetal and neonatal manganese exposure in humans: describing manganese homeostasis during development. Toxicol. Sci. 122 (2), 297–316.
Yoon, M., Taylor, M.D., Clewell, H.J., Andersen, M.E., 2014. Modeling manganese kinetics for human health risk assessment. In: Manganese in Health and Disease. Royal Society of Chemistry, pp. 322–354.

Abstract 4035. Poster Board P734, Society of Toxicology, 2022

Bright ideas. Sustainable change. RAMBOLL

Incorporation of rapid association/dissociation processes in tissues into the monkey and human physiologically based pharmacokinetic models for manganese

AUTHORS

Jerry Campbell[1], Harvey Clewell[1], Cynthia VanLandingham[2], Robinan Gentry[2], Athena Keene[3], Michael Taylor[4], and Mel Andersen[5]

[1]Ramboll, RTP, NC

[2] Ramboll, Monroe, LA

[3]Afton Chemical Corporation, Richmond, VA

[4]NiPERA, Durham, NC

[5]Andersen ToxConsulting LLC, Denver, NC

ABSTRACT

In published physiologically based pharmacokinetic (PBPK) models for manganese (Mn), the kinetics of transport of Mn to and from tissues was primarily driven by Mn binding in tissues. In subsequent years, appreciation of the role of cellular membrane transporters in the homeostasis of Mn has grown appreciably. Based on these insights, an updated Mn model for primates, following similar work with rats, was developed that accounts for more rapid rates of transporter-mediated entry into tissues, interaction of Mn with cellular binding sites and accumulation of free Mn in tissues after saturation of these Mn-binding sites. This alternative structure successfully described Mn kinetics in tissues in non-human primates and humans exposed to Mn via various routes including diet, oral gavage, inhalation, and intraperitoneal, subcutaneous, or intravenous injection. An important contribution of this effort is showing that the extension of the rate constants for cellular transport and intracellular disposition of Mn established in the monkey were also able to describe kinetic data from humans. The increased biological relevance of the Mn model structure and parameters provides greater confidence in applying the Mn PBPK models to risk assessment. This model is also well-suited to extension to explicitly incorporate emerging information on the role of transporters in tissue disposition, intestinal uptake, and hepatobiliary excretion of Mn.

BACKGROUND

- Early Mn compartmental PK models were unable to capture the rapid rise in tissue Mn concentrations seen during inhalation exposure to high Mn concentrations, due to their reliance on linear first-order processes to simulate Mn tissue kinetics under both normal and deficient dietary conditions. Subsequently, a successful PBPK model structure was developed in the rat, monkey and human that included saturable Mn tissue stores (Nong et al., 2009, Schroeter et al. 2011).
- Since the publication of these models, further investigation of the processes important to metal homeostasis has indicated that uptake into and efflux out of tissues are due to actions of cellular membrane transporters and less avid, more readily reversible binding of Mn within tissues (Aschner and Erikson, 2017; Chen et al., 2015).
- Solute transporter proteins recently identified to be involved in Mn homeostasis in vertebrates include SLC30A10, SLC39A8 and SLC39A14 (Mercadante et al., 2019; Park et al. 2015; Tuschl et al., 2016).
- In light of these findings, Yoon et al. (2019) recast the published PBPK model for the adult rat (Nong et al., 2009) to have more rapid tissue uptake and more rapid binding and association of Mn with binding sites in tissues.
- In the current study, the same model structure with more rapid association-dissociation processes for Mn binding in tissues was incorporated into the non-human primate and human Mn PBPK model (Schroeter et al. 2011), based on the current understanding of the role of transporters in the influx and efflux of Mn.

STRUCTURE OF MANGANESE PBPK MODEL

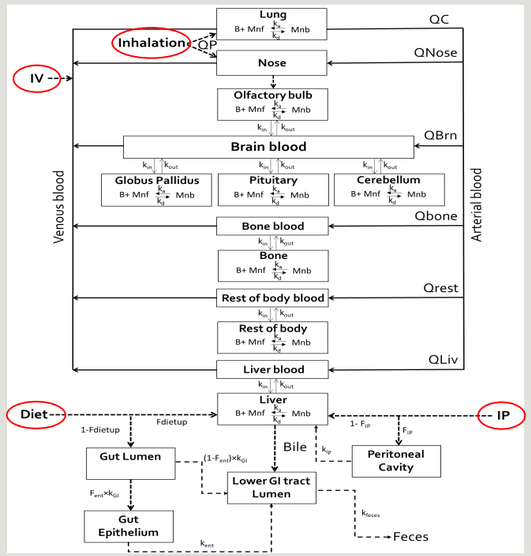

- Structure of model is unchanged from Schroeter et al. (2011), except that the dose dependent uptake to the globus pallidus and pituitary compartments in Schroeter et al. (2011) was not required to reproduce the non-human primate data with the revised model

STRUCTURE OF MANGANESE TISSUE SUBMODELS

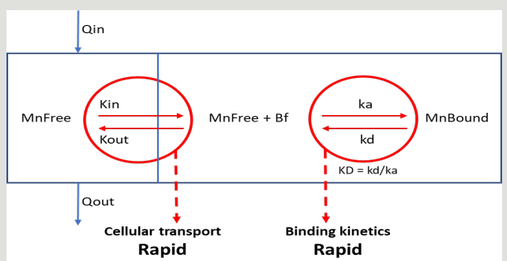

- Kin and Kout are diffusion rate constants for Mn influx and efflux, respectively
- ka and kd are Mn association and dissociation rate constants
- The available binding sites (Bf) are equal to the maximal binding capacity in a tissue (Bmax) minus the amount of Mn bound

MODEL PARAMETERIZATION

- Mn tissue binding (ka and kd) constants were retained from rat model.
- Parameter optimization for the monkey Mn transporter model was conducted to simultaneously estimate three parameters (Kin, Kout and Bmax) for each tissue.
- The datasets used for optimization included the Dorman et al. (2006a) baseline diet values and 1.5 mg/m3 inhalation time-course data and the whole-body clearance of ^{54}Mn: IP (Dastur et al. 1971), IV and oral (Furchner et al. 1966) (below).
- Apart from physiological parameters, other human parameters were scaled allometrically from the monkey.

SIMULATION OF MN TISSUE TIME-COURSES IN MONKEYS FROM INHALATION

1.5 MG MN/M^3, 90 DAYS, 6 H/D, 5 D/W (DORMAN ET AL. 2006)

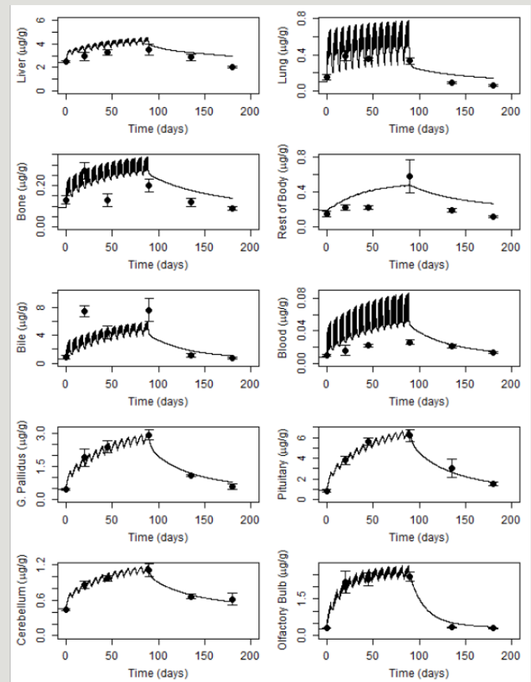

SIMULATION OF WHOLE-BODY ^{54}MN CLEARANCE IN MONKEYS FOLLOWING IP (DASTUR ET AL. 1971), IV AND ORAL (FURCHNER ET AL. 1966) DOSING

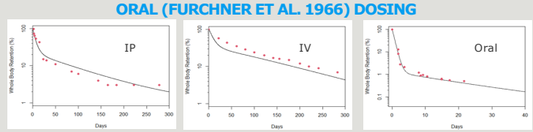

MODEL VALIDATION

PREDICTED FECAL EXCRETION OF 54MN IN MONKEYS COMPARED WITH THE DATA FROM NEWLAND ET AL. (1987)

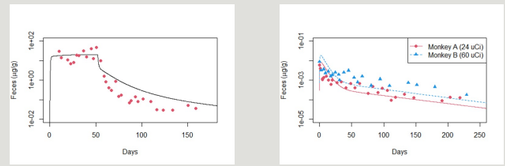

One monkey injected subcutaneously with 200 µCi $^{54}MnCl_2$ and 400 mg $MnCl_2$

Two monkeys exposed by inhalation to a nebulized aerosol of carrier-free $^{54}MnCl2$

PREDICTED MN TISSUE CONCENTRATIONS IN MONKEYS FROM REPEATED INHALATION

90 DAYS, 6 H/D, 5 D/W (DORMAN ET AL. 2006)

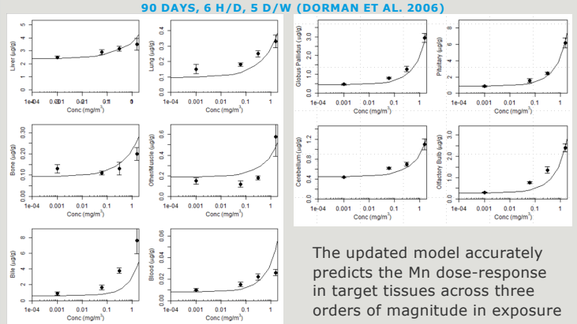

The updated model accurately predicts the Mn dose-response in target tissues across three orders of magnitude in exposure

PREDICTION OF WHOLE-BODY ^{54}MN CLEARANCE IN HUMAN SUBJECTS

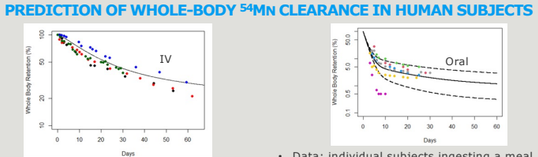

- Green circles: average for 8 subjects (Mena et al. 1967)
- Others: 3 individual subjects (Mahoney and Small 1968)
- Data: individual subjects ingesting a meal labeled with ^{54}Mn (Davidsson et al. 1988)
- Dashed curves show the effect of simultaneous 3-fold opposed changes in FDIETUP and KBILEC, to indicate the impact of variability in these two parameters

CONCLUSIONS

- PBPK models with more loosely bound tissue Mn better represent the known biochemistry of Mn compared to earlier models with much more tightly bound, slowly exchangeable Mn.
- Despite the improved fidelity with Mn biology in the new model, both the older and newer PBPK models adequately describe the dose dependence of Mn concentration in various brain regions with increasing inhalation exposures or dietary intakes to support risk assessments of manganese exposure.

ACKNOWLEDGEMENT: Funded by AftonChemical, Richmond, VA.

CONTACT: Jerry Campbell (jcampbell@ramboll.com)